Geochemical Controls on Arsenic Release into Groundwaters from Sediments: In Relation to the Natural Reactive Barrier

by

Michelle M. Berube

B.S., Union College, 2015

A THESIS

submitted in partial fulfillment of the requirements for the degree

MASTER OF SCIENCE

Department of Geology
College of Arts and Sciences

KANSAS STATE UNIVERSITY
Manhattan, Kansas

2017

Approved by:

Major Professor
Saugata Datta

Abstract

Elevated levels of dissolved arsenic (As), iron (Fe) and manganese (Mn) are seen in the shallow, anoxic groundwaters of southeast Bangladesh on the Ganges- Brahmaputra- Meghna River delta. Over the past decade the mechanisms of As release have been widely debated. It is understood that As can sorb onto Fe-bearing minerals and can be subsequently released when reactions, such as microbially driven processes, occur. This study takes a multi-disciplinary approach to understand the extent of the natural reactive barrier along the Meghna River and to evaluate the role of the natural reactive barrier in As sequestration and release in groundwater aquifers. River water and groundwater interactions occur in the hyporheic zone, which is defined as the transient subsurface region where river water and groundwater mix. The natural reactive barrier can develop within the hyporheic zone, where Fe-bearing minerals accumulate with a potential for As sorption, along with reworking and re-deposition of sediments along the riverbank. Shallow sediment cores, and groundwater and river water samples were collected from the east and west banks of the Meghna River in Jan. 2016. Groundwater and river water samples were tested for total dissolved Fe, Mn, and As concentrations; $\delta^{2}H$, $\delta^{18}O$ isotopic ratios. Fluorescence spectroscopic characterization of groundwater organic matter provided insight into the hydro-geochemical reactions active in the groundwater and the hyporheic zone. Eight sediment cores of ~1.5 m depth were collected ~10 m away from the edge of the river. Vertical solid-phase concentration profiles of Fe, Mn, and As were measured by four different methods (hand-held XRF, and ICP-OES analysis of 3 digestions: aquaregia (HNO_3: HCl 1:3), 1.2 M HCl, and 1 M NaH_2PO_4 + 1 M L-ascorbic acid extractions). Enrichment of solid phase Fe, Mn, and As and the presence of possible Fe and Mn oxides in the sediments illustrate the existence of a natural reactive barrier at this reach of the Meghna. HCl extractions of sediment revealed solid-phase As accumulation along the west riverbank reaching concentrations of ~1500 mg/kg. Aqueous geochemical results showed the highest dissolved As concentrations in shallow wells (<30 m depth), where organic matter was fresh, humic-like, and aromatic. Humic-like dissolved organic matter present in the groundwater may enhance Fe oxide dissolution. Microbial reduction of organic matter prompts the reduction of Fe^{3+} to Fe^{2+}, causing As to mobilize into groundwater. This study quantified the extent of As accumulation in the sediments along a 1 km stretch of the Meghna River. These findings contribute to the understanding of geochemical processes involved in As release into groundwaters from sediments within a fluvial deltaic environment.

Table of Contents

List of Figures

List of Tables

Acknowledgements

I have found that one of the greatest joys is to work hard at work worth doing, and what makes this project so special is the amazing people helping and supported along this challenging and rewarding journey. I would like to thank all of you. No one achieves anything alone, and this work would not have been possible without all of you.

I would like to specially thank my funders, in particular KSU Geology alumni Paul and Deanna Strunk for their generous donations, the Geological Society of America (GSA), Kansas State University Geology Department, Texas A&M, and the National Science Foundation Hydrologic Sciences Program (Tulane University and Kansas State University), for their research investment funds which allowed this work to be made possible.

I would like to thank everyone from the University of Dhaka, especially Dr. Kazi Matin Ahmed for all of your amazing support, and Musabbir Ahmed Khan for your help in the field, we couldn't have done this without you.

To everyone at the University Of Texas A&M especially Dr. Peter Knappett, Kimberly Myers I cannot even put into words how much I appreciate how much you have done to help our research. To my committee member Dr. Peter Knappett, thank you for all of the time and effort you have put into this project. You have guided me and inspired me and for that I thank you. Kim thank you so much for all your support and care through this process. To Katrina Jewell; thank you for all of your support and for being such a great friend, from field work in Bangladesh, to conferences in Colorado and Japan, we have been through it all together.

There are so many people from Kansas State University that made this work possible. First my committee members; Dr. Pamela Kempton for her incredible and helpful advice, and all of her edits with writing, Dr. Ganga Hettiarachchi for sharing her wisdom and providing insight that changed the way we look at this research. I would also like to thank Dr. Matt Kirk for help with the Ion Chromatography. I would also like to thank Harshad Kulkarni for all of his work and help in this research. In addition, I would like to especially thank Joseph Weeks and Madhubhashini Galkaduwa for spending hours and hours working with me in the Agronomy Department, I am so grateful to have had your help through this process. A special shout out to Mike Vega for always being there for support, bounce ideas off, and helping me gather and organize field supplies.

I would also like to thank all of the K-State students, I could not have done this without you guys! In particular Ian Andree, Beth Morter, Katie Garth, Grant Zwiefelhofer, Jacob Hughes,

Sam Berkelhammer and Kyle Marquart, thank you all for being such amazing friends. A special thanks to my amazing mentor, office mate and true true friend Colleen Gura, you have been my rock through the last two years and I am so appreciative.

Last and certainly not least, I would like to thank my advisor and great friend Dr. Saugata Datta. Over the last two years you have challenged me, and pushed me to realize my potential, as a scientist and as a person. You made this work possible, and without you I would not be this strong, brave, and driven geologist. Thank you for all of your time, guidance, support, advice and for giving me this once in a lifetime opportunity to work on a project that is bigger than any one person.

I am so grateful to have had this amazing experience working with so many people from all branches of science. Collaboration and teamwork are some of most important things in this world and I thank all of you for these adventures we have shared.

CHAPTER 1 - Introduction

1.1 History of Arsenic in Groundwater in Bangladesh

Water is one of the most important resources on earth, and having clean water is a priority when it comes to quality of life. The Bengal Basin, comprises most of Bangladesh, and parts of Western India (West Bengal), and is regarded as one of the most severely arsenic affected geological regions in the world. The Bengal Basin was formed by the sedimentation of the two major Himalayan river systems the Ganges and Brahmaputra. Surface water in much of southeast Asia is contaminated with E.-coli, and other pathogens (Knappett et al., 2011), so groundwater is their major source of clean water (Harvey et al., 2006). More than 95% of the population of the Bengal Basin (>120 million people) rely on groundwater for drinking, and ~70% of all irrigation in this region is groundwater fed (Hasan et al., 2007). The presence of elevated dissolved As in groundwater has endangered the lives of ~35 million people in Bangladesh and ~15 million people in West Bengal (Smedley and Kinniburgh, 2002). Arsenic concentrations in groundwater vary widely, ranging from <0.005 mg/L to 4.1 mg/L in West Bengal and up to 4.7 mg/L in Bangladesh (Ghosh and Mukherjee, 2002). The World Health Organization standard of As in drinking water is 0.01 mg/L in Bangladesh (BGS, 2001; WHO, 2010). The background dissolved As concentration in natural water has been reported to be 0.001- 0.002 mg/L (WHO, 2010).

The assessment of As contamination in groundwaters of Bangladesh was initiated in mid-1996 by the British Geologic Survey to understand the basic hydrochemistry of Bangladesh aquifers and establish the extent of As contamination (BGS, 1999, 2001). It was originally found that ~ 2 million tube wells in Bangladesh were contaminated with As higher than the Bangladesh drinking water standard water (0.05 mg/L) (BGS, 2001). More recently it has been estimated that As has contaminated between 25% and 33% of the ~11 million tube wells providing water in Bangladesh alone (Ahmed et al., 2004; McArthur et al., 2004). Past research conducted by the BGS found that the higher elevated regions in north and northwest Bangladesh have significantly less As contaminated groundwater (known as the Pleistocene uplands) (Morgan and McIntire, 1959) (Figure 1.1), whereas groundwater located in the lowland regions of south and southeast Bangladesh has relatively high As concentrations (BGS, 2001); these are known as the Holocene lowlands (Morgan and McIntire, 1959).

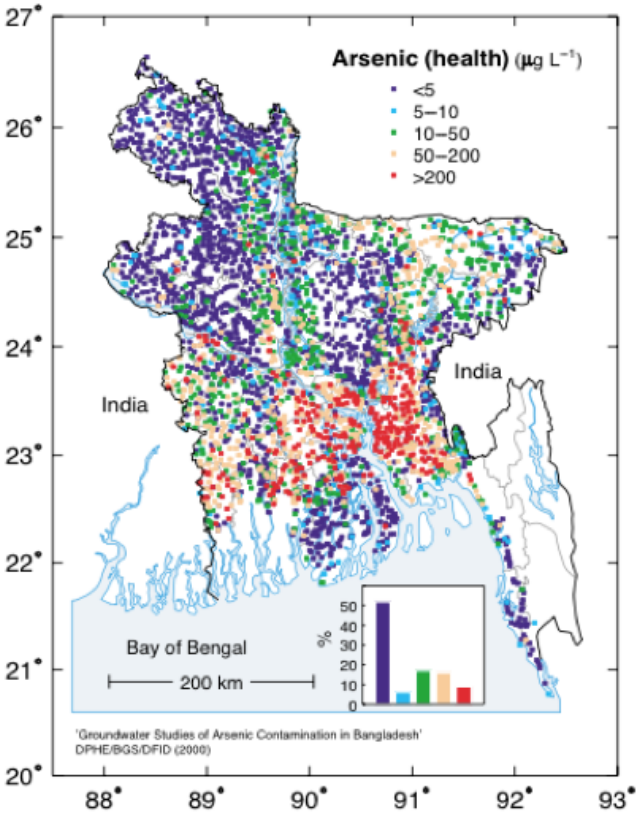

Figure 1.1 Distribution of dissolved As concentration in groundwater aquifers in Bangladesh, based on the DPHE/BGS National Hydrochemical Survey (BGS, 2001).

1.2 Arsenic Geochemistry and Release Mechanisms

Arsenic is a redox sensitive element, meaning that changes in redox conditions influence the mobility, form, toxicity, and interactions with solids and dissolved species. As^{3+} is more soluble, mobile, toxic, bioavailable, and forms weak complexes; upon changes in the hydrochemistry, the weak bonds break easily resulting in mobilization of As^{3+} in solution (Tufano and Fendorf, 2008). Typically, $H_2AsO_4^-$ and $HAs_2O_4^{2-}$ species occur under oxidizing conditions (Eh>100 mV and pH 6-7.5), whereas under reducing conditions (Eh < 100 mV and pH 6-7.5) $H_3AsO_3^0$ typically dominates. However, both As^{3+} and As^{5+} species occur in nature as the rate of redox transformation is slow (Smedley and Kinniburgh, 2002; Mukherjee et al., 2009). In general, redox conditions of the environment strongly govern the ratio of As^{3+} to As^{5+} species.

Previous research has been conducted on source, toxicity and remediation techniques of As in groundwaters (Nagorski et al., 1999; Feris et al., 2004; Ravenscroft et al., 2005; Nimick et al., 2005). There are a number of hypotheses suggesting how the As accumulates in the

groundwater, however, these mechanisms of As release are to some extent still poorly understood. The As release mechanisms are associated with the burial of fresh sediment and the generation of anaerobic groundwater conditions (BGS, 2001). Weathered sediments from the Himalayas have been implicated as primary sources of geogenic As (Nordstrom, 2002; Postma et al., 2010). Arsenic can be released primarily from minerals through weathering, following sediment transport, and deposition. Arsenic sorbs to and is then released from oxides of Fe, Al, and Mn through microbially mediated reductive dissolution (Nickson et al., 1998; Harvey et al., 2002; Islam et al., 2004; Datta et al., 2009; Mladenov et al., 2010, 2015). Once the reducing conditions are achieved, As can be released from the sediments into the groundwater. The mechanisms of As release can also be impacted by changes in the water table level (BGS, 2001).

Changing river levels alter hydraulic gradients, which may control the short-range changes of As concentrations in groundwater (BGS, 2001). It is evident that changes in river water level may have an impact on the As release mechanism (Jung et al., 2015). Considerable volumes of groundwater discharge to rivers in deltas and low-lying areas (Larsen et al., 2008; Knappett et al., 2012; Kolker et al., 2013) carrying nutrients and heavy metals (Sawyer et al., 2013; Musial et al., 2016). The fluctuations in river water level, changes in reducing and oxidizing conditions and subsequent changes in geochemical conditions in the hyporheic zone may promote release of As (Datta et al., 2009; Knappett et al., 2016).

1.3 Hyporheic Zone and Natural Reactive Barrier in Context of Oxyanion Mobility

The hyporheic zone (HZ) is defined as the small transient subsurface region where groundwater is discharging to river water and where oxygen-rich river water meets anoxic groundwater (Datta et al., 2009; Sawyer et al., 2013; Musial et al., 2016; Knappett et al., 2016). The HZ is considered to be part of the aquifer that has at least 1% of recently recharged water from a river for some part of the year (Brunke and Gonser, 1997). Brunke and Gonser (1997), define the HZ as a zone of intense exchange of water solutes. Triska et al. (1989), define the HZ as the area where 10-98% of the water originated from the river, and White (1993) defines the HZ as the saturated pore spaces beneath the stream bed and into the stream banks which contain some proportion of channel water or have been altered by surface water infiltration.

The size of the hyporheic zone can change based on tides and monsoon seasons, causing the HZ to expand into a reduced aquifer or contract; as a result of this expansion and/or contraction the ambient geochemical conditions can be altered in the hyporheic zone (Sawyer et al., 2013;

Musial et al., 2016; Knappett et al., 2016). From the literature it is known that heavy metals and metalloids tend to occur in this transient interface between river water and groundwater. Previous works have found that during gaining river conditions, groundwater flows into the river through a thin "iron curtain" (Beck et al., 2010), "geochemical barrier" (Charette and Sholkovitz, 2002; Charette et al., 2005), or natural reactive barrier "NRB" (Datta et al., 2009) that resides in the hyporheic zone. It has been determined that the natural reactive barrier can develop along freshwater-groundwater interfaces of major rivers of fluvial deltaic environments (Datta et al., 2009; Jung et al., 2015). Datta et al. (2009) define the natural reactive barrier as the region where layers of reactive Fe-bearing minerals form within a sub oxic or oxidized zone. The high solid phases of Fe and As usually reside within the shallow 1-5 m depth along the edges of major rivers. When groundwater discharges through sandy riverbank sediments into the oxygenated river water, the mobile phases of Fe and As build a natural reactive barrier (Jung et al., 2015). The Fe usually forms Fe oxides and hydroxides in various forms, from amorphous to crystalline, and As tends to adsorb onto these Fe minerals (Bostick and Fendorf, 2003). The precipitation of Fe oxides in the subsurface sediments can act as a "geochemical barrier" because they retain and accumulate dissolved cation species, such as As, as groundwater flows towards the river (Charette and Sholkovitz, 2002; Jung et al., 2015). In the natural reactive barrier, As can bind to the Fe minerals and then be released from the Fe complexes following a changes in redox conditions (Datta et al., 2009).

1.4 Hypotheses and Objectives

Growing evidence supports the important role of processes in the hyporheic zone and the natural reactive barrier in regulating groundwater As (Nagorski et al., 1999; Feris et al., 2004; Nimick et al., 2005; Jung et al., 2015; Knappett et al., 2016). A better understanding of patterns of fluctuating As concentration with water exchange processes along the hyporheic zone is required to fully evaluate the geochemical controls of As release (Datta et al., 2009; Jung et al., 2015). The release of As by geochemical processes in the Ganges Brahmaputra Meghna River delta has broad implications for groundwater quality, yet little work has been done to understand the fate of As during groundwater discharge and the role of the natural reactive barrier in the affected areas. However, there is a need for a better understanding of the controls of this process of As sorption and release in the HZ and natural reactive barrier may help explain the spatial distribution of As

in shallow groundwater along the Meghna River delta (Harvey et al., 2006; McArthur et al., 2008; van Geen et al., 2008; Datta et al., 2009; Neumann et al., 2010).

This present study has been conducted to understand the potential geochemical controls on As trapping in sediments along the hyporheic zone of the Meghna River in southeast Bangladesh. The setting of this study is a fluvial deltaic environment with a history of elevated groundwater As, in an aquifer with well documented chemistry, hydrology, and sediment geochemistry from pervious studies (Knappett et al., 2014; 2016; Berube et al., In Review). This investigation seeks to demonstrate the role of the natural reactive barrier in relation to Fe and As sorption, Fe reduction and dissolved As mobilization in groundwater. Here we take a multi disciplinary approach using shallow sediment cores, and river water and groundwater samples collected from the east and west banks of the Meghna River to understand the extent of the natural reactive barrier and its possible role in As sequestration and release in groundwater aquifers.

Objectives:

(1) Characterize the groundwater chemistry and organic matter of the aquifers, as they relate to As mobilization. (2) Determine the lateral and temporal extent of the NRB in the HZ at our study site using riverbank sediments within the shallow sediments up to ~2.5 m deep. (3) Identify the geochemical reactions occurring within the natural reactive barrier and investigate how they control As mobility. (4) Determine effects of fluctuations in river water level and groundwater table within the HZ and natural reactive barrier possibly impacting As sequestration and release.

Hypotheses:

(1) The natural reactive barrier is the main control on the distribution of As- and Fe-bearing mineral species in the riverbank sediments up to ~10 m away from the river. (2) River water and groundwater interactions within the NRB impact the sequestration of As within Fe-bearing minerals. (3) Geochemical processes and redox conditions in the natural reactive barrier and the HZ control the release of As from sediments to groundwater. Reductive dissolution is one of the mechanisms driving As release into groundwater. (4) The presence of organic matter in the groundwater may enhance As release into groundwater from sediments through microbially mediated reduction of Fe^{3+} to Fe^{2+}.

CHAPTER 2 - Background

2.1 Arsenic Mobility in Groundwater

Reduced aquifers in Bangladesh and southeast Asia often have high concentrations of mobile, reduced metals such as Fe^{+2} and Mn^{+2} (McArthur et al., 2012). These metals precipitate as oxides when they come into contact with oxygen. As a result, natural reactive barriers consisting of net positively charged Fe^{+3} and Mn^{+4} oxide coatings can form along the interface between groundwater aquifers and the river water they interact with (Datta et al., 2009; Beck et al., 2009; 2010; 2013; Jung et al., 2015). Within these zones, across a range of groundwater pH, oxides can accumulate oxyanions, such as As^{3+}, $H_3AsO_3^0$ and As^{5+}, $H_3AsO_4^-/H_2AsO_4^{2-}$ (Wilkie and Hering, 1998; Dixit and Hering, 2003; Datta et al., 2009).

Arsenic concentrations in sediments have been extensively studied in southeast Asia. Recent studies, including Datta et al. (2009), Jung et al. (2009, 2011, and 2015), have found high concentrations of solid phase As in sediments along the Meghna River in Bangladesh. Stahl et al. (2016), found sediments enriched in As on a point bar along the Red River in Vietnam, and Jung et al. (2009), recorded elevated sediment As and Fe in sediments along a coastal groundwater aquifer.

One key factor leading to As mobilization is thought to be river level fluctuations (Jung et al., 2015). Tidal fluctuations affect river water levels, and impact aqueous and solid-phase geochemistry within the HZ. Periods of high river water level leads to losing river conditions, which enriches O_2 and nutrient concentrations within the aquifer (Wondzell et al., 1996). Periods of low river water level cause reducing groundwater to flow towards the river (Figure 2.1). As a result, toxic As may be removed from the discharged groundwater for an extended time afterwards (Datta et al., 2009; Knappett et al., 2016).

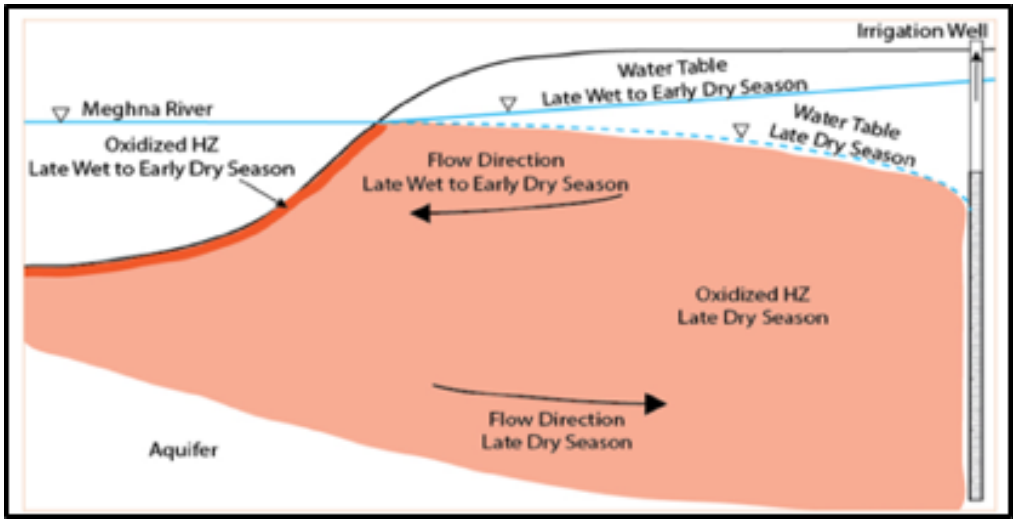

Figure 2.1 Conceptual model of natural reactive barrier, showing seasonal variations caused by fluctuations along the Meghna River (Knappett et al., 2016).

2.2 Organic Matter and Arsenic Release

A number of mechanisms have been reported as processes that contribute to As contamination in groundwater. One of the leading, and widely accepted, mechanisms to date is the reductive dissolution of Fe minerals containing sorbed As (Nickson et al., 1998, 2000; Bhattacharya et al., 2006). Reductive dissolution of Fe-As minerals allows for the release of As into groundwater as Fe^{3+} is reduced to Fe^{2+}. One accepted process leading to Fe mineral reduction is microbially mediated metabolism of organic matter (Chapelle and Lovley, 1992; Lovley, 1996; Nealson, 1997; Nickson et al., 2000; BGS, 2001; Dowling et al., 2002; Ravenscroft et al., 2005; Datta et al., 2011; Sankar, 2013). Recent studies have examined the role of organics, such as anoxic microorganisms and sedimentary carbon, in mediating the process of reductive dissolution. Labile carbon can increase dissolved As concentrations by stimulation of microbially mediated reductive dissolution of Fe minerals (Harvery, 2002; Saunders, 2008).

Organic carbon occurs as a result of decomposition of plant or animal material in soil or water and may dissolve when in contact with water (Soderberg, 2013). Dissolved organic carbon (DOC) concentrations can be influenced by rainfall, runoff and flow path changes which affect DOC production and transportation. Dissolved organic carbon, in combination with other organic compounds involved in most ecological processes, has been referred to as Dissolved Organic Matter (DOM). The biochemical composition of DOM strongly influences its biogeochemical role in freshwater ecosystems (Fellman et al., 2010). The chemical nature of organic matter (OM) has

been investigated intensively, due to its involvement in environmental processes such as the complexation of trace metals (Hering and Kraemer, 1998), binding of organic contaminants (Perminova et al., 1999), and carbon cycling in ecosystems (Stevenson and Cole, 1999; Ohno 2002).

Fluorescence spectroscopy has been used to understand the chemical characteristics of DOC and sources of DOC in natural waters (McKnight et al., 2001). Fluorescence characterization of DOM also provides reliable information about the sources, and biological reactivity of OM (Miller et al., 2009, Mladenov et al., 2010; Fellman et al., 2010). The extent to which microbially mediated release of As occurs is limited by labile DOC availability. The relative importance of DOC sources fueling microbial reduction is debated in the literature. Strong arguments exist for more reactive surface water-derived (Harvey et al., 2006; Neumann et al., 2010; Stahl et al., 2016), and residual buried detrital sources of organic carbon (McArthur et al., 2008). Thus there is a need to characterize DOC and DOM in groundwater as it pertains to As cycling.

2.3 Geochemical Significance of Oxyanions (As) Mobility

Along the Meghna riverbank, As-rich reducing groundwater interacts with oxic river water. During gaining river conditions, the groundwater and river water interact, creating a redox transition zone spanning a wide range of redox conditions within small spatial distances. It is this zone, within the natural reactive barrier, where enrichment of sediment in Fe and As occurs (Datta et al., 2009; Jung et al., 2011; Jung et al., 2015). This study is relevant to As transport in fluvial deltaic environments of southeast Asia where aquifers with elevated As is widespread (Smith et al., 2000). The consumption of groundwater containing hazardous concentrations of As by over 100 million people in southeast Asia has long been recognized as the cause of acute arsenicosis, and other related diseases in the area (Smith et al., 2000; BGS, 2001). The presence of elevated concentrations of As concomitantly in the groundwaters in south and southeast Asia poses serious health concerns for the millions of local inhabitants. Literature has shown that consumption of water-borne As, extracted from contaminated aquifers, is known to cause a variety of neurotoxic effects, arsenicosis and other serious diseases (Smith et al., 2000). Arsenic tainted groundwater is regularly extracted from millions of wells that have been installed in the shallow, unconfined aquifers in Bangladesh (BGS. 2001).

Growing evidence supports the important role of processes in the HZ and the natural reactive barrier in regulating groundwater As (Nagorski et al., 1999; Feris et al., 2004; Nimick et

al., 2005; Jung et al., 2015; Knappett et al., 2016). The release of As by geochemical processes in the Ganges Brahmaputra Meghna River delta has broad implications for groundwater quality, yet little work has been done to understand the fate of As during groundwater discharge and the role of the natural reactive barrier in the affected areas. It has been suggested that tidal fluctuations of the Meghna River can significantly impact As release mechanisms in groundwater. Semi-diurnal tidal fluctuations can influence the river and hyporheic zone up to 400 km north of the southern border with the Bay of Bengal (Knappett et al., 2016). There are a few controls of river water changes including: seasonal monsoons, tides and irrigation pumping (Knappett et al., 2016) along the Meghna River. A better understanding of patterns of fluctuating As concentration with water exchange processes along the hyporheic zone is required to fully evaluate the geochemical controls of As release (Datta et al., 2009; Jung et al., 2015).

CHAPTER 3 - Study Area

3.1 Regional Geology

Bangladesh is a part of the Bengal Basin which is surrounded by the Himalayas to the north, India to the west and the Bay of Bengal to the south. Two major age units have been classified in the basin: the older Pleistocene sediments and the younger Holocene sediments (Morgan and McIntyre, 1959; Mukherjee et al., 2008; McArthur et al., 2008; Datta et al., 2011). These two units have been well defined and extensively studied in Western Bengal, but to a lesser extent in Bangladesh. Three major rivers—Ganges, Brahmaputra and Meghna—drain through the Bengal Basin to the Bay of Bengal (Figure 3.1). Figure 3.1 Ganges-Brahmaputra-Meghna River system catchments draining into the Bay of Bengal (Whitehead et al., 2015). Bangladesh is covered with Quaternary sediments deposited by the Ganges-Brahmaputra-Meghna river system. The sediments are thick, with most areas having a good water-bearing capacity (Rahman, 2013). Alluvial aquifers are the main source of groundwater for the villages in the study area. The aquifers are mostly unconfined to semi-confined, and the unconfined water table occurs at shallow depths 2-5 m below ground surface. Younger alluvial deposition by the Ganges Brahmaputra Meghna River system during the Holocene covers most of these areas. The shallow, younger alluvial sediments deposited during the Holocene are known to be enriched in As at depths less than 60 m in the Bengal Basin, in eastern India and through Bangladesh (McArthur, et al., 2001; Dowling et al., 2002; Datta et al., 2011). Older deposits, below the alluvial deposits, formed during the Pleistocene have been reported as mostly arsenic free. The original source of As in the basin is the As-rich Himalayan rocks, which eroded and transported to the Bengal Basin (Nickson et al., 2000; McArthur, et al., 2001). The sedimentary As accumulated in this fluvial system has formed in the foreland basin of the Himalayan mountain chain (Nickson et al., 2000).

Figure 3.1 Ganges-Brahmaputra-Meghna River system catchments draining into the Bay of Bengal (Whitehead et al., 2015).

3.2 Local Geology

The occurrence, movement and storage of groundwater are governed by the lithology, geological structure, thickness and the depth of occurrence of different geological formations along with the tectonic activities prevailing in the area. As previously mentioned, Bangladesh can be divided into three major physiographic units: the Tertiary hills, the Pleistocene uplands and the Holocene alluvial lowlands. The Pleistocene and Holocene Quaternary sediments are composed of sand, silt and clay. Due to weathering and oxidation processes, the Pleistocene sediment are reddish brown color and contain secondary clays and iron oxides. Since the Pleistocene, the valleys have been filled in with fresher alluvium of mostly greyish color, labelled Holocene sediments. These Holocene sediments were deposited under reducing conditions and contain large amounts of organic matter (Pasupuleti, 2005). The lithology of this study area has been previously studied extensively (Knappett et al., 2016; Shuai et al., 2017; Berube et al., In Review). A vertical division exists between the shallow, gray, reducing, high As, aquifer, and the deeper, orange, low-As aquifers on both side of the river. Knappett et al., 2016, broadly classified based on grain size and color. Three grain size classes were considered: silt or clay, fine-medium sand, and medium-coarse sand. Similarly, two groupings of color were used: gray and brown, yellow or orange. The latter indicates oxidized sand, is often associated with Pleistocene age sediment, and contains low

arsenic groundwater (Horneman et al., 2004; van Geen et al., 2007). Based on available borehole data (Knappett et al., 2014; Knappett et al., 2016) the study area and the adjoining area is divided into four hydro-stratigraphic units. These units, in order of depth, are the upper aquitard, the upper aquifer, the lower aquitard and the lower aquifer. Grain sizes and color were estimated by hand at 1 or 2 ft. intervals for well boreholes on the riverbank on the east side of the Meghna (Shuai et al. 2017) and the top 1-3 m of the riverbank generally contained silt, clay and very find sand. Next, from 2.4 m to 17 m depth, the riverbank aquifer varies from very fine sand to medium-coarse sand. Sands are grey in color, and quartz components of sands were relatively well sorted (Berube et al., In Review). Figure 3.2 shows the sediment types with depth at the study site on the east and west riverbank, in relation to some of the groundwater sample well locations. It is important to note that more water samples were collected from the east side which are not shown in this profile, the purpose of this image is just to get an overall sense of the depths and locations of some of the tubewells samples.

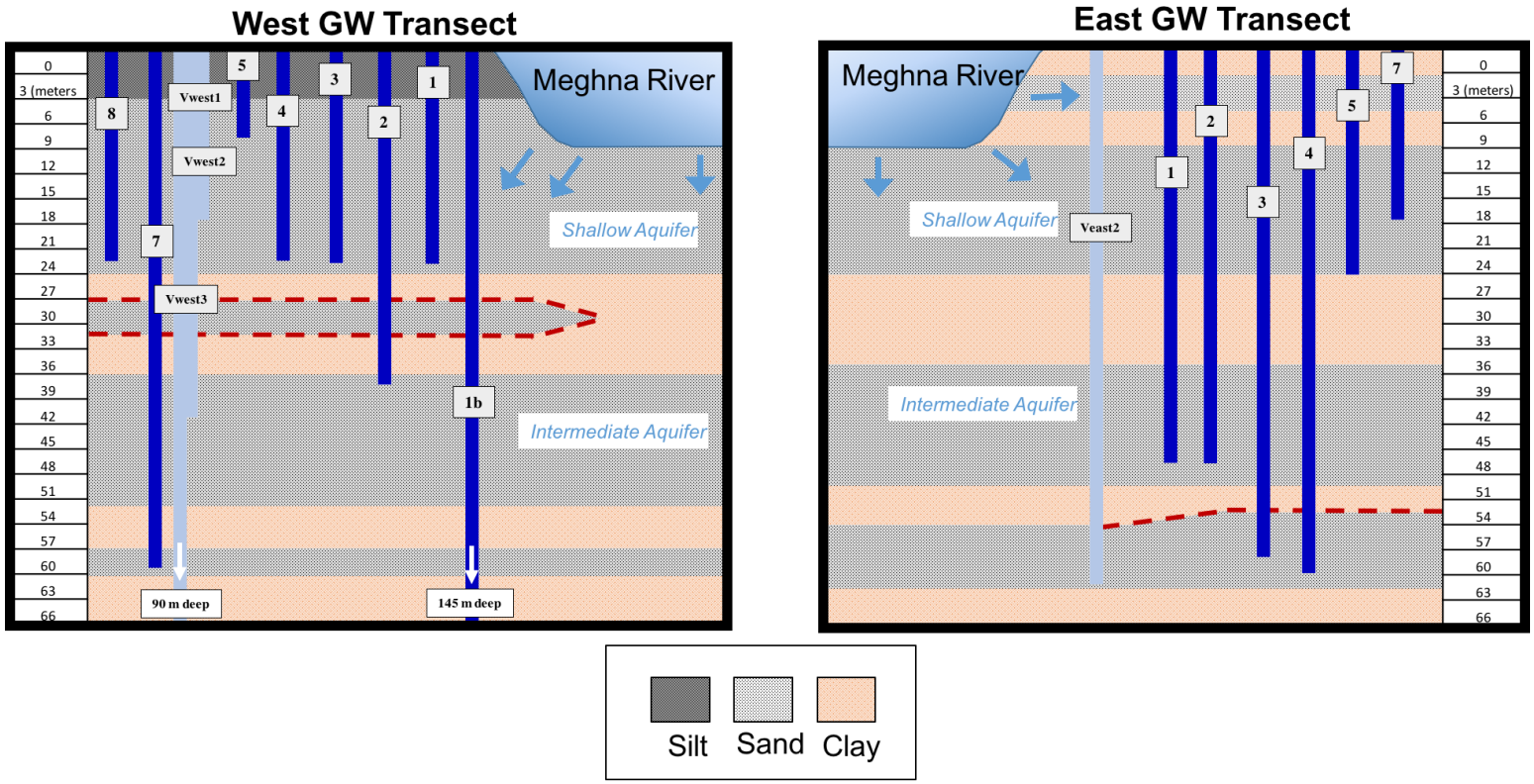

Figure 3.2 This diagram shows a schematic view and vertical profile of the sediment types at the study transects along the Meghna River on the east and west river banks.

3.3 Study Location

The groundwater table reaches its maximum level during the monsoon period (June-October) and its minimum level during the dry season (November-May) (Pasupuleti, 2005). The Meghna River watershed includes the Meghalaya and Assam Hills of India in the North, which represent the wettest place in the world, receiving ~14 meters of rainfall a year. Bangladesh receives the majority of its rainfall during the monsoon season (June-October) (Hossain and Siddique, 2015). Down-gradient, the Meghna River floodplain consists of a low-lying landscape of meandering channels, meander scrolls, and natural levees formed by the river and its tributaries (Hossain and Siddique, 2015). Surficial sediments in the region are Holocene-aged deposits consisting of mica-rich sand, silt, and clays (Weinmann et al., 2008). This research was conducted along a relatively straight 4-km reach of the Meghna River, located in central Bangladesh approximately 35 km east of Dhaka (Figure 3.3). The Meghna merges with the Ganges and Brahmaputra Rivers ~20 km south of the study site. The area of study is densely populated rural villages, two on the east bank of the river (Ulukandi and Baherchar) and one unnamed village on the west bank of the river (located northeast of Nainabad). The study area spans a distance of about 4 km north and south along the edge of the river and covers about 1 km inland to towards villages on the east and west banks of the river (Figure 3.3). Figure 3.3 (b) shows the area of Bangladesh that was sampled and (c) shows a more detailed map of the study site, with the location of sediment samples and the groundwater transects wells on the east and west riverbanks. Field work was performed in Jan. 2016, during the dry season in Bangladesh.

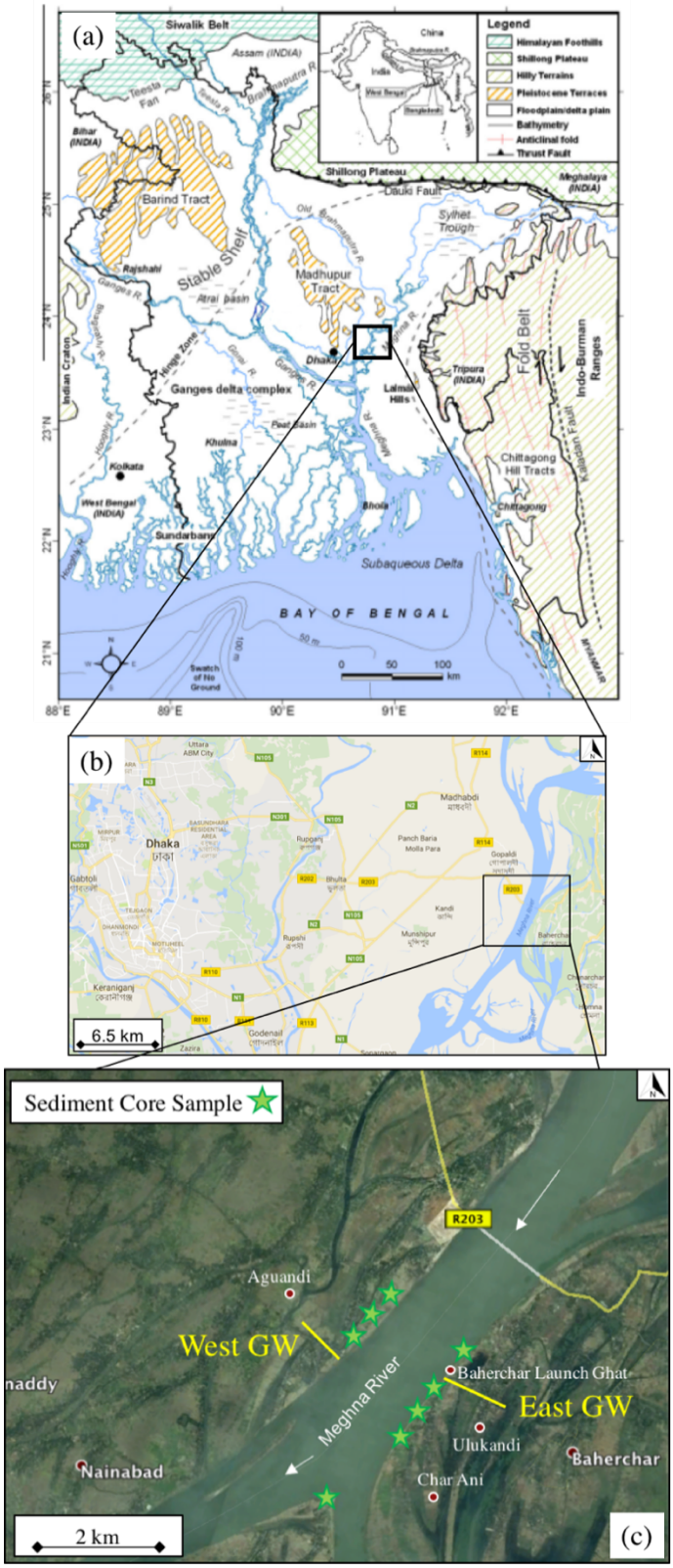

Figure 3.3 Map of study locations (a) geologic map of Bangladesh (b) study site in relation to Dhaka, the capital city of Bangladesh (c) study site with locations of groundwater transects and sediment core samples.

CHAPTER 4 - Methods

4.1 Well Sampling and Aqueous Field Measurements

In total 34 groundwater samples and five river water samples were collected along the east and west sides of the Meghna River (Figure 4.1). The well locations were selected based on proximity to the river along two transects perpendicular to the river on the east and west, and the ease of access to the tube wells.

4.1.1 Well Sampling Methods

A transect of 15 wells, (seven east and eight west) running perpendicular to the river on the east and west sides (Figure 4.1 a, b), was chosen for groundwater sampling. These are labeled TWeast or TWwest, respectively (Figure 4.1). In addition, four groundwater samples were taken from previously installed monitoring wells (Knappett et al., 2016): one from the east bank labeled Veast2 and three from the west bank labeled Vwest1, 2, and 3. Vwest1, 2, and 3 are located ~200 m northeast of the West GW Transect, Veast 2 is located in line with the East GW transect Figure 4.2 shows a schematic view and vertical profile of the groundwater transects on the east and west banks. The reason the groundwater was sampled along a transect perpendicular to the river is because the HZ and natural reactive barrier extend laterally from the river, so the water samples must be taken from this zone specifically. In addition to the transect wells, 15 other groundwater samples were collected from the village of Baherchar, on the east bank. This is an area where As concentrations had never been measured before. These well sites were selected along a transect running semi-parallel to the river on the east side, based on access to the tube wells and proximity to the original perpendicular groundwater transect (Figure 4.3). Figure 4.3 shows the locations of these additional 15 groundwater samples, labeled BA1-15 for Baherchar. Overall, groundwater samples were collected from a variety of well depths; shallow wells are considered <30 m, and deep wells are considered >30 m. In the results and discussion sections, groundwater characterization was completed based on these distinctions of shallow (<30 m) and deep (>30 m).

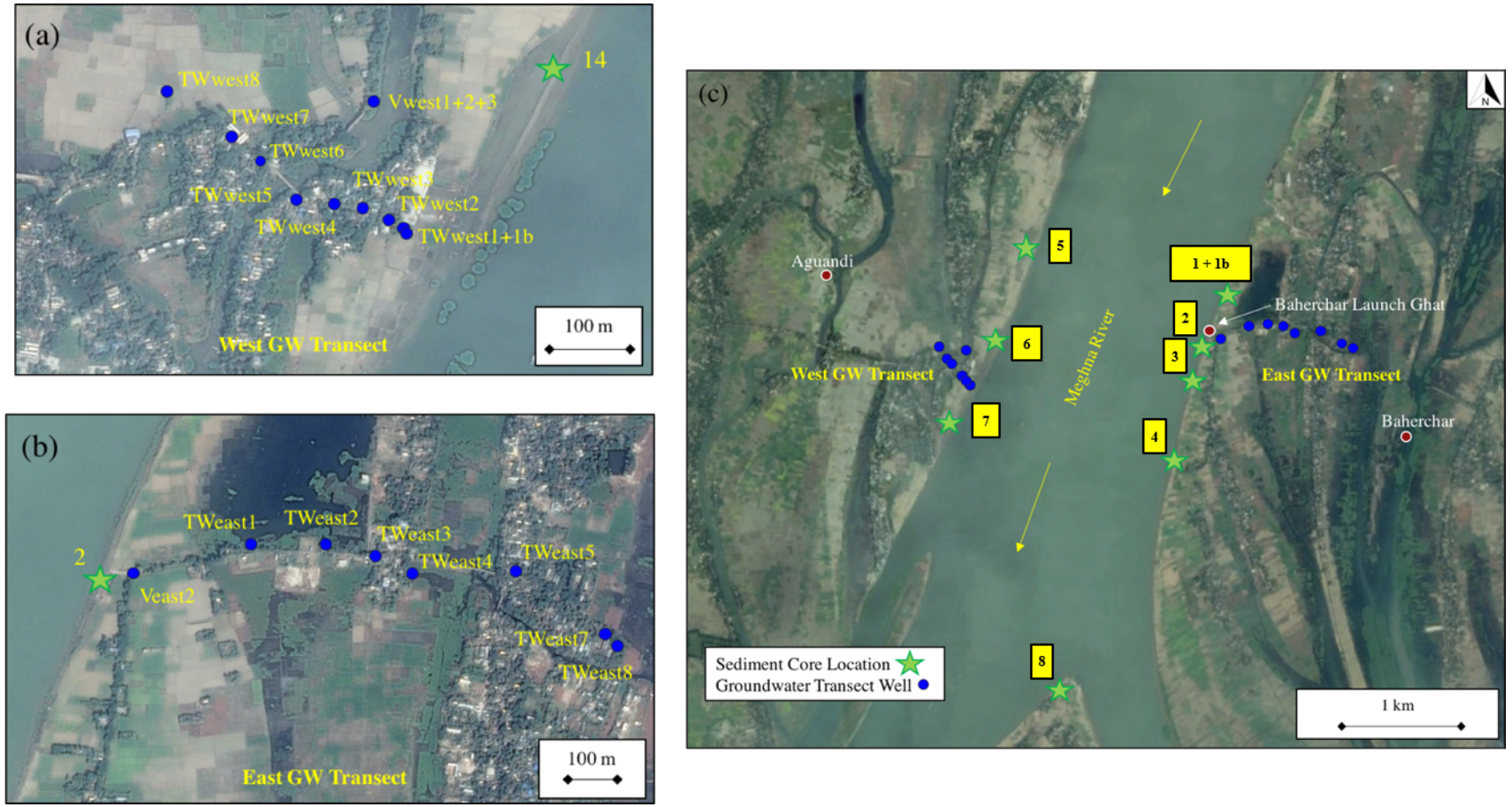

Figure 4.1 Water sampling sites (a) West GW transect (b) East GW transect (c) study location overview with groundwater and sediment core locations.

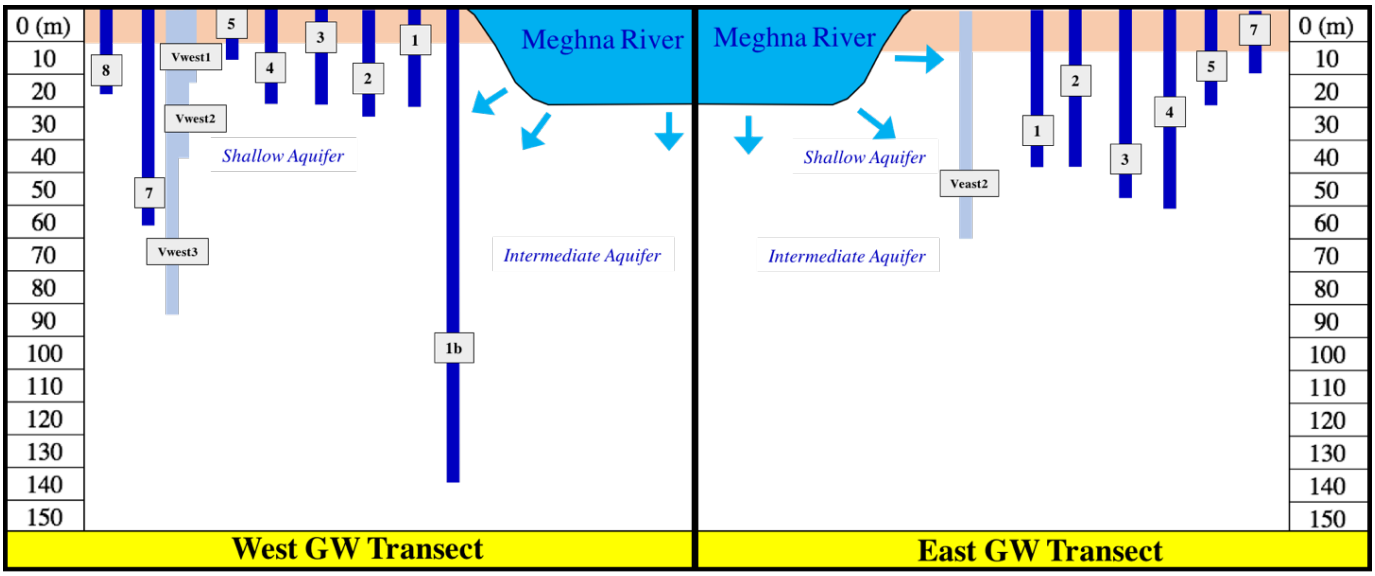

Figure 4.2 Conceptual vertical profile of groundwater samples from the East and West groundwater transects. Dark blue wells are private tubewells (East and West), light gray wells are monitoring wells (Veast and Vwest) (not to horizontal scale).

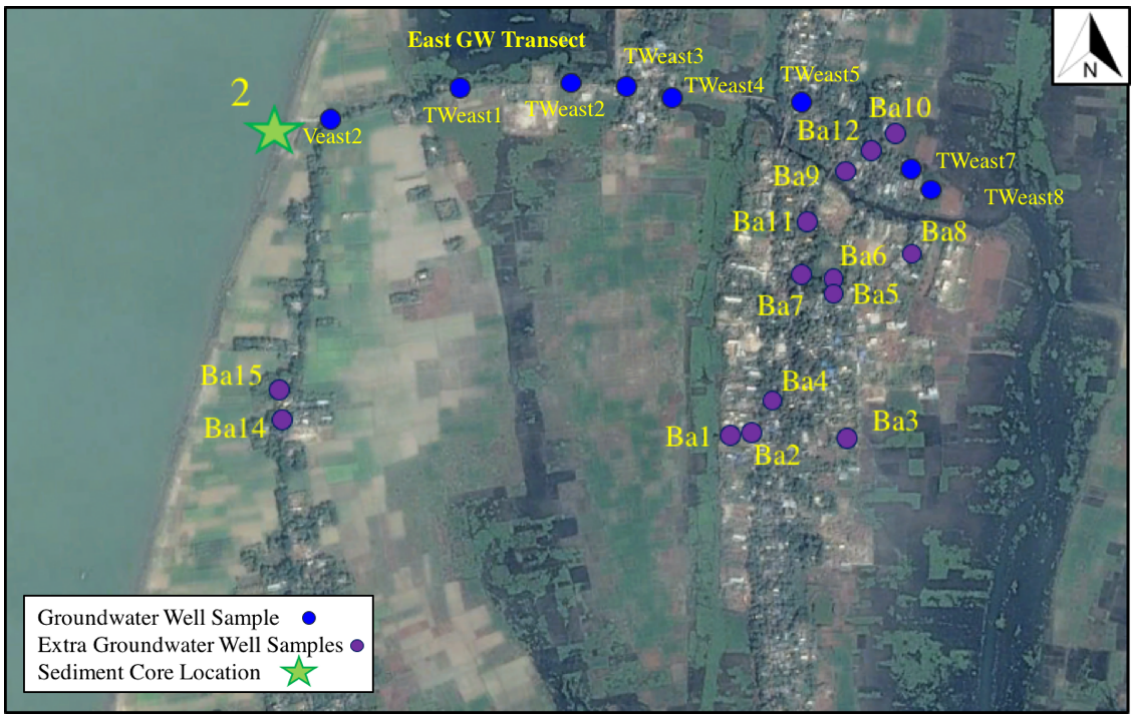

Figure 4.3 Groundwater samples sites on the east bank: East GW Transect (blue) and additional wells (BA 1-15) not located along the transect (purple).

4.1.2 Field Measurements

Physical and chemical parameters were measured on groundwater wells including temperature pH, oxidation-reduction potential (ORP), and specific conductance were obtained using a calibrated YSI Professional Plus multimeter (YSI Inc., Yellow Springs, OH). Each monitoring well (Veast and Vwest) was purged for at least 15 minutes at a flow rate of 4-6 L/min using a submersible pump (Typhoon DTW 50ft, Groundwater Essentials, Bradenton, FL). Samples were taken only when pH, ORP, specific conductance and temperature stabilized for three or more consecutive readings. The private hand pump tube wells were pumped for approximately 15 minutes and also sampled after the above parameters stabilized. For the hand pumped wells the following additional parameters were monitored: alkalinity, dissolved oxygen (DO), NO_3^-, NO_2^-, NH_3, PO_4^{3-}, SO_4^2, dissolved As_T, dissolved Mn_T, dissolved Fe_T, Cl^-, S^{2-}, and dissolved SiO_2. Total As was measured using EZ Arsenic Test Kit (HACH Cat. No. 28228-00) and Arsenic Test Kit (HACH Cat. No 2800000). Dissolved Fe_T, and DO were measured using CHEMetrics test kits (CHEMetrics, Inc., Midland, VA). Dissolved Mn_T, S^{2-}, PO_4^{3-}, Cl^- and dissolved SiO_2, were measured using a V-2000 Multi-Analyte Photometer (CHEMetrics, Inc.). A HACH 1900 Portable Spectrophotometer (HACH Company, Loveland, CO) was used to measure NO_3^-, NO_2^-, and NH_3. Pocket Colorimeter II (HACH, Cat. No. 58700-29) was used to measure SO_4^2. The additional 15 hand pump tube wells on the east bank were each purged for ~15 minutes, but only As_T was measured in the field, due to time constraints. Groundwater samples were collected from each well for laboratory analysis of anions and cations, stable isotopes (δ^2H, $\delta^{18}O$), and dissolved organic matter characterization.

4.2 Aqueous-Phase Laboratory Analyses

4.2.1 Anions and Cations (IC)

Groundwater samples were collected in new plastic bottles pre-rinsed three times with the sample water. Filtered and un-acidified samples were used for the analysis of anions (Cl^-, Br^-, F^-, SO_4^{2-}, NO_3^-, NO_2^- and PO_4^{3-}). For cation analysis samples were filtered using a 0.45 μm nitrocellulose membrane filter (Millipore Millex- HP) and acidified in the field using Optima Grade HNO_3 (0.2% v/v) for the analysis of cations (Ca^{2+}, K^+, Na^+, NH_4^+ Mg^{2+}) by Ion Chromatography (IC). Ion analysis in the lab was performed with by IC at the Department of Geology in Kansas State University.

4.2.2 δ^2H and $\delta^{18}O$ Stable Isotopes

Un-filtered, un-acidified water samples were collected in glass vials for isotope analysis. The stable isotopes (δ^2H, $\delta^{18}O$) of all the groundwater samples were measured using PICARRO Cavity Ring Down Spectrometer (L1102-I, Santa Clara, CA, USA) in the Department of Biology at Kansas State University.

4.2.3 TOC, DOC and DOM

To analyze water samples for total dissolved carbon (TOC) analysis, water samples were filtered through a 0.45 μm hydrophilic polyether sulfone millipore syringe filter and stored in 60 ml clear glass bottles. These were acidified in the field with 0.12 ml of Optima grade HCl. Total organic carbon concentration was determined using a TOC-5000 analyzer (Department of Civil Engineering, Kansas State University), with a confidence interval of ± 0.02 mg Carbon (C)/L (as described in Kulkarni, 2016) Absorbance and fluorescence spectral characterization of DOM was performed on filtered (0.7 μm glass fiber filters) and un-acidified samples (Horiba Aqualog Benchtop Fluorometer, Department of Engineering, Kansas State University). The protocol for absorbance fluorescence spectroscopy is as follows:

- The fluorometer lamp of the instrument was allowed for approximately 45 minutes to warm up and the quartz cuvette was rinsed ~20 times with distilled water before testing all samples
- All the sides of 3-Q-10 sealed water sample and starna quinine sulfate sample were cleaned to remove dust around the cuvette prior to test each sample
- The cuvette was checked for any peaks between emission 300 and 400 nm (not noise) and the highest peak was recorded between emission 300 and 400 nm in the Aqualog logbook.xls
- The water Raman scan was checked to record the Raman peak at ~397 nm (Raman peak X and Y) in the Aqualog logbook.xls and the area under the Raman peak was calculated
- An ultra-pure water sample was run first to check for any contamination on the cuvette. Then to acquisition 3D EEM, all samples were run three times to cross match the results
- All Aqualog fluorescence raw data were exported as ASCII file format and corrected using MATLAB (Kulkarni, 2016) to correct excitation emission matrices and calculate indices

Instrumental parameters, spectral corrections, normalization, and blank subtraction post-processing, methods to compute absorbance and fluorescence indices, were the same as described in Kulkarni (2016), and were completed by Harshad Kulkarni (Kansas State Engineering PHD).

4.3 Shallow Riverbank Sediment Coring

Eight sediment cores were collected from the riverbank of the Meghna River. Five cores were located on the east bank (Cores 1, 1b, 2, 3 and 4), three cores on the west bank (Cores 5, 6 and 7), and one core was taken from a southern mid channel bar (Core 8). Figure 4.4 shows the relative location and distances between each core on the east and west banks. On the east bank, in order of location from north to south, Core 1, the deepest of the cores, was collected to a depth of ~244 cm and samples were collected at intervals of 0-60 cm, 60-122 cm, 122-183 cm, and 183-244 cm. Core 1b, taken ~10 m west of Core 1, the only riverbed core was collected to a depth of ~122 cm at intervals of 0-60 cm and 60-122 cm. Core 2, Core 3, and Core 4, located farther south, in consecutive order, and were each collected to a depth of ~122 cm at intervals of 0-60 cm and 60-122 cm (Figure 4.5b).

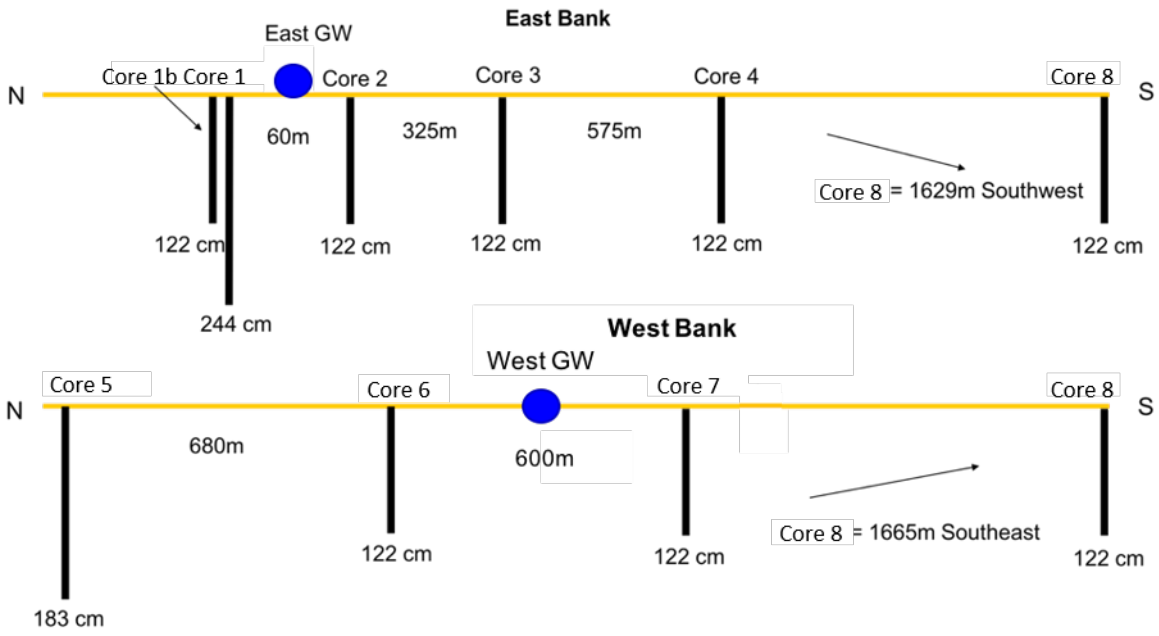

Figure 4.4 Relative location and depth (m) of each sediment core on the east and west riverbanks.

On the west bank, in order of location from north to south, Core 5 the second deepest core, was collected to a depth of ~183 cm and samples were collected at intervals of 0-60 cm, 60-122 cm, and 122-183 cm. Farther south were Core 6 and Core 7; each were collected to a depth of ~122 cm at intervals of 0-60 cm and 60-122 cm (Figure 4.5b). Core 8, the only island core, was located on the western side of the large mid channel bar at the southern point of the study are (Figure 4.5b). Core 8 was collected to depth of ~122 cm at intervals of 0-60 cm and 60-122 cm.

Sediment cores were collected using a hand auger core collector into clear PVC tubes (Figure 4.4 c, d) to obtain relatively undisturbed samples. In the field each interval of sediment extracted was labeled T and B, indicating the top of the core and bottom of the core, respectively. Hand augured cores were flushed with nitrogen and stored on ice at 4 °C until transport. Upon arrival at Kansas State University the cores were frozen until analysis at the Department of Geology, Kansas State University.

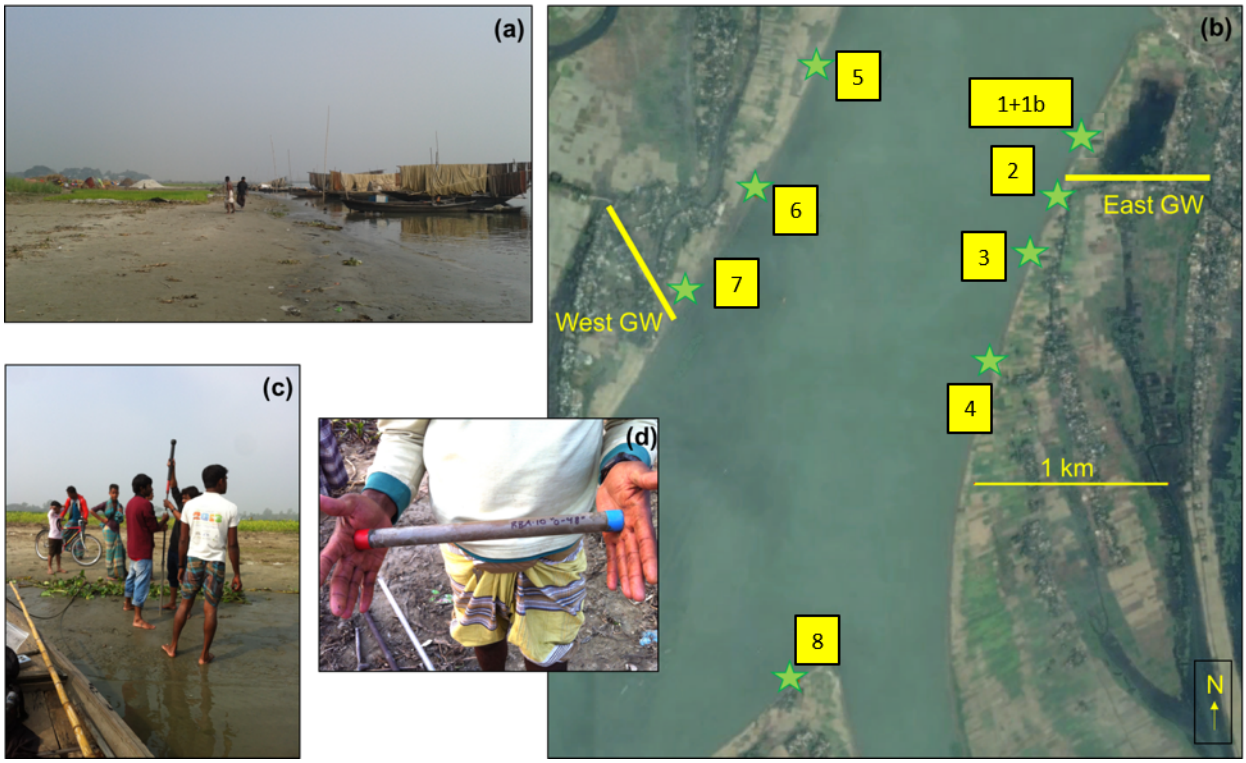

Figure 4.5 (a) Example site of sediment core location, (b) overview of all sediment site locations, (c) hand auger sediment sampling process, and (d) core sample example.

4.3 Sediment Characterization and Analytical Methods

4.3.1 Shallow Sediment Core Analysis Preparation

Prior to analysis, sediment cores were thawed within an anaerobic chamber. Approximately 4 cm of sediment was removed from the top and bottom of each core, labeled T and B, respectively. The 4 cm of sediment from each core was used for all analyses. Samples were then dried for 48 h in the anaerobic chamber and preserved in O_2-impermeable Remel® bags (Mitsubishi Gas Company, Remel®, Cat no. 2019-11-02), along with O_2 absorber pouches (Mitsubishi Gas Company, AnaeroPouch® Anaero; Cat no. 23-246-379).

Sediment samples were analyzed for grain size distribution using a Malvern Mastersizer 3000 laser diffraction particle size analyzer, mineralogical composition by X-Ray Diffraction (XRD) (PANanalytical Empyrean, Cat no. 205069), and element abundances by handheld X-Ray Fluorescence (XRF) (Bruker Tracer III- SD, Cat no. T3S2778). In addition, three individual leaching extractions were performed on the sediments: aquaregia (1:3, HNO_3: HCl), 1.2 M HCl, and 1 M sodium phosphate (NaH_2PO_4), following the procedure in Datta et al., 2009.

4.3.2 Particle Size Analysis

Particle size analysis (PSA) was performed using a Malvern Mastersizer 3000 laser diffraction particle size analyzer with a Hydro EV wet dispersion accessory. Prior to analysis the samples were pretreated with hydrogen peroxide to remove any organic material that could cause clumping. Approximately 0.5 g of dried sample was put into a 50 mL centrifuge tube with 1 ml 30% hydrogen peroxide and 5 ml deionized water. Tubes were left to react for ~5 minutes, and were then filled up to 30 mL with deionized (DI) water. The tubes were then placed in an 80°C water bath, for ~12 hr. Samples were removed and cooled to room temperature, then washed (2x) with DI water and centrifuged at 6000 rpm for 2 min, after which the supernatant liquid was decentered. After the final round of washing, DI water was added to the tubes to return the volume to 30 ml. For the particle size analysis using the Mastersizer, the propeller on the wet dispersion accessory was set for 1500rpm. The tubes were shaken for 15 seconds to ensure a representative sample was taken, then a pipette was used to extract a 1-2 ml sample, which was analyzed by the Mastersizer. Particle size data are originally reported as "% by volume" by the Mastersizer software and then converted to "% finer than" for final reported values (Appendix E). The USDA grain size chart shows diameters of sediment sizes for sand, silt, and clay as greater than 50 μm, between 50 and 2 μm, and less than 2 μm, respectively (USDA). However, due to the method of particle size analysis (Laser Particle Siser), the sizes of sand and clay were modified to between 50 and 8 μm for sand and >8 μm for clay (Konert and Vandenberghe, 1997). Grain size fraction for clay, silt and sand is; clay < 8 μm, 8 μm < silt < 63 μm, and sand > 63 μm, respectively (Konert and Vandenberghe, 1997).

4.3.3 X-Ray Powder Diffraction Analysis

X-Ray Diffraction (XRD) analysis was conducted to determine the bulk mineral composition of the sediments. XRD analyses were conducted using a PANalytical Empyrean X-Ray Diffractometer, using a PIXcel 3D scanning line detector. X-rays were generated with a Cu

tube and Ni-filter at a setting of 45 kV, 40 mA through a rage of 2.5°-70° (2θ). Approximately 3-4 g of the air-dried sediment was homogenized to a fine powder with an agate mortar and pestle. The sediment was then frontloaded and packed firmly into a 27 mm sample holder mounted into a spinning sample stage and rotated at 4 rpm. Peak data for each sample were analyzed using HighScore Plus® software and compared to International Center for Diffraction Data (ICDD) reference data cards to determine the mineralogy of the sample. A mineral was included in sample when the top three to four most intense peaks, as determined by I/I_0 on the ICDD reference card, matched peaks in the sample XRD spectra (Appendix F). All software generated matches were manually verified before a mineral was included in the sample assemblage.

4.3.4 Bulk Sediment X-Ray Fluorescence Analysis

X-Ray Fluorescence (XRF) analysis was conducted to determine the bulk elemental composition of the sediments using a Bruker Tracer III Handheld XRF. This was determined using the Bruker mudrock calibration (Rowe, 2012), which was refined with the addition of chemical data from shale samples located in Kansas and Oklahoma (Rowe, per coms, 2015). The same sediment fraction that was analyzed for XRD was analyzed for XRF. Samples were prepared by grinding ~3-4 g to a fine powder (~50 μm) using an agate mortar and pestle, and put into small plastic Chemex® XRF sample cups. One end of the cup was covered with a plastic cap and the other end was covered with 4μm thick Prolene® film. Each sample was analyzed for trace elements (Co, Ni, Cu, Zn, Ga, As, Rb, Sr, Y, Zr, Nb, Mo, Ba, Pb, Th and U) and major elements (Mg, Al, Si, P, S, K, Ca, Ti, V, Cr, Mn and Fe). Each sample was analyzed 6 times for major and trace elements. The sample cups were shaken and tapped on the counter to compact the sediment and to ensure homogenization between each analyses.

Trace elements were analyzed with the following settings and procedure:

- Yellow filter (12 mil Al + 1 mil Ti)
- 40kV and 12.4μA for 120 seconds

Major elements were analyzed with the following settings and procedure:

- No filter
- 15kV and 25μA for 180 seconds
- Vacuum pump was attached to create a vacuum in the interior of the gun. This improves the intensity of the analysis for lighter mass elements

The mudrock calibration converts the photon intensity peaks generated from the XRF to elemental concentration data. Concentrations are originally reported in weight percent then converted to mg/kg. Only the Fe, Mn, and As concentrations were used for this study, but the results for all major and trace element concentrations are recorded in the Appendix. The 6 values for each sample were averaged, high and low values and standard deviation was recorded in the Appendix. Standard RTC-WS-220 (Rowe, 2012) was analyzed between every five or six samples to ensure quality control.

4.3.5 Chemical Extractions

4.3.5.1 Aquaregia Extraction

The procedure used for these analyses is the standard aquaregia chemical extraction procedure used at the Soil Chemistry Testing Laboratory of the Agronomy Department at Kansas State University, which has been adapted from the Soil Science Society of America Soil Testing Manual.

Iron, Mn, and As concentrations in sediments were acquired through aquaregia digestion. About 0.5 g of finely homogenized (< 2 mm) sediments were placed in glass digestion tubes with. The mass was recorded to 2 significant digits for dilution calculations completed after ICP-OES analysis. Freshly aquaregia (1:3, HNO_3: HCl) (Assay 67-70% HNO_s, Optima grade and Assay 32-35% HCl, Fisher Chemical, Optima grade) was prepared and 5 mL was added to each glass digestion tube containing sediment, and left to equilibrate overnight for 12 hours in a fume hood. Samples were each vortexed for ~2 minutes the following morning then placed in the digestion heating block. The samples were heated to 75˚C (30 min), 90˚C (30 min), 110˚C (30 min) and then to 140˚C until the total volume was reduced to ~1 ml. The time for the last step varied for each tube. As they approached the 1mL mark, tubes were closely watched so as not to overshoot this mark and dry out. Between each 30-minute increment samples were vortexed for 30 seconds to ensure the sample reacted entirely with aquaregia acid. Once the solution was reduced to ~1 ml, samples were allowed to cool to room temperature. Each tube was then diluted to 25 ml using 0.1 % HNO_3 (Optima grade), vortexed to ensure mixing, and then filtered through 2.5 μm (Whatman 42) filter paper into clean Falcon® tubes and refrigerated at 5°C until the time of analysis. Inductively Coupled Plasma Optical Emission Spectroscopy (ICP-OES) analysis was conducted on the filtered solution to more accurately quantify the concentrations of certain elements present in the selected sediment samples.

Analyses were conducted with a Varian 720-ES Inductively Coupled Plasma-Optical Emission Spectrometer. Samples were grouped into two suits based on dilution necessary to fall within the maximum detection limits of the instrument. Five multi-element standards of varying concentrations were custom made for each suite with standard stock solution of Fe, Mn, and As using the sample addition method. During analysis, 2 samples were randomly selected for a duplicate measurement and 2 more samples were spiked with a known amount of one of standard so that quality control could be constrained (Appendix K). Only 3 out of the 8 sediment samples were analyzed for Aquaregia digestion due to time constraints.

4.3.5.2 HCl Extractions

Iron, Mn, and As concentrations in sediments were acquired through HCl extractions. Sediment samples were leached with a 1.2 M HCl solution (OPTIMA Grade, Fisher Chemical), designed to extract As co-precipitated with acid volatile sulfides, carbonate minerals, manganese oxides, and readily reactive iron oxyhydroxides (Datta et al., 2009). About 0.5 g of finely homogenized (< 2 mm) sediment was placed in a 15 ml clean Falcon® tube with 10 ml of 1.2 M Optima Grade HCl (Fisher Chemical). The clean Falcon® tubes were then shaken for 20 hrs. at room temperature. Following the shaking tubes were centrifuged for 10 minutes, and filtered through 2.5 μm through Whatman No. 42 filter paper into clean Falcon® tubes. Samples were refrigerated at 5°C until the time of analysis, for As_T, Fe_T, and Mn_T. Analyses were conducted with a Varian 720-ES Inductively Coupled Plasma-Optical Emission Spectrometer, following the same procedure as observed in the aquaregia extractions. Samples were grouped into two suits based on dilution necessary to fall within the maximum detection limits of the instrument. During analysis, 2 samples were randomly selected for a duplicate measurement and 2 more samples were spiked with a known amount of one of standard so that quality control could be constrained (Appendix K). All 8 of the sediment samples were analyzed for the HCl extractions.

4.3.5.3 Phosphate Extractions

Iron, Mn, and As concentrations in sediments were acquired through phosphate extractions. Sediment samples were leached with a 1 M sodium phosphate (NaH_2PO_4) solution to extract more labile phosphate-mobilizable As (Datta et al., 2009). Phosphate-mobilizable As was extracted using a 1 M sodium phosphate solution with 0.1 M L-ascorbic acid, adjusted to pH 5 using ~30 NaOH pellets (Datta et al 2009). The phosphate solution was purged with N_2 for 30 minutes with nitrogen to remove dissolved oxygen. A separate fraction of sediments (not the same as HCl or

aquaregia extractions) of ~ 0.5 g of sediment, stored under anaerobic conditions, was placed in a clear glass serum vial in a nitrogen-filled glove bag. 10 ml of the 1 M phosphate solution was added to each vial. The serum vial was crimp sealed and wrapped with aluminum foil. Samples were shaken for 24 hrs. at room temperature. The solution was then filtered through 2.5 μm through Whatman No. 42 filter paper into clean glass vials, under anaerobic conditions, and resealed. Samples were refrigerated at 5°C until the time of analysis, for As_T, Fe_T, and Mn_T. Analyses were conducted with a Varian 720-ES Inductively Coupled Plasma-Optical Emission Spectrometer, following the same procedure as observed in the aquaregia and HCl extractions. Samples were grouped into two suits based on dilution necessary to fall within the maximum detection limits of the instrument. During analysis, 2 samples were randomly selected for a duplicate measurement and 2 more samples were spiked with a known amount of one of standard so that quality control could be constrained. All 8 of the sediment samples were analyzed for the phosphate extractions.

CHAPTER 5 - Results

5.1 Aquifer Characterization

5.1.1 Field Measurements

Groundwater parameters were measured in the field, including temperature (°C), specific conductance (us/cm), pH, Oxidation- Reduction Potential (ORP) (mV), dissolved oxygen (DO) (mg/L), and Alkalinity (mg/L). Groundwater temperature did not very significantly with depth or distance from the river. Groundwater temperature ranged from 24.5 to 27 °C. Conductivity did vary significantly with depth or distance from the river, these values ranged from 1,124 to 3,820 us/cm. The pH of groundwater samples ranged from 6.5 to 7.1, and did not vary with depth or distance from the river. ORP provides information on the state of the groundwater, reduced or oxidized. ORP values ranged from -185 to 201 mV. Negative ORP was seen at shallow groundwater (<30 m); less negative, and in some cases positive, ORP was seen in deep groundwater (>30 m). Groundwater samples were measured for, NO_3^-, NO_2^-, NH_3, PO_4^{3-}, SO_4^2, dissolved As_T, dissolved Mn_T, dissolved Fe_T, Cl^-, S^{2-}, and dissolved SiO_2. All results from field measurements can be found in the Appendix. In the field river water samples were analyzed for temperature (°C), specific conductivity (μs/cm), and pH. Average temperature was 26.2°C, average conductivity was 77.8 us/cm and average pH was 7.0.

5.2 Aqueous-Phase Chemistry

5.2.1 Water Chemistry

The following ions were all determined by Ion Chromatography at KSU, with the exception of S^{2-}, which was measured in the field. There were seven private tube wells from the east bank and eight private tube wells from the west bank. The TW in each well name stands for transect well (TW). One monitoring well was sampled from the east bank (Veast2), and three monitoring wells were sampled from the west bank (Vwest1, Vwest2, and Vwest3). The lithology of the aquifers was used to determine the difference between shallow and deep aquifers. The shallow groundwater wells were considered to be those <30 m deep; deep groundwater wells are those >30 m, because this is the middle of the clay layer that divides the two aquifers.

5.2.2 Anions

The highest concentrations of NO_3^-, NO_2^-, PO_4^{3-}, and SO_4^{2-} were found at shallow wells (<30 m), and highest concentrations of Br^-, and Cl^- were found at the transition between shallow to deep groundwater at ~ 30 m. There were no significant trends with depth for F^- and S^{2-}.

Almost all of the groundwater samples contained NO_3^- concentration of >0.5 mg/L. Nitrate concentrations ranged from ~0 to 3.4 mg/L, with the minimum and maximum observed at TWwest1b (~146 m) and TWeast7 (~16 m), respectively. Shallow wells (<30 m) had the highest concentrations of NO_3^-, >2 mg/L (TWwest2, TWwest3, TWwest4, TWeast5, TWeast7). The lowest concentrations of NO_3^- (0 – 1.5 mg/L) were found at well depths greater than 50 m (Figure 5.1), and the very deepest wells (>80 m) had little to no NO_3^-. Excluding those analyses that are below detection limits, NO_2^- concentrations in the 4 samples above the detection limit ranged from 0.8 to 1.4 mg/L, with minimum and maximum at TWwest4 (~27 m) and TWwest7 (~64 m), respectively (Figure 5.1). Ten out of the eighteen groundwater samples reported PO_4^{3-} below detection or ~0 mg/L. Not taking those BDL into account, PO_4^{3-} concentrations in the 10 samples about detection limit ranged from 0.08 to 0.33 mg/L, with minimum and maximum observed at TWwest2 (~34 m) and TWwest1 (~27 m), respectively. Sulfate concentrations ranged from ~0.9 to 56 mg/L, with minimum and maximum observed at Vwest1 (~28 m) and TWeast5 (~27 m), respectively (Figure 5.1). Highest concentrations of NO_3^-, NO_2^-, PO_4^{3-}, and SO_4^{2-} were found at shallow depths (<30 m) (Figure 5.1).

Chloride concentrations ranged from ~13 to 475 mg/L, with the minimum and maximum observed at TWwest8 (~25 m) and TWeast4 (~61 m), respectively. Bromide concentrations ranged from ~0.09 to 1.9 mg/L, with the minimum and maximum observed at TWwest1 (~27 m) and TWeast4 (~61 m), respectively (Figure 5.1).

No significant trends with depth were observed for F^- or S^{2-}. Fluoride concentrations ranged from 0.1 to 0.9 mg/L with minima and maxima observed at TWest2 (~34 m) and Vwest3 (~92 m), respectively. Sulfide concentrations (measured in the field), ranged from 0.02 to 0.5 mg/L (not including the three wells with S^{2-} BDL). The minimum and maximum S^{2-} concentrations were observed at TWeast1 (~52 m) and TWwest5 (~18 m), respectively.

Table 5.A Range of anion concentrations in groundwater

Anion	Range (mg/L)	Range (mmol/L)	Anion	Range (mg/L)	Range (mmol/L)
F^-	0.13 - 0.92	7.0 – 48.50	NO_3^-	0 - 3.37	0 – 544.0
Cl^-	12.87 - 475.26	358.0 – 13410.0	PO_4^{3-}	0 - 0.33	0 – 0.17
NO_2^-	0 - 1.39	0 – 30.0	SO_4^{2-}	0.915 - 55.93	0.45 – 27.30
Br^-	0.09 - 1.89	1.0 – 23.70	S^{2-}	0 - 0.48	0 – 15.0

Table 5.B Statistical analyses of anion concentration for groundwater (mg/L)

	F^-			Cl^-		
	n	Avg.	Stdev.	n	Avg.	Stdev.
Shallow GW (<30 m)	8	0.24	0.15	8	133.89	92.32
Deep GW (>30 m)	10	0.46	0.23	10	211.06	188.33
	NO_3^-			PO_4^{3-}		
	n	Avg.	Stdev.	n	Avg.	Stdev.
Shallow GW (<30 m)	8	0.31	0.42	8	0.18	0.13
Deep GW (>30 m)	10	0.14	0.44	10	0.04	0.05
	NO_2^-			Br^-		
	n	Avg.	Stdev.	n	Avg.	Stdev.
Shallow GW (<30 m)	8	2.25	0.57	8	0.23	0.08
Deep GW (>30 m)	10	0.96	0.84	10	0.88	0.73
	SO_4^{2-}			S^{2-}		
	n	Avg.	Stdev.	n	Avg.	Stdev.
Shallow GW (<30 m)	8	11.72	18.54	8	0.18	0.16
Deep GW (>30 m)	10	2.40	2.98	10	0.08	0.07

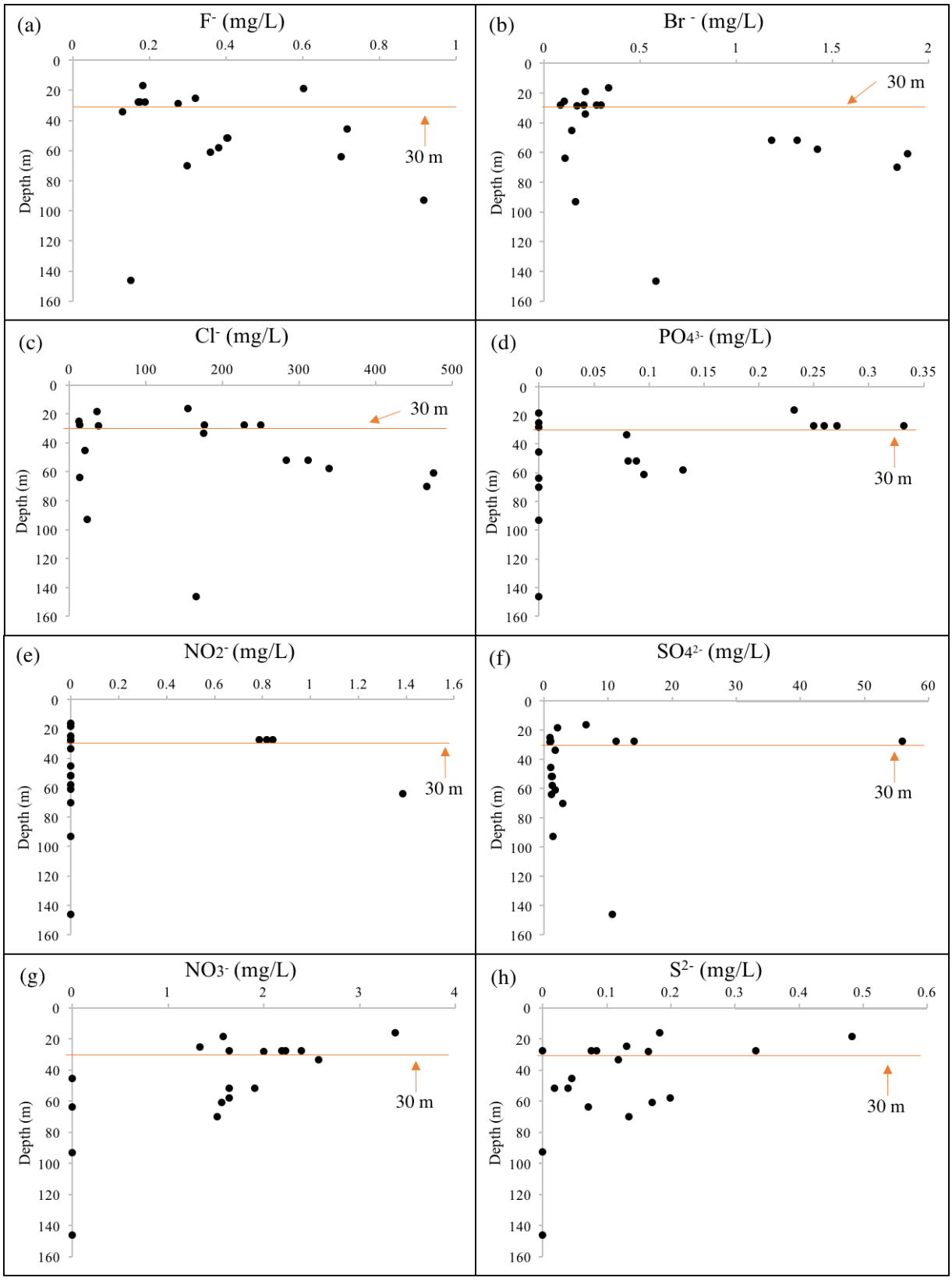

Figure 5.1 Vertical distribution of anion concentrations in groundwater, with depth (a b c d e f g h).

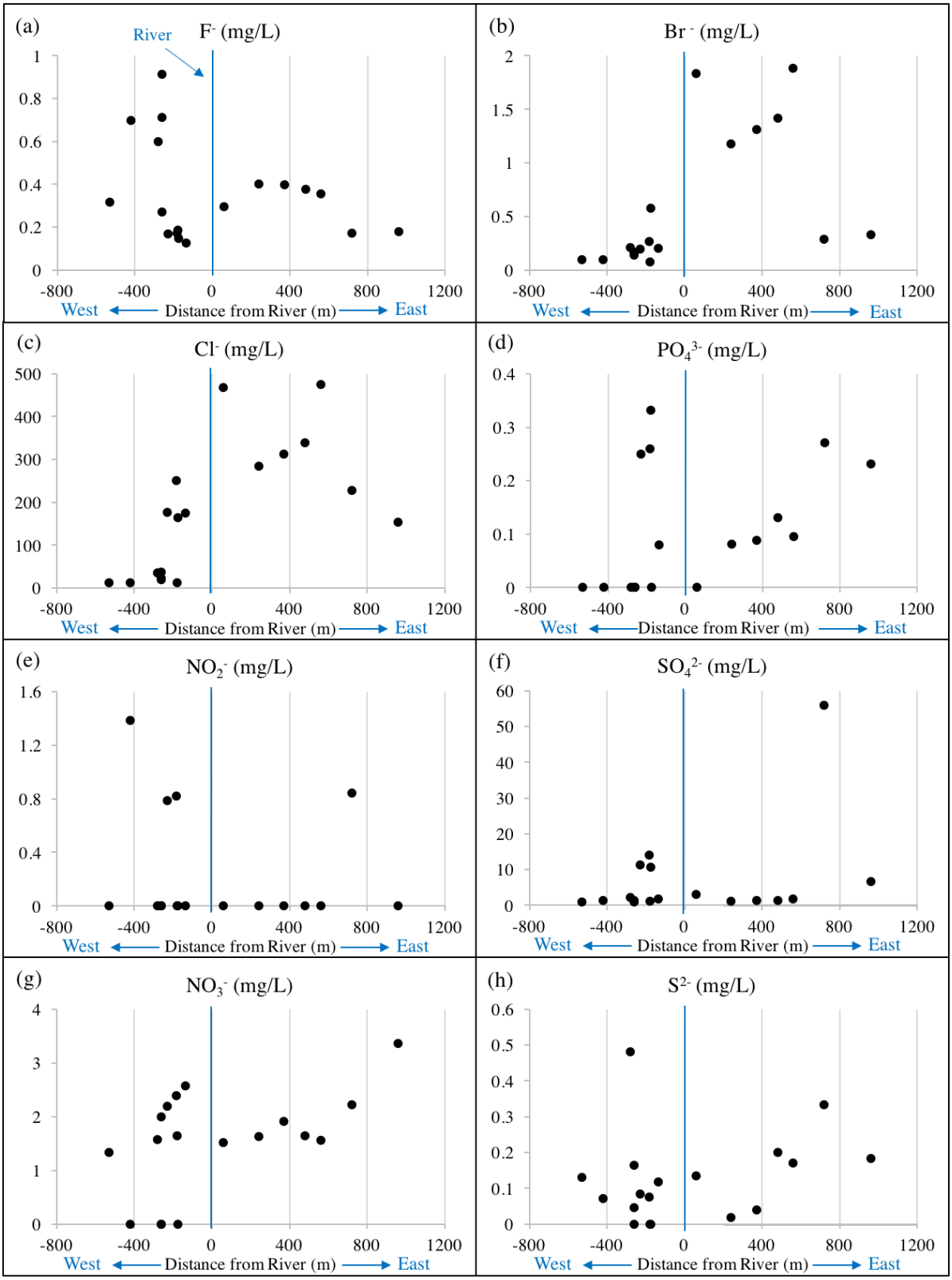

Figure 5.2 Lateral distribution of anion concentrations in groundwater, well location with distance from the river (a b c d e f g h).

5.2.3 Cations

The concentrations of Ca^{2+}, K^+, Mg^{2+} and NH_4^+ were detected at the highest concentrations within shallow wells (<30 m). In contrast, the highest concentrations of Na^+ was found in intermediate groundwater at the transition between shallow deep groundwaters (~50 m) depth. Calcium concentrations ranged from ~21 to 221 mg/L with minimum and maximum values at Vwest3 (~93 m) and TWwest3 (~27 m), respectively. Potassium concentrations ranged from ~1 to 10 mg/L with minimum and maximum values at TWeast1 (~52 m) and TWwest3 (~27 m), respectively. Magnesium concentrations ranged from ~8 to 49 mg/L with minimum and maximum values at Vwest2 (~45 m) and TWwest4 (~27 m), respectively. Ammonium concentrations ranged from ~0.7 to 6.5 mg/L (excluding seven wells with BDL NH_4^+). Minimum and maximum NH_4^+ concentrations were observed at Vwest2 (~45 m) and TWwest8 (~25 m), respectively (Figure 5.3). Deep groundwater wells had lower concentrations of Ca^{2+}, K^+, and Mg^{2+} (>30 m).

A spike in Na^+ concentrations was observed at the transition between shallow and deep groundwater (between 50 – 60 m). Sodium concentrations ranged from ~13 to 338 mg/L, with minimum and maximum values at TWwest8 (~25 m) and TWeast4 (~61 m), respectively (Figure 5.3).

Table 5.C Range of cation concentration in groundwater

Cation	Range (mg/L)	Range (mmol/L)
Na^+	13.6 - 337.49	0.59 – 14.74
NH_4^+	0 - 6.45	0 – 0.359
K^+	1.395 - 10.01	0.0357 – 5.508
Ca^{2+}	21.36 - 220.74	0.308 – 5.508
Mg^{2+}	8.15 - 49.27	0.335 – 2.027

Table 5.D Statistical analyses of cation concentration for groundwater (mg/L)

	Na^+			NH_4^+			K^+		
	n	Avg.	Stdev.	n	Avg.	Stdev.	n	Avg.	Stdev.
Shallow GW (<30 m)	8	68.65	55.02	8	3.55	2.34	8	5.59	2.32
Deep GW (>30 m)	10	205.40	118.26	8	0.36	0.69	8	2.17	0.57
	Mg^{2+}			Ca^{2+}					
	n	Avg.	Stdev.	n	Avg.	Stdev.			
Shallow GW (<30 m)	8	32.82	13.18	8	130.02	67.62			
Deep GW (>30 m)	10	20.03	9.97	10	56.73	57.25			

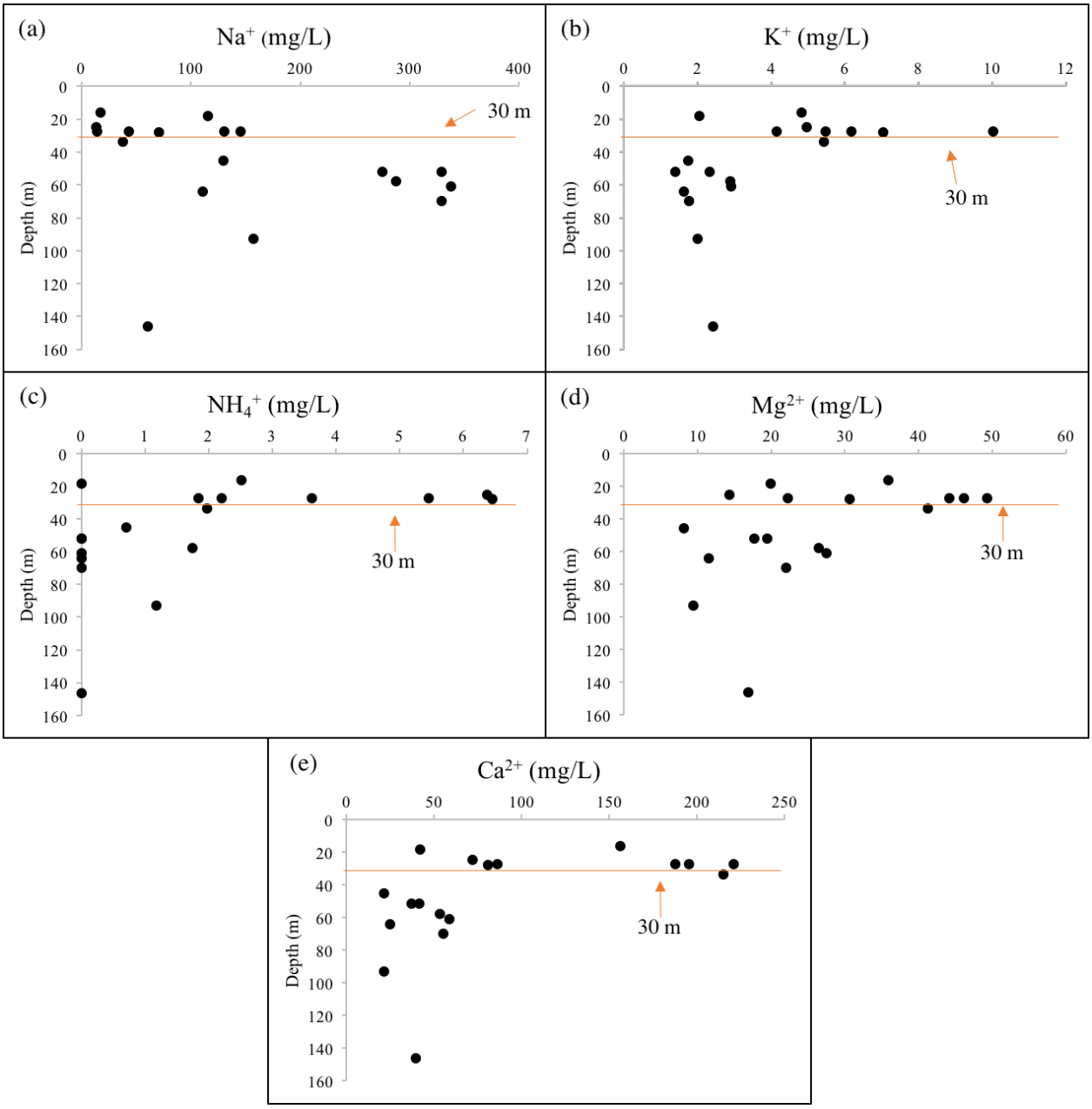

Figure 5.3 Vertical distribution of cation concentrations in groundwater (a b c d e).

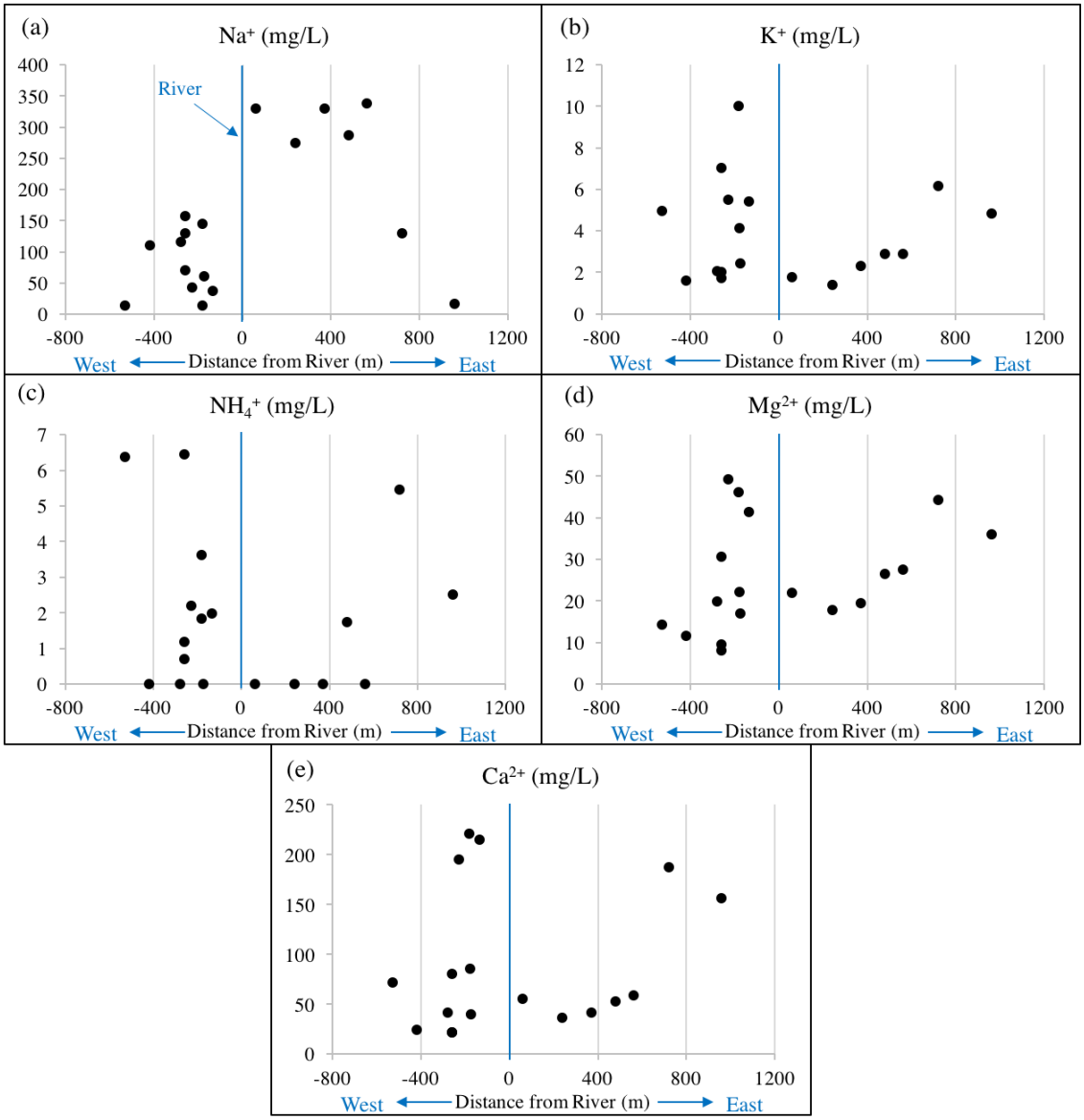

Figure 5.4 Lateral distribution of cation concentrations in groundwater, location of wells with distance from the river, on the east and west bank (a b c d e).

5.2.4 Total dissolved iron, manganese and arsenic in groundwater

Total dissolved Fe_T, Mn_T, and As_T concentrations, measured in the field, ranged widely (Table 5.E, Table 5.F). Highest concentrations of Fe_T were seen in the shallow wells (Figure 5.5). The highest concentrations of As_T were found in the shallow groundwater (<30 m) and lower concentration was seen in the deeper wells (>30 m). Iron concentrations ranged from ~0.3 to 5.9 mg/L, with minimum and maximum values at TWeast3 (~58 m) and TWwest1b (~146 m), respectively. There were four sites with Fe_T below detection limit (<0.20 mg/L) and four sites with

Fe_T above detection limit (>10 mg/L). Manganese concentrations ranged from ~0.01 to 4 mg/L, with minimum and maximum values at Vwest1 (~28 m) and TWwest2 (~34 m), respectively, not including three wells with BDL (~0 mg/L). Total dissolved As_T ranged from ~0 to 0.5 mg/L (Figure 5.5). The highest concentrations of As_T were found in the shallow groundwater (<30 m) and lower concentration was seen in the intermediate and deeper wells (>30 m).

Table 5.E Range of Fe, Mn and As concentrations in groundwater

Cation	Range	Range (mmol/L)
$As_{(t)}$	0 – 500 ppb	0 – 0.0067
$Mn_{(t)}$	0 - 3.97 (mg/L)	0 - 0.723
$Fe_{(t)}$	0 - >10 (mg/L)	0 - 0.179

Table 5.F Statistical analyses of Fe, Mn and As concentration for groundwater

	$As_{(t)}$ (ppb)			$Mn_{(t)}$ (mg/L)			$Fe_{(t)}$ (mg/L)		
	n	Avg.	Stdev.	n	Avg.	Stdev.	n	Avg.	Stdev.
Shallow GW (<30 m)	8	387.50	172.69	8	1.73	1.27	8	5.39	3.50
Deep GW (>30 m)	10	41.00	126.18	10	1.48	1.26	10	1.19	1.89

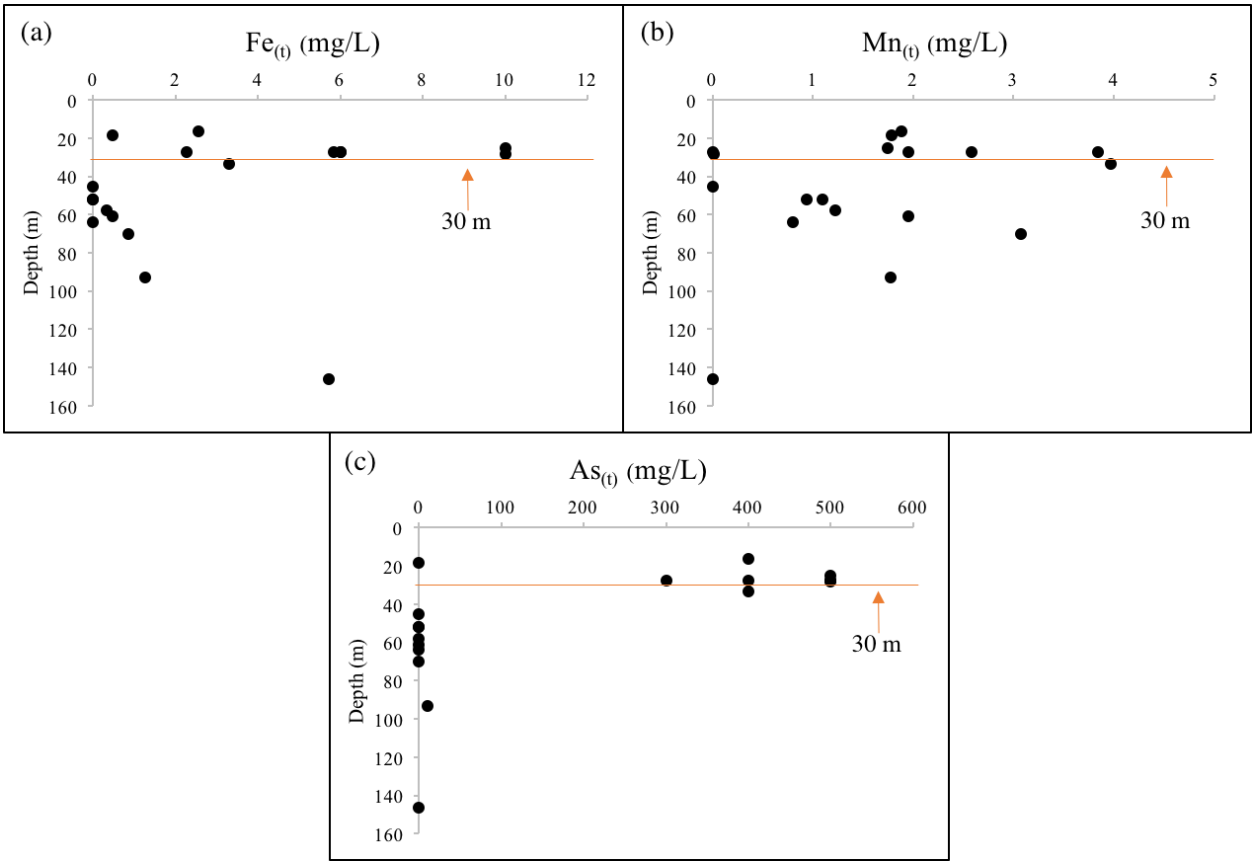

Figure 5.5 Vertical distribution of dissolved Fe, Mn and As concentrations with depth in groundwater (a b c)

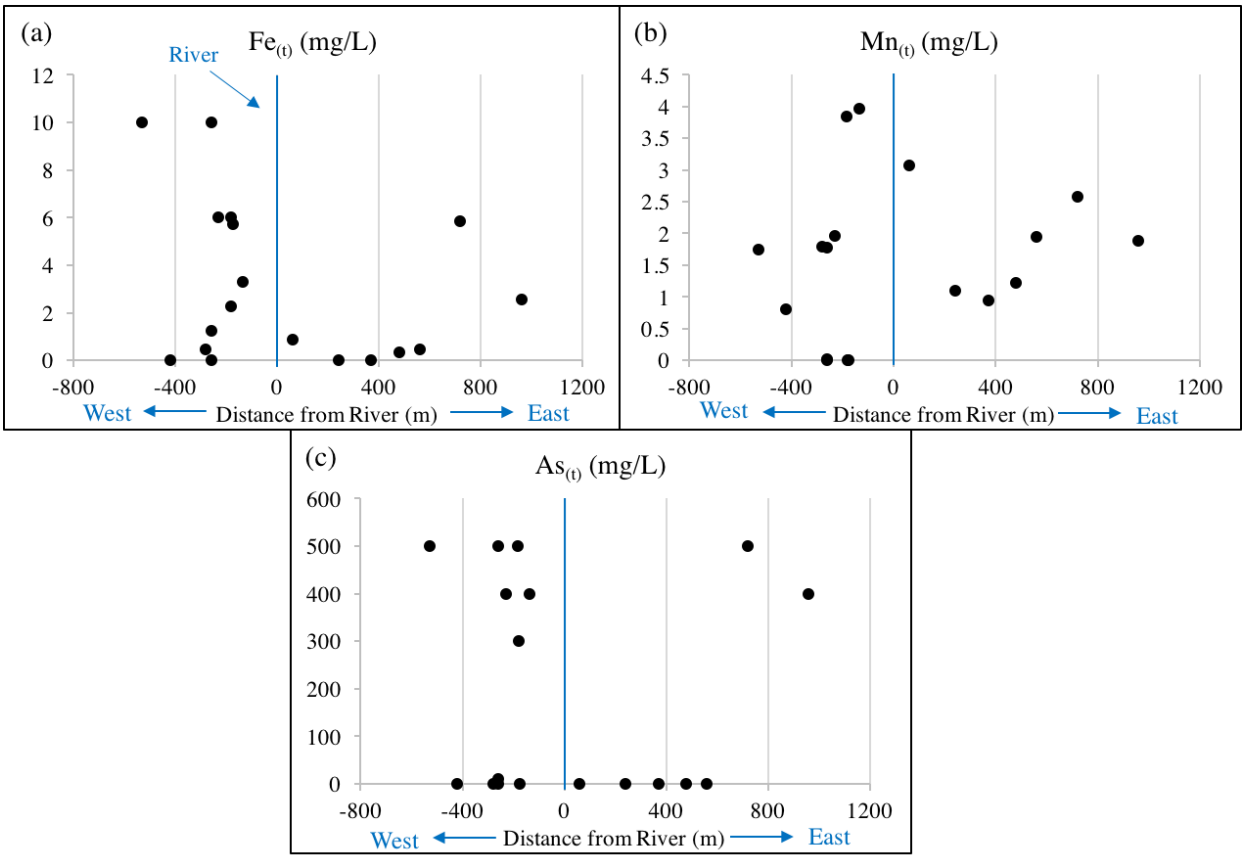

Figure 5.6 Lateral distribution of dissolved Fe, Mn and As concentrations in groundwater (a b c)

5.2.5 Stable isotopes δ^2H and $\delta^{18}O$

Nine shallow groundwater samples (<30 m) and nine deep groundwater samples (>30 m) were analyzed for isotope composition. To better interpret the isotopic compositions, the deep groundwater samples (>30 m) was broken into two groups: intermediate (50-80 m) and deep (>30 m). The groundwaters sampled in this study had hydrogen (δ^2H) isotope ratios ranged from -38 to -11‰ and stable oxygen ($\delta^{18}O$) isotope ratios that ranged from -6 to -2.5‰ (Figure 5.8) (Table 5.G). The averages for shallow groundwater (<30 m) for δ^2H and $\delta^{18}O$ were about -21.5 and -3.9‰, respectively. The intermediate depths (50-80 m) had slightly more negative values for δ^2H and $\delta^{18}O$ with averages of -26.9 and -4.4‰, respectively. Only two deep groundwater samples (>80 m) were measured, these δ^2H and $\delta^{18}O$ values were even more depleted with averages of -31 and -5‰, respectively, as seen in Table 5.H. There were no significant differences observed for the east groundwater sites verses the west groundwater site in terms of isotopic signature (Figure 5.9).

All groundwater samples fell below the Local Meteoric Water Line (LMWL) indicating that the groundwater recharge originates from local rainfall or surface water bodies, with or without evaporation (Ahmed and Burgess, 1995; Zheng et al., 2004; Majumder et al., 2011). A more negative oxygen isotope value as seen in the intermediate and deep groundwater samples (Figure 5.8), may suggest progressive depletion of the vapor mass and thus of the precipitation by the condensation process, preferentially removing the δ^2H and $\delta^{18}O$ isotopes.

Table 5.G Range of groundwater isotope signatures

	δ^2H (‰)	$\delta^{18}O$ (‰)
Range	-38 to -11	-6 to -2.5
Avg.	-25.65	-4.335
Stdev.	7.49	0.88

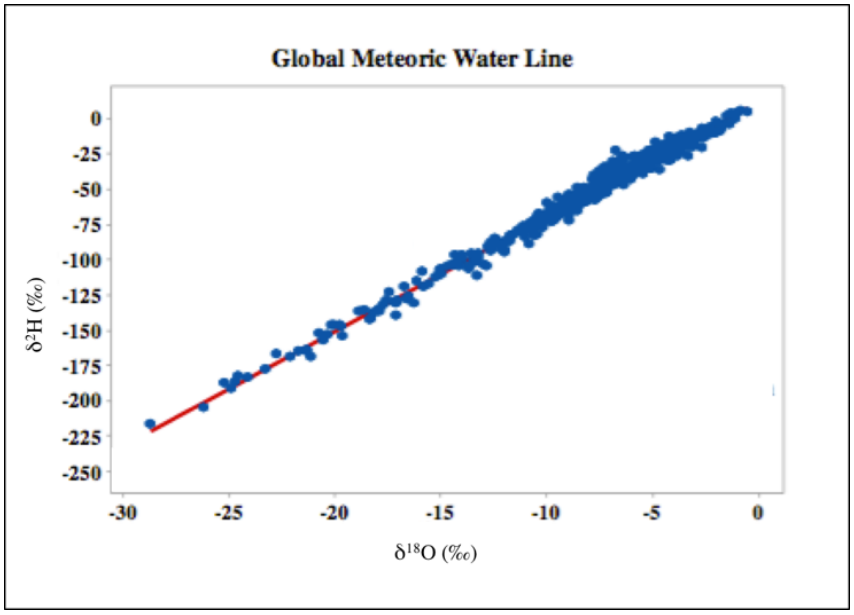

Figure 5.7 Global network of isotopes in precipitation (GNIP), (Hughes and Crawford, 2012).

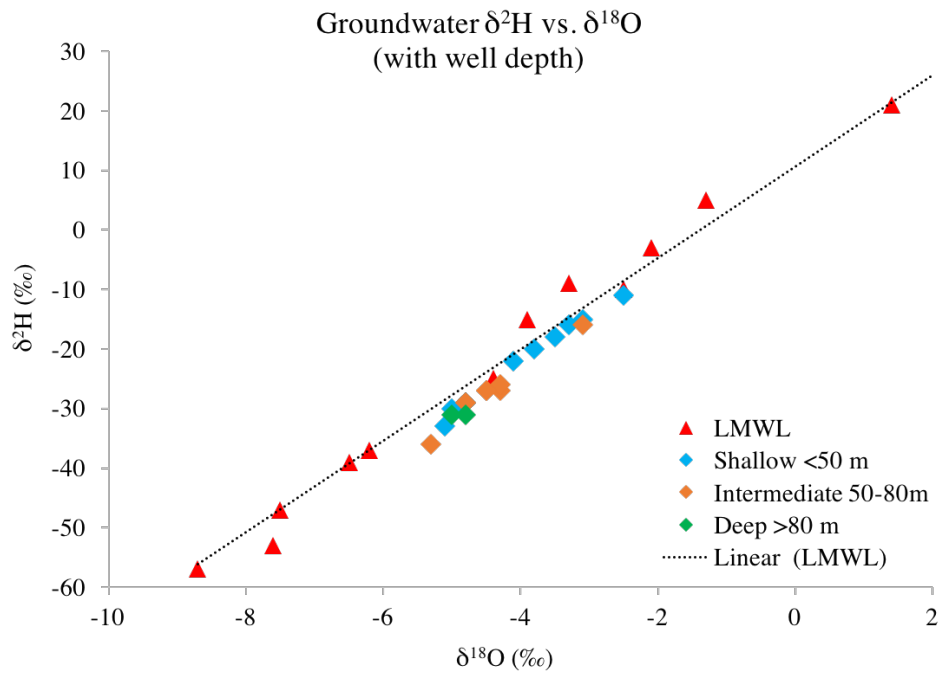

Figure 5.8 δ^2H and $\delta^{18}O$ of groundwater in comparison to the Local Meteoric Water Line (LMWL) and well depth. (LMWL data from Majumder et al., 2011).

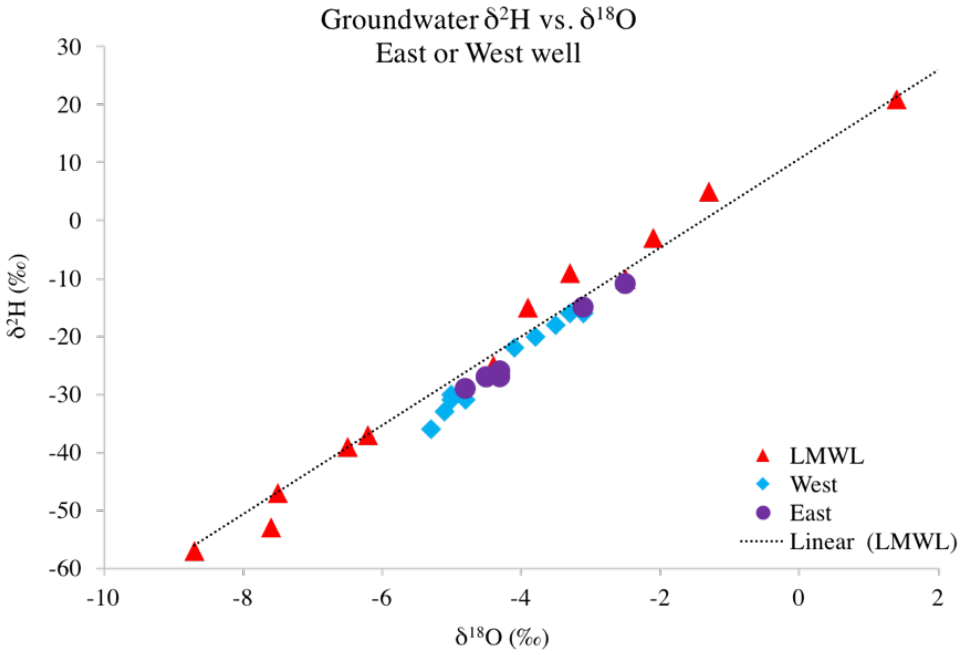

Figure 5.9 δ^2H and $\delta^{18}O$ of groundwater in comparison to the Local Meteoric Water Line (LMWL) and well location (east or west bank). (LMWL data from Majumder et al., 2011)

Table 5.H Statistical analyses of isotope signatures in groundwater

	δ^2H (‰)			$\delta^{18}O$ (‰)		
	n	Avg.	Stdev.	n	Avg.	Stdev.
Shallow <30 m	10	-21.56	7.57	9	-3.92	0.91
Intermediate 50-80m	7	-26.86	5.87	7	-4.4	0.67
Deep >80 m	2	-31	0	2	-4.9	0.14

5.2.6 DOC and Fluorescence Characteristics of Groundwater and River Water

Groundwater (n=35) and surface water (n=5) samples were analyzed using absorption and three dimensional fluorescence excitation emission spectroscopy to characterize the dissolved organic matter (DOM). Parameters such as Abs_{254}, and spectral slope ratio (S_R) were calculated from the absorption spectroscopy (Moran et al., 2000; Weishaar et al., 2003; Vahatalo and Wetzel, 2004; Helms et al., 2008) which provides insight source of OM and on aromaticity of DOM.

Analysis of DOM in this study found that characteristics were different in shallow aquifers (<30 m) as compared to deeper aquifers (>30 m). The statistical differences in OM characters were seen at 50 m depth. Analyses of OM revealed that DOM characteristics were similar for all shallow samples on both the east and west banks.

Intensities of several fluorescence indices were computed from an excitation emission matrix (EEM). Fluorescence index (FI) indicates the extent of terrestrial or microbial origin of DOM, and was calculated as the ratio of fluorescence intensities at 470 nm and 520 nm emission and 370 nm excitation (McKnight et al., 2001; Cory and McKnight, 2005). Freshness index (β: α) provides information on freshness (extent of decomposition) of DOM, and was calculated as the ratio of emission intensity at 380 nm to the maximum intensity between 420 nm to 435 nm (Parlanti et al., 2000). Humification index (HIX) was calculated as the ratio of peak area under emission spectra at 435 nm – 480 nm to peak area from 300 nm to 345 nm, and determines the extent of humification of DOM (Ohno, 2002; Zsolnay, 2003).

A variety of indices have been used from detailed EEMs, on the basis of spectrofluorometric analyses, to explain DOC characteristics. Dissolved organic carbon concentrations and DOM properties of the Meghna River water and groundwater were compared for sample location on the east and west bank (well depth or distance from the river). Figure 5.10 shows the depths (m) of samples collected and distance (m) from the river.

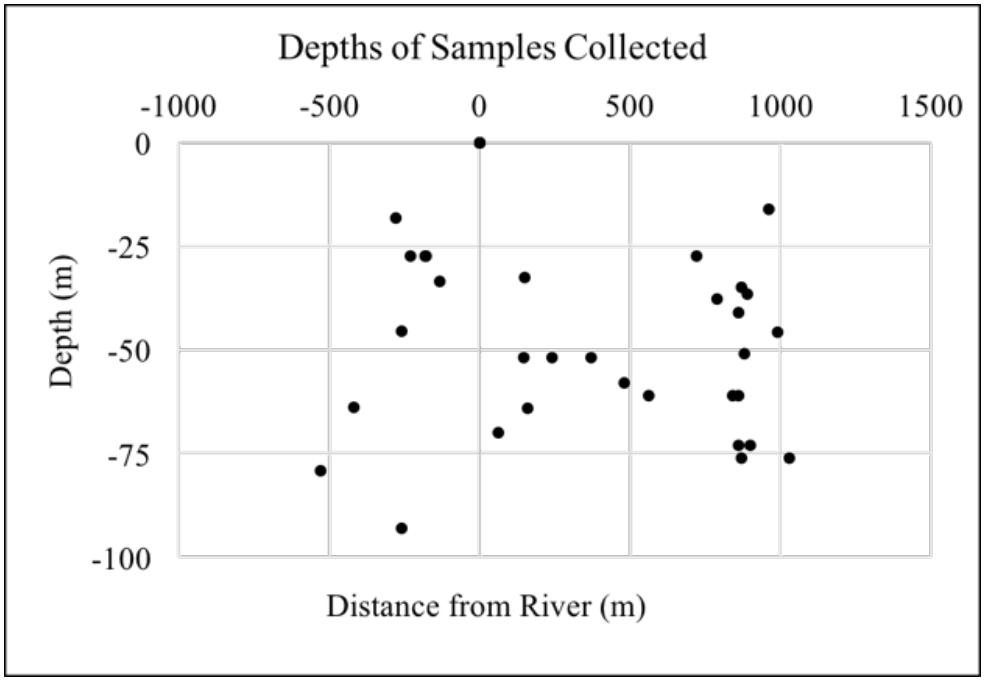

Figure 5.10 Depth of well samples collected and distances from the Meghna River.

Dissolved organic carbon concentrations ranged from 2.9 to 18.1 mg/L in groundwater wells (Figure 5.11), observed at 45 m and 51 m depths, respectively. Average DOC was 6.5 mg/L ± 3.3 (n=29). DOC was not reported for river water samples.

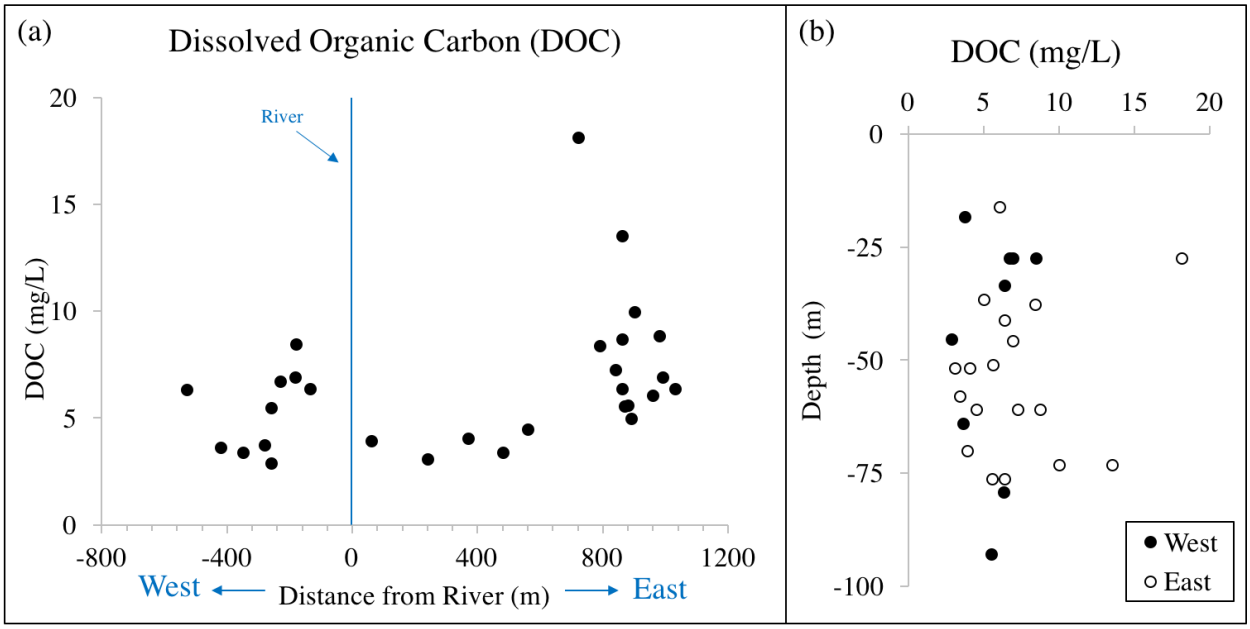

Figure 5.11 Total dissolved organic carbon (DOC) of groundwater (a) DOC with distance from the river (b) DOC with depth.

Fluorescence Index (FI) was calculated as the ratio of intensity at 470 nm to intensity at 520 nm at a fixed excitation wavelength of 370 nm (Cory and McKnight, 2005). FI concentrations ranged from 1.6 to 1.9 from wells 35 m and 64 m depth, respectively, with average of 11.7 ± 0.13 (n = 33). Fluorescence Index in surface water ranged from 1.6 to 1.7 with an average of 1.6 ± 0.04 (n=5). Samples with higher FI (500 m east of river) were collected at depths greater than 50 m. Shallower samples (< 50 m depth) collected beyond 500 m east of river showed lower FI. High FI values (~1.8) indicate DOC consisting of microbial-derived substances and low FI values (~1.2) suggest terrestrially-derived substances (terrestrial plant and soil organic matter) (McKnight et al., 2001). Overall shallow groundwater had lower FI indicating DOC more terrestrial-derived in shallow groundwater, and more microbial-derived DOC in deep groundwaters.

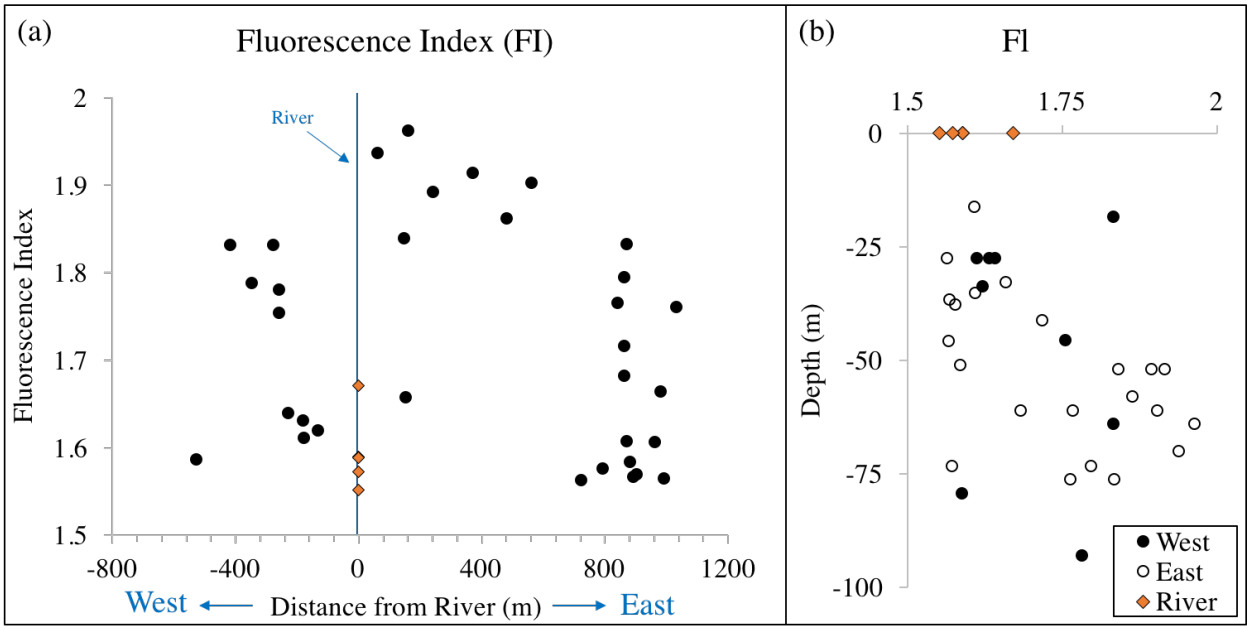

Figure 5.12 Fluorescence Index (FI) of groundwater and river water samples (a) FI with distance from the river (b) FI with depth.

Freshness Index (β:α) ranged from 0.6 to 0.9, with an average of 0.7 ± 0.1 (n=33), minimum and maximum values from groundwater wells, 73 m and 52 m depth, respectively (Figure 5.13). For river water the Freshness Index ranged from 0.71 to 0.74, with an average of 0.73 ± 0.02 (n=5). Higher (β:α) indicates recently derived DOM, and lower β:α indicates more decomposed derived DOM (Parlanti et al., 2000; Wilson and Xenopolus, 2008; Fellman et al., 2010). Samples within 500 m east of river had higher β:α than samples further away ($p<0.05$). Samples with higher β:α (< 500 m east of river) were collected at depths greater than 50 m. Shallow samples (<30 m depth) collected beyond 500 m east of the river showed lower β:α. Dissolved organic matter in samples

close to the river and deeper (on east) was more fresh, DOM was less fresh (more decomposed) in shallow groundwater and at sites farther from the river.

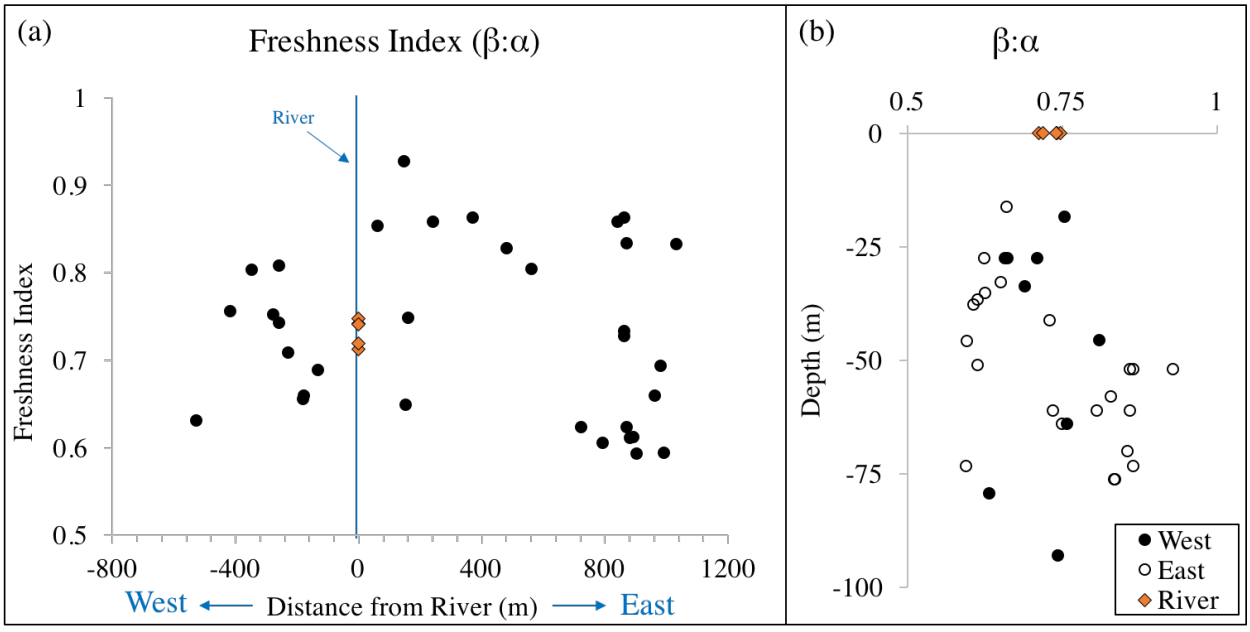

Figure 5.13 Freshness Index (β:α) of groundwater and river water samples (a) β:α with distance from the river (b) β:α with depth.

Humification Index (Figure 5.14) ranged from 1.5 to 18.4, with an average of 8.5 ± 4.5 (n=33), minimum and maximum values from groundwater wells, 52 m and 33m depth, respectively. For river water, HIX ranged from 3.6 to 7.9, with an average of 5.7 ± 2.02 (n=5). Higher HIX values indicate higher extents of humification, whereas lower HIX indicate lower extents of humification (Ohno, 2002; Zslonay, 2003). Samples <500 m east of the river had lower HIX than samples taken further away ($p<0.05$). Samples with lower HIX (<500 m east of river), were collected at depths >30 m. Shallower samples (<30 m depth) collected beyond 500 m east of the river showed higher HIX, and deep groundwater samples (>30 m depth) showed lower HIX. Extent of humification increased as the distance from the river to the east increased.

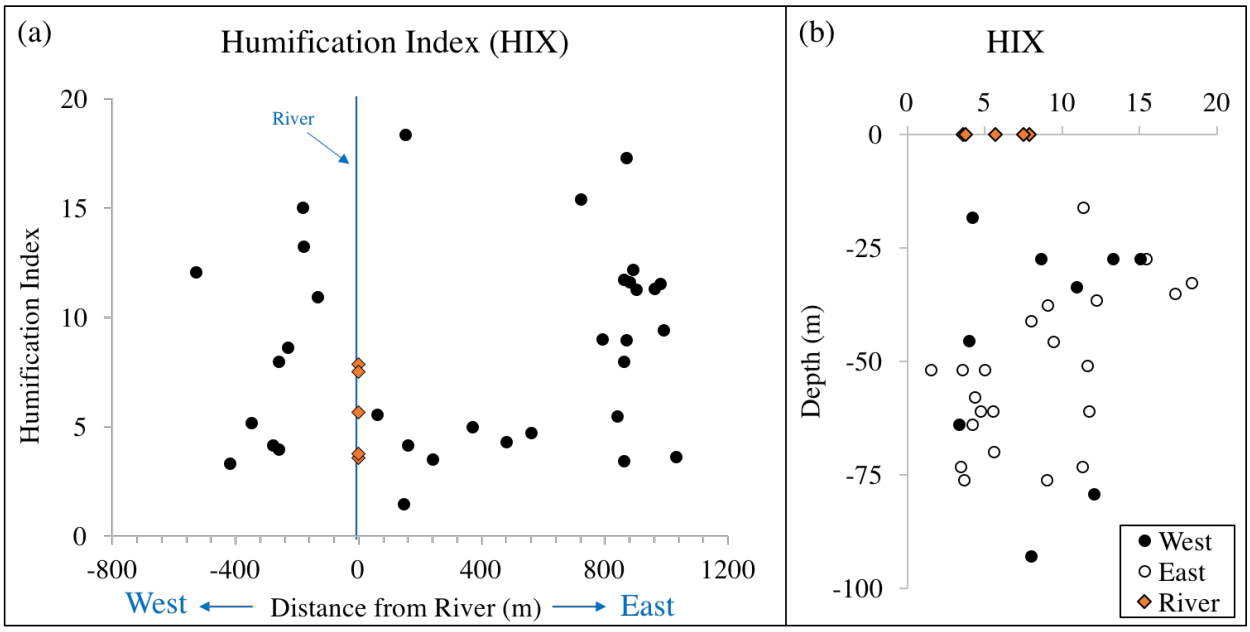

Figure 5.14 Humification Index (HIX) of groundwater and river water samples (a) HIX with distance from the river (b) HIX with depth.

Spectral Slope Ratio (S_R) ranged from 0.3 to 0.78, with average of 0.5 ± 0.17 (n= 33). Minimum and maximum from groundwater wells, 64 m and 12 m depth, respectively (Figure 5.15). For river water, S_R ranged from 0.5 to 0.6, with average of 0.5 ± 0.04 (n=5). There was one outlier for the S_R ratios with an S_R of 3.3. Spectral Slope Ratio (S_R) infers to the source and nature of the DOM. S_R >1 indicates marine-like DOM, S_R <1 indicates terrestrially dominated DOM (Helms et al., 2008). All samples, groundwater and river water had S_R<1. Indicating terrestrially dominated DOM, with the exception of the out one liar (not shown in figure).

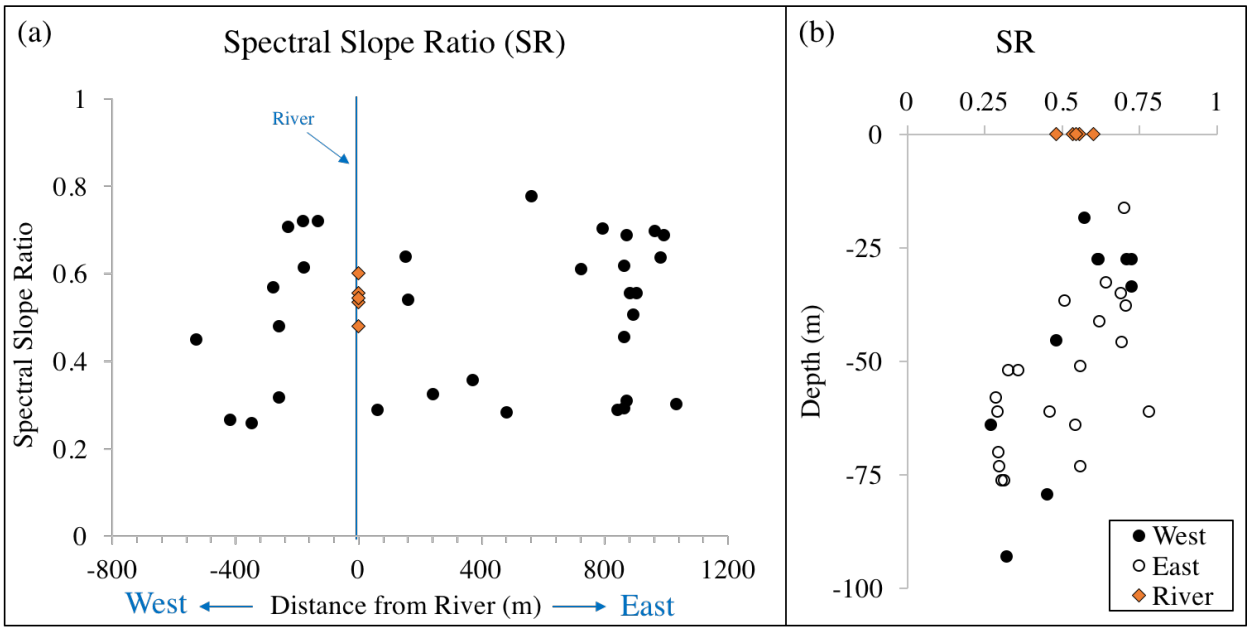

Figure 5.15 Spectral Slope Ratio (SR) of groundwater and river water samples (a) SR with distance from the river (b) SR with depth.

Absorbance at 254 nm (Abs_{254}) ranged from 0.002 A.U. to 0.2 A.U., with average 0.05 ± 0.05 (n=33), minimum and maximum from groundwater wells, 52 m and 27 m depth, respectively (Figure 5.16). For river water, Abs_{254} ranged from 0.03 to 0.04, with average of 0.031 ± 0.004 (n=5). Aromatic OM had highest absorptivity at 254 nm (Weishaar et al., 2003). Samples within 500 m of the river, had higher Abs_{254} than farther samples ($p<0.05$). Samples with higher Abs_{254} (within 500 m east of river), were collected at depths greater than 50 m. Shallow samples (<30 m depth) collected beyond 500 m east of river showed higher Abs_{254}. DOM was more aromatic in shallow groundwater and at sites farther from the river on the east bank.

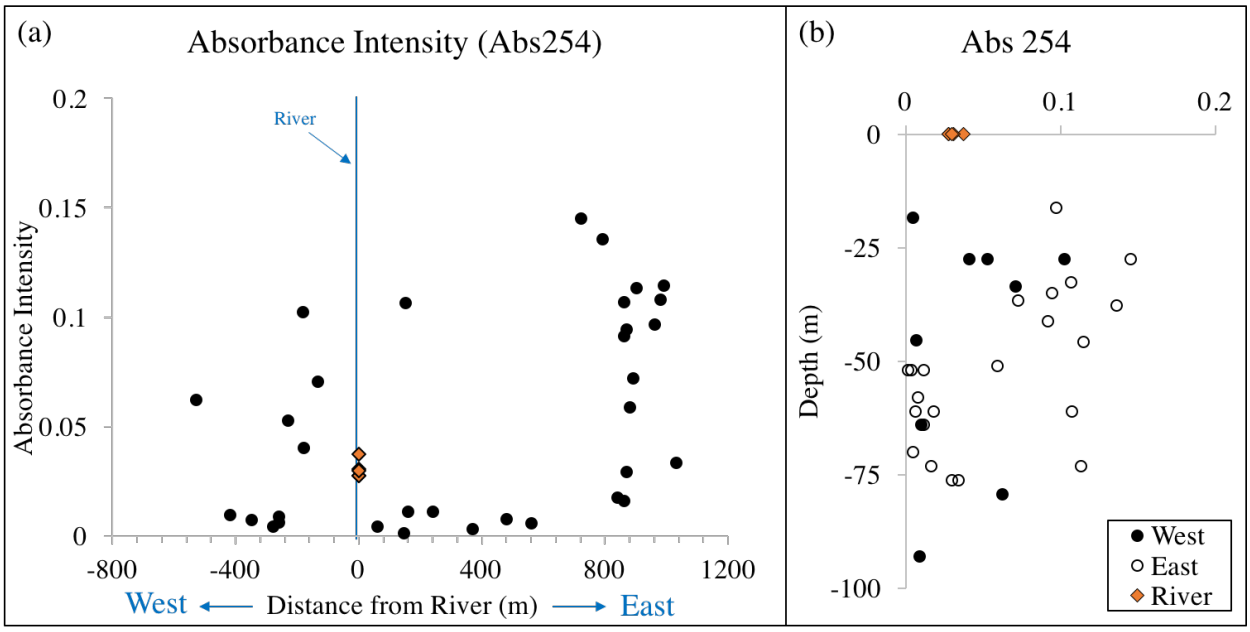

Figure 5.16 Absorbance Intensity (Abs_{254}) of groundwater and river water samples (a) Abs_{254} with distance from the river (b) Abs_{254} with depth.

5.2.7 Fluorescence Spectroscopic Studies

The measurements of DOM fluorescence are often reported as 3D excitation-emission matrices (EEMs), which are produced from many emission spectra combined at consecutively increasing excitation wavelengths (Fellman et al., 2010). The technique is used for visual inspection and analysis of EEMs or fluorescence peaks (Coble et al., 1990; Coble, 1996); it facilitates comparison of the intensity of individual peaks across a range of sample dates (Baker, 2001). Samples within 500 m east of the river had lower Humic: Protein ratios than samples farther away. Samples with lower Humic: Protein ratios (within 500 m) were collected at depths greater than 30 m (Figure 5.17). Shallow samples (less than 30 m depth) collected beyond 500 m east of the river showed higher Humic: Protein ratios. This shows that the humic-like character of DOM was highest in shallow wells (<30 m) and increased as the distance from the river to east increased.

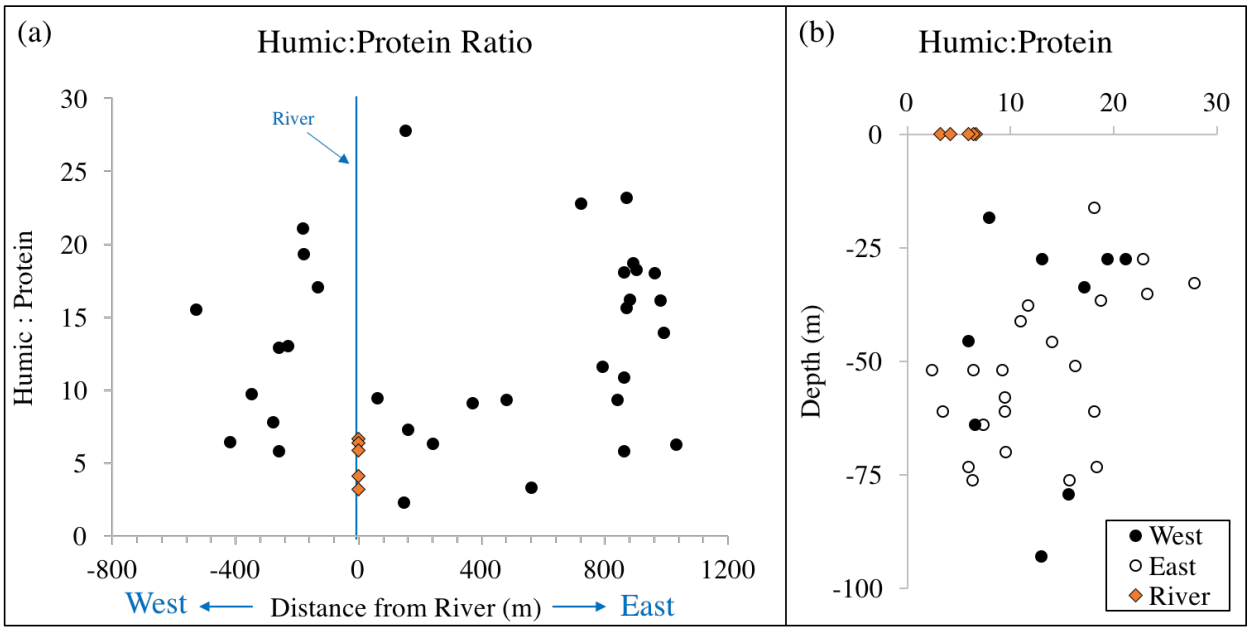

Figure 5.17 Humic:Protein characteristics of groundwater and river water samples (a) Humic:Protein with distance from the river (b) Humic:Protein with depth.

Five primary peaks have been used within the large number of natural and anthropogenic fluorophores identified (Westerhoff et al., 2001; Coble, 2007; Hudson et al., 2007). Peaks A, C and M are humic-like peaks and peaks B and T are protein-like peaks. These have been deliberately connected to ecologically significant characteristics of DOM (Coble et al., 1990; Coble, 1996; Fellman et al., 2010). Figure 5.18 shows the humic-like peaks (A, C and M) compared to sample location (depth and distance from the river). Figure 5.19 shows protein-like peaks (B and T) compared to sample location (depth and distance from the river). Peaks A, B, C, T and M have been defined by Coble et al., 1996 (Figure 5.20) by the excitation wavelengths and emission wavelengths described in Table 6.I. Figure 5.21 shows the EEM spectra for a few samples with peaks labeled manually based on the Ex and Em wavelengths.

Table 5.I Major fluorescent components (Coble et al., 1996)

Peak	Excitation$_{mas}$ (nm)	Emission$_{max}$ (nm)	Composition
B	275	310	Tyrosine- like, protein-like
T	275	340	Tryptophan-like, protein- like
A	260	380-460	Terrestrial Humic- like
M	312	380-420	Maine humic- like
C	350	420-480	Terrestrial Humic- like

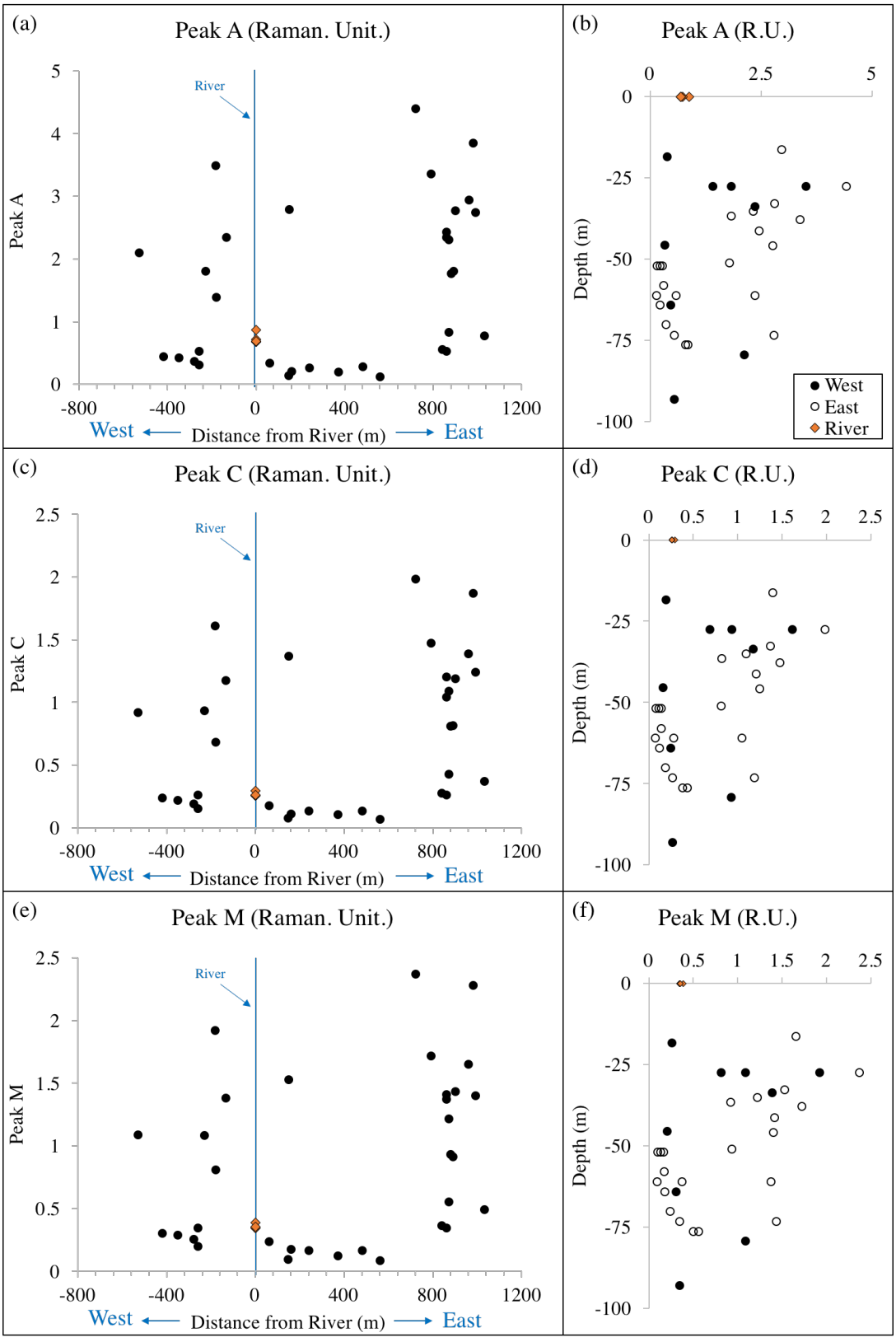

Figure 5.18 Characteristic humic-like peaks (A, C and M) for groundwater and river water (a c e) show peaks with distance from the river, (b d f) show peaks with depth.

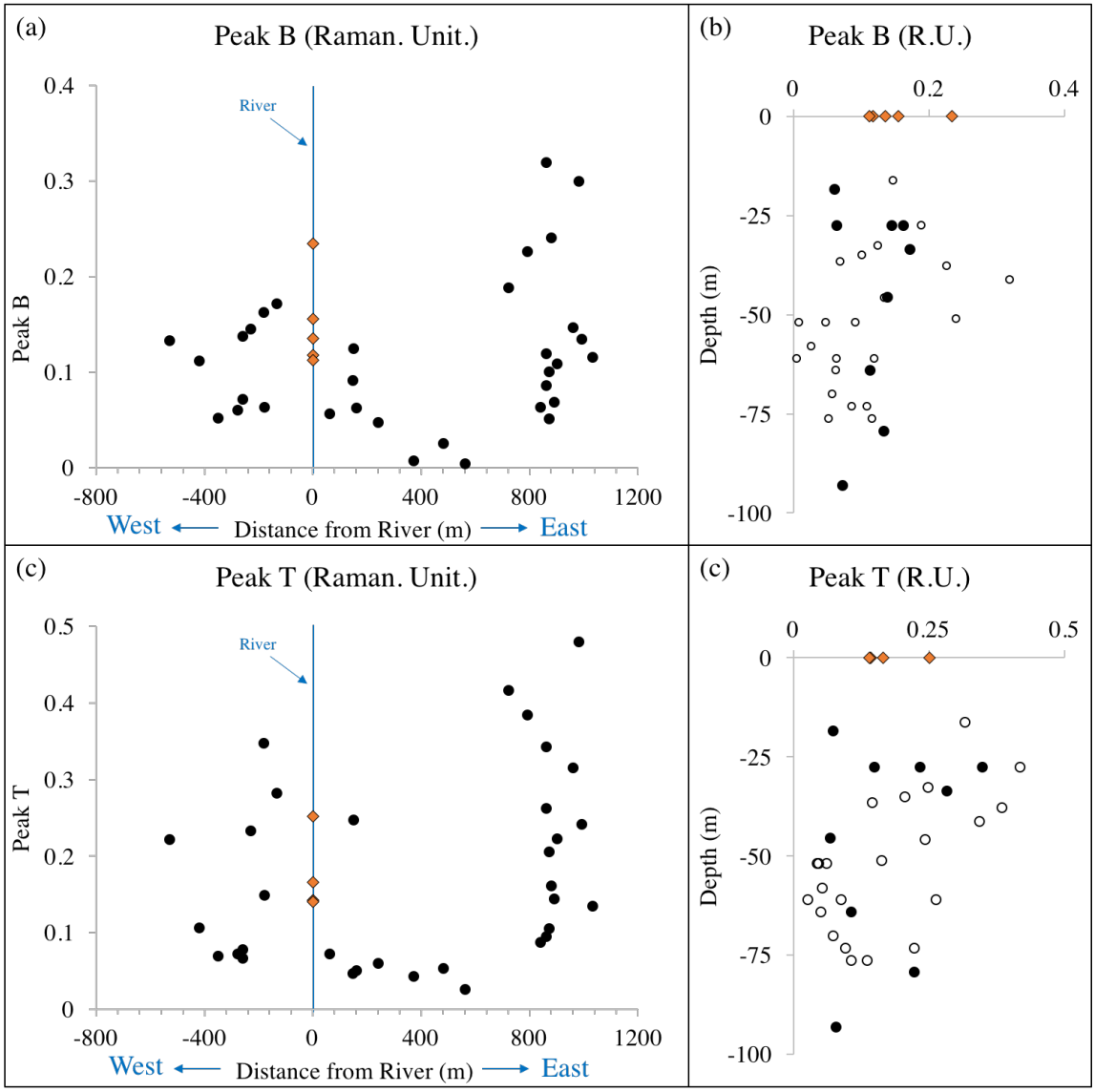

Figure 5.19 Characteristic protein-like peaks (B and T) for groundwater and river water (a c) show peaks with distance from the river, (b d) show peaks with depth.

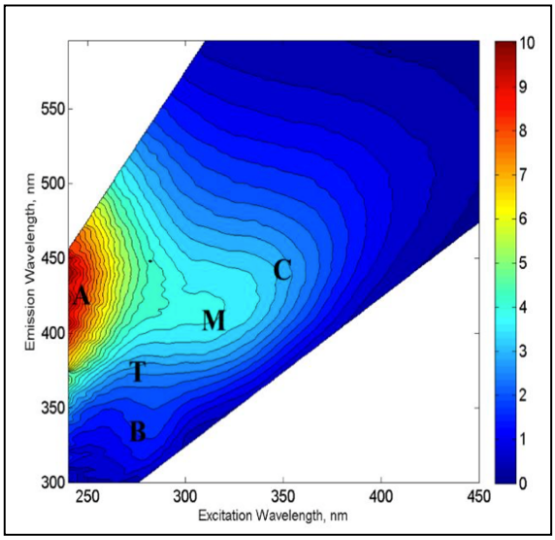

Figure 5.20 Sample 3-D Excitation Emission Matrix (EEM) with peaks A, C and M (humic-like) and peaks B and T (microbial-like) (Coble, 1996).

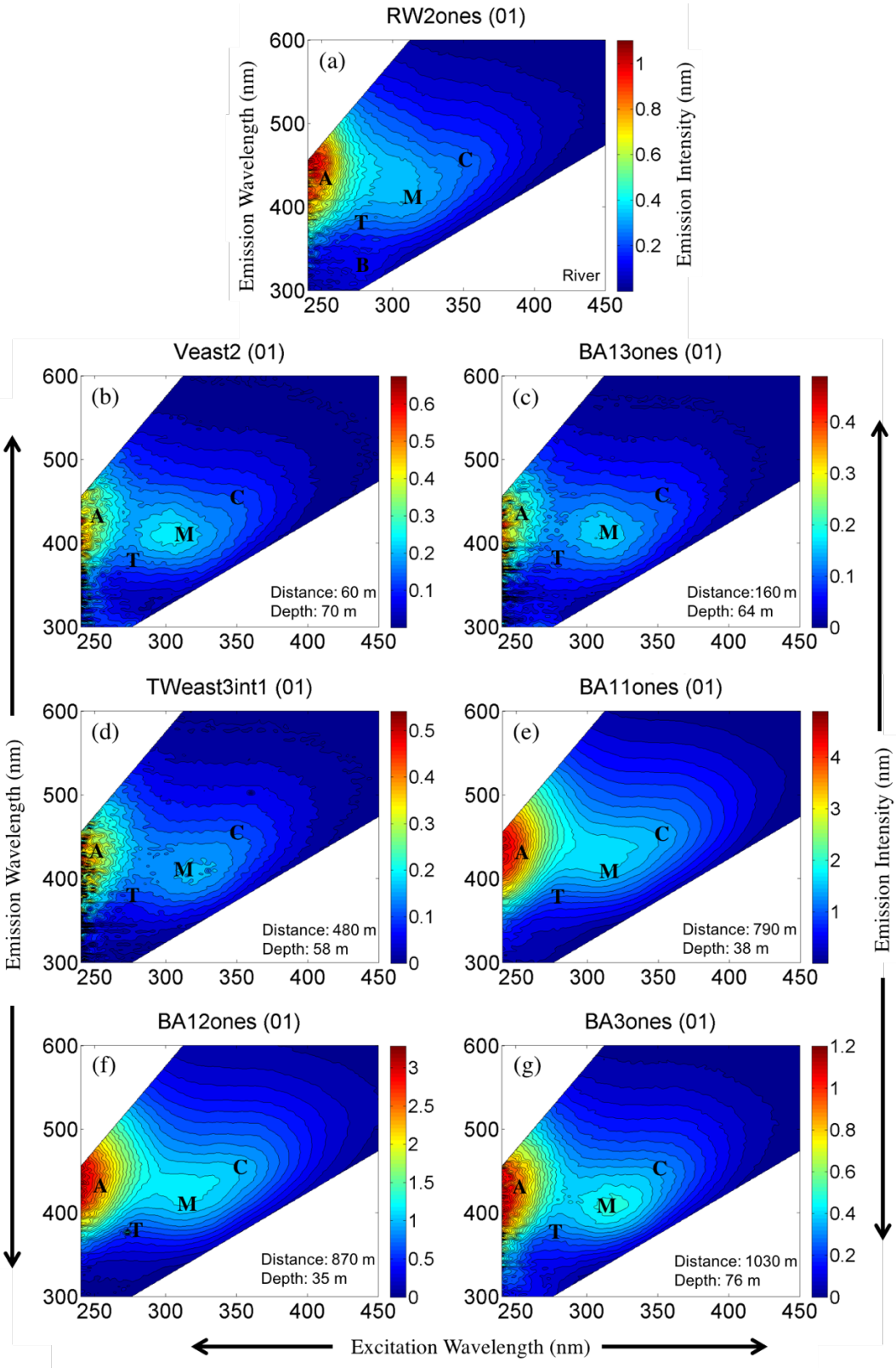

Figure 5.21 Excitation Emission Matrix (EEM) showing primary peaks (a) from the river (b c d e f g) groundwater with increasing distance from the river on the east bank.

5.3 Vertical Solid-Phase Analyses

5.3.1 Riverbank Sediment Cores

Eight sediment cores were analyzed for grain size distribution, mineral assemblage and elemental concentrations using XRF and ICP-OES. Grain size distribution was determined through particle size analysis and mineral assemblage was identified using XRD. Three chemical extractions (aquaregia (HNO_3: HCl 1:3), 1.2 M HCl, and 1 M NaH_2PO_4 + 1 M L-ascorbic acid) were utilized for solid phase Fe, Mn, and As concentrations (Figure 5.25 and Figure 5.29). Aqua Regia extractions target As bound to the refractory mineral phases. The 1.2 M HCl extraction targeted co-precipitated As specifically with readily reactive crystalline Fe oxides and oxyhydroxides, Mn oxides as well as acid volatile sulfides, and carbonate minerals (Keon et al., 2001; Datta et al., 2009). Phosphate extractions are used to extract adsorbed phases of As to Fe hydroxides by inner-sphere mechanisms.

Of the eight sediment cores collected, three cores were located on the west bank (Cores 5, 6 and 7), four were located on the east bank (Cores 1, 1b, 2, 3 and 4) and one was located on a southern island mid-channel bar (Core 8). The breakdown of core information, including sampled and measured depth intervals, can be seen in the Appendix. The purpose of the sediment analyses was to see how the composition of sediments changes with depth on the east and west banks and determine if an NRB was present at the site.

Due to time constraints, aquaregia was only performed for three out of the eight sediment cores (Core 1, Core 1b and Core 2) (Figure 5.25). Examination of sediments using particle size analysis demonstrated that the sediments were mostly silt and sand with minor clay fraction (Figure 5.23, Figure 5.26 and Figure 5.27). The sediments were predominantly composed of quartz, muscovite and some biotite, feldspars, and amphibole. X-ray diffraction (XRD) analysis tentatively revealed Fe and Mn oxides and hydroxides in the river bank sediment at various depths (Figure 5.24).

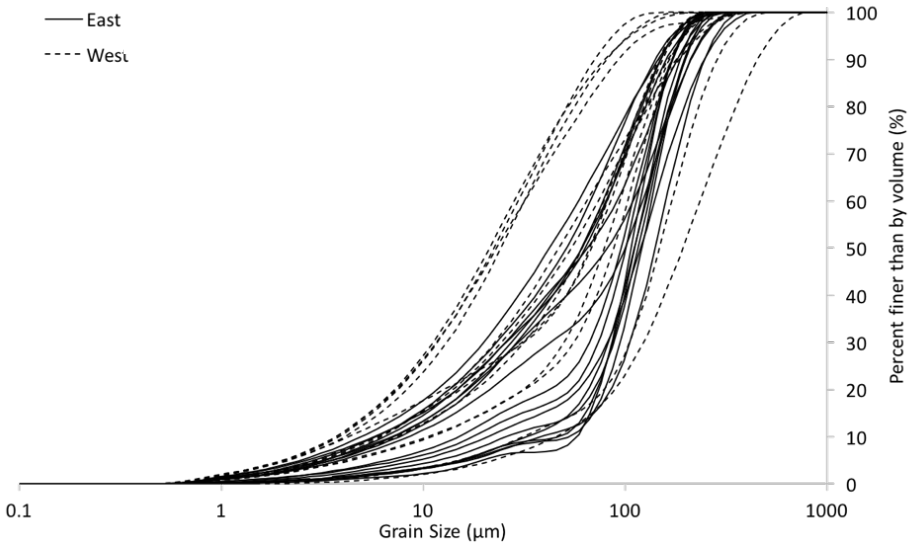

Figure 5.22 Grain size distribution of riverbank sediments for east and west riverbanks, as determined by Particle Size Analysis.

5.3.1.1 East Bank (Cores 1, 1b, 2, 3, and 4)

Core 1 was the deepest core (~244 cm). Based on particle size analysis, Core 1 had a coarse sediment layer towards the surface (~0-60 cm depth), only about 2% clay, 8% silt, and 90% sand fraction (Figure 5.23). Between ~173-244 cm depth there was another coarse layer (~70% sand), with only 10% clay, and 20% silt. The remainder of the core averaged with 10-12% clay, 40-50% silt, and 30-40% sand (Figure 5.23). Quartz, muscovite, amphibole, chlorite, feldspars (albite or anorthite), and Mn oxide (possible birnessite) were found throughout the core. Biotite, Fe oxides (possibly magnetite and goethite), Mn oxide (birnessite) and Fe carbonate (possibly ankerite) were observed towards the surface (~0-60 cm) of Core 1 (Figure 5.24). Deeper portions of the same core (~183- 244 cm) showed pyrite peaks (122-244 cm), possible iron oxides, tentatively hematite (122-183 and ~244 cm) (Figure 5.24*)*.

Handheld XRF analyses indicate that Fe, Mn, and As concentrations in Core 1 ranged from 26,255 to 39,252, 456 to 758, and 3 to 8 mg/kg, respectively. Aquaregia extractions of the same core demonstrated Fe, Mn, and As concentrations range from 15,232 to 30,684, 144 to 435, and 3 to 59 mg/kg, respectively (Figure 5.25). Iron, Mn, and As concentrations from 1.2 M HCl leaching showed ranges from 3,924 to 14,908, 58 to 314, and 8 to 142 mg/kg, respectively. Lastly, phosphate leaching for Core 1 demonstrated Fe, Mn, and As concentrations ranged from 781 to 2,632, 12 to 162, and 0.3 to 5 mg/kg, respectively. The vertical profiles of Core 1, from XRF and all three extractions, show an Fe and Mn zone of increase at approximately 120-173 cm depth

(Figure 5.25). Arsenic extraction results along the sediment profile was more heterogeneous. Two zones of interest were observed by aquaregia and phosphate extractions at approximately 120-150 cm and 173-244 cm depth. Arsenic extracted by HCl leaching increased in the profile starting at ~140 cm and continuing to increase towards to the core bottom (~244 cm) (Figure 5.25). The coarse grain layer (~173-244 cm depth), containing oxides, may be correlated to the observed As, as demonstrated by the HCl extraction. The peaks of Fe and Mn at depth 120-173 cm may also be correlated to the observed oxides (Figure 5.25).

In contrast to Core 1, Core 1b (riverbed), Core 2, Core 3 and Core 4 (riverbank) were only sampled at two shallow intervals of ~ 0-60 cm and ~60-120 cm depth. In Core 1b, particle size analysis demonstrated mostly sand fraction throughout. When comparing the two depth intervals, 0-60 cm depth had more silt fraction (~ 3% clay, 22% silt, and 75% sand) than 60-122 cm depth (~3% clay, 10% silt and 87% sand) (Figure 5.23). Quartz, amphibole and iron carbonate (possibly siderite) were identified throughout the core (0-60 cm and 60-120 cm). Chlorite and Mn oxides (possibly birnessite) were present between 60 to 120 cm depth. In Core 1b, Fe, Mn, and As ranged from 24,994 to 25,784, 432 to 438, and 3 to 4 mg/kg, respectively, as demonstrated by handheld XRF (Figure 5.25). Iron and Mn as demonstrated by the aqua regia leach method, in Core 1b, ranged from 17,641 to 18,133, and 223 to 303 mg/kg, respectively. Aquaregia extraction data for As was not obtained for Core 1b at the surface (0-60 cm), but at 60-120 cm depth As was 3 mg/kg (Figure 5.25). 1.2M HCl extractable Fe, Mn, and As for the same core, ranged from 4,027 to 7,097, 56 to 135 and 82 to 84 mg/kg, respectively. Lastly, phosphate leached Fe, Mn, and As from Core 1b ranged from 1,112 to 1,343, 33 to 39 and 20 to 39 mg/kg, respectively (Figure 5.25).

Core 2 particle size analysis did not show significant variation of grain sizes from shallow to deep (~4% clay, ~9-16% silt, with the remainder sand fraction) (Figure 5.23). Quartz, feldspars (albite, anorthite), amphibole, and Mn oxides (possibly birnessite) were identified throughout the core (0-60 cm and 60-120 cm). Muscovite was observed at the surface only (0-61 cm). For the same core, Fe, Mn, and As ranged from 22,356 to 39,870, 425 to 688, and 2 to 7 mg/kg, respectively, as demonstrated by handheld XRF. Iron, Mn, and As, as demonstrated by aquaregia, in Core 2 ranged from 10,898 to 13,965, 134 to 142, and 16 to 37 mg/kg, respectively (Figure 5.25). 1.2 M HCl extractable Fe, Mn, and As for the same core, ranged from 2,775 to 4,746, 32 to 343 and 538 to 660 mg/kg, respectively (Figure 5.25). Lastly, phosphate leached Fe, Mn, and As for Core 2 ranged from 760 to 2,378, 6 to 162 and 9 to 10 mg/kg, respectively (Figure 5.25).

Particle analysis for Core 3 showed a clay and silt rich layer towards the bottom of the core. At the surface (~0-60 cm) the sediment was about ~5% clay and ~17% silt, with the remainder sand fraction. From ~80 to 122 cm depth there was ~11-15% clay and 45-56 % silt, with remainder stand fraction (Figure 5.23). Quartz, muscovite and amphibole were identified at all depths (~0-33, 33-91, and 91-122 cm). Manganese oxides (possibly birnessite or hausmannite) and Fe-carbonates (tentatively ankerite or siderite) were identified between ~33-92 cm depth and ~122 cm depth. Iron oxides (possibly hematite) was identified between 33-92 cm depth. For the same core, Fe, Mn, and As ranged from 23,869 to 38,352, 440 to 647, and 4 to 5 mg/kg, respectively, as demonstrated by handheld XRF. Measurements by aquaregia were not obtained for Core 3. 1.2 M HCl extractable Fe, Mn, and As for the same core, ranged from 2,278 to 4,613, 83 to 254, and 18 to 226 mg/kg, respectively (Figure 5.25). Lastly, phosphate leached Fe, Mn, and As for Core 3 ranged from 281 to 360, 35 to 113, and 0.08 to 0.12 mg/kg (Figure 5.25).

Core 4 had a silt size dominated layer deeper in the core (at ~60 cm), ~12% clay and ~45% silt. At the surface (~0 cm) and at the bottom (~122 cm), Core 4 had ~2% clay and 11% silt, with remainder sand fraction (Figure 5.23). Quartz, feldspar, muscovite, amphibole and Mn oxides (possibly birnessite) were identified throughout the core (0-61 cm and 61-122 cm). In Core 4, Fe, Mn, and As ranged from 24,868 to 29,069, 468 to 491, and 2 to 6 mg/kg, respectively, as demonstrated by handheld XRF (Figure 5.25). HCl extractable Fe, Mn, and As for the same core, ranged from 2,010 to 3,878, 139 to 389, and 14 to 20 mg/kg, respectively. Lastly, phosphate leached Fe, Mn, and As ranged from 170 to 269, 30 to 70, and 0.09 to 0.47 mg/kg, respectively (Figure 5.25).

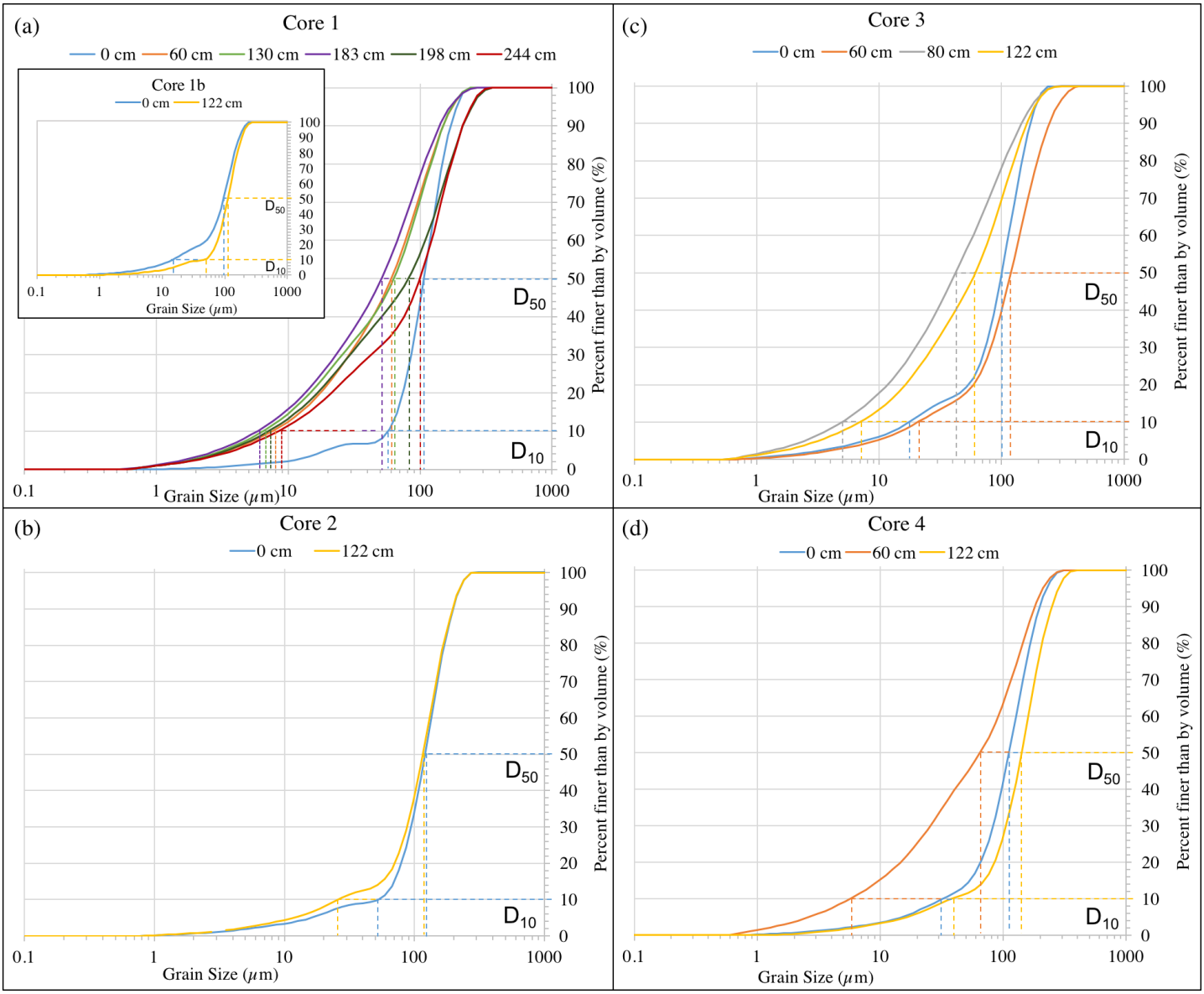

Figure 5.23 Grain size distribution of riverbank sediment (East), as determined by Particle Size Analysis. (a) Core 1 and 1b (b) Core 2 (c) Core 3 and (d) Core 4. Grain Size (μm) is in logarithmic scale.

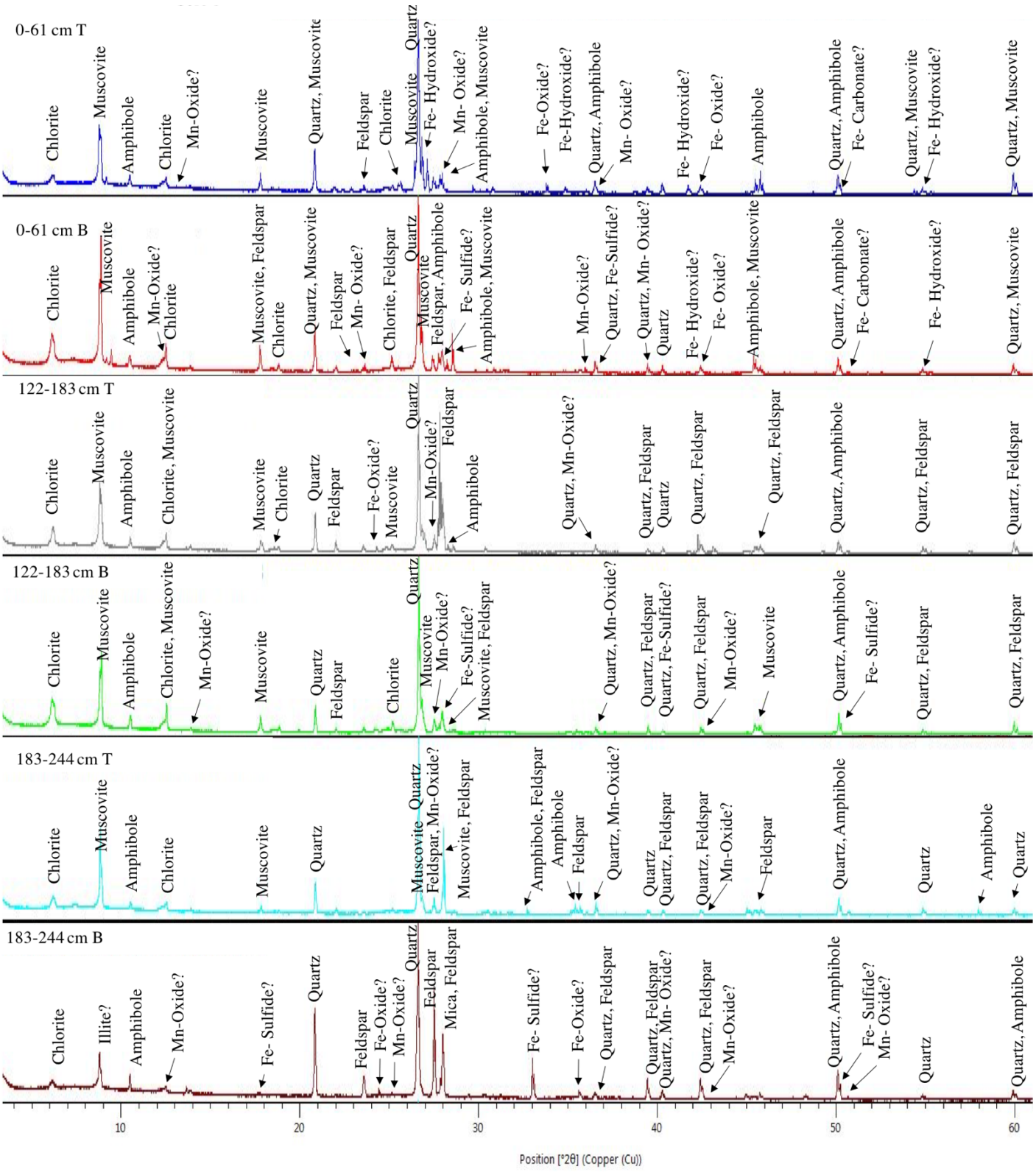

Figure 5.24 Mineral assemblage of riverbank sediment for Core 1 (depth intervals 0-61 cm, 61-122 cm, 122-183 cm and 183-244 cm), as determined by X-Ray Diffraction.

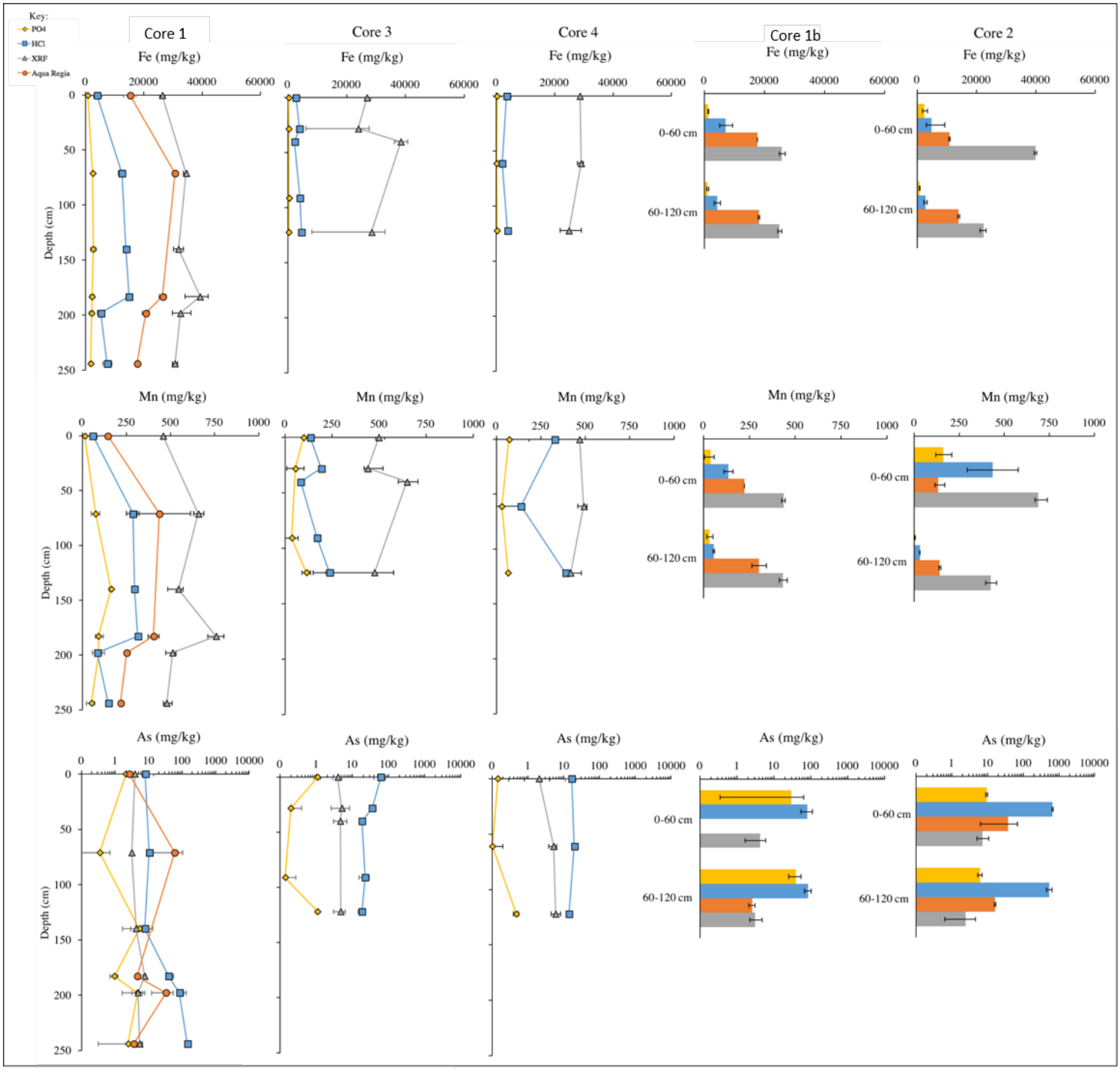

Figure 5.25 Extracted Fe, Mn, and As concentrations (mg/kg) for riverbank sediments (East) (Core 1, 1b, Core 2, Core 3, and Core 4). XRF analyses, in gray and three chemical leaching procedures: Aquaregia in orange, HCl in blue and Phosphate in yellow.

5.3.1.2 West Bank (Cores 5, 6, and 7)

Core 5 was the second deepest core extending from the surface to ~183 cm. Grain size increased with depth; between ~130 and 183 cm there was a coarse layer with low clay and higher sand fraction (Figure 5.26). The grain sizes were relatively constant from the surface to about 80 cm depth with ~12% clay, 50- 54% silt and remainder sand fraction. At about 112 cm, there was a silt rich layer, just above the coarse sand layer at the bottom of the core. At about ~112 cm the core had only ~12% clay and ~77% silt, with remainder stand, whereas between 130 and 183 cm depth there was <1% clay, ~14% silt and ~75% sand (Figure 5.26). Quartz and chlorite were identified at all depths (0-183 cm). Muscovite was identified between 0-122 cm depth and biotite was identified at the bottom of the core (122-183 cm depth). Iron and Mn oxides were identified at various depths in the core. Manganese oxides (possibly birnessite) and iron-carbonate (possibly ankerite, siderite, or lepidochrosite) were identified between 0-61 and 61-183 (Figure 5.28).

Iron, Mn, and As in Core 5 ranged from 29,821 to 57,254, 369 to 935, and 4 to 14 mg/kg, respectively, as demonstrated by handheld XRF (Figure 5.29). HCl extractable Fe, Mn, and As for the same core ranged from 2,197 to 7,055, 61 to 557, and 15 to 1,533 mg/kg, respectively (Figure 5.29). Lastly, phosphate leached Fe, Mn, and As ranged from 205 to 530, 12 to 216 mg/kg, and 0 to 3 mg/kg (Figure 5.29). The maximum for all three occurs at depth 0 cm and minimum is at the bottom of the core (~183 cm). The vertical profile of Core 5 shows two zones of As specifically bound to Fe and Mn- oxides, as demonstrated by the HCl extraction. One zone occurs between 50 and 80 cm depth with As concentrations up to 1,533 mg/kg, and the second enrichment zone is deeper between 112 and 183 cm depth, with As concentrations up to 130 mg/kg. The bottom As accumulation possibly correlates with the Fe-oxides present at depth, and coarse sand layer observed between 112 and 183 cm depth. The low As concentration zone at ~112 cm (17 mg/kg As) is correlated to the silt rich layer observed at ~112 cm depth (Figure 5.26, Figure 5.29).

In contrast to Core 5, Core 6 and Core 7 were only sampled at two shallow intervals of ~0-60 cm and ~60-120 cm depth. For Core 6, grain size distribution showed a clay and silt rich layer ~60-80 cm depth and higher silt fraction at the surface (0-60cm) and at the bottom of the core (~122 cm). About 8% clay, ~28% silt and remainder sand fraction was observed at the surface (0-60cm) and at the bottom of the core (~122 cm). Whereas the fine grain layer ~60-80 cm depth showed 13-16% clay, ~40% silt, with remainder stand fraction (Figure 5.26). Quartz, feldspars (albite, anorthite), muscovite and amphibole were identified throughout the entire core. Manganese

oxides (possibly birnessite) was tentatively identified in the deeper portion of the core between 61 and 122 cm and Fe-sulfide was possibly observed at ~61 cm. Clay, possibly montmorillonite or illite, were also tentatively identified at ~50 cm and ~71 cm depth. For the same core, Fe, Mn, and As ranged from 232,684 to 39,447 mg/kg, 533 to 560, 4 to 9 mg/kg, respectively, as demonstrated by handheld XRF (Figure 5.29). HCl extractable Fe, Mn, and As for the same core, ranged 2,884 to 5,616, 82 to 203, and 43 to 578 mg/kg, respectively (Figure 5.29). Lastly, phosphate leached Fe, Mn, and As ranged from 315 to 362, 1 to 108, and 0 to 1 mg/kg, respectively (Figure 5.29).

Core 7 had relatively similar particle sizes with depth. Overall, Core 7 had ~25% clay and ~75% silt (Figure 5.26). This core had the most clay fraction observed out of all the sediment cores. Quartz, feldspars (albite, anorthite), muscovite, and amphibole were identified at all depths (0-61 cm and 61-122 cm). Manganese oxides (possibly birnessite) were seen at the surface and bottom of the core (0-61 cm and ~122 cm) and iron carbonates (possibly siderite) at ~122 cm. Chlorite was also identified between 0-61 cm and ~122 cm. Iron, Mn, and As concentrations for this core ranged from 39,592 to 44,285, 582 to 684, and 4 to 7 mg/kg, respectively, as demonstrated by handheld XRF. HCl extractable Fe, Mn, and As for the same core, ranged from 6,916 to 7,815, 291 to 365, and 17 to 738 mg/kg, respectively. Lastly, phosphate leached Fe, Mn, and As ranged from 175 to 384, 75 mg/kg to 124 and 0.2 to 1.1 mg/kg, respectively (Figure 5.29).

5.3.1.3 Island (Core 8)

Core 8 was taken from an island in the southern portion of the study site. This core was sampled at two shallow intervals of ~0-60 cm and ~60-120 cm depth. Core 8 had relatively similar particle sizes with depth. Overall this core had 4-5% clay, silt ~20% silt, with remainder silt fraction (Figure 5.27). Quartz, feldspar, amphibole, muscovite and chlorite peaks were identified at the surface. Manganese oxides (possibly birnessite) was also tentatively identified at the surface 0-60 cm). In Core 8, Fe, Mn, and As concentrations ranged from 26,627 to 26,812, 408 to 439, and 4 to 7 mg/kg, respectively, as demonstrated by handheld XRF. HCl extractable Fe, Mn, and As for the same core, ranged from 2,537 to 2,665, 103 to 139, 16 to 17 mg/kg, respectively. Lastly, phosphate leached Fe, Mn, and As ranged from 238 to 293, 52 to 183 mg/kg, and 0.2 to 2.8 mg/kg, respectively (Figure 5.29). All three elements for Core 8 had the lowest concentrations at the surface, then increased with depth to the highest concentrations observed at 122 cm depth.

5.3.2 Riverbank Sediment Core Overview

Out of all four sediment analyses (handheld XRF, aquaregia, HCl and phosphate), handheld XRF demonstrated the highest concentrations of solid phase Fe and Mn (Figure 5.25, Figure 5.29). Aquaregia extractions demonstrated the second highest solid phase Fe and Mn concentrations. The 1.2 M HCl extraction demonstrated the highest concentrations of solid phase As. On the east bank, a maximum of 660 mg/kg As was observed between 0-60 cm depth in Core 2 (Figure 5.25), and on the west bank a maximum of 1,533 mg/kg As was observed at ~71 cm depth in Core 5 (Figure 5.29). Aquaregia extracted As concentrations were considerably lower in the three cores (Figure 5.25). The phosphate extraction also demonstrated low As concentrations in all 8 cores (Figure 5.29).

Grain size distribution of the east bank verses the west bank can be seen in Figure 5.22. In general, there seems to be higher clay and silt fraction in the west bank than in the east bank. The sediments on both the east and west banks contained quartz, feldspar (albite, anorthite), amphibole, muscovite and chlorite. Biotite mica was only identified on the west bank, for example in Core 5 (Figure 5.28). Iron-sulfides (maybe pyrite), Fe-oxides (such as hematite) and possibly Fe and Mn carbonates (such as siderite, ankerite, and birnessite), were tentatively identified on both the east and west banks. We caution it can be stated that the possible Fe and Mn oxides were identified at the same depths where enrichment of solid phase As was observed (as seen in Figure 5.24 and Figure 5.25 on the east bank and Figure 5.28 and Figure 5.29 on the west bank).

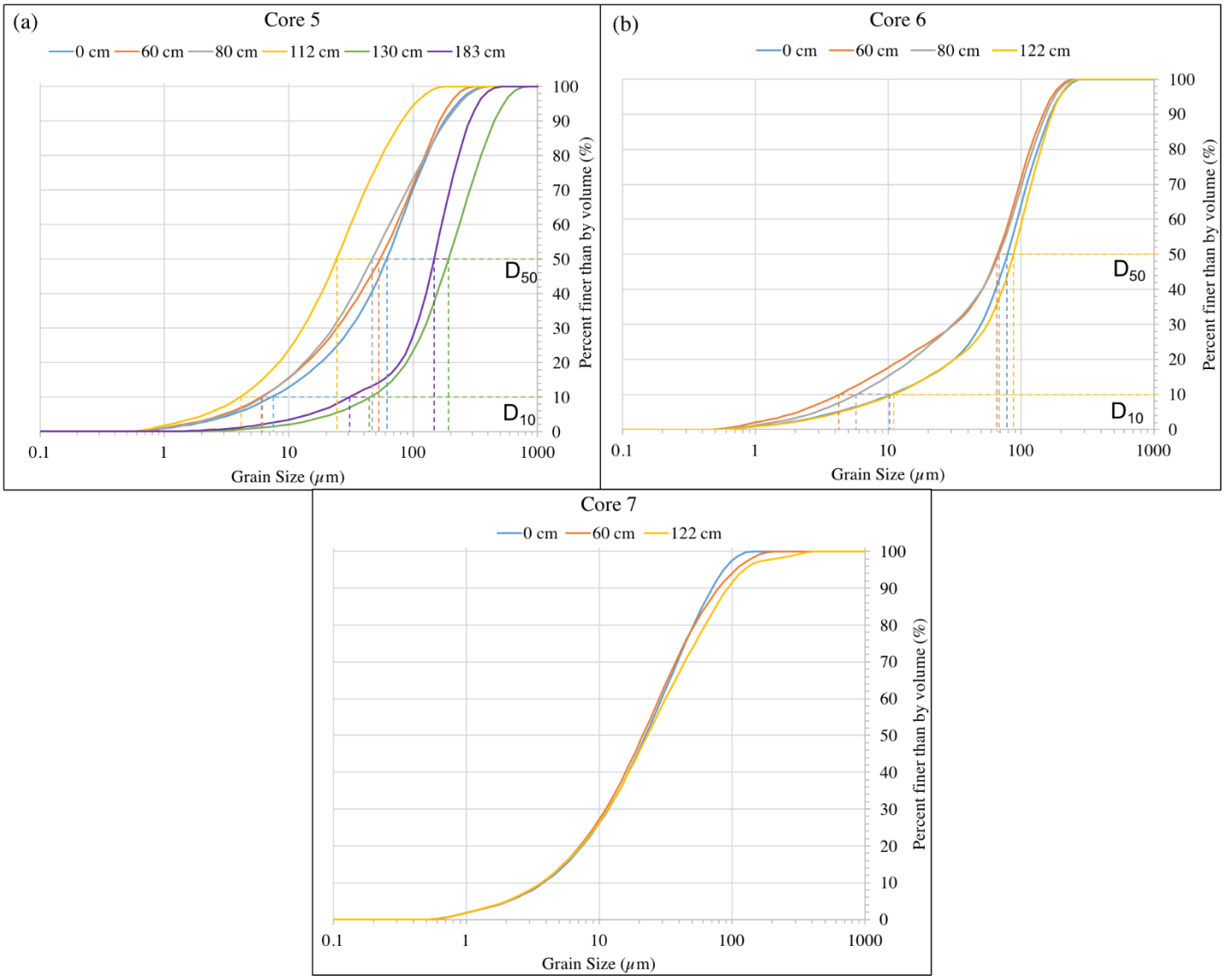

Figure 5.26 Grain size distribution of riverbank sediment (West), as determined by Particle Size Analysis. (a) Core 5 (b) Core 6 and (c) Core 7. Grain Size (μm) is in logarithmic scale.

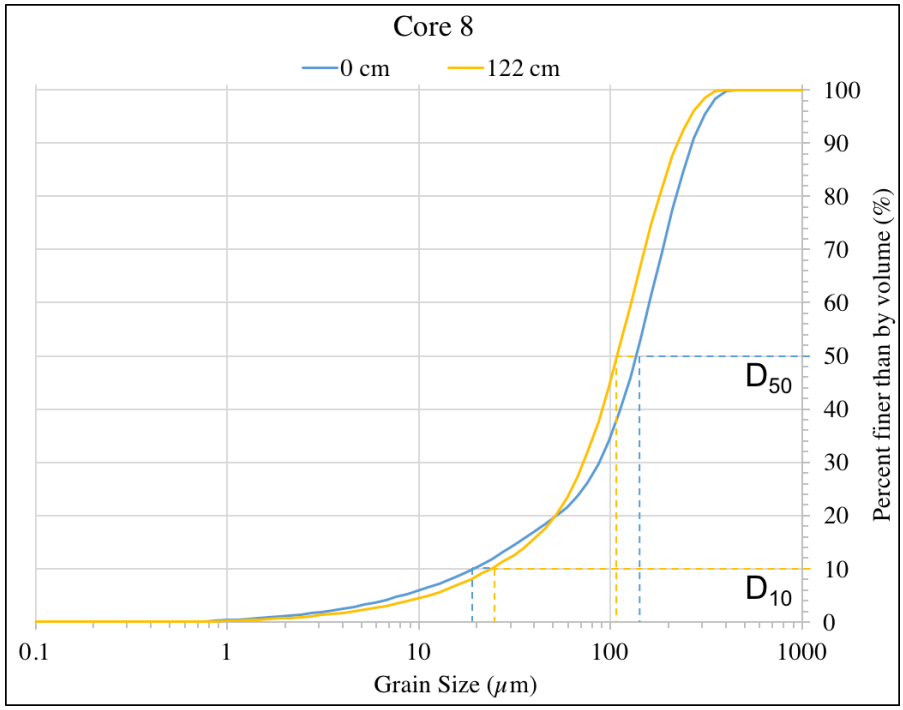

Figure 5.27 Grain size distribution of riverbank sediment for (Island) Core 8, as determined by Particle Size Analysis. Grain Size (μm) is in logarithmic scale.

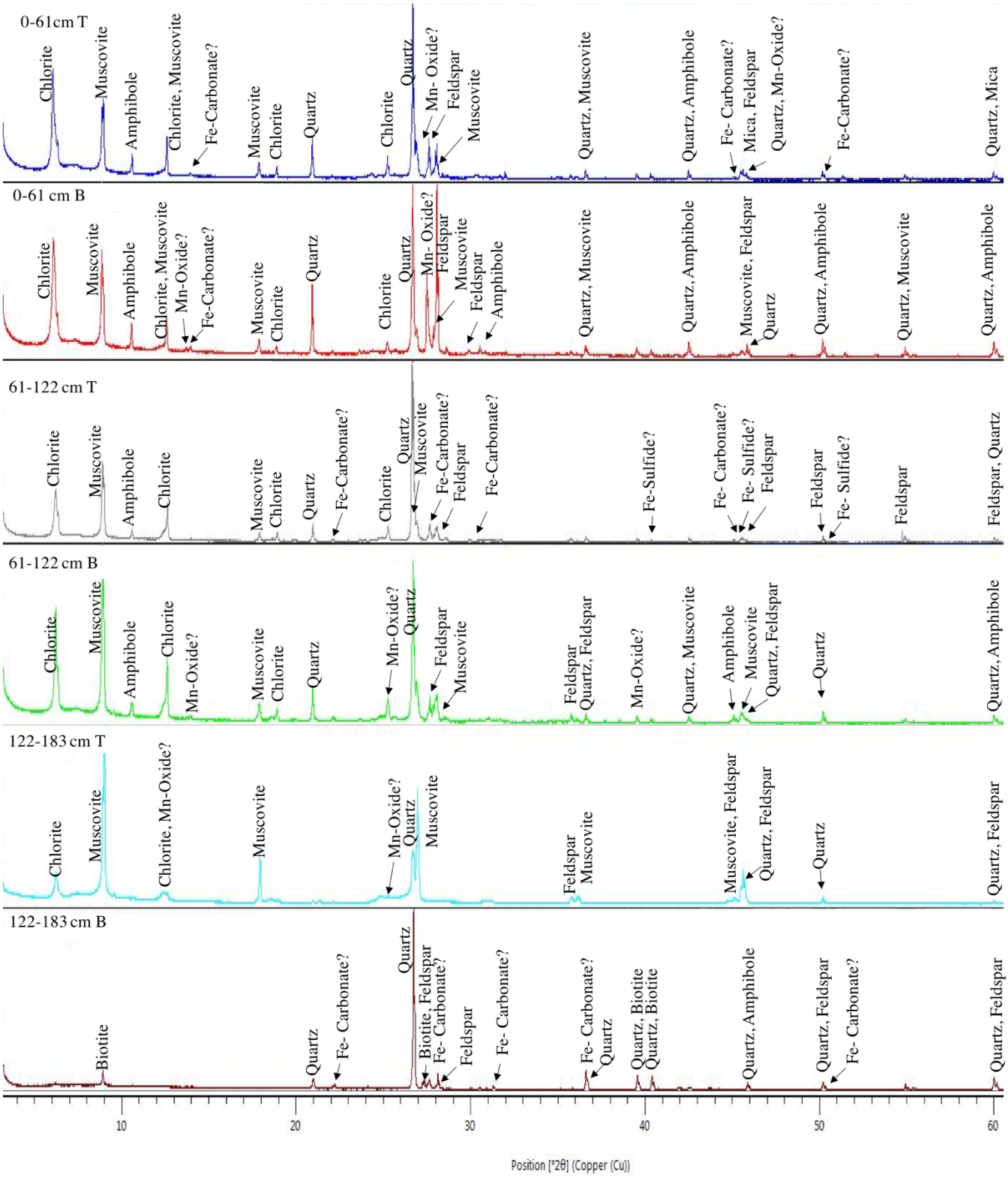

Figure 5.28: Mineral assemblage of riverbank sediment for Core 5 (depth intervals 0-61 cm, 61-122 cm, and 122-182 cm), as determined by X-Ray Diffraction.

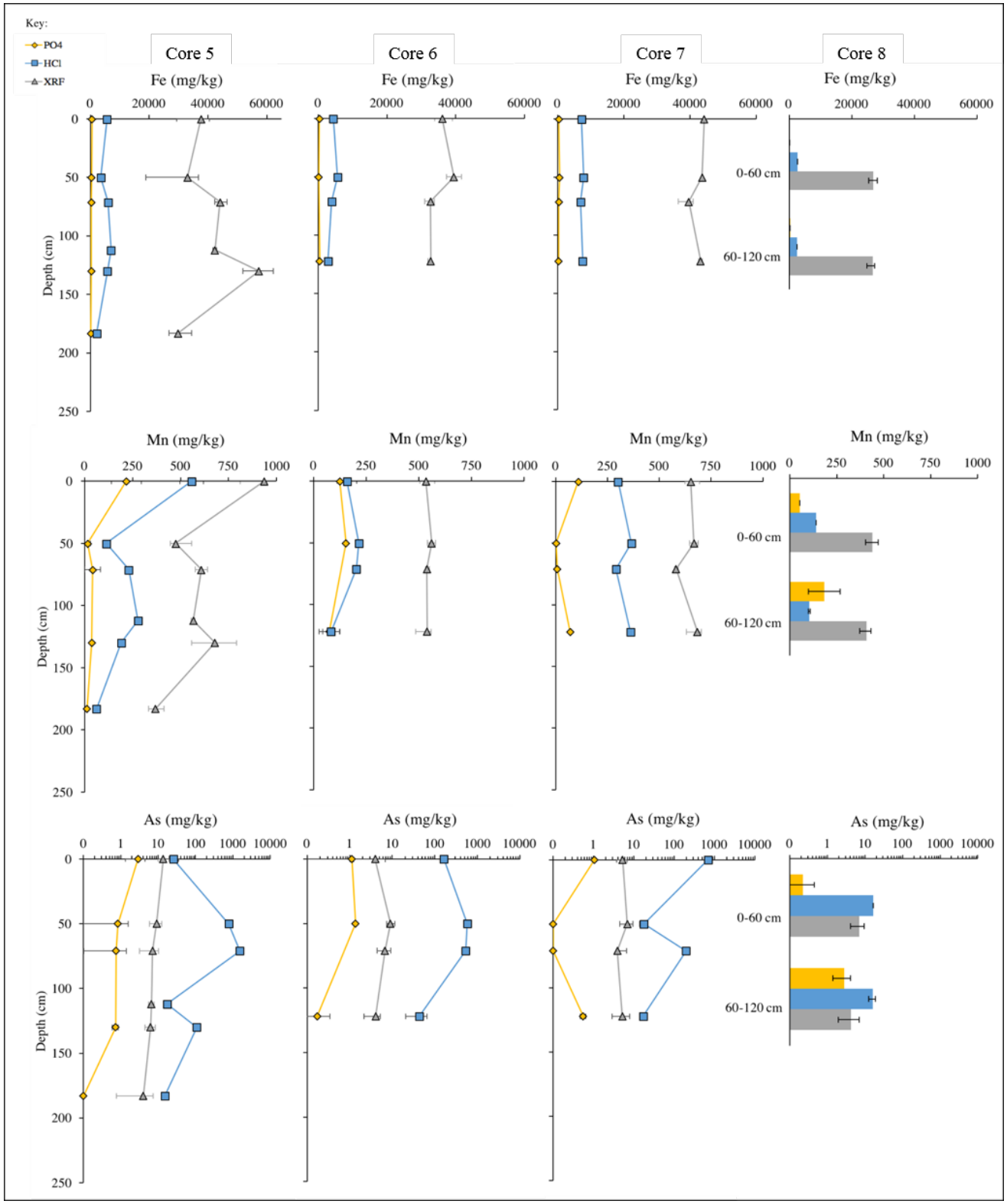

Figure 5.29 Extracted Fe, Mn, and As concentrations (mg/kg) for riverbank sediment (West) (Core 5, Core 6, Core 7) and Island (Core 8). XRF analyses, in gray and two chemical leaching procedures: HCl in blue and Phosphate in yellow.

CHAPTER 6 - Discussion

6.1 Sediment Geochemistry and its Relation to Controlling the Formation of a natural reactive barrier

Solid-phase sediment extractions showed a zone of accumulation of solid phase Fe, Mn, and possibly As between 120 cm and 173 cm on the east bank, and between 0 cm and 120 cm on the west bank. Arsenic extracted by HCl was observed up to ~660 mg/kg on the east bank (Figure 5.25), and up to ~1500 mg/kg on the west bank (Figure 5.29). The 1.2 M HCl extraction targeted co-precipitated As specifically with readily reactive crystalline Fe oxides and oxyhydroxides, Mn oxides as well as acid volatile sulfides, and carbonate minerals (Keon et al., 2001; Datta et al., 2009). It is postulated that solid phase As is associated with crystalline Fe and Mn oxide phases, sulfides or carbonate (Figure 5.24, Figure 5.28), based on the presence of these minerals at depth and the occurrence of elevated As concentrations from the HCl extractions which specifically targets As bound to these phases.

In contrast to HCl extractions, As was leached to much lesser extent via the phosphate and aqua regia extractions (Figure 5.25, 5.29). A maximum of ~10 mg/kg (phosphate) and ~70 mg/kg (aquaregia) was observed on both the east and west riverbanks. Phosphate extractions specifically target As strongly adsorbed to amorphous Fe oxide-hydroxides through the process of ligand exchange (Keon et al., 2001; Jung et al., 2006). With the addition of ascorbic acid, phosphate extractions can target As bound to amorphous hydrous oxides of Fe and Al (Wenzel et al., 2001; He et al., 2010). For ascorbic acid and phosphate extractions, Jung et al. (2006 and 2012), postulates that L-ascorbic acid (anti-oxidant) targets reactive oxygen species and regenerates other antioxidants and liberates sorbed As. Phosphates are used to extract adsorbed phases of As to Fe hydroxides by inner-sphere mechanism because phosphate displaces adsorbed As in the Fe hydroxides. It has been reported that As leached by phosphate extractions to some extent represents only about 10% of total sediment As (Wenzel et al., 2001). Similar concentrations of phosphate extractable As have been found in aquifer sediments with high Fe(II)/Fe ratios (Zheng et al., 2005), in which As was bound to surfaces of Fe-bearing minerals like magnetite, viviantite, siderite or green rust (Saunders and Swann, 1992; Dixit and Hering, 2003). Therefore, we may assume that only a small portion of As in the sediments of our study area is easily extractable by this leaching technique. In addition, an even smaller portion may be bound to refractory phases such as silicates or potentially mobilized due to addition of P or changes in pH (as also seen in Wenzel et al., 2001).

We thus postulate that the solid phase As seen in our sediments, on the west bank may have been bound to crystalline Fe and Mn oxide phases in the natural reactive barrier, such as those that have been tentatively identified at the site using XRD (Figure 6.1, Figure 6.2, Figure 6.3).

Previous studies have documented an enriched layer of solid-phase Fe and As within the top most 1 m of Meghna River sediments (Datta et al., 2009; Jung et al., 2015). The zones of solid phase Fe, Mn, and As enrichment on the east and west banks occurred at the same depths as the tentatively identified Fe-and Mn- oxides. This points to the existence of a natural reactive barrier between 120 -173 cm depth on the east riverbank and between 0-120 cm on the west riverbank at the study site. The sediment has a mineral assemblage of mostly quartz, muscovite mica and some biotite, feldspars (anorthite, albite), amphibole, and some chlorite. Interestingly, and with caution, we state that some Fe and Mn oxides (birnessite and hematite), Fe-carbonates (ankerite and siderite), and Fe-sulfide (possibly in some form of pyrite) were identified at various depths in the sediment cores. These minerals may have been the hosts of sorbed As, as they occurred at the same depths as the spikes in solid-phase As concentration (Figure 6.1, Figure 6.2, Figure 6.3).

Total solid phase As found in our riverbank sediment was lower when compared to previous studies investigating As concentrations in natural reactive barrier sediments in similar floodplain regions for example other locations in Bangladesh (Zheng et al., 2005; Datta et al., 2009; Jung et al., 2015). High values of As extracted from sediments along Meghna banks as previously observed (i.e. up to 23,740 mg/kg; Datta et al., 2009) were not seen at our study area. This may have partly been due to a silt layer capping the aquifer, limiting groundwater discharge (Jung et al., 2015). Jung et al. (2015) identified the formation of the reactive barrier (Fe(III) oxyhydroxides) trapping As in discharging groundwater along the sand-covered riverbank. But the NRB was not formed along the silt-clay covered riverbank, most likely due to limited infiltration of surface water and low groundwater discharge. Particle size analysis at the study site revealed grain sizes (Figure 5.23, Figure 5.26, Figure 5.27) mostly within the silt and sand fraction. Most cores on the east and west banks had grain size distributions that remained relatively constant with depth, except for Core 1 and Core 5. In Core 1 (east bank) there was a sand rich layer on the surface, with less sand fraction at depths 130-193 cm (Figure 5.23). Core 1 showed HCl extracted As concentrations that were higher at the bottom of the core between 130-244 cm depth (Figure 5.25). In Core 5 (west bank) the sand fraction increased with depth towards the bottom (Figure

5.26). This demonstrates how grain sizes can influence development of a natural reactive barrier and the extent of sediment As enrichment.

The extraction methods may have also contributed to lower observed As concentrations. A major limitation for any extraction procedure is re-adsorption of As on remaining mineral phases (Tipping et al., 1985; Kheboian et al., 1987; Wenzel et al., 2001). All of the extraction methods used in this study are semi-quantitative (Tessier et al., 1979). For extractions targeting amorphous and crystalline forms of hydrous Fe oxides, using acidified 0.25 M $NH_2OH{\cdot}HCl$ (Wenzel et al., 2001), As recovery can be reduced in the presence of goethite, indicating re-adsorption onto goethite surfaces (Wenzel et al., 2001). This process of re-adsorption may have contributed to the low As concentrations extracted from the sediments during the aquaregia digestion. Regardless, it is apparent that As in the subsurface sediments is sorbing sorbed to crystalline Fe oxides and oxyhydroxides and possibly Mn- oxides.

Iron oxide minerals, ferrihydrite, hematite (Akai et al., 2004), and goethite (Akai et al., 2004; Rowland et al., 2008; Datta et al., 2009; Postma et al., 2010), and other Fe-bearing minerals such as biotite, hornblende, magnetite and vivantite (Datta et al., 2009) have been identified in shallow aquifer sediments in Bangladesh, West Bengal, and other similar deltaic environments. At our study site we tentatively identified Fe- and Mn-bearing oxides in the shallow subsurface (Figure 5.24, Figure 5.28). As previously mentioned, the more As in the subsurface sediments is associated with minerals that could be leached with HCl, as opposed to phosphate and aqua regia extractions, suggesting that As is mostly sorbed to crystalline Fe oxides and oxyhydroxides (Figure 6.1, Figure 6.2, Figure 6.3). It is possible that the As-enriched Fe oxides could be formed by oxidation of Fe^{2+} and As^{3+} near the top of the hyporheic zone (Breit et al., 2004, Datta et al., 2009). The exposure of As to oxidants such as O_2 may enable bacterial oxidation and co-precipitation. Arsenic also may be bound to the Fe oxide minerals through a ligand exchange method. In ligand exchange, the As oxyanion competes and exchanges with surface-OH or $-OH_2$ groups that are directly coordinated to structural Fe^{3+} at the Fe oxide surface. The general reaction leading to As sorption, possibly seen at the study site, is demonstrated below:

1. Fe (II) oxide + oxidant → Fe (III) oxide
2. Fe (III) oxide + As (II) → Fe (III) oxide-As (III)

If this is the case, a possible oxidant would be O_2. As a result of As sorption, we would expect to see a decrease in dissolved As concentrations along the groundwater flow path to the river as As is removed from the groundwater and adsorbed onto the solid phase. The active removal of dissolved As from groundwater as it passed through the natural reactive barrier was observed in a study conducted parallel to ours at the same study location (Berube et al., In Review). Berube et al. (In Review) is further discussed in detail in Sections 6.2 and 6.3. It is possible that As was removed from the groundwater and incorporated into Fe^{3+} minerals/oxides within the natural reactive barrier (Ebinger and Schulze, 1990; Jung et al., 2015).

Many studies have found evidence to support the existence and formation of natural reactive barriers (Datta et al., 2009) or "iron curtains" (Charette and Sholokovitz, 2006) along major river hyporheic zones. natural reactive barriers allow for the sequestration of As on Fe-oxide and hydroxide minerals present in the sediments (Datta et al., 2009; Jung et al., 2012; Jung et al., 2015, Berube et al., In Review). The conditions of discharging reducing groundwater interacting with oxic river water favors the trapping of groundwater As onto the Fe^{3+} oxyhydroxides in the reactive barrier at this site (Knappett et al., 2016). A large flux of anoxic groundwater, high in Fe^{2+} and As, discharges from the floodplain aquifers towards the river. The groundwater mixes with the oxic river water and amorphous and crystalline iron oxides will precipitate and incorporate As along the natural reactive barrier (as seen in Datta et al., 2009; Jung et al., 2015; Knappett et al., 2016, Berube et al., In Review). Postma et al., 2010 and Stahl et al., 2016 both observed enriched As and Fe layer in river sediments, attributed to redisposition.

The distribution of Fe, Mn, and As in the natural reactive barrier illustrates a step in the dynamic redox cycling of As to and from the Fe- and Mn-rich sediments. This raises the question of how long it actually takes to accumulate these elements in the natural reactive barrier sediments. It has been postulated that buildup of As up to these concentrations can take up to hundreds or thousands of years (Jung et al., 2015). Redox cycling, seasonality, Fe, Mn, and As concentrations in groundwater and sediment, all contribute to the sorption and release of As from the sediments to groundwaters. The possible mechanisms of As mobilization and contamination in groundwater at this study site are discussed in detail in Section 6.3, but first we must understand the groundwater characteristics at our study site, and how these may contribute to As cycling.

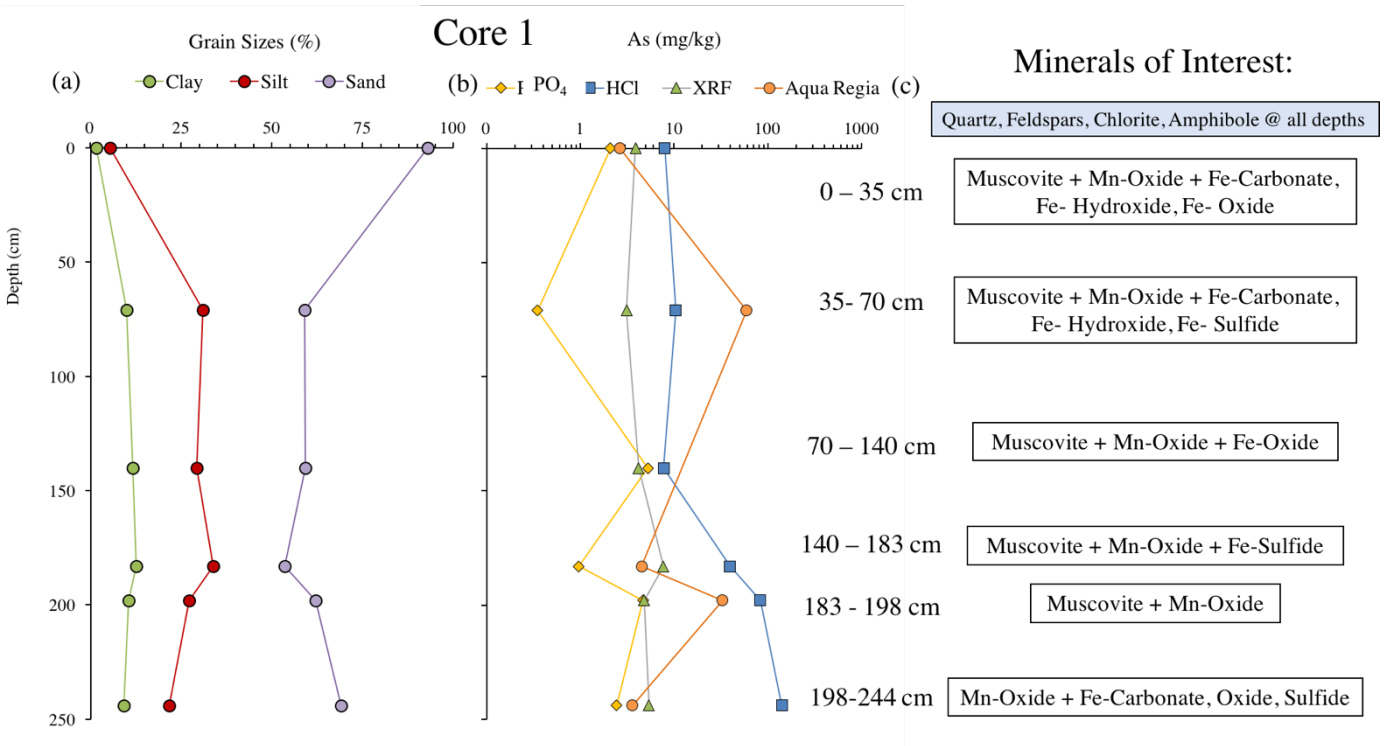

Figure 6.1 (a) Core 1 grain size distribution (b) XRD mineral assemblage, and (c) riverbank sediment As concentrations (mg/kg). XRF analyses, in gray and 3 chemical leaching procedures: Aquaregia in orange, HCl in blue, and Phosphate in yellow.

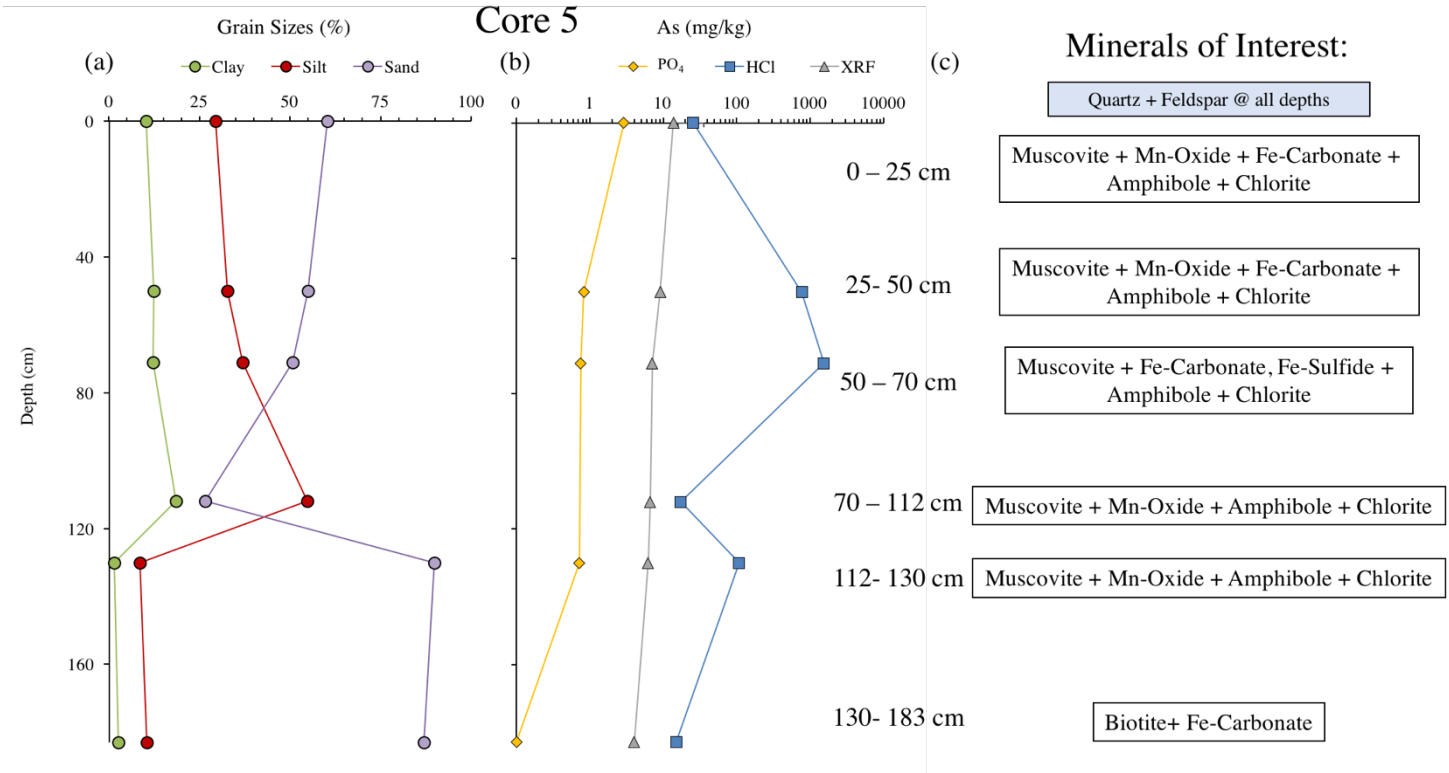

Figure 6.2 (a) Core 5 grain size distribution, (b) XRD mineral assemblage, and (c) riverbank sediment As concentrations (mg/kg). XRF analyses, in gray and 3 chemical leaching procedures: Aquaregia in orange, HCl in blue, and Phosphate in yellow.

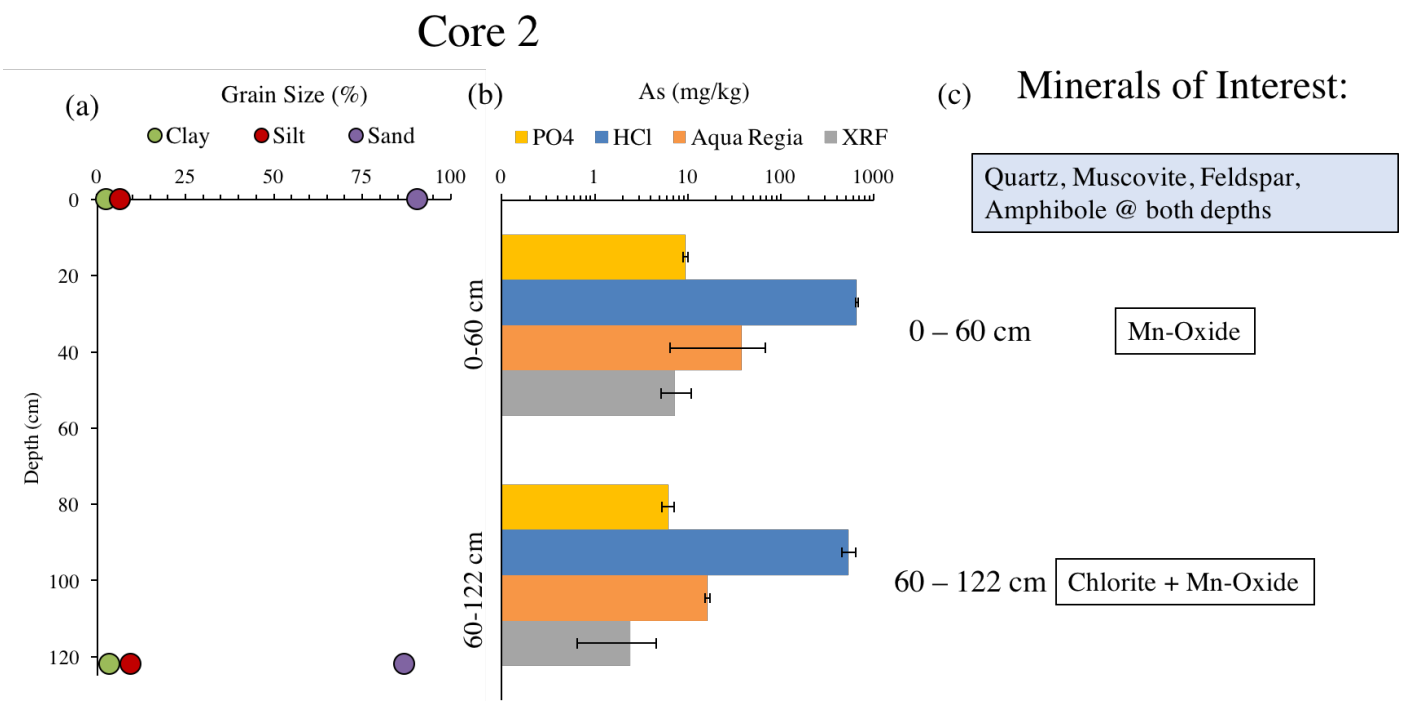

Figure 6.3 (a) Core 2 grain size distribution, (b) XRD mineral assemblage, and (c) riverbank sediment As concentrations (mg/kg). XRF analyses, in gray and 3 chemical leaching procedures: Aquaregia in orange, HCl in blue, Phosphate in yellow.

6.2 Shallow vs. Deep Groundwater Characterization

In general, groundwater well samples on the east bank had similar characteristics to those on the west bank. Differences in overall chemical signature, redox state, organic matter characterization, and ion concentrations were observed between shallow (<30 m) and deep (>30 m) groundwater, most likely due to the hydro-geochemical division of the shallow and deep aquifers in this region. On the east side of the river there were five shallow wells with higher Cl^- and Br^- concentrations relative to the other samples on the east bank, and on the west bank there were four shallow wells with elevated F^- relative to the other samples on the west bank. Concentrations of elements may be affected by the presence of different minerals, possibly carbonates, their stability fields, and weathering rates along groundwater flow paths. Relative to the deep groundwater samples, shallow groundwater in this study had higher concentrations of cations (NH_4^+, Ca^{2+}, K^+ and Mg^{2+}) and anions (S^{2-}, NO_3^-, Cl^- and Br^-), possibly due to infiltration of surface water to the shallow groundwater. Zheng et al. (2004), found most of their shallow depth samples from southeast Bangladesh were characterized by high bicarbonate concentrations, close

to saturation with respect to calcite, and low in dissolved O_2. Highest concentrations of total dissolved Fe (up to ~10 mg/L), Mn (up to ~4 mg/L), and As (up to ~500 mg/L) were found in the shallow groundwater (<30 m). This indicates that shallow groundwater, is enriched in ions and highly contaminated by dissolved As (Figure 5.5).

δ^2H and $\delta^{18}O$ variations of groundwater at our study site were shown to closely follow that of the meteoric water line, suggesting recharge during the wet season without much evaporation (Figure 5.7) (as in Ahmed and Burgess, 1995; Zheng et al., 2004; Barua, 2015). All groundwater samples fell below the Local Meteoric Water Line (LMWL), indicating that the groundwater recharge originates from local rainfall and surface water bodies, with or without evaporation (Ahmed and Burgess, 1995; Zheng et al., 2004; Majumder et al., 2011). There were no significant differences in isotopic signature observed for the east groundwater sites verses the west groundwater sites. Isotopic signatures of shallow groundwater on the east bank were similar to those on the west bank, and the same was seen for the deep groundwater (Figure 5.9). Infiltration of surface water as recharge for groundwater has also been seen in previous published works from this region. Surface water contamination could also possibly account for the elevated cations and anions observed in the shallow groundwater (Figure 5.1, Figure 5.3). The groundwaters sampled in this study had hydrogen (δ^2H) isotope ratios ranged from -38 to -11‰ and stable oxygen ($\delta^{18}O$) isotope ratios that ranged from -6 to -2.5‰ (Figure 5.8). A trend with depth was observed for the δ^2H and $\delta^{18}O$ averages (Figure 5.8). The δ^2H and $\delta^{18}O$ averages for shallow groundwater (<30 m) were less negative then the deeper aquifers (>30 m). The two deepest samples (>80 m) showed even more negative values for δ^2H and $\delta^{18}O$ with averages of -31 and -5‰, respectively (Figure 5.8). More negative oxygen isotope values trending with depth from the shallow to deep well samples (Figure 5.8) may suggest progressive depletion of the vapor mass and precipitation by the condensation process. $\delta^{18}O$ values suggest possibly the recharge source for the deep more depleted groundwaters could be from the coast or further up in elevation. Burgess and Hoque (2012), believe the deeper aquifers east of the Meghna are recharged from the Tripura hills in India which are higher in elevation, than the floodplains that recharge the shallow aquifers.

Redox conditions directly control the release of As to groundwater, especially in the reduction of Fe-oxyhydroxides (Nickson et al., 2000). High aqueous As concentrations are accompanied by reduced conditions, particularly those in which reduced Fe is high as well (Figure 5.5). Oxidative Redox Potential (ORP) is critical in predicting the states of chemical species in the

water, such as dissolved metals. ORP measures the capacity of water to either release or accept electrons from chemical reactions. Negative ORP values indicate a reducing environment and a positive ORP values indicate an oxidizing environment. Overall, ORP shows moderate to highly reduced groundwater conditions on both the east and west groundwaters. ORP values of groundwater on the west bank ranged from -3.9 to -141 mV and on the east bank ranged from -46 to 200.5 mV. Shallow groundwaters (<30 m) were more reducing, whereas deep aquifers (> 30 m) seemed to be less reducing, and in some cases, slightly oxidizing. The dissolved oxygen was very low in shallow aquifers, ranging mostly between 0-1 mg/L and slightly higher (up to 3 mg/L) in deeper aquifers. The cause of low As in deep groundwaters has been attributed partially to these waters not being sufficiently reducing (Zheng et al., 2004), as seen by the ORP values in this study.

The hyporheic zone has been shown to extend a maximum of 50 m away from the river at the Veast site (Knappett et al., 2016; Berube et al., In Review). An additional study (Berube et al., In Review) conducted in parallel with ours, looked closely at the hyporheic zone chemistry, and interactions on a smaller scale, up to 50 m away from the river. Shallow drive point piezometer wells were installed on the east river bank in a transect running parallel to the east groundwater transect (TWeast) from the study site, starting at Veast2 and moving towards the river (Figure 4.2, Figure 4.3). Changes in dissolved ion concentrations and redox signatures along the groundwater flow path on the east bank were measured. Hydraulic gradients were measured over the course of two years and it was found that under natural, dry season conditions lateral gradients across the 85 m transect varied from nearly flat at high tide, to quite steep at low tide (Berube et al., In Review). In the discharge zone under the seepage face, reversals in vertical hydraulic gradients were observed from losing conditions (downward flow) during the peak river height to gaining conditions (upward flow) in the trough. Evidence of river water mixing with groundwater up to 50 m way from the river was discovered, and two zones of mixing were identified (Berube et al., In Review). The first mixing zone was the natural reactive barrier or recent river water mixing, which extended about 3 m below the seepage face and 10-20 m laterally. The natural reactive barrier was characterized by temperature and ORP that was intermediate between the warm, reducing aquifer and the colder, oxidizing river.

6.3 Extent of Sediment and Groundwater Interactions

Field work for this study, as well as the study conducted in parallel (Berube et al., In Review), was performed during the dry season. At this point during the dry season, the river was

under gaining conditions. During gaining conditions, the aquifers drain towards the river. As this happens the dissolved As draining from aquifers may get trapped as is it sorbs to Fe- bearing minerals in the natural reactive barrier sediments. Enrichment of As in shallow subsurface riverbank sediment along the Meghna River has been attributed to redox trapping of groundwater As by Fe^{3+} oxyhydroxides precipitated in the hyporheic zone during the dry season when the hydraulic gradient drives groundwater flow from the aquifer to the river (Datta et al., 2009; Jung et al., 2012, 2015; Berube et al., In Review). This may be a process occurring at our site, which explains the sediment Fe, Mn, and As enrichment along the Meghna. Higher As concentrations, up to 660 mg/kg (east bank) and up to 1500 mg/kg (west bank), were observed in zones interpreted as natural reactive barriers (Figure 5.25, 5.29). The As accumulation in the sediments may occur all throughout the dry season, until the conditions shift, from gaining to losing at the start of the monsoon season. During losing conditions, the hyporheic zone invades more towards the aquifers, carrying with it the suboxic natural reactive barrier Fe-As oxide complexes (Knappett et al., 2016). The built-up As may then be re-mobilized into the aquifer, possibly by reductive dissolution of Fe minerals (Nickson et al., 1998, 2000; McArthur et al., 2001; Bhattacharya et al., 2002; Harvey et al., 2002; Anawar et al., 2003; McArthur et al., 2004; Datta et al., 2009). However, this method is still debated and it is important to consider all processes and interactions that may be active along the groundwater flow path.

Elevated dissolved As has been primarily attributed to reductive dissolution of secondary Fe-(oxy)hydroxide minerals (authigenic goethite, ferrihydrite, and amorphous Fe(oxy)hydroxides) (Bhattacharya et al., 1997; McArthur et al., 2001; Uddin et al., 2001). Nonetheless, previous studies have attributed oxidation of As-rich pyrite as the mechanism for mobilizing As in groundwater, due to pumping and water table drawdown causing more oxidizing conditions. This suggests that As sorbs to authigenic pyrite in aquifers (Lowers et al., 2007), and would be mobilized by competitive displacement of PO_4^{3-} (Mallick and Rajgopal, 1995). In addition, chemical weathering of detrital basic minerals such as biotite (Seddique et al., 2008; Itai et al., 2008) or chlorite (Masuda et al., 2012) in the aquifer, due to the enforced infiltration of surface water, is a possible mechanism for releasing As into the aquifer. These studies found results that contradict the reduction-dissolution of As-bearing Fe oxyhydroxides: higher As concentrations in groundwater with low dissolved Fe and high ORP (Masude et al., 2008). Sequential extractions of aquifer sediments in Seddique et al. (2008), revealed that most of the As was fixed in silicates in

the sandy aquifer and biotite was presumed to be a host phase of As and weathering of biotite was the proposed mechanism for As release into groundwater.

Low ORP in the shallow groundwaters supports the reductive dissolution of Fe-oxides as the possible primary source of As in our groundwater. However, multiple processes may be responsible for As accumulation in groundwater, depending on the redox conditions and minerals present in the sediments. Thus some of the dissolved As present in our groundwaters may be due to chemical weathering of chlorite or biotite. These mechanisms of As mobilization and accumulation in groundwaters are extensively studied and debated due to the complexity of Fe, As, and S biogeochemical cycles (Zheng et al., 2004). There is also the possibility of re-oxidation and re-mobilization of sequestered As from adsorbed phases (Mukherjee, 2006). A number of additional factors, not described in detail here, can contribute to desorption of As in groundwater. These include ligand exchange and ligand enhanced dissolution of Fe-oxides and sulfides. Thus, further investigation is required to determine the dominant processes at this study site. However, as previously mentioned, the more recent consensus for mobilizing sorbed As is reductive dissolution of metal oxides and hydroxides (FeOOH/hydrous ferric oxides and Mn oxides and hydroxides) (Bhattacharya et al., 1997; McArthur et al., 2001).

At our study site, Knappett et al. (2016) has shown that seasonal fluctuations in water level, changing hydraulic gradients and seasonal irrigation pumping influence the extent of mixing and geochemical conditions of the hyporheic zone. Hyporheic zone exchange is a significant component of stream flow and groundwater interactions (van Geen et al., 2013; Stahl et al., 2016; Knappett et al., 2016). Berube et al., In Review, found evidence of river mixing with groundwater up to 50 m away from the river in the natural reactive barrier (recent water mixing). The chemistry of the hyporheic zone on the east bank of this study site changes throughout the year based on gaining or losing conditions of the river, induced by irrigation pumping and early monsoon levels (Knappett et al., 2016).

Human activities may contribute to reversing the natural hydraulic gradients in gaining rivers in deltas (Larsen et al., 2008), such as large scale groundwater pumping for irrigation (Harvey et al., 2006) or municipal uses (Knappett et al., 2016; Stahl et al., 2016). Gaining rivers accumulate Fe, Mn, and As as discharging reducing groundwater interacts with oxic river water, as seems to be occurring at multiple study sites along the Meghna River banks (Jung et al., 2012; 2015; Knappett et al., 2016; Berube et al., In Prep). These conditions favor the trapping of

groundwater As onto the Fe^{3+} oxyhydroxides in the natural reactive barrier that expands through fluctuations in river level. A large flux of anoxic groundwater, high in Fe^{2+} and As, discharges from the floodplain aquifers towards and mixes with the oxic river water such that iron oxides precipitate and become incorporated into the natural reactive barrier (Datta et al., 2009; Postma et al., 2010; Jung et al., 2015; Knappett et al., 2016). During losing conditions the natural reactive barrier and hyporheic zone expand further into the floodplain aquifers and changing redox conditions allow for the release of As to groundwater through reductive dissolution. Organic matter present in the groundwater may contribute to the reduction of Fe oxides; this is largely driven by bacterially catalyzed oxidation of OM (Bhattacharya et al., 1997; McArthur et al., 2001).

Kinetic sorption reactions and OM are significant in controlling the mobility of As in the environment, further discussed in Section 6.4 and 6.5. The profiling of Fe, Mn, and As concentrations in sediment and mineral assemblage in riverbank sediments from cores along the Meghna River sheds light on the sources and destination of As in sediments and groundwater in the GBMR system. A zone of Fe, Mn, and As between 120 cm and 173 cm on the east bank and between 0 cm and 120 cm on the west bank, was identified, possibly associated with crystalline Fe and Mn oxides phases, tentatively identified at this site (Figure 5.24, Figure 5.28). Thus it is likely that As and Mn are incorporated into Fe^{3+} minerals/oxides by replacing Fe in mineral structures within the natural reactive barrier at the study site. Reductive dissolution of Fe-oxides containing sorbed As may be occurring in the shallow groundwater and is possibly microbially driven. These two As cycling mechanisms may be causing the elevated As concentrations in our shallow groundwater (Berube et al., In Review).

6.4 Characteristics of DOM and its relation to Arsenic Release from Sediments

6.4.1 DOM Properties and Sources of DOM in Waters

Organic carbon occurs as a result of decomposition of plant or animal material. Organic matter present in soil or water may then dissolve when contacted by water (DOC). This DOC moves with both ground and surface waters. Based on OM characterization, shallow groundwaters on the east bank (<30 m) were found to contain microbial and terrestrial-derived DOC, with decomposed, more humified, and aromatic OM (Figure 5.12, Figure 5.13, Figure 5.14). Deep groundwater on the east bank (>30 m) was found to contain mostly microbially derived DOC, with fresher, less humified and less aromatic OM. On average, shallow groundwater had higher DOC concentrations than deep groundwater (Figure 5.11). High flow rates may increase DOC concentration in the shallow groundwater, due to increased runoff and infiltration through shallow organic-rich soils. DOC is expected to be lost to microbial respiration as the water ages (Mladenov et al., 2009), possibly contributing to the low DOC concentrations seen in the deeper aquifers (Figure 5.11). Also, rainfall and runoff distribution may affect DOC production and transportation. The O- and H-isotopes ratios (Figure 5.8) support infiltration of surface water to shallow groundwaters.

Previous studies have found that DOC concentrations tend to be substantially higher in shallow groundwater than in deeper groundwater (Sutton et al., 2009; Datta et al., 2011; Sankar et al., 2014; Barua, 2015). It has been found that low DOC concentrations in deep Pleistocene aquifers of the Bengal Basin may limit the release of As from those sediments, whereas high DOC concentrations in shallow Holocene aquifers in the Bengal Basin may enhance As mobility from sediments (Postma et al., 2007; Harvey et al., 2002; Berg et al., 2008; Fendorf et al., 2010). This suggests that the shallow groundwater sample may be from Holocene aquifers and deep samples may be from Pleistocene aquifers. However, no dating of sediments was completed in this study, and the Holocene and Pleistocene aquifers are not well defined in this region of southeast Bangladesh, so it cannot be confirmed whether the shallow aquifers are actually Holocene. However, negative ORP values and low DO in shallow aquifers, compared to higher ORP values in the deeper aquifers, further suggests that the shallow aquifers might be Holocene, and the deep aquifers may be Pleistocene.

Fluorescence Index (FI) provides an indication of the type of microbial activity occurring in both shallow and deep aquifers (Figure 5.12). The FI in shallow groundwater and river water

from this study ranged from 1.5 to 1.7 and in deep groundwater ranged from 1.6 to 1.9 (Figure 5.12). Lower values of FI (~1.3-1.4) indicate terrestrial sources of DOM while higher values (~1.7-1.9) indicate microbially derived DOM (McKnight et al., 2001; Cory and McKnight, 2005). This points to microbially derived DOM in both the shallow and deep aquifers, but with a contribution from terrestrial sources of OM in the shallow aquifers and river water (McKnight et al., 2001). S_R values were <1, consistent with terrestrial sources of DOM in the shallow aquifer and river water (Figure 5.15). Terrestrial sources of OM (terrestrial plant and soil OM) are present in the shallow groundwater, with some microbial sources, possibly extracellular release and leachate from bacteria. A possible source of the terrestrial OM in the shallow aquifers could be humic substances leaching from surface soil (Soderberg, 2013). Wastewater influencing the shallow aquifers would account for the microbial influence of OM (Mladenov et al., 2009). Infiltration from surface water recharge is a probable source for the OM in shallow aquifers (Figure 5.8). Microbially derived OM dominates in deep groundwaters. Deep groundwater has less potential to mix with surface water, so microbially derived OM was expected in that case.

Based on the freshness index, humification index and absorbance intensity the shallow groundwaters contain fresher OM (Figure 5.13), more humic OM (Figure 5.14), more aromatic OM (Figure 5.16). Humification index is an indicator of humic substances and extent of humification. Low humification and freshness index in deep groundwater and river water indicates that the DOC in the deep aquifers and river water has a less humic component. Low absorbance index in both river water and deep groundwater indicates that aromaticity is high only in the shallow groundwaters. Plant dominated DOM and reduced sedimentary peat, or other dispersed sedimentary organic carbon, could be significant sources of the aromatic DOM in shallow groundwater (Mladenov et al., 2009).

Looking at OM characteristics of groundwater with increasing distance from the river may provide insight to mixing, source, and evolution of OM in aquifers near the river (<500 m) verses farther away from the river (>500 m). It was observed that, on the east bank, aquifers within 500 m of the river had a different DOM signature than the groundwater farther away (>500m). Taking only distance from the river into consideration, groundwater OM was more decomposed, humified, and aromatic as distance from the river increased. These observations might be due to the proximity of the samples to the river and interaction with the hyporheic zone. Fluorescence index indicated that the groundwater OM became more terrestrially-derived as distance from the river to

the east increased (Figure 5.12), possibly indicating higher extent of vertical infiltration from surface water at sites farther away from the river.

Furthermore, taking into consideration peaks A, C, and M (humic-like, terrestrial derived OM), and B and T (protein-like, microbial derived OM), from the fluorescence spectroscopic studies (Figure 5.18, Figure 5.19), differences were observed for the shallow (<30 m) vs deep aquifers (>30 m). Shallow groundwater was found to have higher humic peaks (A, C, M) (Figure 5.18). Peaks A and C are considered to be derived primarily from vascular plant sources, aromatic in nature (Coble et al., 1998). Based on Figure 5.19 there were no significant trends in protein peaks (B and T) between the shallow and deep groundwater. However, looking closely at peak T (Tryptophan-like) in Figure 5.19, there was slightly higher tryptophan in shallow groundwater. This was surprising because previous studies have found a higher protein signature in deep groundwaters because of the microbial activity and dominance of microbially derived DOM (Kulkarni, 2016). The presence of tryptophan-like components in shallow wells may suggest the presence of some labile organic carbon derived from microbial sources (pond microbial organic compounds: bacteria and algae).

Collectively these data suggest a greater presence of humic and aromatic material, with a combination of terrestrial and microbially derived OM in shallow groundwater (>30 m). Whereas deep groundwater (>30 m) was less humic and aromatic, with a mostly microbially derived OM.

6.4.2 Role of DOM and Arsenic Release from Sediments

Dispersed sedimentary OM has been suggested as a source of labile DOM to fuel microbial reactions in the reducing aquifers of Bangladesh (Mladenov et al., 2009), although the process of mobilization of sedimentary OM has not been directly demonstrated in these environments. High humic-like OM in the shallow aquifers of the Ganges Brahmaputra Meghna River delta may point to OM becoming more reactive due to increased functional groups (Wolt, 1994; Ohno, 2002), or an OM source that may participate in humic DOM-stimulated reductive dissolution (Ohno, 2002; Zsolnay, 2003; Mladenov et al., 2009; Kulkarni 2016). Humic substances have been known to be involved in complexation reactions with Fe and As, competition with As for sorption sites, and electron shuttling reactions (Lovley et al., 1996; 1998; 1999; Scott et al., 1998; Klapper et al., 2002; Bauer and Blodau, 2006; Jiang et al., 2008; Wolf et al., 2009; Sharma, 2010; Mladenov et al., 2010; Liu et al., 2011; Kulkarni, 2016).

A dual role of natural DOM in Bangladesh aquifers has been established by Mlandenov et al. (2009). First, DOM is a labile substrate for Fe and humic reducing bacteria and second, DOM is an electron shuttle via humic substances to enhance microbial Fe reduction. The presence of humic, terrestrial DOM, as seen in the shallow wells, may enhance the reactions that contribute to As mobilization and accumulation in groundwater (Wang and Mulligan, 2006; Mlandenov et al., 2009; Mikutta and Kretzschmar, 2011; Kulkarni, 2016). Furthermore, as seen in Mladenov et al. (2015), associations between dissolved As, Fe, fulvic acid concentration and fluorescence properties of isolated fulvic acids (FA) suggest that aromatic, terrestrially derived fulvic acids promote As–Fe–FA complexation reactions that may enhance As mobility. It is possible that the process of enhanced As mobility due to aromatic, terrestrially derived humic OM substances (Mladenov et al., 2015) are enhancing As mobility in the groundwaters at our study site.

The vertical and lateral extent of the hyporheic zone has the potential to impact the characteristics of OM in the aquifers. Organic matter serves as an electron shuttle and enhances the reductive dissolution process under reducing conditions. Kulkarni (2016) recently suggested that As can bind with non-aromatic portion of the humic-like DOM under reducing conditions and increase its solution concentrations (Kulkarni, 2016). The influence of the hyporheic zone interactions on OM (fulvic acids) and other redox acid species has been investigated in a few of studies (Wang and Mulligan, 2006; Miller et al., 2009). Both DOC, OM, and N dynamics may be influenced by hyporheic zone interactions, and changing hydraulic gradients. Fluorescence spectroscopy of OM specifically, humic substances and fulvic acids, have provided insight into redox reactions in aquifers as well in dynamic hyporheic zone catchment systems. Hyporheic zone exchange is an important process in determining energy flow, electron transport in ecosystems (Miller et al., 2009). It has been suggested that fulvic acids are involved in rapid electron-transfer processes in and near stream channels and may be important in determining ecological energy flow (Miller et al., 2009, Kulkarni, 2016). It has also been determined that electron transport and rates of electron shuttling in aquifers may significantly contribute to As mobilization (Scott et al., 1998; Klapper et al., 2002; Jiang et al., 2008; Wolf et al., 2009; Mladenov et al., 2009, 2010, 2015; Kulkarni, 2016). The high As concentrations and presence of decomposed, humified and aromatic DOM and high amounts of DOC in shallow groundwater aquifers at this study site supports the hypothesis that presence of humic substances contribute to As mobilization.

There is broad consensus that microbial reduction of Fe^{3+} oxides, containing As, results in the mobilization of As into the dissolved phase in the presence of labile organic carbon where humic like organic matter aides in electron shuttling, reducing the Fe minerals (Scott et al., 1998; Klapper et al., 2002; Jiang et al., 2008; Wolf et al., 2009; Mladenov et al., 2009, 2010, 2015; Kulkarni, 2016). Reductive dissolution requires the breakdown of a mineral as a result of a reduction process, which involves the consumption of electrons by the mineral, causing the mineral to release the sorbed As. Mineral (hydro)oxides may act as a surface catalyst or as an electron-transfer intermediate. Arsenic release may be enhanced by the redox reactions between natural organic matter (NOM), As and substrates, resulting in the reduction of As^{+5} to the more mobile As^{+3} phase (Figure 6.4 (Process B)) (Wang and Mulligan, 2006). Microbial reduction of OM is one of the proposed methods that is responsible for the dissolution of iron minerals and arsenic release in aquifers under reducing conditions. Microbial reduction of OM prompts the reduction of Fe oxides, like FeOOH, from Fe^{3+} to Fe^{2+} and thus the release of sorbed As into the groundwater. The following chemical equation demonstrates the process of reductive dissolution:

$$\text{Fe(III) oxide-As(V)} + e^- \rightarrow Fe^{2+} + \text{As(V), As(III)}$$

Microbial reduction of OM, under reducing conditions, is one of the proposed methods responsible for the dissolution of Fe minerals and As release in aquifers. In a reducing environment, the electron donor for reduction of Fe^{3+} oxides and hydroxides can be OM in sediments (Figure 6.4 (Process C)) (Nickson et al., 2000; McArthur et al., 2001; BGS, 2001; Dowling et al., 2002; Ravenscroft et al., 2005; Datta et al., 2011; Sankar, 2013, Chapelle and Lovley, 1992; Nealson, 1997; Bhattacharya et al., 2002; Smedley and Kinninburgh, 2002; van Geen et al., 2003, 2004; Horneman et al., 2004; Zheng et al., 2005; Wang and Mulligan, 2006). Several other publications have shown that OM has the potential to influence the solubility and mobility of As through competitive adsorption, complexation and redox reactions (Wang and Mulligan, 2006) as well as inhibit As mobility by forming insoluble metal complexes (Lin et al., 2004; Wang and Mulligan, 2006), and by an increase in As adsorption (Xu et al., 1991; Redman et al., 2002; Saada et al., 2003).

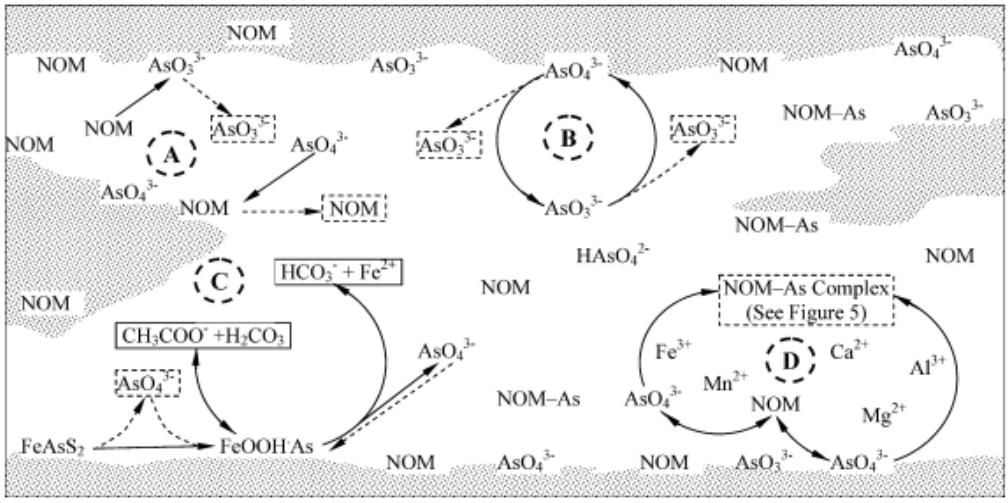

Figure 6.4 Model for the mechanisms of the effects of natural organic matter on arsenic release (Wang and Mulligan, 2006)

It has been shown that OM can catalyze oxidation and reduction reactions among chemical species (Schwarzenbach et al., 1990; Scott et al., 1998; Redman et al., 2002, Mladenov et al., 2019, 2015) and they may serve as an electron shuttle between kinetically inert redox species or micro-organisms and As species (Scott et al., 1998). In addition, the source of the OM and microbial activity that drives the reduction of iron oxides in the reductive dissolution mechanism of As release is still controversial. The high total dissolved As concentrations in shallow groundwater, high DOC concentrations and presence of decomposed, humic-like and aromatic OM in shallow groundwater aquifers at this study site supports the role of humic substances contribute to As mobilization. Organic matter characterization and occurrence of high solid phase As, possibly bound to crystalline Fe-oxides in NRB sediments, leads us to believe that in the shallow groundwater at our study site, reductive dissolution, possibly microbially driven, is occurring causing the elevated As concentrations in our shallow groundwater aquifers.

CHAPTER 7 - Conclusions

Based on the Fe and Mn concentrations in the sediments, specifically from HCl leaching, it is possible that Mn, as well as As, are being incorporated into Fe^{3+} minerals/oxides and replacing Fe in mineral structures within the natural reactive barrier (Ebinger and Schulze, 1990; Jung et al., 2015). Only a small portion of As in the sediments of our study area is readily bioavailable, or easily extractable; an even smaller portion is bound to refractory phases such as silicates or potentially mobilized due to addition of P or changes in pH (Wenzel et al., 2001). Solid-phase sediment extractions showed a zone of accumulation of Fe, Mn, and As between 120 cm and 173 cm on the east bank and between 0 cm and 120 cm on the west bank as seen in the HCl data. Arsenic was bound possibly bound with crystalline Fe and Mn oxides phases within the natural reactive barrier. The positive correlation between sediment grain size and solid-phase concentrations of Fe and As at several sites along the riverbank strongly suggest the role of mixing between surface water and groundwater and thus the existence of active natural reactive barriers along the study stretch of the Meghna River. The sediment mineral assemblage contains mostly quartz, mica (muscovite, biotite), feldspar (anorthite, albite), amphibole, and chlorite. With caution, we state that some Fe and Mn oxides (birnessite and hematite), Fe-carbonates (ankerite and siderite) and Fe-sulfide (possibly in some form of pyrite) were identified at various depths in the sediment cores. These minerals may have been the hosts of sorbed As, as they occurred at the same depths as the spikes in solid phase As.

During the early dry season, a large flux of anoxic groundwater, high in Fe^{2+} and As, discharges from the floodplain aquifers towards the river (Knappet et al., 2016; Berube et al., In Review). At this time, substantial quantities of As and Mn are produced as groundwater flows towards the river through the hyporheic zone. As the groundwater mixes with the oxic river water, crystalline and crystalline-amorphous Fe oxides will precipitate and incorporate As along the natural reactive barrier (Datta et al., 2009; Postma et al., 2010; Jung et al., 2015; Knappett et al., 2016). The enriched As in the subsurface sediments was associated with minerals that could be leached with HCl, suggesting that As is mostly sorbed to crystalline Fe oxides and oxyhydroxides, and less with crystalline silicate minerals. It is possible that the As-enriched Fe oxides could be formed by oxidation of Fe^{2+} and As^{3+} near the top of the hyporheic zone (Breit et al., 2004, Datta et al., 2009). The exposure of As to oxidants, possibly O_2, may enable bacterial oxidation and co-precipitation.

Sorption reactions are significant in controlling the mobility of As in the environment. Gaining rivers accumulate Fe, Mn, and As from reducing aquifers within the natural reactive barrier that expands through tidal river level fluctuations. During losing conditions, as the natural reactive barrier and hyporheic zone expand further into the floodplain aquifers, losing rivers likely mobilize As that may have taken thousands of years to accumulate (Jung et al., 2015).

The high As concentrations and presence of decomposed, humified and aromatic DOM and high amounts of DOC in shallow groundwater aquifers at this study site illustrate the potential for humic substances to contribute to As mobilization. The OM present in the aquifers may contribute to the reduction of Fe oxides, and subsequent release of As into the shallow aquifers, through electron donation. On average, shallow groundwater on the east side of the river had higher DOC concentrations then deep groundwater (Figure 5.11). Based on the fluorescence characterization, shallow groundwaters on the east bank (<30 m) were found to contain microbial and terrestrial-derived DOC, and decomposed, humified, and aromatic OM. Deeper aquifers had a significantly larger microbial OM signature than the shallow aquifers and was less aromatic and slightly less decomposed and humified. A possible source of the OM in the shallow aquifers could be from infiltration of surface water to groundwater, i.e. humic substances leaching from surface soil. This assumption is supported by the oxygen and hydrogen isotope ratios because recharge to the groundwater is infiltration of surface water (Figure 5.8). The terrestrially derived source of OM, and high humic-like peaks are be expected at this site. Mixing of shallow groundwater and surface water allow for infiltration of OM from the river and other surface water sources. Whereas deep aquifers have little potential to mix with surface water, so their OM source is mostly microbially derived.

Natural OM present in the aquifers and sediment play critical roles in As mobilization, because of OM's ability to enhance redox reactions. Microbial reduction of OM is one of the proposed methods that is responsible for the dissolution of iron minerals and arsenic release in aquifers under reducing conditions. Microbial reduction of OM prompts the reduction of Fe oxides, like FeOOH, from Fe^{3+} to Fe^{2+} in the aquifers and thus the release of sorbed As into the groundwater. The OM characterization and high solid phase As, possibly bound to crystalline Fe-oxides, in NRB sediments, supports reductive dissolution, possibly microbial driven, occurring and causing the elevated As concentrations in our shallow groundwater aquifers.

Arsenic cycling such as mobilization specifically into shallow aquifers and in general in the Ganges Brahmaputra Meghna River Deltas, as well as As trapping as shallow groundwater discharges to the river is very complex and numerous factors contribute to the processes involved. Even after many years of research, these are still poorly understood. Our study examines how sediment character, mineralogy, organic matter and dissolved species interact and influence trapping and release of As and the accumulation of dissolved As in groundwater. Further investigation of organic matter in the hyporheic zone and in the aquifers farther from the river would help in the interpretation of the processes occurring at our site. A better understand of the kinetics, reaction rates, and rates of exchange at our site is required to fully understand natural reactive barrier interactions. These previously unrecognized interaction zones within shallow aquifers lining rivers in Bangladesh may be important sinks and sources of As, and may help understand other causes of high solid-phase concentrations of Fe and As in riverbed sediments. The processes taking place within the hyporheic zone of reducing aquifers with high concentrations of dissolved Fe, Mn, and As, must be studied to understand how changes to the levels in rivers, groundwater tables, and oceans will impact the locations of As accumulation and release. These findings are important in advancing scientific understanding of the fate and transport of As in the environment, implications on the control of As mobility as well as remediation technologies to reduce and avoid further contamination.

CHAPTER 8 - References

1. Anawar, H.M; Akai, J; Komaki, K. Terao, H; Yoshioka, T; Ishizuka, T; Safiullah, S; Kato, K. (2003). Geochemical occurrence of arsenic in groundwater of Bangladesh: source and mobilization processes. J Geochem Explorer 77:109–131

2. Ahmed, K.M; Hoque, M; Hasan, M.K; Ravenscroft, P; Chowdhury, L.R. (1998). Occurrence and origin of water well CH4 gas in Bangladesh. Journal of Geological Society of India 51:697–708.

3. Baker, A. (2001). Fluorescence excitation–emission matrix characterization of some sewage-impacted river: Environmental Science and Technology 35:948–953.

4. Barua, S; and Datta, S. (2015). Effect on groundwater quality from proximal surface water bodies and effect on arsenic distribution in Bangladesh; Geochemical controls: Kansas State University Masters Thesis.

5. Bauer, M; and Blodau, C. (2006). Mobilization of arsenic by dissolved organic matter from iron oxides, soils and sediments. Science of the Total Environment 354:179–90.

6. Beck, A. J; Cochran, J.K; Sanudo-Wilhelmy, S.A. (2009). Temporal trends of dissolved trace metals in Jamaica Bay, NY: Importance of wastewater input and submarine groundwater discharge in an urban estuary. Estuary Coast 32:535-550.

7. Beck, J. A; Cochran, J. K; Sanudo-Wilhelmy, S.A. (2010). The distribution and speciation of dissolved trace metals in a shallow subterranean estuary. Marine Chemistry 121:145-156.

8. Beck, A. J; Charette, M. A; Cochran, J. K; Gonneea, M.E; Peucker-Ehrenbrink, B. (2013). Dissolved strontium in the subterranean estuary - implications for the marine strontium isotope budget. Geochim Cosmochim Ac 117:33-52.

9. Berg, M; Trang, P.T.K; Stengel, C; Buschmann, J; Viet, P.H; Van Dan, N; Giger, W; Stüben, D. (2008). Hydrological and sedimentary controls leading to arsenic contamination of groundwater in the Hanoi area, Vietnam. The impact of iron-arsenic ratios, peat, river bank deposits, and excessive groundwater abstraction. Chemical Geology 249: 91–112.

10. Berube, M.M; Jewell, K; Myers, K; Knappett, P.S.K; Dimova, N; Hossain, A; Lipsi, M; Hossain, S; Hossain, A; Peterson, J; Ahmed, K.M; Datta, S. (2017). The Fate of Arsenic in Groundwater Discharged to the Meghna River, Bangladesh. Environmental Chemistry (In Review).

11. Bhattacharya, P; Chatterjee, D; Jacks, G., 1997. Occurrence of arsenic-contaminated groundwater in alluvial aquifers from the Bengal Delta Plain, Eastern India: options for a safe drinking water supply. Water Resource Development 13:79–92.

12. Bhattacharya, P; Jacks, G; Ahmed, K.M; Khan, A.A; Routh, J. (2002). Arsenic in groundwater of the Bengal Delta Plain aquifers in Bangladesh. Bull Environ Contamin Toxicol 69:538–545.

13. Bhattacharya, P; Claesson, M; Bundschuh, J; Sracek, O; Fagerberg, J; Jacks, G; Martin, R.A; Storniolo, A.D.R; Thir, J.M. (2006). Distribution and mobility of arsenic in the Río Dulce alluvial aquifers in Santiago del Estero Province, Argentina. Science of Total Environment 358:97–120.

14. Boano, F; Camporeale, C; Revelli, R; Ridolfi, L. (2006). Sinuosity- driven hyporheic exchange in meandering rivers. Geophysica Res. Lett 33(18).

15. Bostick, B. C and Fendorf, S. (2003). Arsenite sorption on troilite (FeS) and pyrite (FeS2). Geochem. Cosmochim. Acta 67:909-921.

16. Breit, G. N; Foster, A. L; Perkins, R. B; Young, J. C; King, T; Welch, A. H. (2004). Arsenic-rich ferric oxyhydroxide enrichments in the shallow subsurface of Bangladesh. Water-Rock Interactions, eds Wanty RB, Seal RRI (Taylor & Francis Group, London): 1457–1461.

17. British Geological Survey (BGS); and Department of Public Health and Engineering (DPHE). (1999). Groundwater studies for arsenic contamination in Bangladesh phase I: Rapid investigation phase, main report. British Geological Survey and Mott MacDonald Ltd.

18. British Geological Survey (BGS), and Bangladesh Department of Public Health Engineering (DPHE). (2001). Arsenic contamination of groundwater in Bangladesh. In Kinniburgh, D.G., Smedley, P.L. (Eds), British Geologic Survey Report 1-4.

19. Brunke, M; and Gonser, T. (1997). The ecological significance of exchange processes between rivers and groundwater: Freshwater Biology 37(1):1-33.

20. Cardenas, M.B. (2009). A model for lateral hyporheic flow based on valley slope and channel sinuosity. Water Resources Res 45.

21. Chapelle, F. H; and Lovley, D. R. (1992). Competitive-exclusion of sulphate reduction by Fe (III)-reducing bacteria - a mechanism for producing discrete zones of high-iron ground-water. Ground Water 30:29-36.

22. Charette, M. A; and Sholkovitz, E. R. (2002). Oxidative precipitation of groundwater-derived ferrous iron in the subterranean estuary of a coastal bay. Geophysics Research Letters 29: 85.1-85.4.

23. Charette, M. A; Sholkovitz, E. R; Hansel, C.M. (2005). Trace element cycling in a subterranean estuary: Part 1. Geochemistry of the permeable sediments. Geochemica et Cosmochima Acta 69(8):2095-2109.

24. Chowdhury M.A.I; Ahmed M.F; Ali M.A. (2003). Influence of up stream sediment on arsenic contamination of groundwater in Bangladesh. In *Fate of Arsenic in the Environment*, eds Ahmed MF, Ali MA, Adeel Z (ITN Centre, BUET): 21–37.

25. Coble, P. G; Green, S. A; Blough, N. V; Gagosian, R. B. (1990). Characterization of DOM in the Black Sea by fluorescence spectroscopy. Nature 348:432–435.

26. Coble, P. G. (1996). Characterization of marine and terrestrial DOM in seawater using excitation–emission matrix spectroscopy. Mar. Chem 51:325–346.

27. Cory, R.M; and McKnight, D.M. (2005). Fluorescence spectroscopy reveals ubiquitous presence of oxidized and reduced quinones in dissolved organic matter. Environmental Science and Technology 39:8142–9.

28. Datta, S; Mailloux, B; Jung, H. B; Hoque, M. A.; Stute, M; Ahmed, K. M; Zheng, Y. (2009). Redox trapping of Arsenic during groundwater discharge in sediments from the Meghna riverbank in Bangladesh. Proceedings of the National Academy of Sciences of the USA 106(40):16930-16935.

29. Datta, S; Neal, A.W; Mohajerin, T.J; Ocheltree, T; Rosenheim, B.E; White, C.D; Johannesson, K.H. (2011). Perennial ponds are not an important source of water or dissolved organic matter to groundwaters with high arsenic concentrations in West Bengal, India. Geophys. Res. Lett 38:1–5.

30. Dixit, S; and Hering, J.G. (2003). Comparison of arsenic (V) and arsenic (III) sorption onto iron oxide minerals: implications for arsenic mobility. Environmental Science and Technology 37(18):4182-4189.

31. Dowling, C.B. (2002). Geochemical study of arsenic release mechanisms in the Bengal Basin groundwater. Water Resour. Res 38:1–18.

32. Ebinger. M.H, and Schulze. D.G. (1990). The influence of pH on the synthesis of mixed FeMn oxide minerals. Clay Min. 25:507-518.

33. Fellman, J.B; Hood, E; Spencer, R.G.M. (2010). Fluorescence spectroscopy opens new windows into dissolved organic matter dynamics in freshwater ecosystems: A review. Limnol. Oceanogr 55(6):2452–2462.

34. Fendorf, S; Eick, M.J. Grossl, P; Sparks. D.L. (1997). Arsenate and chromate retention mechanisms on goethite structure. Environmental Science and Technology 31 (2):315-320.

35. Fendorf, S; Michael, H. A; and van Geen A. (2010). Spatial and temporal variations of groundwater arsenic in south and southeast Asia. Science 328:1123-1127.

36. Feris, K. P; Ramsey, P. W; Rillig, M; Moore, J. N; Gannon, J. E; and Holben, W. E. (2004). Determining rates of change and evaluating group level resiliency differences in hyporheic microbial communities in response to fluvial heavy-metal deposition. Applied and Environmental Microbiology 70:4756–4765.

37. Ghosh, A.R; Mukherjee, A. (2002). Arsenic contamination of groundwater and human health impacts in Burdwan District, West Bengal, India. Geological Society of America Abstracts with Program 34(2):107.

38. Goldberg, S; and Johnston, C.T. (2001). Mechanisms of arsenic adsorption on amorphous oxides evaluated using macroscopic measurements, vibrational spectroscopy and surface complexation modeling. J Colloid Interface Sci. 234(1):204-216.

39. Harvey, C.F; Swartz, C.H; Badruzzaman, A. B. M; Keon-Blute, N; Yu, W; Ali, M. A; Jay, J; Beckie, R; Niedan, V; Brabander, D; Oates, P.M; Ashfaque, K.N; Islan, S. Hemond, H.F; Ahmed, M.F. (2002). Arsenic mobility and groundwater extraction in Bangladesh: Science 298:1602-1606.

40. Harvey, C. F; Ashfaque, K. N; Yu, W; Badruzzaman, A. B. M; Ali, M. A; Oates, P. M; Michael, H. A; Neumann, R. B; Beckie, R; Islam, S; and Ahmed, M. F. (2006). Groundwater dynamics and arsenic contamination in Bangladesh. Chemical Geology 228:112-136.

41. Hasan, M.A; Ahmed, K.M; Sracek, O; Bhattacharya, P; von Brömssen, M; Broms, S., Fogelstrom, J; Mazumder, M.L; Jacks, G. (2007). Arsenic in shallow groundwater of Bangladesh: investigations from three different physiographic settings. Hydrogeology Journal 15(8):1507–1522.

42. He, Y.T; Fitzmaurice, A.G; Bilgin, A; Choi, S; O'Day, P; Horst, J. (2010). Geochemical processes controlling arsenic mobility in groundwater: a case study of arsenic mobilization and natural attenuation. Applied Geochemistry 25:69–80.

43. Helms, J.R; Stubbins, A; Ritchie, J.D; Minor, E.C; Kieber, D.J; Mopper, K. (2008). Absorption spectral slopes and slope ratios as indicators of molecular weight, source, and photobleaching of chromophoric dissolved organic matter. Limnol. Oceanogr. 53:955–969.

44. Hering, J. G; and Kraemer, S. (1998). In Perspectives in Environmental Chemistry; Macalady, D. L., Ed.; Oxford University Press: New York; 57-74.

45. Hisa, T.H; Lo, S.L; Lin, C.F; Lee, D.Y. (1994). Characterization of arsenate adsorption on hydrous iron oxide using chemical and physical methods. Colloids Surfaces A. Physicochem Eng Aspects 85:1–7.

46. Hossain, M.A; and Siddique, M.N.A. (2015). Water- a limiting resource for sustainable agriculture in Bangladesh. EC Agriculture. 1(2):124-137.

47. Horneman, A; van Geen, A; Kent, D; Mathe, P. E; Zheng, Y; Dhar, R. K; O'Connell, S; Hoque, M.A; Aziz, Z; Shamsudduha, M; Seddique, A; and Ahmed, K. M. (2004). Decoupling of arsenic and iron release to Bangladesh groundwater under reducing conditions. Part I: Evidence from sediment profiles. Geochim. Cosmochim. Acta. 68:3459-3473.

48. Hughes, C.E. and Crawford, J. (2012). A new precipitation weighted method for determining the meteoric water line for hydrological applications demonstrated using Australian and global GNIP data. Journal of Hydrology, 464–465:344-351.

49. Hudson, N; Baker, A; Reynolds, D. (2007). Fluorescence analysis of dissolved organic matter in natural, waste and polluted waters—A review: River Res. Applic. 23:631–649.

50. Islam, F.S; Gault, A.G; Boothman, C; Polya, D.A; Charnock, J.M; Chatterjee, D; Lloyd, J.R. (2004). Role of metal-reducing bacteria in arsenic release from Bengal delta sediments. Nature 430:68-71.

51. Itai, T; Takahashi, Y; Seddique, A.A; Maruoka, T; Mitamura, M. (2010). Variations in the redox state of As and Fe measured by X-ray absorption spectroscopy in aquifers of Bangladesh and their effect on As adsorption. Applied Geochemistry 25:34-47.

52. Jiang, J; and Kappler, A. (2008). Kinetics of microbial and chemical reduction of humic substances: implications for electron shuttling. Environmental Science and Technology 42:3563–3569.

53. Jung, H.B; and Zheng, Y. (2006). Enhanced recovery of arsenite sorbed onto synthetic oxides by L- ascorbic acid addition to phosphate solution: calibrating a sequential leaching method for the speciation analyses of arsenic in natural samples. Water Resources 40:2168-2180.

54. Jung, B. H; Charette, A. M; and Zheng, Y. (2009). Field, laboratory and modeling study of reactive transport of groundwater arsenic in a costal aquifer. Environmental Science and Technology 43:5333-5338.

55. Jung, H.B; Bostick, B.C; Zheng, Y. (2012). Field, experimental, and modeling study of arsenic partitioning across a redox transition in a Bangladesh aquifer. Environmental Science and Technology 46:1388-1395.

56. Jung, B. H; Bostick, C. B; Zheng, Y. (2011). Field, experimental and modeling study of arsenic partitioning across a redox transition in a Bangladesh aquifer: Environmental Science and Technology 43:5333-5338.

57. Jung, B.H; Zheng, Y; Rhaman, W.M; Rhaman M.M; Ahmed. M.K. (2015). Redox zonation and oscillation in the hyporheic zone of the Ganges-Brahmaputra Delta: Implications for the fate of groundwater arsenic during discharge. Applied Geochemistry 63:647-660.

58. Keon, N. E; Swartz, C; Brabander, D. J; Harvey, C; Hemond, H. F. (2001). Validation of an arsenic sequential extraction method for evaluation mobility in sediments: Environmental Science and Technology 35:2778–84.

59. Kheboian, C; and Bauer, C. F. (1987). Accuracy of selective extraction procedures for metal speciation in model aquatic sediments: Analytical Chemistry 59(10):1417-1423.

60. Klapper, L; McKnight, D.M; Fulton, J.R; Blunt-Harris, E.L; Nevin, K.P; Lovley, D.R; and Hatcher, P.G. (2002). Fulvic acid oxidation state detection using fluorescence spectroscopy. Environmental Science and Technology 36:3170–5.

61. Knappett, P. S. K; Escamilla, V; Layton, A; McKay, L. D; Emch, M; Williams, D. E; Huq, M. R; Alam, M. J; Farhana, L; Mailloux, B. J; Ferguson, A; Sayler, G. S; Ahmed, K. M; van Geen, A. (2011). Impact of population and latrines on fecal contamination of ponds in rural Bangladesh. Science of the Total Environment 409,17:3174-3182.

62. Knappett, P. S. K; McKey, L. D; Layton, A; Williams, D. E; Alam, Md. J; Huq, Md. R; Feighery, J. E; Culligan, P. J; Mailloux, B. J; Zhuang, J; Escamilla, V; Emch, M; Perfect, E; Sayler, G. S; Ahmed, K. M; van Geen, A. (2012). Implications of fecal bacteria input from latrine-ponds for wells in sandy aquifers. Environmental Science and Technology 46:1361-1370.

63. Knappett, P.S.K; Mailloux, B.J; Choudhury, I; Khan, M.R; Michael, H.A; Barua, S; Mondal, D. R; Steckler, M.S; Akhter; S.H; Bostick, B; Harvey, C.F; Shamsudduha, M. (2016). Vulnerability of low-arsenic aquifers to municipal pumping in Bangladesh. Journal of Hydrology 539:674-686.

64. Kolker, A.S; Cable, J.E; Johannesson, K.H; Allison, M.A; and Inniss, L.V. (2013). Pathways and processes associated with the transport of groundwater in deltaic systems. Journal of Hydrology 498:319-334.

65. Konert, M; and Vandenberghe, J. (1997). Comparison of laser grain size analysis with pipette and sieve analysis: a solution for the underestimation of the clay fraction. Sedimentology 44:523-535.

66. Kulkarni, H.V. (2016). Biogeochemical Interactions of Natural Organic Mater with Arsenic in Groundwater: A Dissertation. Department of Civil Engineering, College of Engineering, Kansas State University, Manhattan Ks.

67. Larsen, F; Pham, N. Q; Dang, N. D; Postma, D; Jessen, S; Pham, V. H; Nguyen, T. B; Trieu, H. D; Tran, L. T; Nguyen, H; Chambon, J. (2008). Controlling geological and hydrogeological processes in an arsenic contaminated aquifer on the red river flood plain, Vietnam. Applied Geochemistry 23:3099-3115.

68. Lowers, H.A; Breit, G.N; Foster, A.L; Whitney, J; Young, J; Uddin, M.N; Muneem, A.A. (2007). Arsenic incorporation into authigenic pyrite, Bengal Basin sediment, Bangladesh. Geochimica et Cosmochimica Acta 71(11):2699–2717.

69. Liu, G; ND Cai, Y. (2011). Complexation of Arsenite with Dissolved Organic Matter: Conditional Distribution Coefficients and Apparent Stability Constants. Chemosphere 81:890–896.

70. Lin, H.H.T; Wang, M.C.M; Li, G.G.C. (2004). Complexation of arsenate with humic substance in water extract of compost. Chemosphere 56:1105–1112.

71. Lovley, D.R; Coates, J.D; Blunt-Harris, E.L; Phillips, E.J.P; Woodward, J.C. (1996). Humic substances as electron acceptors for microbial respiration. Nature 382:445–448.

72. Lovley, D.R; Fraga, J.L; Blunt-Harris, E.L; Hayes, L. A; Phillips, E.J.P; Coates, J.D. (1998). Humic Substances as a Mediator for Microbially Catalyzed Metal Reduction. Acta Hydrochim. Hydrobiol 26:152–157.

73. Lovley, D.R; Fraga, J.L; Coates, J.D; Blunt-Harris, E.L. (1999). Humics as an electron donor for anaerobic respiration. Environmental Microbiology 1:89–98.

74. Mallick, S; Rajgopal, N.R. (1995). Groundwater development in the arsenic affected alluvial belt of West Bengal—some questions. Current Science 70:956–958.

75. Masuda, H; Shinoda, K; Okudaria, T; Takahashi, Y; Hoguchi, N. (2012). Chlorite- source of arsenic groundwater pollution in the Holocene aquifer of Bangladesh. Geochemical Journal 46:381-391.

76. Mukherjee, A. (2006). Deeper Groundwater Chemistry and Flow in the Arsenic Affected Western Bengal Basin, West Bengal, India. Dissertation. University of Kentucky, Lexington.

77. Majumder, R.K; Halim, M.A; Shimada, J; Saha, B.B; Zahid, A; Hasan, M.Q; Islam, M. S. (2011). Hydrochemistry and isotopic studies to identify Ganges River and riverbank groundwater interaction, southern Bangladesh. Arab Journal of Geosciences 6:4585–4591.

78. McArthur, J.M; Ravenscroft, P; Safiulla, S; Thirlwall, M.F. (2001). Arsenic in groundwater: Testing pollution mechanisms for sedimentary aquifers in Bangladesh. Water Resources Res. 37:109–117.

79. McArthur, J.M; Banerjee, D.M; Hudson-Edwards, K.A; Mishra, R; Purohit, R; Ravenscroft, P; Cronin, A; Howarth, R.J; Chatterjee, A; Talukder, T; Lowry, D; Houghton, S; Chadha, D.K. (2004). Natural organic matter in sedimentary basins and its relation to arsenic in anoxic ground water: the example of West Bengal and its worldwide implications. Applied Geochemistry 19:1255-1293.

80. McArthur, J. M; Ravenscroft, P; Banerjee, D. M; Milsom, J; Hudson-Edwards, K. A; Sengupta, S; Bristow, C; Sarkar, A; Tonkin, S; Purohit, R. (2008). How paleosols influence groundwater flow and arsenic pollution: A model from the Bengal Basin and its worldwide implication. Water Resources Research 44(11).

81. McKnight, D. M.; Boyer, E. W.; P. K. Westerhoff, P. T.; Kulbe, D. T. and Andersen, D. T. (2001). Spectrofluorometric characterization of DOM for indication of precursor material and aromaticity. Limnol. Oceanography 46:38–48.

82. Mikutta, C; and Kretzschmar, R. (2011). Spectroscopic evidence for ternary complex formation between arsenate and ferric iron complexes of humic substances. Environmental Science and Technology.

83. Miller, M.P; Mcknight, D.M; Cory, R.M; William, M.W; Runkel, L.R. (2009). Hyporheic exchange and fulvic acid redox reaction in an alpine stream/wetland ecosystem, Colorado front range. Environmental Science and Technology 40:5943-5949

84. Mladenov, N; Zheng, Y; Miller, M.P; Nemergut, D.R; Legg, T; Simone, B; Hageman, C; Rahman, M.M; Ahmed, K.M; McKnight, D.M. (2010). Dissolved organic matter sources and consequences for iron and arsenic mobilization in Bangladesh aquifers. Environmental Science and Technology 44:123–8.

85. Mladenov, N; Zheng, Y; Simone, B; Bilinski, T.M; McKnight, D.M; Nemergut, D; Radloff, K. A; Rahman, M.M; and Ahmed, K.M. (2015). Dissolved Organic Matter Quality in a

Shallow Aquifer of Bangladesh: Implications for Arsenic Mobility. Environment Science and Technology.

86. Moran, M.A; Sheldon, W.M; and Zepp, R.G. (2000). Carbon loss and optical property changes during long-term photochemical and biological degradation of estuarine dissolved organic matter. Limnol. Oceanography 45:1254–1264.

87. Morgan, J.P; and Mcintire, W.G. (1959). Geological Society of America Bulletin Quaternary Geology of the Bengal Basin, East.

88. Mukherjee, A; von Brömssen, M; Scanlon, B; Bhattacharya, P; Fryar, A.E; Hasan, M.A; Ahmed, K.M; Chatterjee, D; Jacks, G; Sracek, O. (2008). Hydrogeochemical comparison and effects of overlapping redox zones on groundwater arsenic near the Western (Meghna sub-basin, India) and Eastern (Meghna sub-basin, Bangladesh) margins of the Bengal Basin. Journal of Cont. Hydrology 99:31-48.

89. Mukherjee, A; Fryar, A.E; Thomas, W.A. (2009). Geologic, geomorphic and hydrologic framework and evolution of the Bengal basin, India and Bangladesh. J. Asian Earth. Sci. 34:227-244.

90. Musial, C. T; Sawyer, A. H; Barnes, R. T; Bray, S; Knights, D. (2016). Surface water-groundwater exchange dynamics in a tidal freshwater zone: Hydrology Process 30:739-750.

91. Nagorski, S. A; and Moore, J. N. (1999). Arsenic mobilization in the hyporheic zone of a contaminated stream. Water Resources Research 35:3441–3450.

92. Nealson, K. H. (1997). Sediment bacteria: Who's there, what are they doing, and what's new? Annual Review Earth Planet. Science 25:403-434.

93. Neumann, R. B; Ashfaque, K. N; Badruzzaman, A. B. M; Ali, M. A; Shoemaker, J. K; Harvey, C. F. (2010). Anthropogenic influences on groundwater arsenic concentrations in Bangladesh. Nature Geoscience 3(1):46–52.

94. Nickson, R; McArthur, J; Burgess, W; Ahmed, K. M; Ravenscroft, P; Rahman, M. (1998). Arsenic poisoning of Bangladesh groundwater. Nature 395:338-338.

95. Nickson, R.T; McArthur, J.M; Ravenscroft, P; Burgess, W.G; and Ahmed, K.M. (2000). Mechanism of arsenic release to groundwater, Bangladesh and West Bengal. Applied Geochemistry 15:403–413.

96. Nimick, D; Cleasby, T; McCleskey, R. (2005). Seasonality of diel cycles of dissolved trace-metal concentrations in a Rocky Mountain stream. Environmental Geology 47:603– 614.

97. Nordstrom, D. K. (2002). Public health - worldwide occurrences of arsenic in ground water. Science 296:2143-2145.

98. Ohno, T. (2002). Fluorescence inner-filtering correction for determining the humification index of dissolved organic matter. Environmental Science and Technology 36:742–746.

99. Parlanti, E; Worz, K; Geoffroy, L; Lamotte, M. (2000). Dissolved organic matter fluorescence spectroscopy as a tool to estimate biological activity in a coastal zone submitted to anthropogenic inputs: Org. Geochemistry 31:1765–1781.

100. Pasupuleti, P.K. (2005). Mobilization of Arsenic in Aquifer Sediments of Matlab Upazila, southeastern Bangladesh: TRITA-LWR Master Thesis. KTH.

101. Perminova, I.V; Grechishceva, N.Y; Petrosyan, V.S. (1999). Environmental Science and Technology 33:3781.

102. Postma, D; Larsen, F; Hue, N. T. M; Duc, M. T; Viet, P. H; Nhan, P. Q; Jessen, S. (2007). Arsenic in groundwater of the red river floodplain, Vietnam: Controlling geochemical processes and reactive transport modeling. Geochim Cosmochim Ac 71:5054-5071.

103. Postma, D; Jessen, S; Nguyen, T. M. H; Mai, T. D; Koch, C. B; Pham, H. V; Nhan, P. Q; Larsen, F. (2010). Mobilization of arsenic and iron from red river floodplain sediments, Vietnam. Geochim Cosmochim Ac 74:3367-3381.

104. Ravenscroft, P; Burgess, W. G; Ahmed, K. M; Burren, M; Perrin, J. (2005). Arsenic in groundwater of the Bengal Basin, Bangladesh; Distribution, field relations, and hydrogeological setting. Hydrogeology Journal 13:727–751.

105. Rahaman, S; Sinha, A C; Pati, R; Mukhopadhyay, D. (2013). Arsenic contamination: a potential hazard to the affected areas of West Bengal, India. Environ. Geochem. Health 35:119–32.

106. Redman, A.D; Macalady, D.L; Ahmann, D. (2002). Natural organic matter affects arsenic speciation and sorption onto hematite. Environmental Science and Technology 36:2889–96.

107. Rowe, H; Hughes, N; Robinson, K. (2012). The quantification and application of handheld energy-dispersive x-ray fluorescence (ed-xrf) in mudrock chemostratigraphy and geochemistry. Chemical Geology 324:122-131.

108. Saada, A; Breeze, D; Crouzet, C; Cornu, S; Baranger, P. (2003). Adsorption of arsenic (V) on kaolinite–humic acid complexes: Role of humic acid nitrogen groups. Chemosphere 51:757–763.

109. Sadiq, M. (1997). Arsenic chemistry in soils: an overview of thermodynamic prediction and field observation. Water Air Soil Pollution 93:117–136.

110. Sankar M.S. (2013). Geochemical Significance of Arsenic and Manganese Toxicity in Groundwaters from Murshidabad District, West Bengal, India. Master of Science Published Thesis.

111. Sankar, M.S; Vega, M; Defoe, P.P; Kibria, M.G; Ford, S; Telfeyan, K; Neal, A; Mohajerin, T.J; Hettiarachchi, G.M; Barua, S; Hobson, C; Johannesson, K; Datta, S. (2014). Elevated arsenic and manganese in groundwaters of Murshidabad, West Bengal, India. Science of Total Environment. 488-489:570–579.

112. Saunders, J.A; Lee, M.-K.K; Shamsudduha, M; Dhakal, P; Uddin, A; Chowdury, M.T; and Ahmed, K.M. (2008). Geochemistry and mineralogy of arsenic in (natural) anaerobic groundwaters. Applied Geochemistry 23:3205–3214.

113. Saunders, J. A, and C. T. Swann (1992). Nature and origin of authigenic rhodochrosite and siderite from the Paleozoic aquifer, northeast Mississippi. Applied Geochemistry 7:375 – 387.

114. Sawyer, A. H; Shi, F. Y; Kirby, J. T; Michael, H. A. (2013). Dynamic response of surface water-groundwater exchange to currents, tides, and waves in a shallow estuary. J Geophys Res-Oceans 118:1749-1758.

115. Schwarzenbach, R.P; Stierli, R; Lanz, K; Zeyer, J. (1990). Quinone and iron porphyrin mediated reduction of nitroaromatic compounds in homogeneous aqueous solution. Environmental Science and Technology 24:1566–1574.

116. Scott, D.T; McKnight, D.M; Blunt-Harris, E.L; Kolesar, S.E; and Lovley, D.R. (1998). Quinone Moieties Act as Electron Acceptors in the Reduction of Humic Substances by Humics-Reducing Microorganisms. Environmental Science and Technology 32:2984–2989.

117. Seddique, A.A; Masuda, H; Mitamura, M; Shinoda, K; Yamanaka, T; Itai, T; Maruoka, T; Uesugi, K; Ahmed, K.M; Biswas, D.K. (2008). Arsenic release from biotite into a Holocene aquifer in Bangladesh. Applied Geochemistry 23:2236-2248.

118. Sharma, P; Ofner, J; Kappler, A. (2010). Formation of binary and ternary colloids and dissolved complexes of organic matter, Fe and As. Environmental Science and Technology 44:4479–85.

119. Shuai, P; Knappett, P; Hossain, S; Hosain, A; Rhodes, K; Ahmed, K, M; M. B. Cardenas (2017). The impact of the degree of aquifer confinement and anisotropy on tidal pulse propagation. Ground Water.

120. Stahl, M. O; Harvey, C. F; van Geen, A; Sun, J; Trang, P. T. K; and Lan, V. M; Phuong, T. M; Viet, P. H; Bostick, B. (2016). River bank geomorphology controls groundwater arsenic concentrations in aquifers adjacent to the red river, Hanoi Vietnam. Water Resources 52:6321-6334.

121. Stevenson, F. J; and Cole, M. A. (1999). Cycles of Soils: Carbon, Nitrogen, Phosphorus, Sulfur, Micronutrients, 2nd ed.; John Wiley & Sons: New York.

122. Smedley, P; and Kinniburgh, D. (2002). A review of the source, behavior and distribution of arsenic in natural waters. Applied Geochemistry 17:517–568.

123. Smith, A. H; Lingas, E. O; Rhaman, M. (2000). Contamination of drinking-water by arsenic in Bangladesh: a public health emergency.

124. Söderberg, L. (2013). Importance of dissolved organic carbon for transport of organic contaminants in groundwater. Published digitally at the Department of Earth Sciences, Uppsala University, Uppsala, ISSN:1401-5765.

125. Sutton, N.B; van der Kraan, G.M; van Loosdrecht, M.C.M; Muyzer, G; Bruining, J; Schotting, R.J. (2009). Characterization of geochemical constituents and bacterial populations associated with As mobilization in deep and shallow tube wells in Bangladesh. Water Resources 43:1720–1730.

126. Sun, X; Doner, H.E. (1996). An investigation of arsenite and arsenate bonding structures on goethite by FTIR. Soil Science 161:865–872.

127. Tareq, S.M; Safiullah, S; Anawar, H.M; Rahman, M.M; Ishizuka, T. (2003). Arsenic pollution in groundwater: a self-organizing complex geochemical process in the deltaic sedimentary environment, Bangladesh. Science of the Total Environment 313:213–226.

128. Tessier, A; Campbell, P.G.C; Bisson, M. (1979). Sequential extraction procedure for the speciation of particulate trace metals. Analytical Chemistry 51(7).

129. Tipping, E; Hetherington, N. B; Hilton, J; Thompson, D. W; Bowles, E; Hamilton-Taylor, J. (1985). Artifacts in the use of selective chemical extraction to determine distributions of metals between oxides of manganese and iron. Analytical Chemistry 57:1944.

130. Tufano, K. J; and Fendorf, S. (2008). Confounding impacts of iron reduction on arsenic retention. Environmental Science and Technology 42:4777–4783.

131. Uddin, A; Shamsudduha, M; Saunders, J.A; Lee, M.K; Amed, K.M; Chowdury, M.T. (2011). Mineralogical profiling of alluvial sediments from arsenic-affected Ganges-Brahmaputra floodplain in central Bangladesh. Applied Geochemistry 26:470-483.

132. Vähätalo, A. V; and Wetzel, R.G. (2004). Photochemical and microbial decomposition of chromophoric dissolved organic matter during long (months-years) exposures. Marine Chemistry 89:313–326.

133. van Geen, A; Zheng, Y; Stute, M; Ahmed, K. M. (2003). Arsenic mobility and groundwater extraction in Bangladesh. Science. 300:584.

134. van Geen, A; Protus, T; Cheng, Z; and Horneman, A. (2004). Testing groundwater for arsenic in Bangladesh before installing a well. Environmental Science and Technology 38:6783-6789.

135. van Geen, A; Zheng, Y; Goodbred, S; Horneman, A; Aziz, Z; Cheng, Z; Stute, M; Mailloux, B; Weinman, B; Hoque, M. A; Seddique, A. A; Hossain, M. S; Chowdhury, S. H; and Ahmed, K. M. (2008). Flushing history as a hydrogeological control on the regional distribution of arsenic in shallow groundwater of the Bengal Basin. Environmental Science and Technology 42(7):2283-2288.

136. Wang, S; and Mulligan, C.N.C. (2006). Effect of natural organic matter on arsenic release from soils and sediments into groundwater. Environmental Geochemical Health 28:197–214.

137. Weishaar, J. L; Aiken, G. R; Bergamaschi, B. A; Fram, M. S; Fujii, R; and Moppe, R. (2003). Evaluation of Specific Ultraviolet Absorbance as an Indicator of the Chemical Composition and Reactivity of Dissolved Organic Carbon. Environmental Science and Technology 37:4702-4708.

138. Weinman, B; Goodbred, S. L; Zheng, Y; Aziz, Z; Steckler, M; van Geen, A; Singhvi, A. K; and Nagar, Y, C. (2008). Contributions of floodplain stratigraphy and evolution to the spatial patterns of groundwater arsenic in araihazar, Bangladesh. Geological Society American Bulletin. 120:1567-1580.

139. Wenzel, W. W; Kirchbaumer, N; Prohaska, T; Stingeder, G; Lombi, E; Adriano, D.C. (2001). Arsenic fractionation in soils using an improved sequential extraction procedure. Analytical Chimica. Acta. 436:309-323.

140. Westerhoff, P; Chen, W; and Esparza, M. (2001). Fluorescence analysis of a standard fulvic acid and tertiary treated wastewater. J. Environ. Qual. 30: 2037–2046.

141. Whitehead, P. G; Barbour, E; Futter, M. N.; Sarkar, S; Rodda, H.; Caesar, J; Butterfield, D; Jin, L; Sinha, R; Nicholls, R; and Salehin, M. (2015). Impacts of climate change and socio-economic scenarios on flow and water quality of the Ganges, Brahmaputra and Meghna (GBM) river systems: low flow and flood statistics. Environmental Science: Processes Impacts17:1057-1069.

142. Wilson, H.F; and Xenopoulos, M. A. (2008). Effects of agricultural land use on the composition of fluvial dissolved organic matter. Nat. Geosci. 2:37–41.

143. Wilkie, J.A; and Hering, J.G. (1998). Rapid oxidation of geothermal As(III) in stream waters of the eastern Sierra Nevada. Environmental Science and Technology 32:657-662.

144. Winkel, L; Berg, M; Amini, M; Hug, S. J; Johnson, C. A. (2008). Predicting groundwater arsenic contamination in southeast Asia from surface parameters: Nat. Geosci. 1:536-542.

145. Wolt, J. D. (1994). Soil Solution Chemistry: Applications to Environmental Science and Agriculture; John Wiley&Sons: New York. 275-292.

146. Wolf, M; Kappler, A; Jiang, J; Meckenstock, R.U. (2009). Effects of humic substances and quinones at low concentrations on ferrihydrite reduction by Geobacter metallireducens. Environmental Science and Technology 43:5679–85.

147. Wondzell, S. M; and Swanson, F. J. (1996). Seasonal and storm dynamics of the hyporheic zone of a 4th-order mountain stream 1; Hydrologic Processes: Journal of the North American Benthological Society. 15(1):3-19.

148. World Health Organization (WHO) Public Health and Environment. (2010). Exposure to arsenic; A major public health concern: World Health Organization.

149. Xu, H; Allard, B; Grimvall, A. (1991). Effects of acidification and natural organic materials on the mobility of arsenic in the environment. Water Air Soil Pollution 57/58:269–278.

150. Zheng, Y; Stute, M; Van Geen, A; Gavrieli, I; Dhar, R; Simpson, H.J; Schlosser, P; Ahmed, K.M. (2004). Redox control of arsenic mobilization in Bangladesh groundwater. Applied Geochemistry 19:201-214.

151. Zheng, Y; van Geen, A; Stute, M; Dhar, R; Mo, Z; Cheng, Z; Horneman, A; Gavrieli, I; Simpson, H.J; Versteeg, R; Steckler, M; Grazioli-Venier, A; Goodbred, S; Shahnewaz, M; Shamsudduha, M; Hoque, M.A; and Ahmed, K.M. (2005). Geochemical and hydrogeological contrasts between shallow and deeper aquifers in two villages of Araihazar, Bangladesh: Implications for deeper aquifers as drinking water sources. Geochim. Cosmochim. Acta. 69:5203–5218.

152. Zsolnay, Á. (2003). Dissolved organic matter: artefacts, definitions, and functions. Geoderma 113:187–209.

Appendix A - Groundwater On Site Parameters

Table A.1 Well locations

Name	Coordinates
TWeast1	23 44' 41.9"N, 90 43' 53.6"E
TWeast2	23 44'42.1"N, 90 43' 59.1"E
TWeast3	23°44'41.10"N, 90 44' 2.7"E
TWeast4	23 44'39.9"N, 90°44'5.10"E
TWeast5	23 44' 40.2"N, 90 44' 11.6"E
TWeast7	23°44'36.00"N, 90°44'18.40"E
TWeast8	23°44'35.40"N, 90°44'19.00"E
Vesat2	23°44'40.82"N, 90°43'46.48"E
Twwest1a	23°44'35.52"N, 90°42'43.52"E
Twwest1b	23°44'35.52"N, 90°42'43.52"E
Twwest2	23°44'35.70"N, 90°42'42.90"E
Twwest3	23°44'36.40"N, 90°42'41.50"E
Twwest4	23°44'36.50"N, 90°42'39.60"E
Twwest5	23°44'37.30"N, 90°42'37.80"E
Twwest6	23°44'39.20"N, 90°42'36.40"E
Twwest7	23°44'41.00"N, 90°42'34.60"E
Twwest8	23°44'43.50"N, 90°42'31.50"E
Vwest1	23°44'42.34"N, 90°42'42.13"E
Vwest2	23°44'42.34"N, 90°42'42.13"E
Vwest3	23°44'42.34"N, 90°42'42.13"E
BA1	23 44’23.1”N, 90°44'7.80"E
BA2	23 44’22.8”N, 90 44’ 6.7”E
BA3	23°44'22.40"N, 90°44'13.70"E
BA4	23 44’ 25.0”N, 90 44’ 9.2”E
BA5	23 44’ 30.4”N, 90 44’ 13.1”E
BA6	23 44’ 30.8”N, 90 44’ 13.2”E
BA7	23 44’ 31.2”N, 90 44’ 11.9”E
BA8	23 44’ 32.0”N, 90 44’ 17.6”E
BA9	23 44’ 36.3”N, 90 44’ 14.4”E
BA10	23 44’ 38.1”N, 90 44” 16.8” E
BA11	23 44’ 33.7”N, 90, 44’ 11.1”E
BA12	23 44’ 37.5”N, 90 44’ 15.8”E

Name	Coordinates
BA13	23 44’ 35.1”N, 90, 43’ 46.6” E
BA14	23 44’ 26.2”N, 90 43’ 42.7”E
BA15	23 44 27.4”N, 90 43’ 42.8”E
RW1	23°44'34.90"N, 90°42'53.90"E
RW2	23°44'30.00"N, 90°43'2.40"E
RW3	23°44'24.00"N, 90°43'17.40"E
RW4	23°44'20.30"N, 90°43'28.60"E
RW5	23°44'17.50"N, 90°43'31.60"E

Table A.2 Groundwater and river water sample locations overview

Location of Sample	Sample ID	Depth (m)	Distance from the river (m)
River Water	RW1	0	0
	RW2	0	0
	RW3	0	0
	RW4	0	0
	RW5	0	0
East Bank Transect Wells	TWeast1	-52	240
	TWeast2	-52	370
	TWeast3	-58	480
	TWeast4	-61	560
	TWeast5	-27	720
	TWeast7	-16	960
	TWeast8	NA	980
	Veast2	-70	60
West Bank Transect Wells	TWwest1	-27	-180
	TWwest 1b	-146	-175
	TWwest2	-34	-135
	TWwest3	-27	-183
	TWwest4	-27	-230
	TWwest5	-18	-280
	TWwest7	-64	-420
	TWwest6	NA	350
	TWwest8	-25	-530
	Vwest1	-28	-260
	Vwest2	-45	-260
	Vwest3	-93	-260
Extra East Bank Wells	BA1	-73	860
	BA10	-51	880
	BA11	-38	790
	BA12	-35	870
	BA13	-64	160
	BA14	-33	150
	BA15	-52	145
	BA2	-61	840
	BA3	-76	1030

Location of Sample	Sample ID	Depth (m)	Distance from the river (m)
	BA4	-76	870
	BA5	-37	890
	BA6	-73	900
	BA7	-41	860
	BA8	-46	990
	BA9	-61	860

Table A.3 Field measurement of groundwater parameters

Sample ID	Location	Depth	Distance from River	T	Conductivity	pH	ORP	DO	Alkalinity
		(m)	(m)	(C)	(us/cm)		(MV)	(mg/L)	(mg/L)
TWeast1	East	51.816	240	25.4	2930	6.92	194.3 to 200.5	1	> 400
TWeast2	East	51.816	370	26.2	3050	6.78	182.4	3-4	375.8
TWeast3	East	57.912	480	26.4	3240	6.82	10.1 to 27.7	1-2	358.7
TWeast4	East	60.96	560	26.3	3820	6.8	-44.8 to -46.0	0-1	301.5
TWeast5	East	27.432	720	26.3	2920	6.8	-185.3	0-1	> 400
TWeast7	East	16.1544	960	26.7	2197	6.98	-76.05	0-1	> 400
Veast2	East	70	60	26.1	3780	6.47	7.9 to 10.0	0-1	310
TWwest1a	West	27.432	180	26	1251	7.01	-131.93	3-4	344.5
TWwest1b	West	146.304	175	25.6	1327.33	6.57	-142.53	2-3	128.3
TWwest2	West	33.528	135	26.3	2850	6.87	-52.2 to -53.2	2-3	> 400
TWwest3	West	27.432	183	26.3	3320	6.91	-86.9	2-3	> 400
TWwest4	West	27.432	230	25.9	2850	6.89	-82.5	1-2	> 400
TWwest5	West	18.288	380	27	1523	6.86	-3.9 to -7.4	0-1	> 400
TWwest7	West	64	420	26.3	1175	6.89	20.9 to 34.1	0-1	312.5
TWwest8	West	25	530	25.9	1124	6.62	-147.9	3-4	295
Vwest 1	West	28.0416	260	26.3	1810.33	6.97	-159.8	0-1	> 400
Vwest2	West	45.4152	260	26.2	1292.33	7.097	140.8 to -136.2	2-3	322.5
Vwest3	West	92.964	260	26.4	1152	7.03	-97.1 to -97.6	1-2	383.8

Table A.4 Field measurement of river water parameters

Sample ID	T	Conductivity	pH	ORP
	(C)	(us/cm)		(MV)
RW1	21.5	107.7	7.8	26.7
RW2	21.3	108.2	7.6	153.6

Table A.5 Field Measurement of Groundwater Well Cations and Anions

Note: For Table A.5, field measurements for cations and anions were only collected for transect wells west (TWwest), transect wells east (TWeast) and monitoring wells (Veast and Vwest). However, arsenic concentrations were measured for all well sites.

Sample	As	Mn	Fe	S	SO_4	PO_4	NH_3	NO_2	NO_3	SiO_2	Cl
	ppb	mg/L	mg/L	mg/L	mg/L	mg/L	mg/L	mg/L	mg/L	mg/L	mg/L
TWwest1a	300	0	2.267	0	0	0	0.089	< 0.015	< 0.23	>10	17.63
TWwest1b	0	0	5.722	0	20	0.625	0.118	0.02	0.58	>10	>40
TWwest2	400	3.968	3.291	0.118	23	1.628	0.859	< 0.015	1.33	>10	>40
TWwest3	500	3.845	>6.0	0.076	40	1.395	0.912	0.097	0.337	>10	>40
TWwest4	400	1.955	>6.0	0.084	0	1.79	0.771	0.078	0.67	>10	>40
TWwest5	0	1.786	0.462	0.482	2.495	0.694	<0.015	<0.015	0.85	>10	39.59
TWwest7	0	0.806	<0.20	0.071	2.51	0.245	0.034	0.018	<0.23		
TWwest8	500	1.745	>10	0.131	6.089	5.075	>2.0	0.039	1.06		
Vwest1	500	0.012	>10	0.165	0	4.366	0.188	0.156	1.27	>10	>40
Vwest2	0	0	<0.2	0	0	0.165	0.128	< 0.015		>10	22.37
Vwest3	10	1.772	1.253	0.045	25	0.517	0.147	< 0.015	0.91	>10	29.55
TWeast1	0	1.095	<0.20	0.018	2.29	0.183	<0.015	<0.015	<0.23	>10	>40
TWeast2	0	0.939	<0.20	0.04	1.02	0.073	<0.015	<0.015	0.63	>10	>40
TWeast3	0	1.228	0.316	0.199	2.98	0.138	0.108	<0.015	0.51	>10	>40
TWeast4	0	1.951	0.457	0.171	2.617	0.099	0.063	<0.015	0.5	>10	>40
TWeast5	500	2.581	5.845	0.333	54.3	4.854	1.347	<0.015	0.7	>10	>40
TWeast7	400	1.879	2.554	0.183	4	2.236	1.543	0.017	0.94	>10	>40
Veast2	0	3.071	0.855	0.135	5.124	0.498	0.03	<0.015	0.84		
BA1	0										
BA2	0										
BA3	0										
BA4	0										
BA5	500										
BA6	500										
BA7	500										
BA8	500										
BA9	100										
BA10	300										
BA11	500										

Sample	As	Mn	Fe	S	SO_4	PO_4	NH_3	NO_2	NO_3	SiO_2	Cl
	ppb	mg/L	mg/L	mg/L	mg/L	mg/L	mg/L	mg/L	mg/L	mg/L	mg/L
BA12	500										
BA13	0										
BA14	200										

Appendix B - Ion Chromatography

Table B.1 Groundwater Ion Chromatography Anion Results

	Depth	F-	Cl-	NO2-	Br-	NO3-	PO4---	SO4--
Well ID	m	mg/L	mg/L	mg/L	mg/L	mg/L	mg/L	mg/L
TW East 1	51.816	0.4045	283.517	0	1.1825	1.6352	0.081	1.1836
TW East 2	51.816	0.4026	311.684	0	1.3171	1.9069	0.0886	1.2763
TW East 3	57.912	0.3807	338.654	0	1.4233	1.6368	0.1309	1.3411
TW East 4	60.96	0.3587	475.276	0	1.8924	1.5635	0.0952	1.8094
TW East 5	27.432	0.1747	228.055	0.8413	0.2967	2.226	0.2707	55.9253
TW East 7	16.1544	0.1825	154.4863	0	0.3371	3.3702	0.2319	6.6172
V East 2	70	0.2987	466.977	0	1.837	1.5134	0	2.9808
TW West 1a	27.432	0.1892	13.3125	0	0.0858	1.6366	0.3321	1.0478
TW West 1b	146.304	0.1508	164.9912	0	0.5826	0	0	10.7186
TW West 2	33.528	0.1301	175.3305	0	0.2144	2.5748	0.0798	1.8035
TW West 3	27.432	0.1756	249.904	0.8172	0.2758	2.3892	0.2597	14.0274
TW West 4	27.432	0.1719	176.3675	0.7862	0.2064	2.191	0.2501	11.2776
TW West 5	18.288	0.6013	36.1635	0	0.2167	1.579	0	2.1119
TW West 7	64	0.7006	12.9916	1.3866	0.1085	0	0	1.2474
TW West 8	25	0.3198	12.8662	0	0.1079	1.3351	0	0.9335
V West 1	28.0416	0.275	37.4654	0	0.1739	1.9997	0	0.9154
V West 2	45.4152	0.7153	20.2657	0	0.1457	0	0	1.0455
V West 3	92.964	0.9159	23.3794	0	0.1656	0	0	1.4274

Table B.2 Groundwater Ion Chromatography Cation Results

	Depth	Na+	NH4+	K+	Mg++	Ca++
Well ID	m	mg/L	mg/L	mg/L	mg/L	mg/L
TW East 1	51.816	274.975	0	1.3949	17.6853	36.823
TW East 2	51.816	329.17	0	2.3288	19.4795	41.564
TW East 3	57.912	287.642	1.7388	2.8977	26.4893	53.124
TW East 4	60.96	337.485	0	2.9009	27.4414	58.635
TW East 5	27.432	130.051	5.4478	6.1727	44.2337	187.44
TW east 7	16.1544	17.1817	2.5102	4.82	35.9261	156.1292
V East 2	70	329.17	0	1.77	21.9609	55.148
TW West 1a	27.432	13.7631	1.8334	4.1417	22.2035	85.8885
TW West 1b	146.304	60.4094	0	2.4238	16.8604	39.7298

	Depth	**Na+**	**NH4+**	**K+**	**Mg++**	**Ca++**
Well ID	m	mg/L	mg/L	mg/L	mg/L	mg/L
TW West 2	33.528	37.8315	1.9743	5.4284	41.3167	214.948
TW West 3	27.432	145.23	3.6222	10.0183	46.1436	220.742
TW West 4	27.432	42.9457	2.1983	5.4773	49.2668	195.39
TW West 5	18.288	115.5731	0	2.0448	19.8981	41.8064
TW West 7	64	110.7462	0	1.6213	11.5553	24.5786
TW West 8	25	13.603	6.3688	4.9645	14.259	71.9742
V west 1	28.0416	70.8151	6.448	7.0468	30.6406	80.7733
V west 2	45.4152	129.2582	0.7067	1.7428	8.1514	21.4158
V west 3	92.964	157.292	1.1802	2.0075	9.4004	21.3556

Appendix C - Stable Isotopes

Table C.1 Groundwater Stable Isotope Ratios

Sample ID	Depth (m)	Distance (m)	δ 2H (‰)	δ 18O (‰)
TW-east 1	51.816	240	-27	-4.3
Tw-east 2	51.816	370	-26	-4.3
Tw-east 3	57.912	480	-27	-4.5
Tw-east 4	60.96	560	-29	-4.8
Tw-east 5	27.432	720	-15	-3.1
Tw-east 7	16.1544	960	-11	-2.5
Tw-east 8	NA	980	-38	-6
V-east 2	70	60	-27	-4.5
Tw-west1a	27.432	180	-20	-3.8
Tw-west-1b	146.304	175	-31	-4.8
TW-west 2	33.528	135	-18	-3.5
TW-west 3	27.432	183	-16	-3.3
TW-west 4	27.432	230	-22	-4.1
TW-west 5	18.288	380	-33	-5.1
Tw-west 6	NA	350	-31	-4.9
Tw-west 7	64	420	-36	-5.3
Tw-west 8	25	530	-16	-3.1
V-west 1	28.0416	260	-30	-5
V-west 2	45.4152	260	-29	-4.8
V-west 3	92.964	260	-31	-5

Appendix D - DOM Characterization

Table D.1 Groundwater OM Characteristics

Sample	Depth (m)	Distance (m)	DOC	SR	FI	FrI	HIX	abs254
TWeast1	-51.816	240	3.088	0.325468	1.893155	0.858922	3.534309	0.011328
TWeast2	-51.816	370	4.044	0.357412	1.914669	0.86359	4.993707	0.003434
TWeast3	-57.912	480	3.397	0.283993	1.862189	0.828047	4.339047	0.007882
TWeast4	-60.96	560	4.48	0.777716	1.903062	0.805274	4.744234	0.005947
TWeast5	-27.432	720	18.13	0.612427	1.56333	0.62391	15.394904	0.145253
TWeast7	-16.154	960	6.048	0.699225	1.607425	0.659682	11.336448	0.096842
TWeast8		980	8.826	0.638986	1.66522	0.693729	11.533801	0.108252
Veast2	-70	60	3.924	0.290828	1.937331	0.853983	5.564562	0.004656
BA1	-73.152	860	13.53	0.294005	1.795376	0.863581	3.438888	0.016502
BA2	-60.96	840	7.245	0.290329	1.766369	0.85876	5.508181	0.018007
BA3	-76.2	1030	6.38	0.303284	1.761768	0.833168	3.635404	0.033703
BA4	-76.2	870	5.551	0.310826	1.833268	0.834347	8.976352	0.029603
BA5	-36.5	890	4.987	0.506797	1.567538	0.613006	12.195975	0.072204
BA6	-73.152	900	9.986	0.556546	1.570604	0.59414	11.287097	0.113319
BA7	-41.148	860	6.386	0.619182	1.71716	0.728494	7.993548	0.091543
BA8	-45.72	990	6.913	0.689268	1.5658	0.594641	9.428898	0.11446
BA9	-60.96	860	8.702	0.457001	1.682505	0.734272	11.745423	0.106942

Sample	Depth (m)	Distance (m)	DOC	SR	FI	FrI	HIX	abs254
BA10	-51	880	5.585	0.556562	1.583946	0.612219	11.629441	0.059198
BA11	-37.7	790	8.388	0.703967	1.576634	0.605963	9.026357	0.13595
BA12	-35	870		0.689014	1.608471	0.624355	17.297085	0.094502
BA13	-64.008	160		0.540661	1.96293	0.749407	4.174947	0.01123
BA14	-32.6136	150		0.639334	1.657836	0.649786	18.355916	0.10654
BA15	-51.816	145		3.274646	1.840054	0.927658	1.495038	0.001494
RW1	0	0		0.534945	1.670604	0.712451	3.570187	0.037622
RW2	0	0		0.601763	1.58932	0.719503	7.872604	0.027593
RW3	0	0		0.556001	1.551644	0.741536	7.511772	0.027815
RW4	0	0		0.544407	1.589006	0.747654	3.756379	0.030872
RW5	0	0		0.480414	1.572949	0.740755	5.681363	0.029833
TWwest1	-27.432	-180	8.4685	0.614906	1.611609	0.660347	13.254734	0.04064
TWwest2	-33.528	-135	6.35	0.722206	1.620472	0.689223	10.945521	0.070597
TWwest3	-27.432	-183	6.91	0.721651	1.63135	0.65674	15.023946	0.102515
TWwest4	-27.432	-230	6.723	0.707702	1.640092	0.709218	8.62071	0.052835
TWwest5	-18.288	-280	3.733	0.570844	1.832242	0.753232	4.186179	0.004499
TWwest6		-350	3.399	0.260485	1.78834	0.80428	5.203162	0.007719
TWwest7	-64	-420	3.63	0.268057	1.832147	0.757044	3.330456	0.009947
TWwest8	-25	-530	6.317	0.45009	1.586909	0.63151	12.064101	0.062472
TWwest7	-64	-420	3.63	0.268057	1.832147	0.757044	3.330456	0.009947

Sample	Depth (m)	Distance (m)	DOC	SR	FI	FrI	HIX	abs254
Vwest2	-45.4152	-260	2.871	0.480338	1.754499	0.808578	3.970902	0.006412
Vwest3	-92.964	-260	5.482	0.319147	1.780734	0.742887	7.986852	0.008964

Table D.2 Groundwater OM Peaks Characterization

Sample	Depth (m)	Distance (m)	A	B	T	C	M	humic/protein
TWeast1	-51.816	240	0.276067	0.047992	0.06026	0.135059	0.165471	5.326432768
TWeast2	-51.816	370	0.21302	0.007659	0.043213	0.10685	0.12667	8.777716622
TWeast3	-57.912	480	0.293639	0.025917	0.053181	0.138359	0.169196	7.600622013
TWeast4	-60.96	560	0.13833	0.004662	0.026178	0.068831	0.08652	9.52273022
TWeast5	-27.432	720	4.410742	0.188297	0.417124	1.983808	2.369891	14.47660554
TWeast7	-16.154	960	2.955332	0.146554	0.315858	1.390478	1.653625	12.97421996
TWeast8	980		.858508	0.299595	0.480388	1.87033	2.282861	10.27163284
Veast2	-70	60	0.353174	0.057088	0.073014	0.180408	0.237669	5.928048762
BA1	-73.152	860	0.539175	0.086044	0.09572	0.264727	0.346551	6.329377655
BA2	-60.96	840	0.574039	0.063439	0.08739	0.277116	0.36732	8.078519383
BA3	-76.2	1030	0.790834	0.115978	0.135396	0.374652	0.494467	6.603519059
BA4	-76.2	870	0.84523	0.051658	0.10607	0.428428	0.555404	11.59630503
BA5	-36.5	890	1.820216	0.06885	0.144643	0.815753	0.915609	16.63557119
BA6	-73.152	900	2.784173	0.108856	0.22261	1.189466	1.436777	16.3226877
BA7	-41.148	860	2.445816	0.319605	0.342821	1.207337	1.411554	7.645694764
BA8	-45.72	990	2.759766	0.1347	0.242156	1.243806	1.402903	14.34626223

Sample	Depth (m)	Distance (m)	A	B	T	C	M	humic/protein
BA9	-60.96	860	2.35699	0.119518	0.262896	1.044501	1.374066	12.48792408
BA10	-51	880	1.783258	0.240427	0.161839	0.813693	0.933604	8.776667678
BA11	-37.7	790	3.374476	0.226087	0.384283	1.474073	1.718922	10.75981945
BA12	-35	870	2.322246	0.100693	0.205583	1.089959	1.218759	15.12023143
BA13	-64.008	160	0.215933	0.062691	0.050582	0.113714	0.177631	4.478366424
BA14	-32.6136	150	2.800193	0.124938	0.247964	1.369545	1.529093	15.2823825
BA15	-51.816	145	0.153586	0.091378	0.046577	0.079361	0.098491	2.402508064
RW1	0	0	0.879905	0.234133	0.251482	0.292807	0.38609	3.209954388
RW2	0	0	0.730579	0.117525	0.141931	0.257461	0.34566	5.140370622
RW3	0	0	0.686678	0.13533	0.142341	0.258361	0.34731	4.654245492
RW4	0	0	0.69095	0.155542	0.165304	0.257861	0.346731	4.037893569
RW5	0	0	0.697409	0.112713	0.14057	0.262104	0.352931	5.181729528
TWwest1	-27.432	-180	1.40256	0.064017	0.149194	0.685454	0.809903	13.59177997
TWwest2	-33.528	-135	2.357082	0.172146	0.282745	1.175758	1.385056	10.81115256
TWwest3	-27.432	-183	3.502103	0.162516	0.347971	1.614303	1.922309	13.78823555
TWwest4	-27.432	-230	1.818131	0.145326	0.233738	0.933885	1.086894	10.12733997
TWwest5	-18.288	-280	0.380386	0.060275	0.072749	0.192746	0.258913	6.254848749
TWwest6		-350	0.436518	0.052166	0.069983	0.222759	0.288538	7.759498645
TWwest7	-64	-420	0.458474	0.112344	0.106554	0.241209	0.304519	4.58753392
TWwest8	-25	-530	2.112946	0.132912	0.222438	0.922143	1.088548	11.60443788

Sample	Depth (m)	Distance (m)	A	B	T	C	M	humic/protein
TWwest7	-64	-420	0.458474	0.112344	0.106554	0.241209	0.304519	4.58753392
Vwest2	-45.4152	-260	0.322736	0.137988	0.066881	0.156774	0.202409	3.328561178
Vwest3	-92.964	-260	0.541386	0.072091	0.07857	0.263897	0.346582	7.64540923

Table D.3 Parafac Modeling

Sample	MaxInt	C1	C2	C3	Corr C1	Corr C2	Corr C3	Total Fl Int	%C1	%C2	%C3	Hum:Protein	S1	S2
TWeast1	0.52048	0.428506693	0.548050731	0.154006264	0.223029163	0.285249444	0.08015718	0.588435788	37.90203925	48.47588302	13.62207773	6.341024032	-0.010918	-0.033547
TWeast2	0.46217	0.356121559	0.496344594	0.093274239	0.164588701	0.229395581	0.043108555	0.437092837	37.65531871	52.48211859	9.862562708	9.139352515	-0.007752	-0.021689
TWeast3	0.5389	0.414392459	0.583578024	0.106348652	0.223316096	0.314490197	0.057311289	0.595117582	37.52470149	52.84505227	9.630246241	9.383950472	-0.009053	-0.031876
TWeast4	0.31901	0.366831553	0.544519075	0.272052762	0.117022934	0.17370703	0.086787551	0.377517515	30.99801438	46.01297241	22.98901322	3.349903976	-0.013937	-0.01792
TWeast5	6.1405	0.749328977	0.593184137	0.058829639	4.601254584	3.642447192	0.361243395	8.604945172	53.47221269	42.3296967	4.198090611	22.82035293	-0.012437	-0.020308
TWeast7	4.4265	0.685658521	0.578446294	0.070075124	3.035067444	2.560492518	0.310187538	5.9057475	51.39175768	43.35594297	5.252299352	18.03928038	-0.013875	-0.019843
TWeast8	5.6483	0.68644596	0.650927097	0.082793686	3.877252718	3.676631521	0.467643574	8.021527813	48.33558903	45.8345543	5.829856667	16.15308038	-0.013892	-0.021741
Veast2	0.75337	0.379579107	0.546670818	0.097502701	0.285963512	0.411845394	0.07345561	0.771264516	37.07722912	53.39872195	9.524048932	9.499736059	-0.009773	-0.033604
BA1	0.8823	0.520849863	0.707303156	0.209956834	0.459545834	0.624053575	0.185244914	1.268844323	36.21766876	49.18283224	14.599499	5.849550112	-0.017852	-0.060719
BA2	1.0345	0.463714054	0.644737116	0.117972925	0.479712189	0.666980547	0.122042991	1.268735727	37.81025308	52.57048669	9.619260229	9.395809825	-0.017024	-0.058638
BA3	1.1981	0.566318352	0.724394625	0.205393417	0.678506018	0.8678972	0.246081853	1.792485071	37.85281275	48.41865711	13.72853014	6.284100991	-0.014239	-0.046948
BA4	1.4141	0.53134076	0.681137443	0.07726345	0.751368969	0.963196457	0.109258245	1.823823671	41.19745678	52.81192874	5.990614479	15.69277841	-0.01489	-0.047904
BA5	2.6577	0.728178086	0.508092811	0.066062688	1.935278899	1.350358264	0.175574806	3.461211969	55.91333083	39.01402966	5.072639513	18.7136027	-0.012126	-0.023928
BA6	3.9075	0.73345101	0.559023276	0.070673316	2.865959823	2.184383451	0.276155982	5.326499256	53.80569274	41.00973916	5.184568107	18.28800971	-0.012153	-0.021837
BA7	3.6902	0.667950914	0.630135162	0.119064179	2.464872465	2.325324773	0.439370634	5.229567871	47.13338703	44.46495065	8.401662328	10.90240646	-0.015372	-0.024826
BA8	3.8916	0.760775865	0.533988648	0.092804884	2.960635355	2.078070223	0.361159486	5.399865064	54.8279507	38.48374354	6.688305755	13.95146957	-0.014255	-0.020682
BA9	3.3262	0.64770271	0.713927648	0.075268828	2.154388754	2.374666144	0.250359176	4.779414074	45.07641984	49.68529839	5.238281776	18.09022925	-0.009578	-0.020958
BA10	2.5036	0.762231736	0.537185019	0.080081887	1.908323375	1.344896414	0.200493012	3.453712801	55.25425781	38.94059788	5.805144307	16.22610063	-0.014504	-0.026061
BA11	4.8909	0.711352477	0.555788686	0.109100987	3.479153829	2.718306886	0.533602017	6.731062732	51.68803155	40.38451273	7.927455718	11.61438771	-0.016302	-0.023157
BA12	3.2871	0.751942835	0.552450107	0.056260118	2.471711292	1.815958747	0.184932634	4.472602673	55.26337734	40.60183476	4.134787901	23.18503739	-0.014715	-0.021357
BA13	0.47082	0.37257858	0.587856418	0.130997902	0.175417447	0.276774559	0.061676432	0.513868438	34.1366455	53.86097652	12.00237797	7.331682289	-0.009595	-0.017746
BA14	4.0566	0.723168508	0.581335628	0.04689536	2.93360537	2.358246108	0.190235716	5.482087194	53.51256313	43.01730389	3.470132986	27.81733939	-0.015953	-0.024953
BA15	0.26816	0.458731487	0.558396538	0.434308746	0.123013436	0.149739616	0.116464233	0.389217284	31.60533729	38.47198511	29.9226776	2.341946911	-0.006711	-0.002049
RW1	1.3259	0.590800613	0.499027075	0.339941585	0.783342532	0.661659999	0.450728547	1.895731079	41.32139527	34.90262973	23.775975	3.20592636	-0.016963	-0.03171
RW2	1.0831	0.62459903	0.524338191	0.17217321	0.67650321	0.567910695	0.186480803	1.430894707	47.27833614	39.68920226	13.0324616	6.673147487	-0.016676	-0.027712

Sample	MaxInt	C1	C2	C3	Corr C1	Corr C2	Corr C3	Total Fl Int	%C1	%C2	%C3	Hum:Protein	S1	S2
RW3	1.0077	0.644882482	0.5668315	0.189371074	0.649848078	0.571196102	0.190829231	1.411873411	46.02736143	40.45660878	13.5160298	6.39862234	-0.017108	-0.03077
RW4	1.0578	0.602928392	0.539578921	0.277809292	0.637777653	0.570766582	0.293866669	1.502410904	42.45028114	37.99004525	19.55967361	4.11255975	-0.017813	-0.03272
RW5	1.0533	0.617535695	0.565399825	0.200952935	0.650450348	0.595535636	0.211663727	1.45764971	44.62322759	40.85588133	14.52089108	5.886629715	-0.017803	-0.037058
TWwest1	2.0918	0.705637981	0.564087494	0.065698155	1.476053529	1.179958219	0.137427401	2.793439149	52.84001012	42.2403409	4.919648982	19.32665346	-0.012953	-0.021065
TWwest2	3.5497	0.682819055	0.616027468	0.075989887	2.423802801	2.186712702	0.269741304	4.880256806	49.66547658	44.80732856	5.527194866	17.09236013	-0.014512	-0.020095
TWwest3	4.9906	0.712014571	0.613436004	0.062807435	3.55337992	3.061413722	0.313446784	6.928240426	51.28834598	44.18746369	4.524190332	21.10340252	-0.014795	-0.020502
TWwest4	2.685	0.698593689	0.625883125	0.101632547	1.875724056	1.680496192	0.272883388	3.829103636	48.98598299	43.88745648	7.12656053	13.0320144	-0.014435	-0.020398
TWwest5	0.78489	0.444949559	0.546698932	0.126393966	0.34923646	0.429098524	0.09920536	0.877540344	39.79719702	48.89786862	11.30493435	7.845694885	-0.004977	-0.008719
TWwest6	0.81717	0.4865596	0.583881449	0.109805925	0.397601909	0.477130404	0.089730108	0.96446242	41.22523597	49.47112444	9.30363959	9.748481714	-0.01157	-0.044415
TWwest7	0.92718	0.473775558	0.53178965	0.154633799	0.439275221	0.493064728	0.143373366	1.075713315	40.8357148	45.83607182	13.32821338	6.502881078	-0.011973	-0.044666
TWwest8	3.0796	0.705464516	0.563766447	0.081650423	2.172548523	1.736175151	0.251450641	4.160174316	52.22253585	41.73323084	6.044233304	15.54469557	-0.011036	-0.024521
TWwest7	0.92718	0.473775558	0.53178965	0.154633799	0.439275221	0.493064728	0.143373366	1.075713315	40.8357148	45.83607182	13.32821338	6.502881078	-0.011973	-0.044666
Vwest2	0.59114	0.489761603	0.553253478	0.178387753	0.289517674	0.327050261	0.105452136	0.722020072	40.09828612	45.29656087	14.60515301	5.846898484	-0.006268	-0.01305
Vwest3	0.9288	0.5377732	0.59145522	0.087444288	0.499483748	0.549343608	0.081218255	1.130045611	44.20031751	48.61251642	7.187166063	12.91368992	-0.00884	-0.027698

Appendix E - Fluorescence Spectroscopy (EEM's and Peaks)

Protocol for fluorescence spectroscopy

The quinine sulfate was scanned and recorded the emission at 450 nm (observed) in the Aqualog logbook.xls.

- Cuvette check- Integration time = 0.25 sec Gain = High Increment = 3.28 nm Excitation = 240 nm
- Raman scan check and calculate the area under Raman Peak- Integration time = 0.25 sec Gain = High Increment = 3.28 nm Excitation = 350 nm
- Quinine sulfate scan and record the emission at 450 nm-

Integration time = 0.25 sec

Increment = 0.41 nm ☐ Acquisition 3D EEM-

Integration time = 0.25 and 1 second Excitation = 240-450 nm Gain = High

Gain = High Excitation = 347.5 nm

Increment = 3.28 nm Emission = 300-550 nm

3-D Excitation Emission Matrix (EEM's)

Figure E.1 East Groundwater EEM's

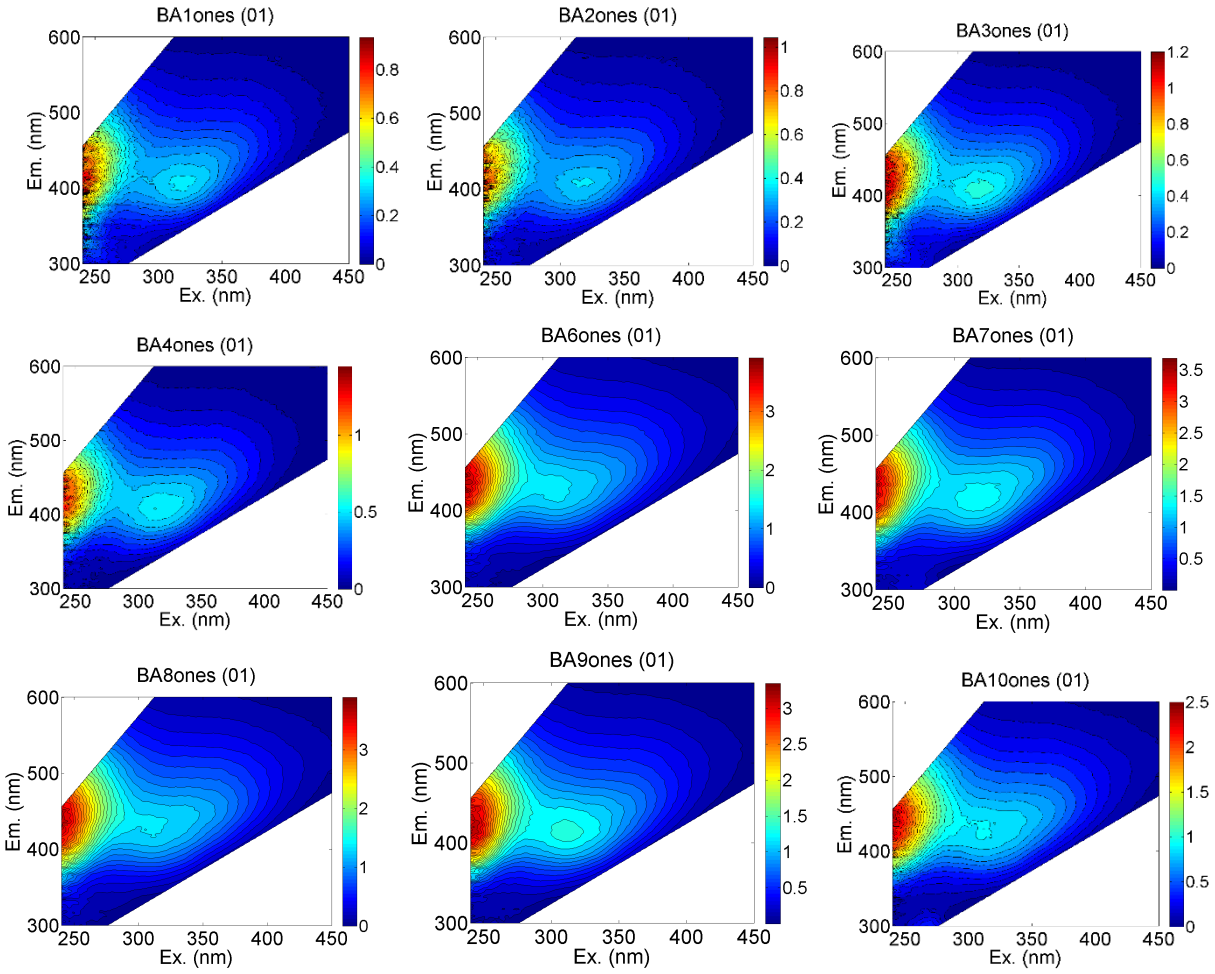

Figure E.1 East Groundwater EEM's

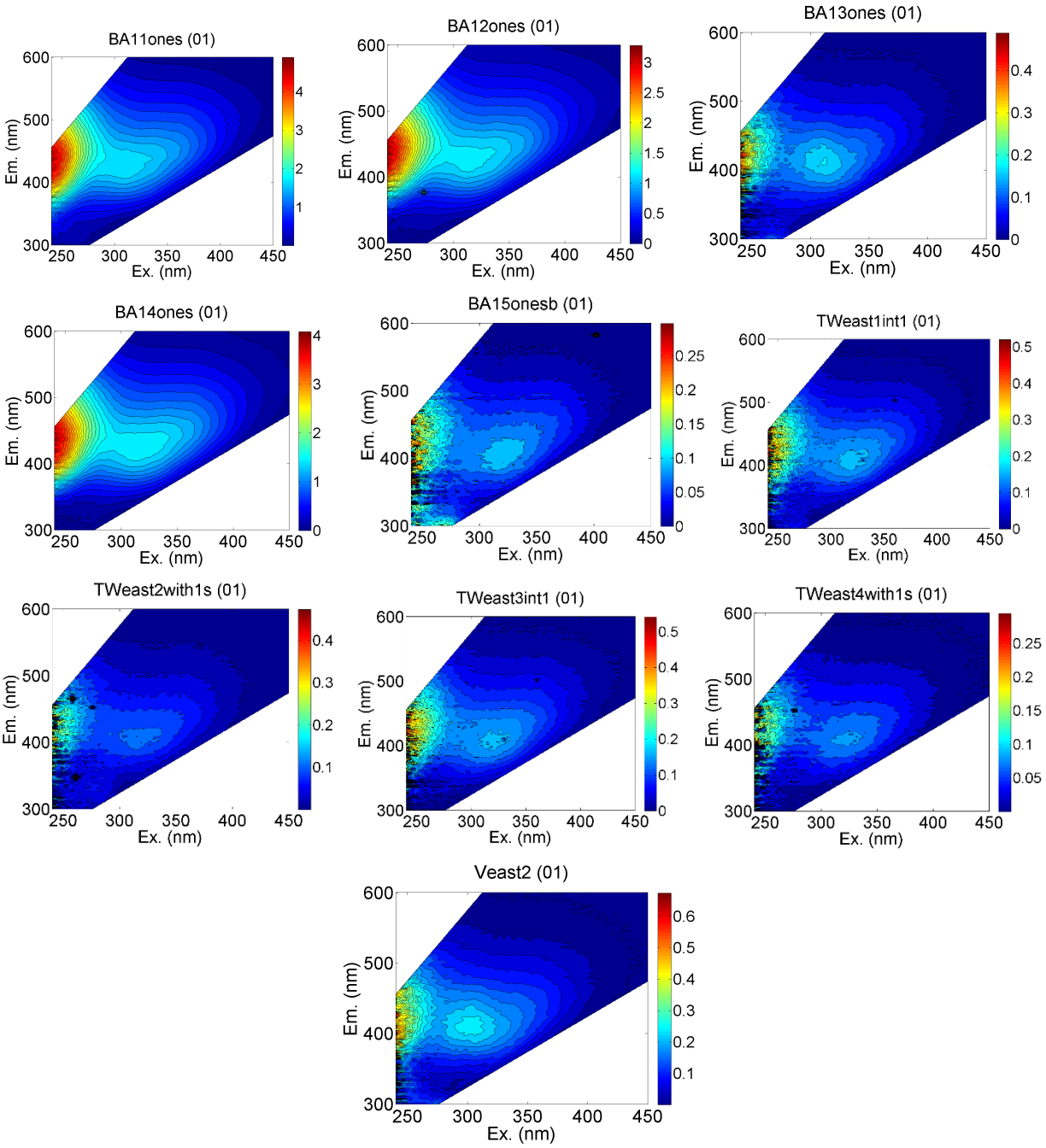

Figure E.2 West Groundwater EEM's

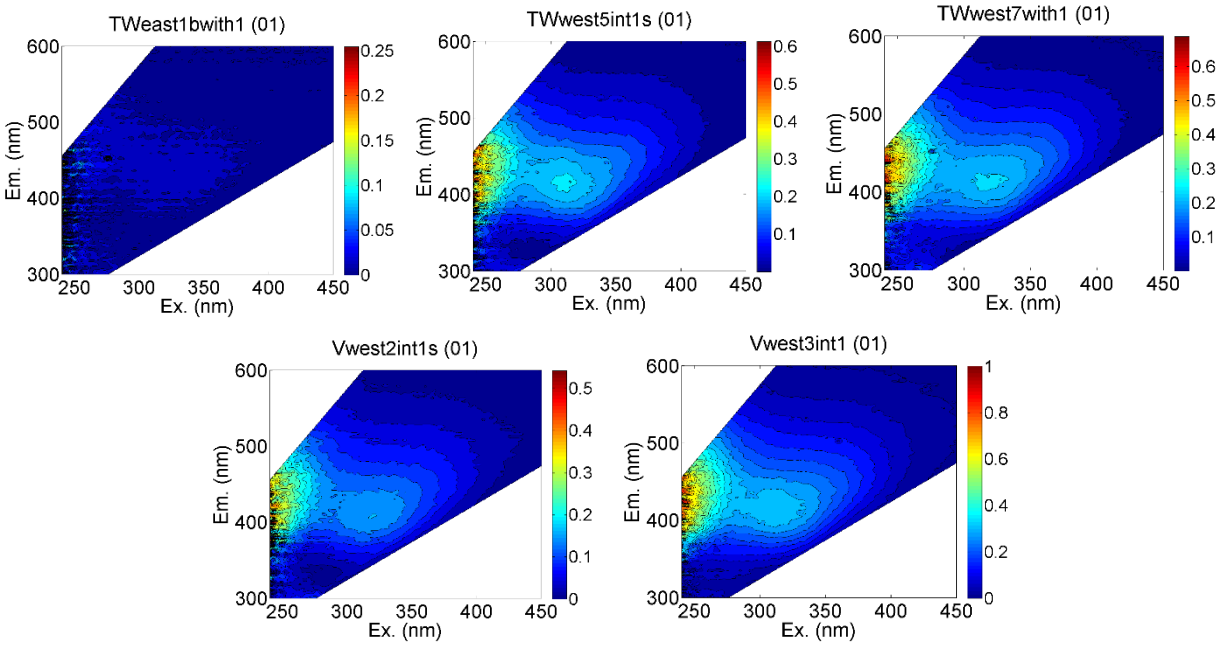

Figure E.3 River Water EEM's

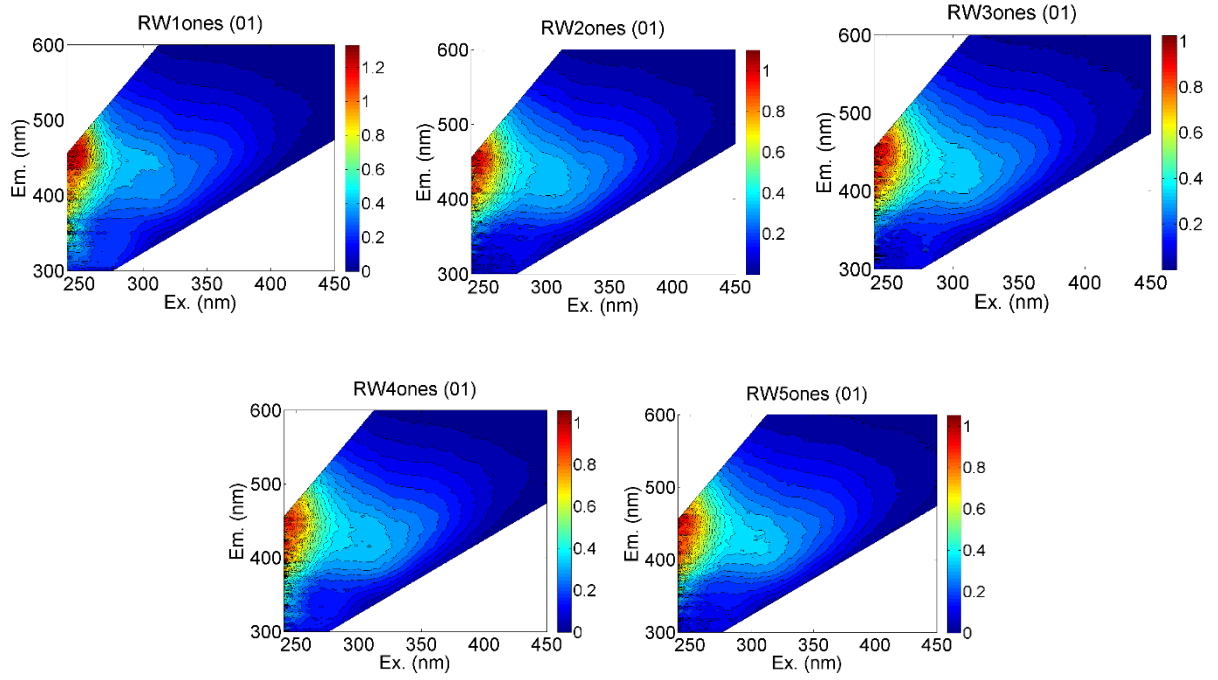

Appendix F - Sediment Field Parameters

Table F.1 Coordinates of sediment cores

Core Name	Bank	Coordinates
Core 1	East	23°44'41.90"N, 90°43'44.80"E
Core 1b	East	23°44'41.91"N, 90°43'44.40"E
Core 2	East	23°44'39.90"N, 90°43'44.00"E
Core 3	East	90°43'46.48"E, 90°43'39.00"E
Core 4	East	23°44'13.00"N, 90°43'32.10"E
Core 5	West	23°45'1.30"N, 90°43'1.80"E
Core 6	West	23°44'40.90"N, 90°42'50.90"E
Core **7**	West	23°44'24.90"N, 90°42'37.90"E
Core 8	East	23°43'21.40"N, 90°42'56.90"E

Table F.2 Description of sediment core depth intervals, and estimated depth

Location	Core #	Depth Intervals (cm)	Graph Depth (cm)	Location	Core #	Depth Intervals (cm)	Graph Depth (cm)
East	1	0-61 T	0	West	5	0-61 T	0
		61-122 B	112			0-61 B	50
		122- 183 T	130			61-122 T	71
		122- 183 B	183			61-122 B	112
		183- 244 T	198			122- 183 T	130
		183- 244 B	244			122- 183 B	183
East	1b	0-61 T	0	West	6	0-61 T	0
		0-61 B	50			0-61 B	50
		61-122 T	70			61-122 T	71
		61-122 B	122			61-122 B	122
East	2	0-61 T	0	West	7	0-61 T	0
		0-61 B	50			0-61 B	50
		61-122 T	70			61-122 T	71
		61-122 B	122			61-122 B	122
East	3	0-33 T	0	Island	8	0-61 T	0
		0-33 B	28			61-122 B	122
		33-91 T	40			61-122 T	71
		33-91 B	91			61-122 B	122
		91-122 B	122				
East	4	0-61 T	0				
		0-61 B	50				
		61-122 T	71				
		61-122 B	122				

Appendix G - Particle Size Data

Table G.1 PSA Core 1

Core 1																	
0 cm			**60 cm**			**130 cm**			**183 cm**			**198 cm**			**244 cm**		
Size (μm)	% Volume In	% Cum. Volume	Size (μm)	% Volume In	% Cum. Volume	Size (μm)	% Volume In	% Cum. Volume	Size (μm)	% Volume In	% Cum. Volume	Size (μm)	% Volume In	% Cum. Volume	Size (μm)	% Volume In	% Cum. Volume
0.01	0	0	0.01	0	0	0.01	0	0	0.01	0	0	0.01	0	0	0.01	0	0
0.0114	0	0	0.0114	0	0	0.0114	0	0	0.0114	0	0	0.0114	0	0	0.0114	0	0
0.0129	0	0	0.0129	0	0	0.0129	0	0	0.0129	0	0	0.0129	0	0	0.0129	0	0
0.0147	0	0	0.0147	0	0	0.0147	0	0	0.0147	0	0	0.0147	0	0	0.0147	0	0
0.0167	0	0	0.0167	0	0	0.0167	0	0	0.0167	0	0	0.0167	0	0	0.0167	0	0
0.0189	0	0	0.0189	0	0	0.0189	0	0	0.0189	0	0	0.0189	0	0	0.0189	0	0
0.0215	0	0	0.0215	0	0	0.0215	0	0	0.0215	0	0	0.0215	0	0	0.0215	0	0
0.0244	0	0	0.0244	0	0	0.0244	0	0	0.0244	0	0	0.0244	0	0	0.0244	0	0
0.0278	0	0	0.0278	0	0	0.0278	0	0	0.0278	0	0	0.0278	0	0	0.0278	0	0
0.0315	0	0	0.0315	0	0	0.0315	0	0	0.0315	0	0	0.0315	0	0	0.0315	0	0
0.0358	0	0	0.0358	0	0	0.0358	0	0	0.0358	0	0	0.0358	0	0	0.0358	0	0
0.0407	0	0	0.0407	0	0	0.0407	0	0	0.0407	0	0	0.0407	0	0	0.0407	0	0
0.0463	0	0	0.0463	0	0	0.0463	0	0	0.0463	0	0	0.0463	0	0	0.0463	0	0
0.0526	0	0	0.0526	0	0	0.0526	0	0	0.0526	0	0	0.0526	0	0	0.0526	0	0
0.0597	0	0	0.0597	0	0	0.0597	0	0	0.0597	0	0	0.0597	0	0	0.0597	0	0
0.0679	0	0	0.0679	0	0	0.0679	0	0	0.0679	0	0	0.0679	0	0	0.0679	0	0
0.0771	0	0	0.0771	0	0	0.0771	0	0	0.0771	0	0	0.0771	0	0	0.0771	0	0
0.0876	0	0	0.0876	0	0	0.0876	0	0	0.0876	0	0	0.0876	0	0	0.0876	0	0
0.0995	0	0	0.0995	0	0	0.0995	0	0	0.0995	0	0	0.0995	0	0	0.0995	0	0
0.113	0	0	0.113	0	0	0.113	0	0	0.113	0	0	0.113	0	0	0.113	0	0
0.128	0	0	0.128	0	0	0.128	0	0	0.128	0	0	0.128	0	0	0.128	0	0
0.146	0	0	0.146	0	0	0.146	0	0	0.146	0	0	0.146	0	0	0.146	0	0
0.166	0	0	0.166	0	0	0.166	0	0	0.166	0	0	0.166	0	0	0.166	0	0

Core 1																	
0 cm			**60 cm**			**130 cm**			**183 cm**			**198 cm**			**244 cm**		
Size (μm)	% Volume In	% Cum. Volume	Size (μm)	% Volume In	% Cum. Volume	Size (μm)	% Volume In	% Cum. Volume	Size (μm)	% Volume In	% Cum. Volume	Size (μm)	% Volume In	% Cum. Volume	Size (μm)	% Volume In	% Cum. Volume
0.188	0	0	0.188	0	0	0.188	0	0	0.188	0	0	0.188	0	0	0.188	0	0
0.214	0	0	0.214	0	0	0.214	0	0	0.214	0	0	0.214	0	0	0.214	0	0
0.243	0	0	0.243	0	0	0.243	0	0	0.243	0	0	0.243	0	0	0.243	0	0
0.276	0	0	0.276	0	0	0.276	0	0	0.276	0	0	0.276	0	0	0.276	0	0
0.314	0	0	0.314	0	0	0.314	0	0	0.314	0	0	0.314	0	0	0.314	0	0
0.357	0	0	0.357	0	0	0.357	0	0	0.357	0	0	0.357	0	0	0.357	0	0
0.405	0	0	0.405	0	0	0.405	0	0	0.405	0	0	0.405	0	0	0.405	0	0
0.46	0	0	0.46	0	0	0.46	0	0	0.46	0	0	0.46	0	0	0.46	0	0
0.523	0	0	0.523	0	0	0.523	0	0	0.523	0	0	0.523	0	0	0.523	0	0
0.594	0	0	0.594	0.07	0.07	0.594	0.05	0.05	0.594	0.09	0.09	0.594	0.06	0.06	0.594	0.08	0.08
0.675	0	0	0.675	0.15	0.22	0.675	0.15	0.2	0.675	0.19	0.28	0.675	0.14	0.2	0.675	0.15	0.23
0.767	0	0	0.767	0.22	0.44	0.767	0.22	0.42	0.767	0.27	0.55	0.767	0.21	0.41	0.767	0.21	0.44
0.872	0	0	0.872	0.25	0.69	0.872	0.26	0.68	0.872	0.31	0.86	0.872	0.24	0.65	0.872	0.24	0.68
0.991	0.03	0.03	0.991	0.25	0.94	0.991	0.26	0.94	0.991	0.32	1.18	0.991	0.25	0.9	0.991	0.24	0.92
1.13	0.05	0.08	1.13	0.25	1.19	1.13	0.26	1.2	1.13	0.31	1.49	1.13	0.24	1.14	1.13	0.23	1.15
1.28	0.05	0.13	1.28	0.25	1.44	1.28	0.26	1.46	1.28	0.31	1.8	1.28	0.25	1.39	1.28	0.23	1.38
1.45	0.05	0.18	1.45	0.27	1.71	1.45	0.29	1.75	1.45	0.34	2.14	1.45	0.27	1.66	1.45	0.25	1.63
1.65	0.06	0.24	1.65	0.31	2.02	1.65	0.34	2.09	1.65	0.39	2.53	1.65	0.32	1.98	1.65	0.28	1.91
1.88	0.06	0.3	1.88	0.36	2.38	1.88	0.41	2.5	1.88	0.45	2.98	1.88	0.37	2.35	1.88	0.32	2.23
2.13	0.07	0.37	2.13	0.41	2.79	2.13	0.48	2.98	2.13	0.51	3.49	2.13	0.43	2.78	2.13	0.37	2.6
2.42	0.08	0.45	2.42	0.47	3.26	2.42	0.54	3.52	2.42	0.58	4.07	2.42	0.49	3.27	2.42	0.41	3.01
2.75	0.1	0.55	2.75	0.52	3.78	2.75	0.61	4.13	2.75	0.64	4.71	2.75	0.55	3.82	2.75	0.46	3.47
3.12	0.11	0.66	3.12	0.57	4.35	3.12	0.67	4.8	3.12	0.71	5.42	3.12	0.61	4.43	3.12	0.51	3.98
3.55	0.13	0.79	3.55	0.63	4.98	3.55	0.74	5.54	3.55	0.78	6.2	3.55	0.67	5.1	3.55	0.57	4.55
4.03	0.15	0.94	4.03	0.69	5.67	4.03	0.81	6.35	4.03	0.86	7.06	4.03	0.74	5.84	4.03	0.63	5.18
4.58	0.16	1.1	4.58	0.75	6.42	4.58	0.89	7.24	4.58	0.94	8	4.58	0.81	6.65	4.58	0.69	5.87
5.21	0.16	1.26	5.21	0.81	7.23	5.21	0.97	8.21	5.21	1.02	9.02	5.21	0.88	7.53	5.21	0.75	6.62

Core 1																	
0 cm			**60 cm**			**130 cm**			**183 cm**			**198 cm**			**244 cm**		
Size (μm)	% Volume In	% Cum. Volume	Size (μm)	% Volume In	% Cum. Volume	Size (μm)	% Volume In	% Cum. Volume	Size (μm)	% Volume In	% Cum. Volume	Size (μm)	% Volume In	% Cum. Volume	Size (μm)	% Volume In	% Cum. Volume
5.92	0.16	1.42	5.92	0.87	8.1	5.92	1.05	9.26	5.92	1.11	10.13	5.92	0.95	8.48	5.92	0.81	7.43
6.72	0.16	1.58	6.72	0.93	9.03	6.72	1.13	10.39	6.72	1.2	11.33	6.72	1.03	9.51	6.72	0.87	8.3
7.64	0.16	1.74	7.64	1.01	10.04	7.64	1.23	11.62	7.64	1.3	12.63	7.64	1.11	10.62	7.64	0.93	9.23
8.68	0.18	1.92	8.68	1.1	11.14	8.68	1.34	12.96	8.68	1.42	14.05	8.68	1.21	11.83	8.68	0.99	10.22
9.86	0.22	2.14	9.86	1.21	12.35	9.86	1.47	14.43	9.86	1.55	15.6	9.86	1.32	13.15	9.86	1.06	11.28
11.2	0.3	2.44	11.2	1.36	13.71	11.2	1.62	16.05	11.2	1.7	17.3	11.2	1.45	14.6	11.2	1.15	12.43
12.7	0.4	2.84	12.7	1.54	15.25	12.7	1.78	17.83	12.7	1.87	19.17	12.7	1.59	16.19	12.7	1.25	13.68
14.5	0.52	3.36	14.5	1.74	16.99	14.5	1.95	19.78	14.5	2.04	21.21	14.5	1.75	17.94	14.5	1.38	15.06
16.4	0.64	4	16.4	1.96	18.95	16.4	2.11	21.89	16.4	2.21	23.42	16.4	1.9	19.84	16.4	1.51	16.57
18.7	0.71	4.71	18.7	2.17	21.12	18.7	2.24	24.13	18.7	2.36	25.78	18.7	2.04	21.88	18.7	1.64	18.21
21.2	0.72	5.43	21.2	2.38	23.5	21.2	2.32	26.45	21.2	2.5	28.28	21.2	2.17	24.05	21.2	1.76	19.97
24.1	0.62	6.05	24.1	2.55	26.05	24.1	2.36	28.81	24.1	2.62	30.9	24.1	2.27	26.32	24.1	1.85	21.82
27.4	0.44	6.49	27.4	2.69	28.74	27.4	2.35	31.16	27.4	2.74	33.64	27.4	2.33	28.65	27.4	1.89	23.71
31.1	0.21	6.7	31.1	2.82	31.56	31.1	2.32	33.48	31.1	2.87	36.51	31.1	2.35	31	31.1	1.88	25.59
35.3	0.02	6.72	35.3	2.95	34.51	35.3	2.32	35.8	35.3	3.04	39.55	35.3	2.34	33.34	35.3	1.83	27.42
40.1	0.05	6.77	40.1	3.12	37.63	40.1	2.4	38.2	40.1	3.27	42.82	40.1	2.3	35.64	40.1	1.76	29.18
45.6	0.33	7.1	45.6	3.37	41	45.6	2.63	40.83	45.6	3.59	46.41	45.6	2.27	37.91	45.6	1.71	30.89
51.8	1.05	8.15	51.8	3.72	44.72	51.8	3.03	43.86	51.8	3.99	50.4	51.8	2.27	40.18	51.8	1.75	32.64
58.9	2.35	10.5	58.9	4.2	48.92	58.9	3.62	47.48	58.9	4.44	54.84	58.9	2.36	42.54	58.9	1.96	34.6
66.9	4.25	14.75	66.9	4.75	53.67	66.9	4.36	51.84	66.9	4.89	59.73	66.9	2.57	45.11	66.9	2.39	36.99
76	6.58	21.33	76	5.33	59	76	5.17	57.01	76	5.29	65.02	76	2.96	48.07	76	3.08	40.07
86.4	9.01	30.34	86.4	5.84	64.84	86.4	5.92	62.93	86.4	5.53	70.55	86.4	3.5	51.57	86.4	4	44.07
98.1	11.11	41.45	98.1	6.17	71.01	98.1	6.46	69.39	98.1	5.57	76.12	98.1	4.17	55.74	98.1	5.06	49.13
111	12.42	53.87	111	6.23	77.24	111	6.67	76.06	111	5.37	81.49	111	4.89	60.63	111	6.11	55.24
127	12.6	66.47	127	5.97	83.21	127	6.46	82.52	127	4.93	86.42	127	5.56	66.19	127	6.97	62.21
144	11.56	78.03	144	5.37	88.58	144	5.81	88.33	144	4.28	90.7	144	6.05	72.24	144	7.47	69.68
163	9.5	87.53	163	4.48	93.06	163	4.79	93.12	163	3.49	94.19	163	6.23	78.47	163	7.48	77.16

Core 1																	
0 cm			**60 cm**			**130 cm**			**183 cm**			**198 cm**			**244 cm**		
Size (μm)	% Volume In	% Cum. Volume	Size (μm)	% Volume In	% Cum. Volume	Size (μm)	% Volume In	% Cum. Volume	Size (μm)	% Volume In	% Cum. Volume	Size (μm)	% Volume In	% Cum. Volume	Size (μm)	% Volume In	% Cum. Volume
186	6.84	94.37	186	3.38	96.44	186	3.53	96.65	186	2.63	96.82	186	6.03	84.5	186	6.97	84.13
211	4.15	98.52	211	2.23	98.67	211	2.23	98.88	211	1.78	98.6	211	5.39	89.89	211	5.97	90.1
240	1.45	99.97	240	1.19	99.86	240	1.1	99.98	240	1.02	99.62	240	4.39	94.28	240	4.63	94.73
272	0.01	99.98	272	0.15	100.01	272	0.02	100	272	0.37	99.99	272	3.14	97.42	272	3.15	97.88
310	0	99.98	310	0	100.01	310	0	100	310	0	99.99	310	1.87	99.29	310	1.76	99.64
352	0	99.98	352	0	100.01	352	0	100	352	0	99.99	352	0.7	99.99	352	0.37	100.01
400	0	99.98	400	0	100.01	400	0	100	400	0	99.99	400	0	99.99	400	0	100.01
454	0	99.98	454	0	100.01	454	0	100	454	0	99.99	454	0	99.99	454	0	100.01
516	0	99.98	516	0	100.01	516	0	100	516	0	99.99	516	0	99.99	516	0	100.01
586	0	99.98	586	0	100.01	586	0	100	586	0	99.99	586	0	99.99	586	0	100.01
666	0	99.98	666	0	100.01	666	0	100	666	0	99.99	666	0	99.99	666	0	100.01
756	0	99.98	756	0	100.01	756	0	100	756	0	99.99	756	0	99.99	756	0	100.01
859	0	99.98	859	0	100.01	859	0	100	859	0	99.99	859	0	99.99	859	0	100.01
976	0	99.98	976	0	100.01	976	0	100	976	0	99.99	976	0	99.99	976	0	100.01
1110	0	99.98	1110	0	100.01	1110	0	100	1110	0	99.99	1110	0	99.99	1110	0	100.01
1260	0	99.98	1260	0	100.01	1260	0	100	1260	0	99.99	1260	0	99.99	1260	0	100.01
1430	0	99.98	1430	0	100.01	1430	0	100	1430	0	99.99	1430	0	99.99	1430	0	100.01
1630	0	99.98	1630	0	100.01	1630	0	100	1630	0	99.99	1630	0	99.99	1630	0	100.01
1850	0	99.98	1850	0	100.01	1850	0	100	1850	0	99.99	1850	0	99.99	1850	0	100.01
2100	0	99.98	2100	0	100.01	2100	0	100	2100	0	99.99	2100	0	99.99	2100	0	100.01
2390	0	99.98	2390	0	100.01	2390	0	100	2390	0	99.99	2390	0	99.99	2390	0	100.01
2710	0	99.98	2710	0	100.01	2710	0	100	2710	0	99.99	2710	0	99.99	2710	0	100.01
3080	0	99.98	3080	0	100.01	3080	0	100	3080	0	99.99	3080	0	99.99	3080	0	100.01
3500		99.98	3500		100.01	3500		100	3500		99.99	3500		99.99	3500		100.01

Table G.2 PSA Core 1b

Core 1b					
0 cm			**122 cm**		
Size (μm)	% Volume In	% Cumulative Volume	Size (μm)	% Volume In	% Cumulative Volume
0.01	0	0	0.01	0	0
0.0114	0	0	0.0114	0	0
0.0129	0	0	0.0129	0	0
0.0147	0	0	0.0147	0	0
0.0167	0	0	0.0167	0	0
0.0189	0	0	0.0189	0	0
0.0215	0	0	0.0215	0	0
0.0244	0	0	0.0244	0	0
0.0278	0	0	0.0278	0	0
0.0315	0	0	0.0315	0	0
0.0358	0	0	0.0358	0	0
0.0407	0	0	0.0407	0	0
0.0463	0	0	0.0463	0	0
0.0526	0	0	0.0526	0	0
0.0597	0	0	0.0597	0	0
0.0679	0	0	0.0679	0	0
0.0771	0	0	0.0771	0	0
0.0876	0	0	0.0876	0	0
0.0995	0	0	0.0995	0	0
0.113	0	0	0.113	0	0

Core 1b					
0 cm			**122 cm**		
Size (μm)	% Volume In	% Cumulative Volume	Size (μm)	% Volume In	% Cumulative Volume
0.128	0	0	0.128	0	0
0.146	0	0	0.146	0	0
0.166	0	0	0.166	0	0
0.188	0	0	0.188	0	0
0.214	0	0	0.214	0	0
0.243	0	0	0.243	0	0
0.276	0	0	0.276	0	0
0.314	0	0	0.314	0	0
0.357	0	0	0.357	0	0
0.405	0	0	0.405	0	0
0.46	0	0	0.46	0	0
0.523	0	0	0.523	0	0
0.594	0	0	0.594	0	0
0.675	0.08	0.08	0.675	0	0
0.767	0.12	0.2	0.767	0	0
0.872	0.15	0.35	0.872	0	0
0.991	0.15	0.5	0.991	0	0
1.13	0.15	0.65	1.13	0.02	0.02
1.28	0.14	0.79	1.28	0.06	0.08
1.45	0.15	0.94	1.45	0.07	0.15
1.65	0.17	1.11	1.65	0.08	0.23
1.88	0.2	1.31	1.88	0.09	0.32

Core 1b					
0 cm			**122 cm**		
Size (μm)	% Volume In	% Cumulative Volume	Size (μm)	% Volume In	% Cumulative Volume
2.13	0.22	1.53	2.13	0.1	0.42
2.42	0.25	1.78	2.42	0.12	0.54
2.75	0.28	2.06	2.75	0.14	0.68
3.12	0.32	2.38	3.12	0.16	0.84
3.55	0.36	2.74	3.55	0.19	1.03
4.03	0.39	3.13	4.03	0.21	1.24
4.58	0.43	3.56	4.58	0.23	1.47
5.21	0.47	4.03	5.21	0.25	1.72
5.92	0.5	4.53	5.92	0.26	1.98
6.72	0.53	5.06	6.72	0.26	2.24
7.64	0.57	5.63	7.64	0.28	2.52
8.68	0.63	6.26	8.68	0.3	2.82
9.86	0.7	6.96	9.86	0.34	3.16
11.2	0.8	7.76	11.2	0.41	3.57
12.7	0.93	8.69	12.7	0.51	4.08
14.5	1.07	9.76	14.5	0.62	4.7
16.4	1.21	10.97	16.4	0.74	5.44
18.7	1.32	12.29	18.7	0.82	6.26
21.2	1.36	13.65	21.2	0.84	7.1
24.1	1.34	14.99	24.1	0.78	7.88
27.4	1.25	16.24	27.4	0.63	8.51
31.1	1.12	17.36	31.1	0.43	8.94

Core 1b					
0 cm			**122 cm**		
Size (μm)	% Volume In	% Cumulative Volume	Size (μm)	% Volume In	% Cumulative Volume
35.3	1.03	18.39	35.3	0.25	9.19
40.1	1.07	19.46	40.1	0.2	9.39
45.6	1.35	20.81	45.6	0.41	9.8
51.8	1.97	22.78	51.8	1.01	10.81
58.9	2.97	25.75	58.9	2.08	12.89
66.9	4.31	30.06	66.9	3.62	16.51
76	5.87	35.93	76	5.53	22.04
86.4	7.43	43.36	86.4	7.57	29.61
98.1	8.73	52.09	98.1	9.43	39.04
111	9.52	61.61	111	10.78	49.82
127	9.62	71.23	127	11.35	61.17
144	8.96	80.19	144	11	72.17
163	7.64	87.83	163	9.77	81.94
186	5.86	93.69	186	7.87	89.81
211	3.92	97.61	211	5.63	95.44
240	2.09	99.7	240	3.41	98.85
272	0.3	100	272	1.19	100.04
310	0	100	310	0	100.04
352	0	100	352	0	100.04
400	0	100	400	0	100.04
454	0	100	454	0	100.04
516	0	100	516	0	100.04

Core 1b					
0 cm			**122 cm**		
Size (μm)	% Volume In	% Cumulative Volume	Size (μm)	% Volume In	% Cumulative Volume
586	0	100	586	0	100.04
666	0	100	666	0	100.04
756	0	100	756	0	100.04
859	0	100	859	0	100.04
976	0	100	976	0	100.04
1110	0	100	1110	0	100.04
1260	0	100	1260	0	100.04
1430	0	100	1430	0	100.04
1630	0	100	1630	0	100.04
1850	0	100	1850	0	100.04
2100	0	100	2100	0	100.04
2390	0	100	2390	0	100.04
2710	0	100	2710	0	100.04
3080	0	100	3080	0	100.04
3500		100	3500		100.04

Table G.3 PSA Core 2

Core 2					
0 cm			**122 cm**		
Size (μm)	% Volume In	% Cumulative Volume	Size (μm)	% Volume In	% Cumulative Volume
0.01	0	0	0.01	0	0
0.0114	0	0	0.0114	0	0
0.0129	0	0	0.0129	0	0
0.0147	0	0	0.0147	0	0
0.0167	0	0	0.0167	0	0
0.0189	0	0	0.0189	0	0
0.0215	0	0	0.0215	0	0
0.0244	0	0	0.0244	0	0
0.0278	0	0	0.0278	0	0
0.0315	0	0	0.0315	0	0
0.0358	0	0	0.0358	0	0
0.0407	0	0	0.0407	0	0
0.0463	0	0	0.0463	0	0
0.0526	0	0	0.0526	0	0
0.0597	0	0	0.0597	0	0
0.0679	0	0	0.0679	0	0
0.0771	0	0	0.0771	0	0
0.0876	0	0	0.0876	0	0
0.0995	0	0	0.0995	0	0
0.113	0	0	0.113	0	0

Core 2					
0 cm			**122 cm**		
Size (μm)	% Volume In	% Cumulative Volume	Size (μm)	% Volume In	% Cumulative Volume
0.128	0	0	0.128	0	0
0.146	0	0	0.146	0	0
0.166	0	0	0.166	0	0
0.188	0	0	0.188	0	0
0.214	0	0	0.214	0	0
0.243	0	0	0.243	0	0
0.276	0	0	0.276	0	0
0.314	0	0	0.314	0	0
0.357	0	0	0.357	0	0
0.405	0	0	0.405	0	0
0.46	0	0	0.46	0	0
0.523	0	0	0.523	0	0
0.594	0	0	0.594	0	0
0.675	0	0	0.675	0	0
0.767	0	0	0.767	0	0
0.872	0.07	0.07	0.872	0.08	0.08
0.991	0.08	0.15	0.991	0.09	0.17
1.13	0.08	0.23	1.13	0.09	0.26
1.28	0.08	0.31	1.28	0.1	0.36
1.45	0.08	0.39	1.45	0.1	0.46
1.65	0.09	0.48	1.65	0.11	0.57
1.88	0.1	0.58	1.88	0.12	0.69

Core 2					
0 cm			**122 cm**		
Size (μm)	% Volume In	% Cumulative Volume	Size (μm)	% Volume In	% Cumulative Volume
2.13	0.11	0.69	2.13	0.13	0.82
2.42	0.12	0.81	2.42	0.14	0.96
2.75	0.14	0.95	2.75	0.17	1.13
3.12	0.16	1.11	3.12	0.19	
3.55	0.18	1.29	3.55	0.23	1.55
4.03	0.21	1.5	4.03	0.26	1.81
4.58	0.23	1.73	4.58	0.3	2.11
5.21	0.25	1.98	5.21	0.32	2.43
5.92	0.26	2.24	5.92	0.35	2.78
6.72	0.26	2.5	6.72	0.36	3.14
7.64	0.26	2.76	7.64	0.37	3.51
8.68	0.27	3.03	8.68	0.38	3.89
9.86	0.29	3.32	9.86	0.41	4.3
11.2	0.33	3.65	11.2	0.46	4.76
12.7	0.39	4.04	12.7	0.53	5.29
14.5	0.48	4.52	14.5	0.64	5.93
16.4	0.59	5.11	16.4	0.75	6.68
18.7	0.68	5.79	18.7	0.87	7.55
21.2	0.75	6.54	21.2	0.96	8.51
24.1	0.75	7.29	24.1	0.98	9.49
27.4	0.68	7.97	27.4	0.94	10.43
31.1	0.53	8.5	31.1	0.82	11.25

Core 2					
0 cm			**122 cm**		
Size (μm)	% Volume In	% Cumulative Volume	Size (μm)	% Volume In	% Cumulative Volume
35.3	0.35	8.85	35.3	0.67	11.92
40.1	0.21	9.06	40.1	0.56	12.48
45.6	0.23	9.29	45.6	0.6	13.08
51.8	0.55	9.84	51.8	0.92	14
58.9	1.3	11.14	58.9	1.62	15.62
66.9	2.55	13.69	66.9	2.78	18.4
76	4.28	17.97	76	4.36	22.76
86.4	6.33	24.3	86.4	6.22	28.98
98.1	8.45	32.75	98.1	8.12	37.1
111	10.28	43.03	111	9.73	46.83
127	11.46	54.49	127	10.75	57.58
144	11.73	66.22	144	10.92	68.5
163	10.97	77.19	163	10.17	78.67
186	9.29	86.48	186	8.61	87.28
211	7	93.48	211	6.5	93.78
240	4.52	98	240	4.24	98.02
272	2.03	100.03	272	1.97	99.99
310	0.01	100.04	310	0.01	100
352	0	100.04	352	0	100
400	0	100.04	400	0	100
454	0	100.04	454	0	100
516	0	100.04	516	0	100

Core 2					
0 cm			**122 cm**		
Size (μm)	% Volume In	% Cumulative Volume	Size (μm)	% Volume In	% Cumulative Volume
586	0	100.04	586	0	100
666	0	100.04	666	0	100
756	0	100.04	756	0	100
859	0	100.04	859	0	100
976	0	100.04	976	0	100
1110	0	100.04	1110	0	100
1260	0	100.04	1260	0	100
1430	0	100.04	1430	0	100
1630	0	100.04	1630	0	100
1850	0	100.04	1850	0	100
2100	0	100.04	2100	0	100
2390	0	100.04	2390	0	100
2710	0	100.04	2710	0	100
3080	0	100.04	3080	0	100
3500		100.04	3500		100

Table G.5 PSA Core 3

Core 3											
0 cm			**60 cm**			**80 cm**			**122 cm**		
Size (μm)	% Volume In	% Cumulative Volume	Size (μm)	% Volume In	% Cumulative Volume	Size (μm)	% Volume In	% Cumulative Volume	Size (μm)	% Volume In	% Cumulative Volume
0.01	0	0	0.01	0	0	0.01	0	0	0.01	0	0
0.0114	0	0	0.0114	0	0	0.0114	0	0	0.0114	0	0
0.0129	0	0	0.0129	0	0	0.0129	0	0	0.0129	0	0
0.0147	0	0	0.0147	0	0	0.0147	0	0	0.0147	0	0
0.0167	0	0	0.0167	0	0	0.0167	0	0	0.0167	0	0
0.0189	0	0	0.0189	0	0	0.0189	0	0	0.0189	0	0
0.0215	0	0	0.0215	0	0	0.0215	0	0	0.0215	0	0
0.0244	0	0	0.0244	0	0	0.0244	0	0	0.0244	0	0
0.0278	0	0	0.0278	0	0	0.0278	0	0	0.0278	0	0
0.0315	0	0	0.0315	0	0	0.0315	0	0	0.0315	0	0
0.0358	0	0	0.0358	0	0	0.0358	0	0	0.0358	0	0
0.0407	0	0	0.0407	0	0	0.0407	0	0	0.0407	0	0
0.0463	0	0	0.0463	0	0	0.0463	0	0	0.0463	0	0
0.0526	0	0	0.0526	0	0	0.0526	0	0	0.0526	0	0
0.0597	0	0	0.0597	0	0	0.0597	0	0	0.0597	0	0
0.0679	0	0	0.0679	0	0	0.0679	0	0	0.0679	0	0
0.0771	0	0	0.0771	0	0	0.0771	0	0	0.0771	0	0
0.0876	0	0	0.0876	0	0	0.0876	0	0	0.0876	0	0
0.0995	0	0	0.0995	0	0	0.0995	0	0	0.0995	0	0
0.113	0	0	0.113	0	0	0.113	0	0	0.113	0	0
0.128	0	0	0.128	0	0	0.128	0	0	0.128	0	0
0.146	0	0	0.146	0	0	0.146	0	0	0.146	0	0
0.166	0	0	0.166	0	0	0.166	0	0	0.166	0	0

Core 3											
0 cm			**60 cm**			**80 cm**			**122 cm**		
Size (μm)	% Volume In	% Cumulative Volume	Size (μm)	% Volume In	% Cumulative Volume	Size (μm)	% Volume In	% Cumulative Volume	Size (μm)	% Volume In	% Cumulative Volume
0.188	0	0	0.188	0	0	0.188	0	0	0.188	0	0
0.214	0	0	0.214	0	0	0.214	0	0	0.214	0	0
0.243	0	0	0.243	0	0	0.243	0	0	0.243	0	0
0.276	0	0	0.276	0	0	0.276	0	0	0.276	0	0
0.314	0	0	0.314	0	0	0.314	0	0	0.314	0	0
0.357	0	0	0.357	0	0	0.357	0	0	0.357	0	0
0.405	0	0	0.405	0	0	0.405	0	0	0.405	0	0
0.46	0	0	0.46	0	0	0.46	0	0	0.46	0	0
0.523	0	0	0.523	0	0	0.523	0	0	0.523	0	0
0.594	0	0	0.594	0	0	0.594	0.13	0.13	0.594	0.1	0.1
0.675	0.08	0.08	0.675	0	0	0.675	0.25	0.38	0.675	0.2	0.3
0.767	0.12	0.2	0.767	0.08	0.08	0.767	0.35	0.73	0.767	0.27	0.57
0.872	0.14	0.34	0.872	0.1	0.18	0.872	0.39	1.12	0.872	0.31	0.88
0.991	0.15	0.49	0.991	0.11	0.29	0.991	0.39	1.51	0.991	0.31	1.19
1.13	0.14	0.63	1.13	0.12	0.41	1.13	0.38	1.89	1.13	0.29	1.48
1.28	0.14	0.77	1.28	0.12	0.53	1.28	0.38	2.27	1.28	0.29	1.77
1.45	0.15	0.92	1.45	0.13	0.66	1.45	0.41	2.68	1.45	0.31	2.08
1.65	0.16	1.08	1.65	0.14	0.8	1.65	0.46	3.14	1.65	0.35	2.43
1.88	0.18	1.26	1.88	0.16	0.96	1.88	0.53	3.67	1.88	0.4	2.83
2.13	0.2	1.46	2.13	0.17	1.13	2.13	0.6	4.27	2.13	0.45	3.28
2.42	0.23	1.69	2.42	0.19	1.32	2.42	0.67	4.94	2.42	0.5	3.78
2.75	0.25	1.94	2.75	0.22	1.54	2.75	0.73	5.67	2.75	0.55	4.33
3.12	0.28	2.22	3.12	0.24	1.78	3.12	0.8	6.47	3.12	0.6	4.93
3.55	0.31	2.53	3.55	0.27	2.05	3.55	0.87	7.34	3.55	0.65	5.58

Core 3											
0 cm			**60 cm**			**80 cm**			**122 cm**		
Size (μm)	% Volume In	% Cumulative Volume	Size (μm)	% Volume In	% Cumulative Volume	Size (μm)	% Volume In	% Cumulative Volume	Size (μm)	% Volume In	% Cumulative Volume
4.03	0.34	2.87	4.03	0.3	2.35	4.03	0.95	8.29	4.03	0.71	6.29
4.58	0.37	3.24	4.58	0.32	2.67	4.58	1.04	9.33	4.58	0.77	7.06
5.21	0.4	3.64	5.21	0.35	3.02	5.21	1.13	10.46	5.21	0.83	7.89
5.92	0.42	4.06	5.92	0.37	3.39	5.92	1.22	11.68	5.92	0.9	8.79
6.72	0.44	4.5	6.72	0.4	3.79	6.72	1.31	12.99	6.72	0.97	9.76
7.64	0.47	4.97	7.64	0.43	4.22	7.64	1.41	14.4	7.64	1.04	10.8
8.68	0.5	5.47	8.68	0.47	4.69	8.68	1.52	15.92	8.68	1.14	11.94
9.86	0.56	6.03	9.86	0.52	5.21	9.86	1.65	17.57	9.86	1.26	13.2
11.2	0.65	6.68	11.2	0.6	5.81	11.2	1.8	19.37	11.2	1.42	14.62
12.7	0.76	7.44	12.7	0.69	6.5	12.7	1.98	21.35	12.7	1.6	16.22
14.5	0.9	8.34	14.5	0.79	7.29	14.5	2.19	23.54	14.5	1.81	18.03
16.4	1.04	9.38	16.4	0.9	8.19	16.4	2.41	25.95	16.4	2.03	20.06
18.7	1.15	10.53	18.7	0.98	9.17	18.7	2.65	28.6	18.7	2.25	22.31
21.2	1.22	11.75	21.2	1.04	10.21	21.2	2.88	31.48	21.2	2.44	24.75
24.1	1.21	12.96	24.1	1.06	11.27	24.1	3.09	34.57	24.1	2.61	27.36
27.4	1.13	14.09	27.4	1.04	12.31	27.4	3.28	37.85	27.4	2.73	30.09
31.1	0.99	15.08	31.1	0.99	13.3	31.1	3.44	41.29	31.1	2.82	32.91
35.3	0.85	15.93	35.3	0.95	14.25	35.3	3.56	44.85	35.3	2.89	35.8
40.1	0.82	16.75	40.1	0.98	15.23	40.1	3.67	48.52	40.1	2.97	38.77
45.6	1.02	17.77	45.6	1.15	16.38	45.6	3.77	52.29	45.6	3.11	41.88
51.8	1.57	19.34	51.8	1.52	17.9	51.8	3.88	56.17	51.8	3.34	45.22
58.9	2.53	21.87	58.9	2.13	20.03	58.9	4.01	60.18	58.9	3.69	48.91
66.9	3.92	25.79	66.9	3	23.03	66.9	4.15	64.33	66.9	4.15	53.06
76	5.62	31.41	76	4.07	27.1	76	4.29	68.62	76	4.69	57.75

Core 3											
0 cm			**60 cm**			**80 cm**			**122 cm**		
Size (μm)	% Volume In	% Cumulative Volume	Size (μm)	% Volume In	% Cumulative Volume	Size (μm)	% Volume In	% Cumulative Volume	Size (μm)	% Volume In	% Cumulative Volume
86.4	7.44	38.85	86.4	5.24	32.34	86.4	4.39	73.01	86.4	5.22	62.97
98.1	9.08	47.93	98.1	6.36	38.7	98.1	4.43	77.44	98.1	5.67	68.64
111	10.21	58.14	111	7.28	45.98	111	4.35	81.79	111	5.91	74.55
127	10.56	68.7	127	7.88	53.86	127	4.15	85.94	127	5.86	80.41
144	10.01	78.71	144	8.08	61.94	144	3.81	89.75	144	5.49	85.9
163	8.58	87.29	163	7.87	69.81	163	3.33	93.08	163	4.79	90.69
186	6.53	93.82	186	7.31	77.12	186	2.74	95.82	186	3.85	94.54
211	4.23	98.05	211	6.47	83.59	211	2.06	97.88	211	2.79	97.33
240	1.92	99.97	240	5.45	89.04	240	1.35	99.23	240	1.74	99.07
272	0.01	99.98	272	4.33	93.37	272	0.71	99.94	272	0.73	99.8
310	0	99.98	310	3.19	96.56	310	0.07	100.01	310	0.2	100
352	0	99.98	352	2.09	98.65	352	0	100.01	352	0	100
400	0	99.98	400	1.13	99.78	400	0	100.01	400	0	100
454	0	99.98	454	0.25	100.03	454	0	100.01	454	0	100
516	0	99.98	516	0	100.03	516	0	100.01	516	0	100
586	0	99.98	586	0	100.03	586	0	100.01	586	0	100
666	0	99.98	666	0	100.03	666	0	100.01	666	0	100
756	0	99.98	756	0	100.03	756	0	100.01	756	0	100
859	0	99.98	859	0	100.03	859	0	100.01	859	0	100
976	0	99.98	976	0	100.03	976	0	100.01	976	0	100
1110	0	99.98	1110	0	100.03	1110	0	100.01	1110	0	100
1260	0	99.98	1260	0	100.03	1260	0	100.01	1260	0	100
1430	0	99.98	1430	0	100.03	1430	0	100.01	1430	0	100
1630	0	99.98	1630	0	100.03	1630	0	100.01	1630	0	100

Core 3											
0 cm			**60 cm**			**80 cm**			**122 cm**		
Size (μm)	% Volume In	% Cumulative Volume	Size (μm)	% Volume In	% Cumulative Volume	Size (μm)	% Volume In	% Cumulative Volume	Size (μm)	% Volume In	% Cumulative Volume
1850	0	99.98	1850	0	100.03	1850	0	100.01	1850	0	100
2100	0	99.98	2100	0	100.03	2100	0	100.01	2100	0	100
2390	0	99.98	2390	0	100.03	2390	0	100.01	2390	0	100
2710	0	99.98	2710	0	100.03	2710	0	100.01	2710	0	100
3080	0	99.98	3080	0	100.03	3080	0	100.01	3080	0	100
3500		99.98	3500		100.03	3500		100.01	3500		100

Table G.4 PSA Core 4

Core 4								
0 cm			**60 cm**			**122 cm**		
Size (μm)	% Volume In	% Cumulative Volume	Size (μm)	% Volume In	% Cumulative Volume	Size (μm)	% Volume In	% Cumulative Volume
0.01	0	0	0.01	0	0	0.01	0	0
0.0114	0	0	0.0114	0	0	0.0114	0	0
0.0129	0	0	0.0129	0	0	0.0129	0	0
0.0147	0	0	0.0147	0	0	0.0147	0	0
0.0167	0	0	0.0167	0	0	0.0167	0	0
0.0189	0	0	0.0189	0	0	0.0189	0	0
0.0215	0	0	0.0215	0	0	0.0215	0	0
0.0244	0	0	0.0244	0	0	0.0244	0	0
0.0278	0	0	0.0278	0	0	0.0278	0	0
0.0315	0	0	0.0315	0	0	0.0315	0	0
0.0358	0	0	0.0358	0	0	0.0358	0	0
0.0407	0	0	0.0407	0	0	0.0407	0	0
0.0463	0	0	0.0463	0	0	0.0463	0	0
0.0526	0	0	0.0526	0	0	0.0526	0	0
0.0597	0	0	0.0597	0	0	0.0597	0	0
0.0679	0	0	0.0679	0	0	0.0679	0	0
0.0771	0	0	0.0771	0	0	0.0771	0	0
0.0876	0	0	0.0876	0	0	0.0876	0	0
0.0995	0	0	0.0995	0	0	0.0995	0	0
0.113	0	0	0.113	0	0	0.113	0	0
0.128	0	0	0.128	0	0	0.128	0	0
0.146	0	0	0.146	0	0	0.146	0	0
0.166	0	0	0.166	0	0	0.166	0	0

Core 4								
0 cm			**60 cm**			**122 cm**		
Size (μm)	% Volume In	% Cumulative Volume	Size (μm)	% Volume In	% Cumulative Volume	Size (μm)	% Volume In	% Cumulative Volume
0.188	0	0	0.188	0	0	0.188	0	0
0.214	0	0	0.214	0	0	0.214	0	0
0.243	0	0	0.243	0	0	0.243	0	0
0.276	0	0	0.276	0	0	0.276	0	0
0.314	0	0	0.314	0	0	0.314	0	0
0.357	0	0	0.357	0	0	0.357	0	0
0.405	0	0	0.405	0	0	0.405	0	0
0.46	0	0	0.46	0	0	0.46	0	0
0.523	0	0	0.523	0	0	0.523	0	0
0.594	0	0	0.594	0.14	0.14	0.594	0	0
0.675	0	0	0.675	0.25	0.39	0.675	0	0
0.767	0.02	0.02	0.767	0.33	0.72	0.767	0	0
0.872	0.07	0.09	0.872	0.36	1.08	0.872	0	0
0.991	0.08	0.17	0.991	0.36	1.44	0.991	0	0
1.13	0.09	0.26	1.13	0.34	1.78	1.13	0	0
1.28	0.09	0.35	1.28	0.34	2.12	1.28	0.06	0.06
1.45	0.09	0.44	1.45	0.37	2.49	1.45	0.07	0.13
1.65	0.1	0.54	1.65	0.42	2.91	1.65	0.08	0.21
1.88	0.1	0.64	1.88	0.48	3.39	1.88	0.1	0.31
2.13	0.11	0.75	2.13	0.54	3.93	2.13	0.11	0.42
2.42	0.12	0.87	2.42	0.6	4.53	2.42	0.12	0.54
2.75	0.14	1.01	2.75	0.65	5.18	2.75	0.14	0.68
3.12	0.16	1.17	3.12	0.7	5.88	3.12	0.15	0.83
3.55	0.18	1.35	3.55	0.75	6.63	3.55	0.17	1

Core 4								
0 cm			**60 cm**			**122 cm**		
Size (μm)	% Volume In	% Cumulative Volume	Size (μm)	% Volume In	% Cumulative Volume	Size (μm)	% Volume In	% Cumulative Volume
4.03	0.2	1.55	4.03	0.81	7.44	4.03	0.2	1.2
4.58	0.22	1.77	4.58	0.88	8.32	4.58	0.22	1.42
5.21	0.24	2.01	5.21	0.94	9.26	5.21	0.25	1.67
5.92	0.25	2.26	5.92	1	10.26	5.92	0.27	1.94
6.72	0.26	2.52	6.72	1.07	11.33	6.72	0.28	2.22
7.64	0.27	2.79	7.64	1.14	12.47	7.64	0.3	2.52
8.68	0.28	3.07	8.68	1.22	13.69	8.68	0.31	2.83
9.86	0.31	3.38	9.86	1.32	15.01	9.86	0.33	3.16
11.2	0.37	3.75	11.2	1.44	16.45	11.2	0.35	3.51
12.7	0.44	4.19	12.7	1.59	18.04	12.7	0.4	3.91
14.5	0.54	4.73	14.5	1.76	19.8	14.5	0.46	4.37
16.4	0.65	5.38	16.4	1.95	21.75	16.4	0.54	4.91
18.7	0.76	6.14	18.7	2.15	23.9	18.7	0.64	5.55
21.2	0.85	6.99	21.2	2.35	26.25	21.2	0.74	6.29
24.1	0.9	7.89	24.1	2.53	28.78	24.1	0.81	7.1
27.4	0.9	8.79	27.4	2.67	31.45	27.4	0.85	7.95
31.1	0.88	9.67	31.1	2.75	34.2	31.1	0.84	8.79
35.3	0.87	10.54	35.3	2.77	36.97	35.3	0.78	9.57
40.1	0.95	11.49	40.1	2.73	39.7	40.1	0.69	10.26
45.6	1.19	12.68	45.6	2.67	42.37	45.6	0.63	10.89
51.8	1.69	14.37	51.8	2.64	45.01	51.8	0.7	11.59
58.9	2.52	16.89	58.9	2.72	47.73	58.9	0.98	12.57
66.9	3.69	20.58	66.9	2.96	50.69	66.9	1.57	14.14
76	5.14	25.72	76	3.39	54.08	76	2.54	16.68

Core 4								
0 cm			**60 cm**			**122 cm**		
Size (μm)	% Volume In	% Cumulative Volume	Size (μm)	% Volume In	% Cumulative Volume	Size (μm)	% Volume In	% Cumulative Volume
86.4	6.73	32.45	86.4	4.01	58.09	86.4	3.87	20.55
98.1	8.23	40.68	98.1	4.73	62.82	98.1	5.48	26.03
111	9.4	50.08	111	5.41	68.23	111	7.19	33.22
127	10.02	60.1	127	5.9	74.13	127	8.73	41.95
144	9.93	70.03	144	6.06	80.19	144	9.86	51.81
163	9.13	79.16	163	5.81	86	163	10.34	62.15
186	7.73	86.89	186	5.11	91.11	186	10.06	72.21
211	5.95	92.84	211	4.05	95.16	211	9.04	81.25
240	4.08	96.92	240	2.81	97.97	240	7.44	88.69
272	2.38	99.3	272	1.59	99.56	272	5.52	94.21
310	0.68	99.98	310	0.43	99.99	310	3.59	97.8
352	0	99.98	352	0	99.99	352	1.92	99.72
400	0	99.98	400	0	99.99	400	0.27	99.99
454	0	99.98	454	0	99.99	454	0	99.99
516	0	99.98	516	0	99.99	516	0	99.99
586	0	99.98	586	0	99.99	586	0	99.99
666	0	99.98	666	0	99.99	666	0	99.99
756	0	99.98	756	0	99.99	756	0	99.99
859	0	99.98	859	0	99.99	859	0	99.99
976	0	99.98	976	0	99.99	976	0	99.99
1110	0	99.98	1110	0	99.99	1110	0	99.99
1260	0	99.98	1260	0	99.99	1260	0	99.99
1430	0	99.98	1430	0	99.99	1430	0	99.99
1630	0	99.98	1630	0	99.99	1630	0	99.99

Core 4								
0 cm			**60 cm**			**122 cm**		
Size (μm)	% Volume In	% Cumulative Volume	Size (μm)	% Volume In	% Cumulative Volume	Size (μm)	% Volume In	% Cumulative Volume
1850	0	99.98	1850	0	99.99	1850	0	99.99
2100	0	99.98	2100	0	99.99	2100	0	99.99
2390	0	99.98	2390	0	99.99	2390	0	99.99
2710	0	99.98	2710	0	99.99	2710	0	99.99
3080	0	99.98	3080	0	99.99	3080	0	99.99
3500		99.98	3500		99.99	3500		99.99

Table G.6 PSA Core 5

Core 5																	
0 cm			**60 cm**			**80 cm**			**112 cm**			**130 cm**			**183 cm**		
Size (μm)	% Volume In	% Cum. Volume	Size (μm)	% Volume In	% Cum. Volume	Size (μm)	% Volume In	% Cum. Volume	Size (μm)	% Volume In	% Cum. Volume	Size (μm)	% Volume In	% Cum. Volume	Size (μm)	% Volume In	% Cum. Volume
0.01	0	0	0.01	0	0	0.01	0	0	0.01	0	0	0.01	0	0	0.01	0	0
0.0114	0	0	0.0114	0	0	0.0114	0	0	0.0114	0	0	0.0114	0	0	0.0114	0	0
0.0129	0	0	0.0129	0	0	0.0129	0	0	0.0129	0	0	0.0129	0	0	0.0129	0	0
0.0147	0	0	0.0147	0	0	0.0147	0	0	0.0147	0	0	0.0147	0	0	0.0147	0	0
0.0167	0	0	0.0167	0	0	0.0167	0	0	0.0167	0	0	0.0167	0	0	0.0167	0	0
0.0189	0	0	0.0189	0	0	0.0189	0	0	0.0189	0	0	0.0189	0	0	0.0189	0	0
0.0215	0	0	0.0215	0	0	0.0215	0	0	0.0215	0	0	0.0215	0	0	0.0215	0	0
0.0244	0	0	0.0244	0	0	0.0244	0	0	0.0244	0	0	0.0244	0	0	0.0244	0	0
0.0278	0	0	0.0278	0	0	0.0278	0	0	0.0278	0	0	0.0278	0	0	0.0278	0	0
0.0315	0	0	0.0315	0	0	0.0315	0	0	0.0315	0	0	0.0315	0	0	0.0315	0	0
0.0358	0	0	0.0358	0	0	0.0358	0	0	0.0358	0	0	0.0358	0	0	0.0358	0	0
0.0407	0	0	0.0407	0	0	0.0407	0	0	0.0407	0	0	0.0407	0	0	0.0407	0	0
0.0463	0	0	0.0463	0	0	0.0463	0	0	0.0463	0	0	0.0463	0	0	0.0463	0	0
0.0526	0	0	0.0526	0	0	0.0526	0	0	0.0526	0	0	0.0526	0	0	0.0526	0	0
0.0597	0	0	0.0597	0	0	0.0597	0	0	0.0597	0	0	0.0597	0	0	0.0597	0	0
0.0679	0	0	0.0679	0	0	0.0679	0	0	0.0679	0	0	0.0679	0	0	0.0679	0	0
0.0771	0	0	0.0771	0	0	0.0771	0	0	0.0771	0	0	0.0771	0	0	0.0771	0	0
0.0876	0	0	0.0876	0	0	0.0876	0	0	0.0876	0	0	0.0876	0	0	0.0876	0	0
0.0995	0	0	0.0995	0	0	0.0995	0	0	0.0995	0	0	0.0995	0	0	0.0995	0	0
0.113	0	0	0.113	0	0	0.113	0	0	0.113	0	0	0.113	0	0	0.113	0	0
0.128	0	0	0.128	0	0	0.128	0	0	0.128	0	0	0.128	0	0	0.128	0	0
0.146	0	0	0.146	0	0	0.146	0	0	0.146	0	0	0.146	0	0	0.146	0	0
0.166	0	0	0.166	0	0	0.166	0	0	0.166	0	0	0.166	0	0	0.166	0	0

Core 5																	
0 cm			**60 cm**			**80 cm**			**112 cm**			**130 cm**			**183 cm**		
Size (μm)	% Volume In	% Cum. Volume	Size (μm)	% Volume In	% Cum. Volume	Size (μm)	% Volume In	% Cum. Volume	Size (μm)	% Volume In	% Cum. Volume	Size (μm)	% Volume In	% Cum. Volume	Size (μm)	% Volume In	% Cum. Volume
0.188	0	0	0.188	0	0	0.188	0	0	0.188	0	0	0.188	0	0	0.188	0	0
0.214	0	0	0.214	0	0	0.214	0	0	0.214	0	0	0.214	0	0	0.214	0	0
0.243	0	0	0.243	0	0	0.243	0	0	0.243	0	0	0.243	0	0	0.243	0	0
0.276	0	0	0.276	0	0	0.276	0	0	0.276	0	0	0.276	0	0	0.276	0	0
0.314	0	0	0.314	0	0	0.314	0	0	0.314	0	0	0.314	0	0	0.314	0	0
0.357	0	0	0.357	0	0	0.357	0	0	0.357	0	0	0.357	0	0	0.357	0	0
0.405	0	0	0.405	0	0	0.405	0	0	0.405	0	0	0.405	0	0	0.405	0	0
0.46	0	0	0.46	0	0	0.46	0	0	0.46	0	0	0.46	0	0	0.46	0	0
0.523	0	0	0.523	0	0	0.523	0	0	0.523	0	0	0.523	0	0	0.523	0	0
0.594	0.06	0.06	0.594	0.08	0.08	0.594	0.06	0.06	0.594	0.13	0.13	0.594	0	0	0.594	0	0
0.675	0.14	0.2	0.675	0.18	0.26	0.675	0.15	0.21	0.675	0.27	0.4	0.675	0	0	0.675	0	0
0.767	0.21	0.41	0.767	0.26	0.52	0.767	0.23	0.44	0.767	0.4	0.8	0.767	0	0	0.767	0	0
0.872	0.25	0.66	0.872	0.31	0.83	0.872	0.28	0.72	0.872	0.46	1.26	0.872	0	0	0.872	0	0
0.991	0.26	0.92	0.991	0.32	1.15	0.991	0.3	1.02	0.991	0.47	1.73	0.991	0	0	0.991	0	0
1.13	0.26	1.18	1.13	0.32	1.47	1.13	0.29	1.31	1.13	0.45	2.18	1.13	0	0	1.13	0	0
1.28	0.26	1.44	1.28	0.32	1.79	1.28	0.29	1.6	1.28	0.45	2.63	1.28	0	0	1.28	0.06	0.06
1.45	0.28	1.72	1.45	0.33	2.12	1.45	0.31	1.91	1.45	0.47	3.1	1.45	0	0	1.45	0.07	0.13
1.65	0.32	2.04	1.65	0.37	2.49	1.65	0.35	2.26	1.65	0.53	3.63	1.65	0	0	1.65	0.08	0.21
1.88	0.36	2.4	1.88	0.42	2.91	1.88	0.4	2.66	1.88	0.61	4.24	1.88	0	0	1.88	0.09	0.3
2.13	0.41	2.81	2.13	0.47	3.38	2.13	0.46	3.12	2.13	0.69	4.93	2.13	0.07	0.07	2.13	0.1	0.4
2.42	0.47	3.28	2.42	0.53	3.91	2.42	0.51	3.63	2.42	0.78	5.71	2.42	0.07	0.14	2.42	0.11	0.51
2.75	0.52	3.8	2.75	0.59	4.5	2.75	0.57	4.2	2.75	0.87	6.58	2.75	0.08	0.22	2.75	0.12	0.63
3.12	0.58	4.38	3.12	0.66	5.16	3.12	0.64	4.84	3.12	0.98	7.56	3.12	0.09	0.31	3.12	0.14	0.77
3.55	0.64	5.02	3.55	0.75	5.91	3.55	0.73	5.57	3.55	1.1	8.66	3.55	0.11	0.42	3.55	0.17	0.94

Core 5																	
0 cm			**60 cm**			**80 cm**			**112 cm**			**130 cm**			**183 cm**		
Size (μm)	% Volume In	% Cum. Volume	Size (μm)	% Volume In	% Cum. Volume	Size (μm)	% Volume In	% Cum. Volume	Size (μm)	% Volume In	% Cum. Volume	Size (μm)	% Volume In	% Cum. Volume	Size (μm)	% Volume In	% Cum. Volume
4.03	0.71	5.73	4.03	0.84	6.75	4.03	0.83	6.4	4.03	1.24	9.9	4.03	0.13	0.55	4.03	0.2	1.14
4.58	0.78	6.51	4.58	0.94	7.69	4.58	0.94	7.34	4.58	1.39	11.29	4.58	0.14	0.69	4.58	0.23	1.37
5.21	0.86	7.37	5.21	1.04	8.73	5.21	1.05	8.39	5.21	1.55	12.84	5.21	0.16	0.85	5.21	0.26	1.63
5.92	0.93	8.3	5.92	1.13	9.86	5.92	1.17	9.56	5.92	1.72	14.56	5.92	0.19	1.04	5.92	0.3	1.93
6.72	1	9.3	6.72	1.22	11.08	6.72	1.29	10.85	6.72	1.9	16.46	6.72	0.21	1.25	6.72	0.33	2.26
7.64	1.06	10.36	7.64	1.31	12.39	7.64	1.41	12.26	7.64	2.09	18.55	7.64	0.23	1.48	7.64	0.35	2.61
8.68	1.14	11.5	8.68	1.4	13.79	8.68	1.53	13.79	8.68	2.3	20.85	8.68	0.26	1.74	8.68	0.38	2.99
9.86	1.22	12.72	9.86	1.5	15.29	9.86	1.65	15.44	9.86	2.55	23.4	9.86	0.29	2.03	9.86	0.41	3.4
11.2	1.31	14.03	11.2	1.61	16.9	11.2	1.78	17.22	11.2	2.82	26.22	11.2	0.33	2.36	11.2	0.44	3.84
12.7	1.41	15.44	12.7	1.74	18.64	12.7	1.93	19.15	12.7	3.13	29.35	12.7	0.37	2.73	12.7	0.49	4.33
14.5	1.53	16.97	14.5	1.89	20.53	14.5	2.08	21.23	14.5	3.45	32.8	14.5	0.41	3.14	14.5	0.55	4.88
16.4	1.66	18.63	16.4	2.05	22.58	16.4	2.25	23.48	16.4	3.79	36.59	16.4	0.47	3.61	16.4	0.62	5.5
18.7	1.81	20.44	18.7	2.22	24.8	18.7	2.45	25.93	18.7	4.11	40.7	18.7	0.53	4.14	18.7	0.72	6.22
21.2	1.98	22.42	21.2	2.4	27.2	21.2	2.66	28.59	21.2	4.4	45.1	21.2	0.6	4.74	21.2	0.82	7.04
24.1	2.18	24.6	24.1	2.57	29.77	24.1	2.89	31.48	24.1	4.63	49.73	24.1	0.68	5.42	24.1	0.92	7.96
27.4	2.41	27.01	27.4	2.73	32.5	27.4	3.13	34.61	27.4	4.79	54.52	27.4	0.76	6.18	27.4	1	8.96
31.1	2.67	29.68	31.1	2.89	35.39	31.1	3.36	37.97	31.1	4.85	59.37	31.1	0.84	7.02	31.1	1.05	10.01
35.3	2.99	32.67	35.3	3.05	38.44	35.3	3.58	41.55	35.3	4.82	64.19	35.3	0.92	7.94	35.3	1.05	11.06
40.1	3.34	36.01	40.1	3.22	41.66	40.1	3.75	45.3	40.1	4.7	68.89	40.1	1.01	8.95	40.1	1.02	12.08
45.6	3.74	39.75	45.6	3.41	45.07	45.6	3.88	49.18	45.6	4.5	73.39	45.6	1.12	10.07	45.6	1	13.08
51.8	4.16	43.91	51.8	3.62	48.69	51.8	3.96	53.14	51.8	4.24	77.63	51.8	1.26	11.33	51.8	1.03	14.11
58.9	4.58	48.49	58.9	3.87	52.56	58.9	3.98	57.12	58.9	3.94	81.57	58.9	1.47	12.8	58.9	1.2	15.31
66.9	4.95	53.44	66.9	4.14	56.7	66.9	3.97	61.09	66.9	3.63	85.2	66.9	1.76	14.56	66.9	1.59	16.9
76	5.23	58.67	76	4.43	61.13	76	3.93	65.02	76	3.31	88.51	76	2.16	16.72	76	2.26	19.16

Core 5																	
0 cm			**60 cm**			**80 cm**			**112 cm**			**130 cm**			**183 cm**		
Size (μm)	% Volume In	% Cum. Volume	Size (μm)	% Volume In	% Cum. Volume	Size (μm)	% Volume In	% Cum. Volume	Size (μm)	% Volume In	% Cum. Volume	Size (μm)	% Volume In	% Cum. Volume	Size (μm)	% Volume In	% Cum. Volume
86.4	5.37	64.04	86.4	4.7	65.83	86.4	3.87	68.89	86.4	2.97	91.48	86.4	2.65	19.37	86.4	3.24	22.4
98.1	5.34	69.38	98.1	4.91	70.74	98.1	3.81	72.7	98.1	2.59	94.07	98.1	3.24	22.61	98.1	4.47	26.87
111	5.15	74.53	111	5.02	75.76	111	3.74	76.44	111	2.17	96.24	111	3.89	26.5	111	5.84	32.71
127	4.82	79.35	127	5	80.76	127	3.65	80.09	127	1.69	97.93	127	4.55	31.05	127	7.17	39.88
144	4.38	83.73	144	4.79	85.55	144	3.53	83.62	144	1.18	99.11	144	5.18	36.23	144	8.24	48.12
163	3.89	87.62	163	4.38	89.93	163	3.37	86.99	163	0.69	99.8	163	5.73	41.96	163	8.89	57.01
186	3.38	91	186	3.75	93.68	186	3.15	90.14	186	0.2	100	186	6.16	48.12	186	9	66.01
211	2.85	93.85	211	2.93	96.61	211	2.85	92.99	211	0	100	211	6.44	54.56	211	8.53	74.54
240	2.32	96.17	240	2.01	98.62	240	2.45	95.44	240	0	100	240	6.58	61.14	240	7.57	82.11
272	1.76	97.93	272	1.11	99.73	272	1.96	97.4	272	0	100	272	6.55	67.69	272	6.26	88.37
310	1.21	99.14	310	0.24	99.97	310	1.41	98.81	310	0	100	310	6.36	74.05	310	4.78	93.15
352	0.69	99.83	352	0	99.97	352	0.85	99.66	352	0	100	352	6	80.05	352	3.34	96.49
400	0.18	100.01	400	0	99.97	400	0.32	99.98	400	0	100	400	5.46	85.51	400	2.09	98.58
454	0	100.01	454	0	99.97	454	0	99.98	454	0	100	454	4.74	90.25	454	1.11	99.69
516	0	100.01	516	0	99.97	516	0	99.98	516	0	100	516	3.86	94.11	516	0.34	100.03
586	0	100.01	586	0	99.97	586	0	99.98	586	0	100	586	2.88	96.99	586	0	100.03
666	0	100.01	666	0	99.97	666	0	99.98	666	0	100	666	1.9	98.89	666	0	100.03
756	0	100.01	756	0	99.97	756	0	99.98	756	0	100	756	0.98	99.87	756	0	100.03
859	0	100.01	859	0	99.97	859	0	99.98	859	0	100	859	0.13	100	859	0	100.03
976	0	100.01	976	0	99.97	976	0	99.98	976	0	100	976	0	100	976	0	100.03
1110	0	100.01	1110	0	99.97	1110	0	99.98	1110	0	100	1110	0	100	1110	0	100.03
1260	0	100.01	1260	0	99.97	1260	0	99.98	1260	0	100	1260	0	100	1260	0	100.03
1430	0	100.01	1430	0	99.97	1430	0	99.98	1430	0	100	1430	0	100	1430	0	100.03
1630	0	100.01	1630	0	99.97	1630	0	99.98	1630	0	100	1630	0	100	1630	0	100.03

Core 5																	
0 cm			**60 cm**			**80 cm**			**112 cm**			**130 cm**			**183 cm**		
Size (μm)	% Volume In	% Cum. Volume	Size (μm)	% Volume In	% Cum. Volume	Size (μm)	% Volume In	% Cum. Volume	Size (μm)	% Volume In	% Cum. Volume	Size (μm)	% Volume In	% Cum. Volume	Size (μm)	% Volume In	% Cum. Volume
1850	0	100.01	1850	0	99.97	1850	0	99.98	1850	0	100	1850	0	100	1850	0	100.03
2100	0	100.01	2100	0	99.97	2100	0	99.98	2100	0	100	2100	0	100	2100	0	100.03
2390	0	100.01	2390	0	99.97	2390	0	99.98	2390	0	100	2390	0	100	2390	0	100.03
2710	0	100.01	2710	0	99.97	2710	0	99.98	2710	0	100	2710	0	100	2710	0	100.03
3080	0	100.01	3080	0	99.97	3080	0	99.98	3080	0	100	3080	0	100	3080	0	100.03
3500		100.01	3500		99.97	3500		99.98	3500		100	3500		100	3500		100.03

Table G.7 PSA Core 6

Core 6											
0 cm			**60 cm**			**80 cm**			**122 cm**		
Size (μm)	% Volume In	% Cum. Volume	Size (μm)	% Volume In	% Cum. Volume	Size (μm)	% Volume In	% Cum. Volume	Size (μm)	% Volume In	% Cum. Volume
0.01	0	0	0.01	0	0	0.01	0	0	0.01	0	0
0.0114	0	0	0.0114	0	0	0.0114	0	0	0.0114	0	0
0.0129	0	0	0.0129	0	0	0.0129	0	0	0.0129	0	0
0.0147	0	0	0.0147	0	0	0.0147	0	0	0.0147	0	0
0.0167	0	0	0.0167	0	0	0.0167	0	0	0.0167	0	0
0.0189	0	0	0.0189	0	0	0.0189	0	0	0.0189	0	0
0.0215	0	0	0.0215	0	0	0.0215	0	0	0.0215	0	0
0.0244	0	0	0.0244	0	0	0.0244	0	0	0.0244	0	0
0.0278	0	0	0.0278	0	0	0.0278	0	0	0.0278	0	0
0.0315	0	0	0.0315	0	0	0.0315	0	0	0.0315	0	0
0.0358	0	0	0.0358	0	0	0.0358	0	0	0.0358	0	0
0.0407	0	0	0.0407	0	0	0.0407	0	0	0.0407	0	0
0.0463	0	0	0.0463	0	0	0.0463	0	0	0.0463	0	0
0.0526	0	0	0.0526	0	0	0.0526	0	0	0.0526	0	0
0.0597	0	0	0.0597	0	0	0.0597	0	0	0.0597	0	0
0.0679	0	0	0.0679	0	0	0.0679	0	0	0.0679	0	0
0.0771	0	0	0.0771	0	0	0.0771	0	0	0.0771	0	0
0.0876	0	0	0.0876	0	0	0.0876	0	0	0.0876	0	0
0.0995	0	0	0.0995	0	0	0.0995	0	0	0.0995	0	0
0.113	0	0	0.113	0	0	0.113	0	0	0.113	0	0
0.128	0	0	0.128	0	0	0.128	0	0	0.128	0	0
0.146	0	0	0.146	0	0	0.146	0	0	0.146	0	0
0.166	0	0	0.166	0	0	0.166	0	0	0.166	0	0

Core 6											
0 cm			**60 cm**			**80 cm**			**122 cm**		
Size (μm)	% Volume In	% Cum. Volume	Size (μm)	% Volume In	% Cum. Volume	Size (μm)	% Volume In	% Cum. Volume	Size (μm)	% Volume In	% Cum. Volume
0.188	0	0	0.188	0	0	0.188	0	0	0.188	0	0
0.214	0	0	0.214	0	0	0.214	0	0	0.214	0	0
0.243	0	0	0.243	0	0	0.243	0	0	0.243	0	0
0.276	0	0	0.276	0	0	0.276	0	0	0.276	0	0
0.314	0	0	0.314	0	0	0.314	0	0	0.314	0	0
0.357	0	0	0.357	0	0	0.357	0	0	0.357	0	0
0.405	0	0	0.405	0	0	0.405	0	0	0.405	0	0
0.46	0	0	0.46	0	0	0.46	0	0	0.46	0	0
0.523	0	0	0.523	0.08	0.08	0.523	0	0	0.523	0	0
0.594	0.07	0.07	0.594	0.21	0.29	0.594	0.11	0.11	0.594	0.07	0.07
0.675	0.14	0.21	0.675	0.35	0.64	0.675	0.21	0.32	0.675	0.13	0.2
0.767	0.2	0.41	0.767	0.44	1.08	0.767	0.28	0.6	0.767	0.18	0.38
0.872	0.23	0.64	0.872	0.46	1.54	0.872	0.31	0.91	0.872	0.21	0.59
0.991	0.23	0.87	0.991	0.45	1.99	0.991	0.31	1.22	0.991	0.22	0.81
1.13	0.23	1.1	1.13	0.42	2.41	1.13	0.29	1.51	1.13	0.21	1.02
1.28	0.23	1.33	1.28	0.42	2.83	1.28	0.29	1.8	1.28	0.22	1.24
1.45	0.25	1.58	1.45	0.46	3.29	1.45	0.33	2.13	1.45	0.23	1.47
1.65	0.28	1.86	1.65	0.53	3.82	1.65	0.39	2.52	1.65	0.26	1.73
1.88	0.32	2.18	1.88	0.61	4.43	1.88	0.46	2.98	1.88	0.3	2.03
2.13	0.36	2.54	2.13	0.69	5.12	2.13	0.54	3.52	2.13	0.34	2.37
2.42	0.39	2.93	2.42	0.76	5.88	2.42	0.61	4.13	2.42	0.38	2.75
2.75	0.43	3.36	2.75	0.82	6.7	2.75	0.67	4.8	2.75	0.41	3.16
3.12	0.46	3.82	3.12	0.88	7.58	3.12	0.74	5.54	3.12	0.45	3.61
3.55	0.5	4.32	3.55	0.94	8.52	3.55	0.81	6.35	3.55	0.49	4.1

Core 6											
0 cm			**60 cm**			**80 cm**			**122 cm**		
Size (μm)	% Volume In	% Cum. Volume	Size (μm)	% Volume In	% Cum. Volume	Size (μm)	% Volume In	% Cum. Volume	Size (μm)	% Volume In	% Cum. Volume
4.03	0.53	4.85	4.03	1	9.52	4.03	0.87	7.22	4.03	0.53	4.63
4.58	0.57	5.42	4.58	1.05	10.57	4.58	0.94	8.16	4.58	0.57	5.2
5.21	0.6	6.02	5.21	1.1	11.67	5.21	1	9.16	5.21	0.61	5.81
5.92	0.63	6.65	5.92	1.13	12.8	5.92	1.06	10.22	5.92	0.64	6.45
6.72	0.67	7.32	6.72	1.16	13.96	6.72	1.12	11.34	6.72	0.66	7.11
7.64	0.7	8.02	7.64	1.18	15.14	7.64	1.17	12.51	7.64	0.69	7.8
8.68	0.74	8.76	8.68	1.2	16.34	8.68	1.23	13.74	8.68	0.73	8.53
9.86	0.79	9.55	9.86	1.22	17.56	9.86	1.29	15.03	9.86	0.78	9.31
11.2	0.84	10.39	11.2	1.24	18.8	11.2	1.37	16.4	11.2	0.85	10.16
12.7	0.91	11.3	12.7	1.27	20.07	12.7	1.46	17.86	12.7	0.93	11.09
14.5	0.97	12.27	14.5	1.3	21.37	14.5	1.55	19.41	14.5	1.03	12.12
16.4	1.04	13.31	16.4	1.32	22.69	16.4	1.64	21.05	16.4	1.12	13.24
18.7	1.1	14.41	18.7	1.34	24.03	18.7	1.72	22.77	18.7	1.21	14.45
21.2	1.18	15.59	21.2	1.36	25.39	21.2	1.79	24.56	21.2	1.27	15.72
24.1	1.28	16.87	24.1	1.39	26.78	24.1	1.84	26.4	24.1	1.32	17.04
27.4	1.42	18.29	27.4	1.46	28.24	27.4	1.88	28.28	27.4	1.36	18.4
31.1	1.64	19.93	31.1	1.61	29.85	31.1	1.95	30.23	31.1	1.41	19.81
35.3	1.98	21.91	35.3	1.86	31.71	35.3	2.08	32.31	35.3	1.53	21.34
40.1	2.44	24.35	40.1	2.26	33.97	40.1	2.31	34.62	40.1	1.76	23.1
45.6	3.07	27.42	45.6	2.84	36.81	45.6	2.67	37.29	45.6	2.16	25.26
51.8	3.83	31.25	51.8	3.57	40.38	51.8	3.21	40.5	51.8	2.78	28.04
58.9	4.7	35.95	58.9	4.43	44.81	58.9	3.9	44.4	58.9	3.62	31.66
66.9	5.6	41.55	66.9	5.32	50.13	66.9	4.72	49.12	66.9	4.67	36.33
76	6.44	47.99	76	6.16	56.29	76	5.56	54.68	76	5.81	42.14

Core 6											
0 cm			**60 cm**			**80 cm**			**122 cm**		
Size (μm)	% Volume In	% Cum. Volume	Size (μm)	% Volume In	% Cum. Volume	Size (μm)	% Volume In	% Cum. Volume	Size (μm)	% Volume In	% Cum. Volume
86.4	7.11	55.1	86.4	6.79	63.08	86.4	6.3	60.98	86.4	6.92	49.06
98.1	7.5	62.6	98.1	7.11	70.19	98.1	6.81	67.79	98.1	7.82	56.88
111	7.54	70.14	111	7.04	77.23	111	6.97	74.76	111	8.34	65.22
127	7.2	77.34	127	6.53	83.76	127	6.7	81.46	127	8.35	73.57
144	6.51	83.85	144	5.65	89.41	144	6.02	87.48	144	7.8	81.37
163	5.53	89.38	163	4.49	93.9	163	4.98	92.46	163	6.74	88.11
186	4.38	93.76	186	3.2	97.1	186	3.73	96.19	186	5.31	93.42
211	3.16	96.92	211	1.97	99.07	211	2.43	98.62	211	3.72	97.14
240	2.01	98.93	240	0.95	100.02	240	1.26	99.88	240	2.19	99.33
272	1.04	99.97	272	0	100.02	272	0.11	99.99	272	0.67	100
310	0.08	100.05	310	0	100.02	310	0	99.99	310	0	100
352	0	100.05	352	0	100.02	352	0	99.99	352	0	100
400	0	100.05	400	0	100.02	400	0	99.99	400	0	100
454	0	100.05	454	0	100.02	454	0	99.99	454	0	100
516	0	100.05	516	0	100.02	516	0	99.99	516	0	100
586	0	100.05	586	0	100.02	586	0	99.99	586	0	100
666	0	100.05	666	0	100.02	666	0	99.99	666	0	100
756	0	100.05	756	0	100.02	756	0	99.99	756	0	100
859	0	100.05	859	0	100.02	859	0	99.99	859	0	100
976	0	100.05	976	0	100.02	976	0	99.99	976	0	100
1110	0	100.05	1110	0	100.02	1110	0	99.99	1110	0	100
1260	0	100.05	1260	0	100.02	1260	0	99.99	1260	0	100
1430	0	100.05	1430	0	100.02	1430	0	99.99	1430	0	100
1630	0	100.05	1630	0	100.02	1630	0	99.99	1630	0	100

Core 6											
0 cm			**60 cm**			**80 cm**			**122 cm**		
Size (μm)	% Volume In	% Cum. Volume	Size (μm)	% Volume In	% Cum. Volume	Size (μm)	% Volume In	% Cum. Volume	Size (μm)	% Volume In	% Cum. Volume
1850	0	100.05	1850	0	100.02	1850	0	99.99	1850	0	100
2100	0	100.05	2100	0	100.02	2100	0	99.99	2100	0	100
2390	0	100.05	2390	0	100.02	2390	0	99.99	2390	0	100
2710	0	100.05	2710	0	100.02	2710	0	99.99	2710	0	100
3080	0	100.05	3080	0	100.02	3080	0	99.99	3080	0	100
3500		100.05	3500		100.02	3500		99.99	3500		100

Table G.8 PSA Core 7

Core 7								
0 cm			**60 cm**			**122 cm**		
Size (μm)	% Volume In	% Cum. Volume	Size (μm)	% Volume In	% Cum. Volume	Size (μm)	% Volume In	% Cum. Volume
0.01	0	0	0.01	0	0	0.01	0	0
0.0114	0	0	0.0114	0	0	0.0114	0	0
0.0129	0	0	0.0129	0	0	0.0129	0	0
0.0147	0	0	0.0147	0	0	0.0147	0	0
0.0167	0	0	0.0167	0	0	0.0167	0	0
0.0189	0	0	0.0189	0	0	0.0189	0	0
0.0215	0	0	0.0215	0	0	0.0215	0	0
0.0244	0	0	0.0244	0	0	0.0244	0	0
0.0278	0	0	0.0278	0	0	0.0278	0	0
0.0315	0	0	0.0315	0	0	0.0315	0	0
0.0358	0	0	0.0358	0	0	0.0358	0	0
0.0407	0	0	0.0407	0	0	0.0407	0	0
0.0463	0	0	0.0463	0	0	0.0463	0	0
0.0526	0	0	0.0526	0	0	0.0526	0	0
0.0597	0	0	0.0597	0	0	0.0597	0	0
0.0679	0	0	0.0679	0	0	0.0679	0	0
0.0771	0	0	0.0771	0	0	0.0771	0	0
0.0876	0	0	0.0876	0	0	0.0876	0	0
0.0995	0	0	0.0995	0	0	0.0995	0	0
0.113	0	0	0.113	0	0	0.113	0	0
0.128	0	0	0.128	0	0	0.128	0	0
0.146	0	0	0.146	0	0	0.146	0	0
0.166	0	0	0.166	0	0	0.166	0	0
0.188	0	0	0.188	0	0	0.188	0	0
0.214	0	0	0.214	0	0	0.214	0	0
0.243	0	0	0.243	0	0	0.243	0	0
0.276	0	0	0.276	0	0	0.276	0	0
0.314	0	0	0.314	0	0	0.314	0	0
0.357	0	0	0.357	0	0	0.357	0	0
0.405	0	0	0.405	0	0	0.405	0	0
0.46	0	0	0.46	0	0	0.46	0	0
0.523	0	0	0.523	0	0	0.523	0	0
0.594	0.12	0.12	0.594	0.14	0.14	0.594	0.14	0.14
0.675	0.27	0.39	0.675	0.3	0.44	0.675	0.3	0.44

Core 7								
0 cm			**60 cm**			**122 cm**		
Size (μm)	% Volume In	% Cum. Volume	Size (μm)	% Volume In	% Cum. Volume	Size (μm)	% Volume In	% Cum. Volume
0.767	0.41	0.8	0.767	0.43	0.87	0.767	0.43	0.87
0.872	0.48	1.28	0.872	0.5	1.37	0.872	0.5	1.37
0.991	0.49	1.77	0.991	0.5	1.87	0.991	0.5	1.87
1.13	0.47	2.24	1.13	0.48	2.35	1.13	0.48	2.35
1.28	0.47	2.71	1.28	0.47	2.82	1.28	0.48	2.83
1.45	0.49	3.2	1.45	0.5	3.32	1.45	0.51	3.34
1.65	0.56	3.76	1.65	0.57	3.89	1.65	0.58	3.92
1.88	0.64	4.4	1.88	0.67	4.56	1.88	0.67	4.59
2.13	0.74	5.14	2.13	0.77	5.33	2.13	0.77	5.36
2.42	0.84	5.98	2.42	0.88	6.21	2.42	0.88	6.24
2.75	0.95	6.93	2.75	0.99	7.2	2.75	0.99	7.23
3.12	1.08	8.01	3.12	1.12	8.32	3.12	1.12	8.35
3.55	1.23	9.24	3.55	1.27	9.59	3.55	1.26	9.61
4.03	1.39	10.63	4.03	1.44	11.03	4.03	1.42	11.03
4.58	1.57	12.2	4.58	1.63	12.66	4.58	1.58	12.61
5.21	1.76	13.96	5.21	1.83	14.49	5.21	1.76	14.37
5.92	1.96	15.92	5.92	2.03	16.52	5.92	1.94	16.31
6.72	2.15	18.07	6.72	2.24	18.76	6.72	2.13	18.44
7.64	2.36	20.43	7.64	2.46	21.22	7.64	2.33	20.77
8.68	2.58	23.01	8.68	2.7	23.92	8.68	2.54	23.31
9.86	2.81	25.82	9.86	2.95	26.87	9.86	2.77	26.08
11.2	3.06	28.88	11.2	3.21	30.08	11.2	3	29.08
12.7	3.33	32.21	12.7	3.48	33.56	12.7	3.24	32.32
14.5	3.61	35.82	14.5	3.74	37.3	14.5	3.48	35.8
16.4	3.88	39.7	16.4	4	41.3	16.4	3.69	39.49
18.7	4.13	43.83	18.7	4.22	45.52	18.7	3.86	43.35
21.2	4.35	48.18	21.2	4.39	49.91	21.2	3.99	47.34
24.1	4.51	52.69	24.1	4.5	54.41	24.1	4.05	51.39
27.4	4.63	57.32	27.4	4.55	58.96	27.4	4.05	55.44
31.1	4.68	62	31.1	4.51	63.47	31.1	4.01	59.45
35.3	4.69	66.69	35.3	4.41	67.88	35.3	3.93	63.38
40.1	4.65	71.34	40.1	4.23	72.11	40.1	3.83	67.21
45.6	4.56	75.9	45.6	4	76.11	45.6	3.75	70.96
51.8	4.43	80.33	51.8	3.73	79.84	51.8	3.68	74.64
58.9	4.23	84.56	58.9	3.44	83.28	58.9	3.62	78.26

Core 7								
0 cm			**60 cm**			**122 cm**		
Size (μm)	% Volume In	% Cum. Volume	Size (μm)	% Volume In	% Cum. Volume	Size (μm)	% Volume In	% Cum. Volume
66.9	3.94	88.5	66.9	3.13	86.41	66.9	3.54	81.8
76	3.52	92.02	76	2.81	89.22	76	3.42	85.22
86.4	2.98	95	86.4	2.49	91.71	86.4	3.21	88.43
98.1	2.32	97.32	98.1	2.17	93.88	98.1	2.86	91.29
111	1.59	98.91	111	1.84	95.72	111	2.38	93.67
127	0.88	99.79	127	1.51	97.23	127	1.81	95.48
144	0.21	100	144	1.17	98.4	144	1.21	96.69
163	0.01	100.01	163	0.84	99.24	163	0.7	97.39
186	0	100.01	186	0.52	99.76	186	0.35	97.74
211	0	100.01	211	0.21	99.97	211	0.23	97.97
240	0	100.01	240	0.03	100	240	0.3	98.27
272	0	100.01	272	0	100	272	0.43	98.7
310	0	100.01	310	0	100	310	0.5	99.2
352	0	100.01	352	0	100	352	0.44	99.64
400	0	100.01	400	0	100	400	0.28	99.92
454	0	100.01	454	0	100	454	0.09	100.01
516	0	100.01	516	0	100	516	0	100.01
586	0	100.01	586	0	100	586	0	100.01
666	0	100.01	666	0	100	666	0	100.01
756	0	100.01	756	0	100	756	0	100.01
859	0	100.01	859	0	100	859	0	100.01
976	0	100.01	976	0	100	976	0	100.01
1110	0	100.01	1110	0	100	1110	0	100.01
1260	0	100.01	1260	0	100	1260	0	100.01
1430	0	100.01	1430	0	100	1430	0	100.01
1630	0	100.01	1630	0	100	1630	0	100.01
1850	0	100.01	1850	0	100	1850	0	100.01
2100	0	100.01	2100	0	100	2100	0	100.01
2390	0	100.01	2390	0	100	2390	0	100.01
2710	0	100.01	2710	0	100	2710	0	100.01
3080	0	100.01	3080	0	100	3080	0	100.01
3500		100.01	3500		100	3500		100.01

Table G.9 PSA Core 8

Core 8					
0 cm			**122 cm**		
Size (μm)	% Volume In	% Cum. Volume	Size (μm)	% Volume In	% Cum. Volume
0.01	0	0	0.01	0	0
0.0114	0	0	0.0114	0	0
0.0129	0	0	0.0129	0	0
0.0147	0	0	0.0147	0	0
0.0167	0	0	0.0167	0	0
0.0189	0	0	0.0189	0	0
0.0215	0	0	0.0215	0	0
0.0244	0	0	0.0244	0	0
0.0278	0	0	0.0278	0	0
0.0315	0	0	0.0315	0	0
0.0358	0	0	0.0358	0	0
0.0407	0	0	0.0407	0	0
0.0463	0	0	0.0463	0	0
0.0526	0	0	0.0526	0	0
0.0597	0	0	0.0597	0	0
0.0679	0	0	0.0679	0	0
0.0771	0	0	0.0771	0	0
0.0876	0	0	0.0876	0	0
0.0995	0	0	0.0995	0	0
0.113	0	0	0.113	0	0
0.128	0	0	0.128	0	0
0.146	0	0	0.146	0	0
0.166	0	0	0.166	0	0
0.188	0	0	0.188	0	0
0.214	0	0	0.214	0	0
0.243	0	0	0.243	0	0
0.276	0	0	0.276	0	0
0.314	0	0	0.314	0	0
0.357	0	0	0.357	0	0
0.405	0	0	0.405	0	0
0.46	0	0	0.46	0	0
0.523	0	0	0.523	0	0
0.594	0	0	0.594	0	0
0.675	0.04	0.04	0.675	0	0
0.767	0.09	0.13	0.767	0	0

Core 8					
0 cm			**122 cm**		
Size (μm)	% Volume In	% Cum. Volume	Size (μm)	% Volume In	% Cum. Volume
0.872	0.11	0.24	0.872	0.07	0.07
0.991	0.11	0.35	0.991	0.08	0.15
1.13	0.11	0.46	1.13	0.09	0.24
1.28	0.11	0.57	1.28	0.09	0.33
1.45	0.12	0.69	1.45	0.1	0.43
1.65	0.14	0.83	1.65	0.11	0.54
1.88	0.16	0.99	1.88	0.12	0.66
2.13	0.18	1.17	2.13	0.13	0.79
2.42	0.2	1.37	2.42	0.15	0.94
2.75	0.23	1.6	2.75	0.16	1.1
3.12	0.26	1.86	3.12	0.19	1.29
3.55	0.29	2.15	3.55	0.21	1.5
4.03	0.32	2.47	4.03	0.24	1.74
4.58	0.36	2.83	4.58	0.28	2.02
5.21	0.4	3.23	5.21	0.31	2.33
5.92	0.44	3.67	5.92	0.34	2.67
6.72	0.48	4.15	6.72	0.37	3.04
7.64	0.52	4.67	7.64	0.41	3.45
8.68	0.55	5.22	8.68	0.45	3.9
9.86	0.59	5.81	9.86	0.5	4.4
11.2	0.64	6.45	11.2	0.56	4.96
12.7	0.7	7.15	12.7	0.64	5.6
14.5	0.77	7.92	14.5	0.72	6.32
16.4	0.85	8.77	16.4	0.81	7.13
18.7	0.94	9.71	18.7	0.9	8.03
21.2	1.03	10.74	21.2	0.99	9.02
24.1	1.13	11.87	24.1	1.08	10.1
27.4	1.21	13.08	27.4	1.17	11.27
31.1	1.27	14.35	31.1	1.28	12.55
35.3	1.31	15.66	35.3	1.43	13.98
40.1	1.34	17	40.1	1.66	15.64
45.6	1.38	18.38	45.6	2	17.64
51.8	1.48	19.86	51.8	2.48	20.12
58.9	1.69	21.55	58.9	3.12	23.24
66.9	2.06	23.61	66.9	3.91	27.15
76	2.63	26.24	76	4.8	31.95

Core 8					
0 cm			**122 cm**		
Size (μm)	% Volume In	% Cum. Volume	Size (μm)	% Volume In	% Cum. Volume
86.4	3.41	29.65	86.4	5.73	37.68
98.1	4.36	34.01	98.1	6.6	44.28
111	5.42	39.43	111	7.29	51.57
127	6.47	45.9	127	7.73	59.3
144	7.39	53.29	144	7.83	67.13
163	8.02	61.31	163	7.56	74.69
186	8.26	69.57	186	6.94	81.63
211	8.01	77.58	211	6.02	87.65
240	7.25	84.83	240	4.87	92.52
272	6.04	90.87	272	3.61	96.13
310	4.53	95.4	310	2.37	98.5
352	2.94	98.34	352	1.29	99.79
400	1.52	99.86	400	0.23	100.02
454	0.13	99.99	454	0	100.02
516	0	99.99	516	0	100.02
586	0	99.99	586	0	100.02
666	0	99.99	666	0	100.02
756	0	99.99	756	0	100.02
859	0	99.99	859	0	100.02
976	0	99.99	976	0	100.02
1110	0	99.99	1110	0	100.02
1260	0	99.99	1260	0	100.02
1430	0	99.99	1430	0	100.02
1630	0	99.99	1630	0	100.02
1850	0	99.99	1850	0	100.02
2100	0	99.99	2100	0	100.02
2390	0	99.99	2390	0	100.02
2710	0	99.99	2710	0	100.02
3080	0	99.99	3080	0	100.02
3500		99.99	3500		100.02

Table G.9 East Bank PSA Figures (Core 1, 1b, 2, 3, and 4)

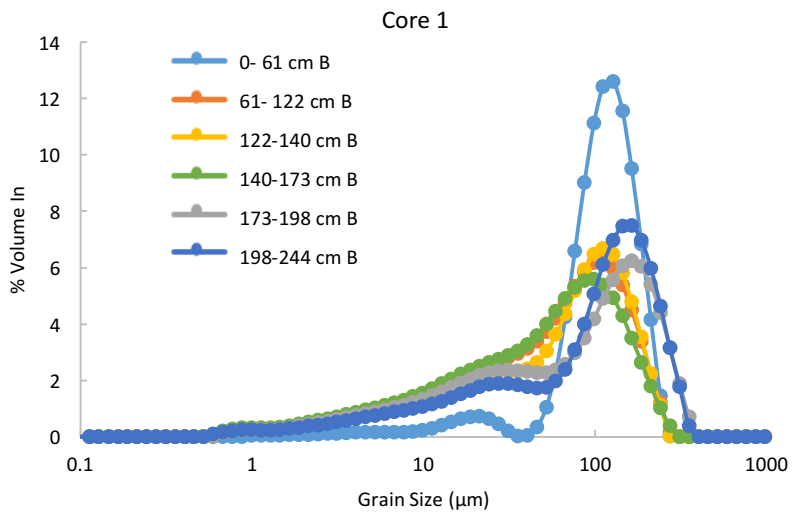

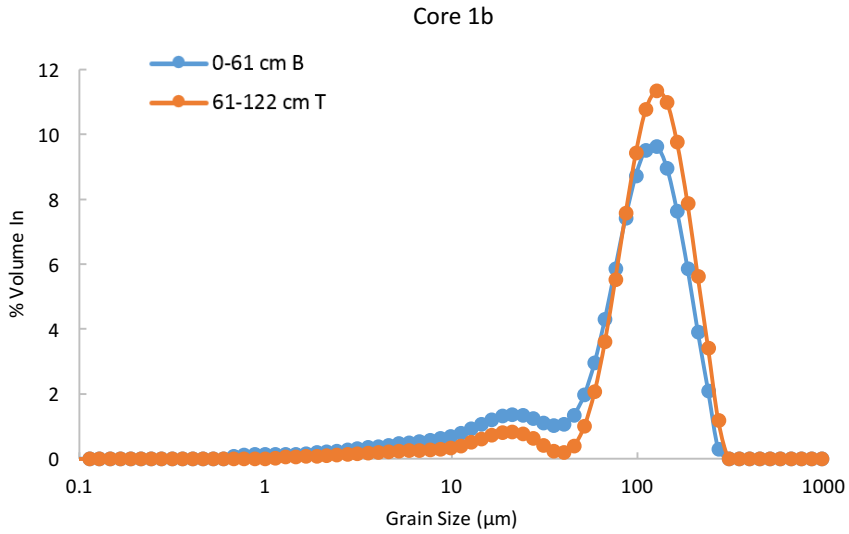

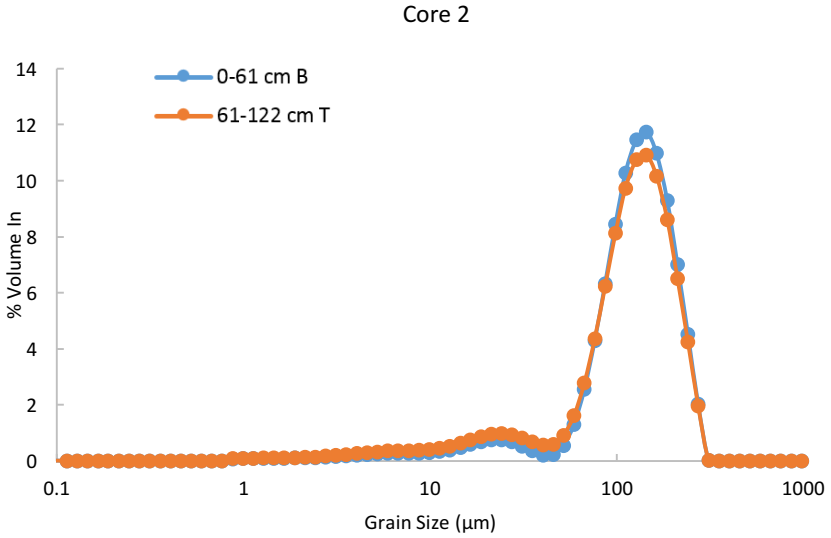

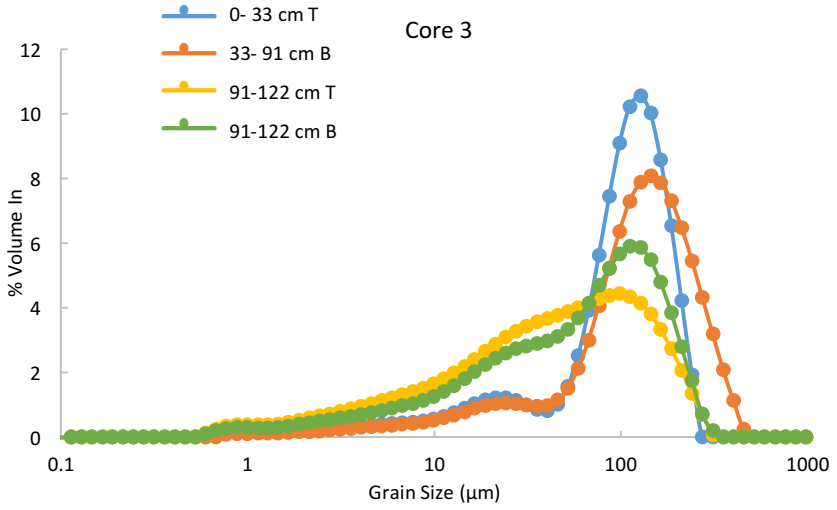

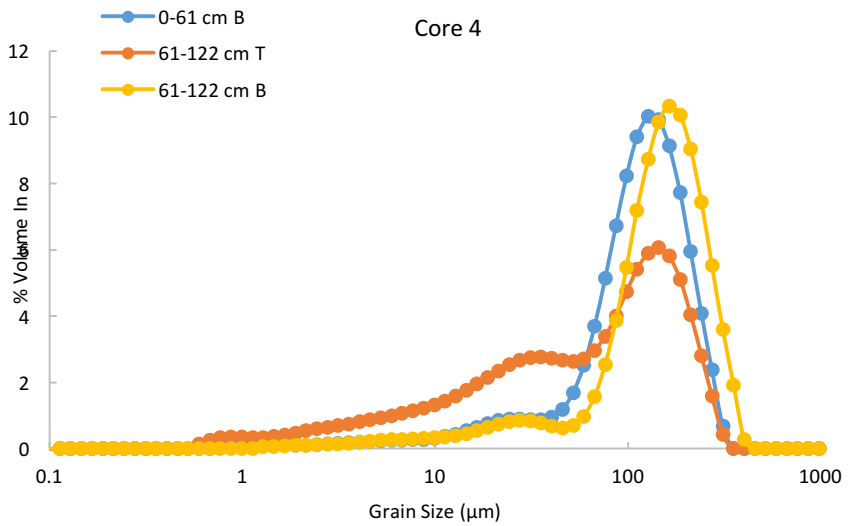
Core 4
0-61 cm B
61-122 cm T
61-122 cm B
% Volume In
12
10
8
6
4
2
0
0.1
1
10
100
1000
Grain Size (µm)

Table G.9 West Bank PSA Figures (Core 5, 6, 7)

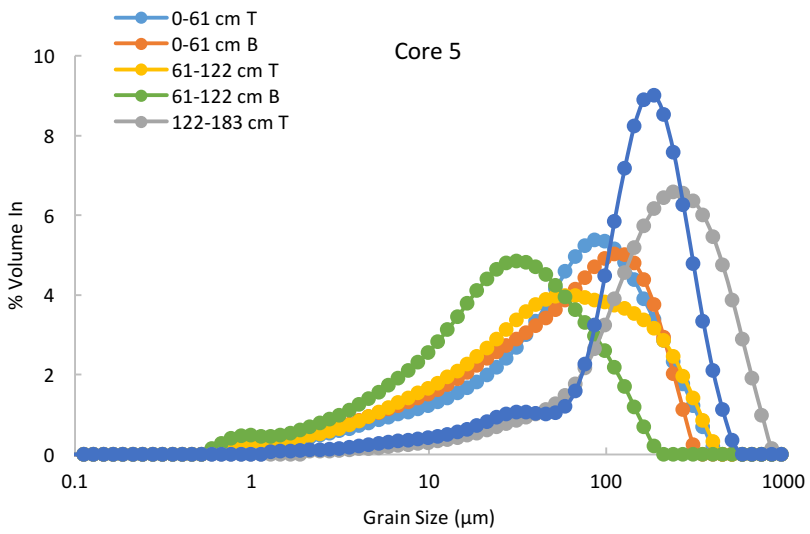

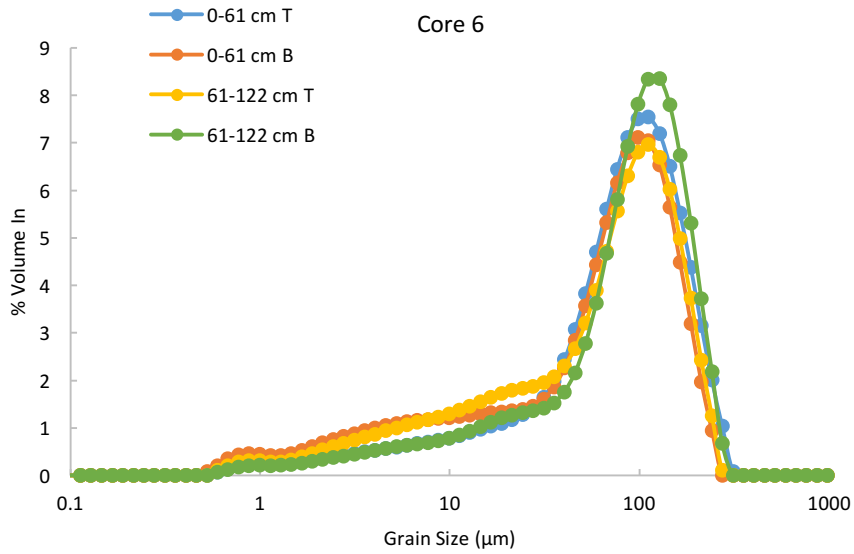

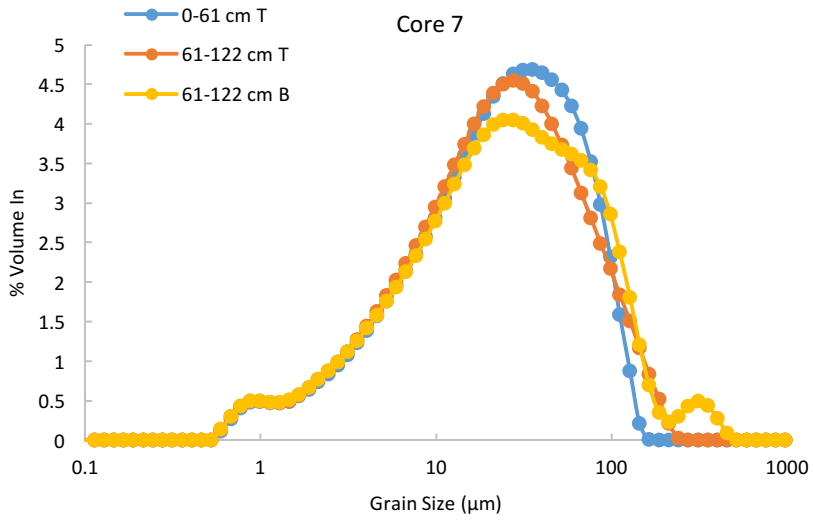

Table G.9 Island Core PSA Figures (Core 8)

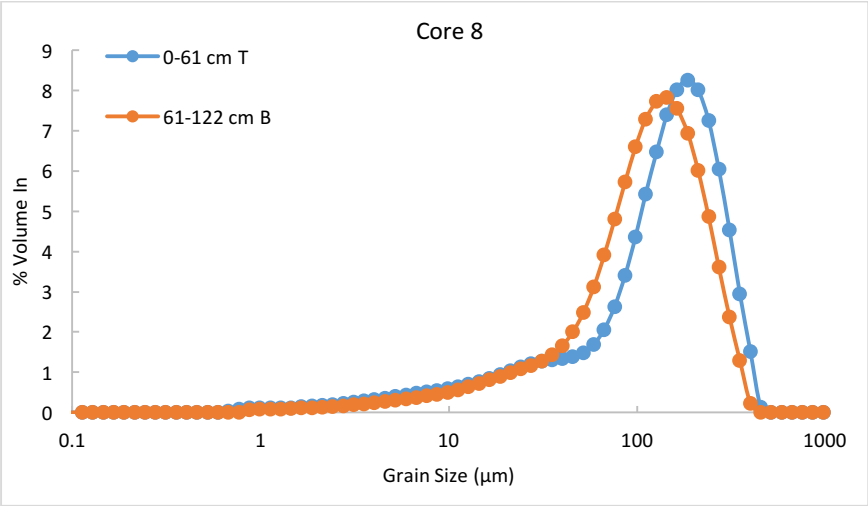

Appendix H - X-Ray Diffraction Mineral Comparison

Table H.1 Mineral Comparison East. Bank Vs West Bank vs. Island

	West			East					Island
Minerals	**Core 5**	**Core 6**	**Core 7**	**Core 1**	**Core 1b**	**Core 2**	**Core 3**	**Core 4**	**Core 8**
Quartz	x	x	x	x	x	x	x	x	x
Albite	x	x	x	x	x	x	x		x
Amphibole	x	x	x	x	x	x	x	x	x
Biotite	x			x			x		
Muscovite	x	x	x	x	x	x	x	x	x
Illite		x	x	x	x	x	x	x	
Chlorite/Serpentine	x		x	x	x	x			x
Birnessite	x	x	x	x	x	x	x	x	x
Ankerite	x			x			x		
Pyrite Peak	x	x		x					
Siderite	x		x		x		x		
Anorthite	x	x	x	x		x	x		
Rutile	x								
Mica		x	x				x	x	
Montmorillonite		x							
Magnetite				x					
Hematite				x			x		
Goethite				x					
Feldspar			x	x	x		x	x	x
Vermiculite	x				x		x		x

Table H.2 Depth Mineral Comparison Core 1

	Core 1					
Depth Interval	**0-61B**	**61-122T**	**122-183T**	**122-183B**	**183-244T**	**183-244B**
Approx. Depth	**50cm**	**70cm**	**130cm**	**183cm**	**198cm**	**244cm**
Minerals						
Quartz	x	x	x	x	x	x
Albite	x	x	x	x		x
Amphibole	x	x	x	x	x	x
Biotite	x					
Muscovite	x	x	x	x	x	
Illite			x			x
Chlorite Serpentine	x	x	x	x	x	
Birnessite	x	x	x	x	x	x
Ankerite	x					x
Pyrite Peak		x		x	x	x
Siderite						
Anorthite		x			x	x
Rutile						
Mica						
Montmorillonite						
Magnetite	x					
Hematite			x			x
Goethite	x					
Feldspar	x					
Vermiculite						

Table H.3 Depth Mineral Comparison Core 1b

	Core 1b	
Depth Interval	**0-61B**	**61-122B**
Approx. Depth	**50cm**	**122cm**
Minerals		
Quartz	x	x
Albite	x	
Amphibole	x	x
Biotite		
Muscovite	x	x
Illite		x
Chlorite Serpentine		x
Birnessite		x
Ankerite		
Pyrite Peak		
Siderite	x	x
Anorthite		
Rutile		
Mica		
Montmorillonite		
Magnetite		
Hematite		
Goethite		
Feldspar		x
Vermiculite	x	

Table H.4 Depth Mineral Comparison Core 2

	Core 2	
Depth Interval	**0-61B**	**61-122B**
Approx. Depth	**50cm**	**122cm**
Minerals		
Quartz	x	x
Albite	x	x
Amphibole	x	x
Biotite		
Muscovite	x	
Illite		x
Chlorite Serpentine		x
Birnessite	x	x
Ankerite		
Pyrite Peak		
Siderite		
Anorthite		x
Rutile		
Mica		
Montmorillonite		
Magnetite		
Hematite		
Goethite		
Feldspar		
Vermiculite		

Table H.5 Depth Mineral Comparison Core 3

	Core 3			
Depth Interval	**33-92T**	**33-92B**	**92-122T**	**92-122B**
Approx. Depth	**40cm**	**91cm**	**105cm**	**122cm**
Minerals				
Quartz	x	x	x	x
Albite	x	x		
Amphibole	x	x	x	x
Biotite	x			
Muscovite		x		x
Illite	x	x	x	
Chlorite Serpentine		x	x	x
Birnessite	x	x		x
Ankerite		x		x
Pyrite Peak				
Siderite	x			
Anorthite		x		
Rutile				
Mica				x
Montmorillonite				
Hematite		x		
Goethite				
Feldspar			x	
Vermiculite	x			

Table H.6 Depth Mineral Comparison Core 4

	Core 4	
Depth Interval	**0-61B**	**61-122B**
Approx. Depth	**50cm**	**122cm**
Minerals		
Quartz	x	x
Albite		
Amphibole	x	x
Biotite		
Muscovite	x	x
Illite	x	
Chlorite Serpentine		
Birnessite	x	x
Ankerite		
Pyrite Peak		
Siderite		
Anorthite		
Rutile		
Mica	x	
Montmorillonite		
Magnetite		
Hematite		
Goethite		
Feldspar	x	x
Vermiculite		

Table H.7 Depth Mineral Comparison Core 5

	Core 5					
Depth Interval	**0-61T**	**0-61B**	**61-122T**	**61-122B**	**122-183T**	**122-183B**
Approx. Depth	**2cm**	**50cm**	**70cm**	**120cm**	**130cm**	**183cm**
Minerals						
Quartz	x	x	x	x	x	x
Albite		x	x	x		x
Amphibole	x	x		x		x
Biotite						x
Muscovite	x	x	x	x	x	
Illite						
Chlorite Serpentine	x	x	x	x	x	
Birnessite (Manganese Oxide)	x	x		x	x	
Ankerite	x		x			x
Pyrite Peak			x			
Siderite				x		x
Anorthite					x	
Rutile (Ti Oxide)					x	x
Mica						
Montmorillonite						
Magnetite						
Hematite						
Goethite						
Feldspar						
Vermiculite		x				

Table H.8 Depth Mineral Comparison Core 6

	Core 6			
Depth Interval	**0-61T**	**0-61B**	**61-122T**	**61-122B**
Approx. Depth	**2cm**	**50cm**	**70cm**	**120cm**
Minerals				
Quartz	x	x	x	x
Albite	x	x	x	x
Amphibole	x	x	x	x
Biotite				
Muscovite		x		x
Illite	x		x	x
Chlorite Serpentine				
Birnessite		x	x	x
Ankerite				
Pyrite Peak			x	
Siderite				
Anorthite	x			
Rutile				
Mica	x		x	
Montmorillonite		x		x
Magnetite				
Hematite				
Goethite				
Feldspar				
Vermiculite				

Table H.9 Depth Mineral Comparison Core 7

	Core 7			
Depth Interval	**0-61T**	**0-61B**	**61-122T**	**61-122B**
Approx. Depth	**2cm**	**50cm**	**70cm**	**120cm**
Minerals				
Quartz	x	x	x	x
Albite				x
Amphibole	x	x	x	x
Biotite				
Muscovite	x	x		x
Illite			x	
Chlorite Serpentine	x	x		x
Birnessite	x			x
Ankerite				
Pyrite Peak				
Siderite				x
Anorthite			x	
Rutile				
Mica			x	
Montmorillonite				
Magnetite				
Hematite				
Goethite				
Feldspar		x		
Vermiculite				

Table H.10 Depth Mineral Comparison Core 8

	Core 8
Depth Interval	**0-61T**
Approx. Depth	**0cm**
Minerals	
Quartz	x
Albite	x
Amphibole	x
Biotite	
Muscovite	x
Illite	
Chlorite Serpentine	x
Birnessite	x
Ankerite	
Pyrite Peak	
Siderite	
Anorthite	
Rutile	
Mica	
Montmorillonite	
Magnetite	
Hematite	
Goethite	
Feldspar	x
Vermiculite	x

Appendix I - X-Ray Diffraction Spectra

Figure I.1: XRD Spectra Core 1 0-24T

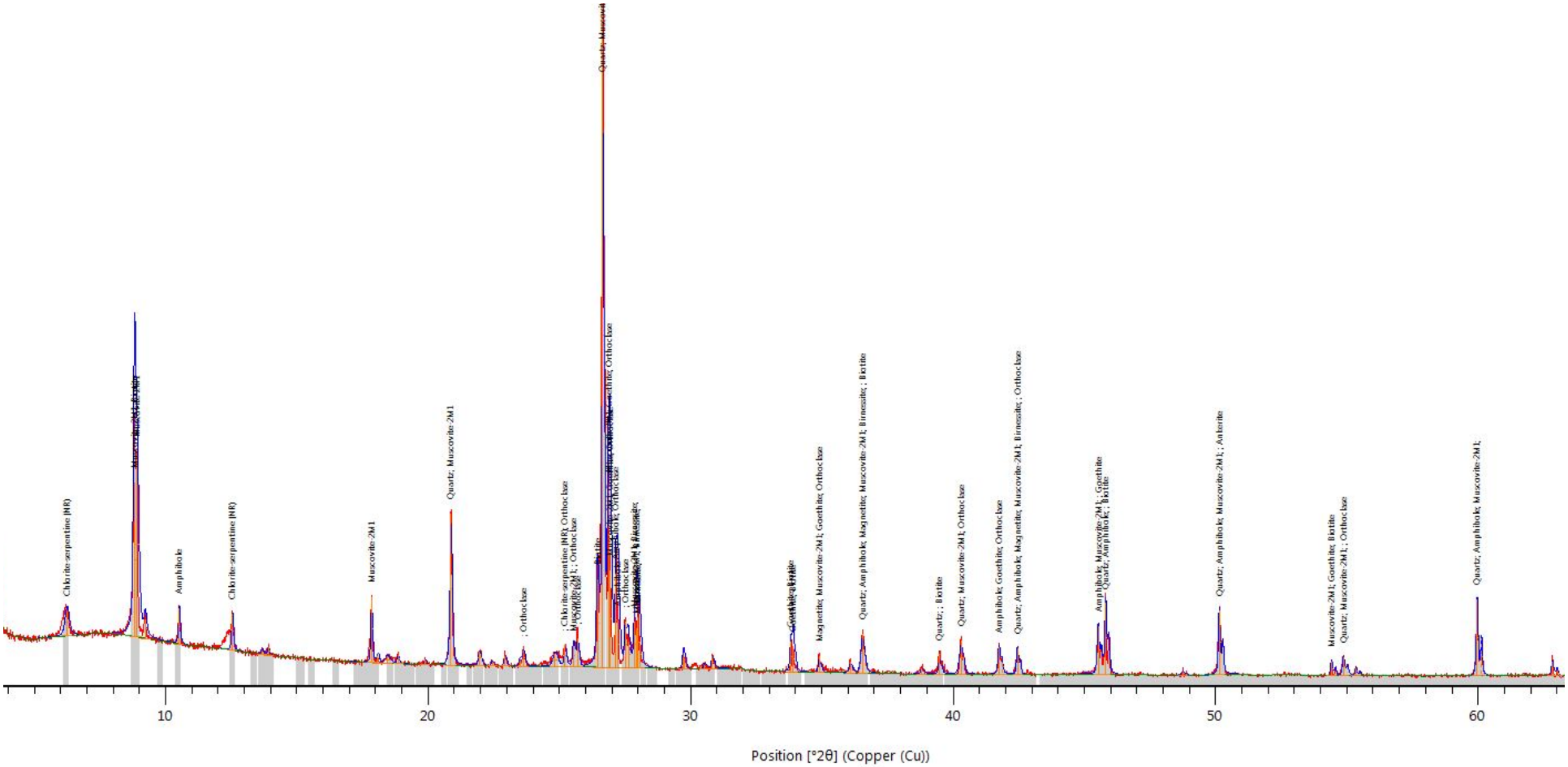

Figure I.2: XRD Spectra Core 1 0-24B

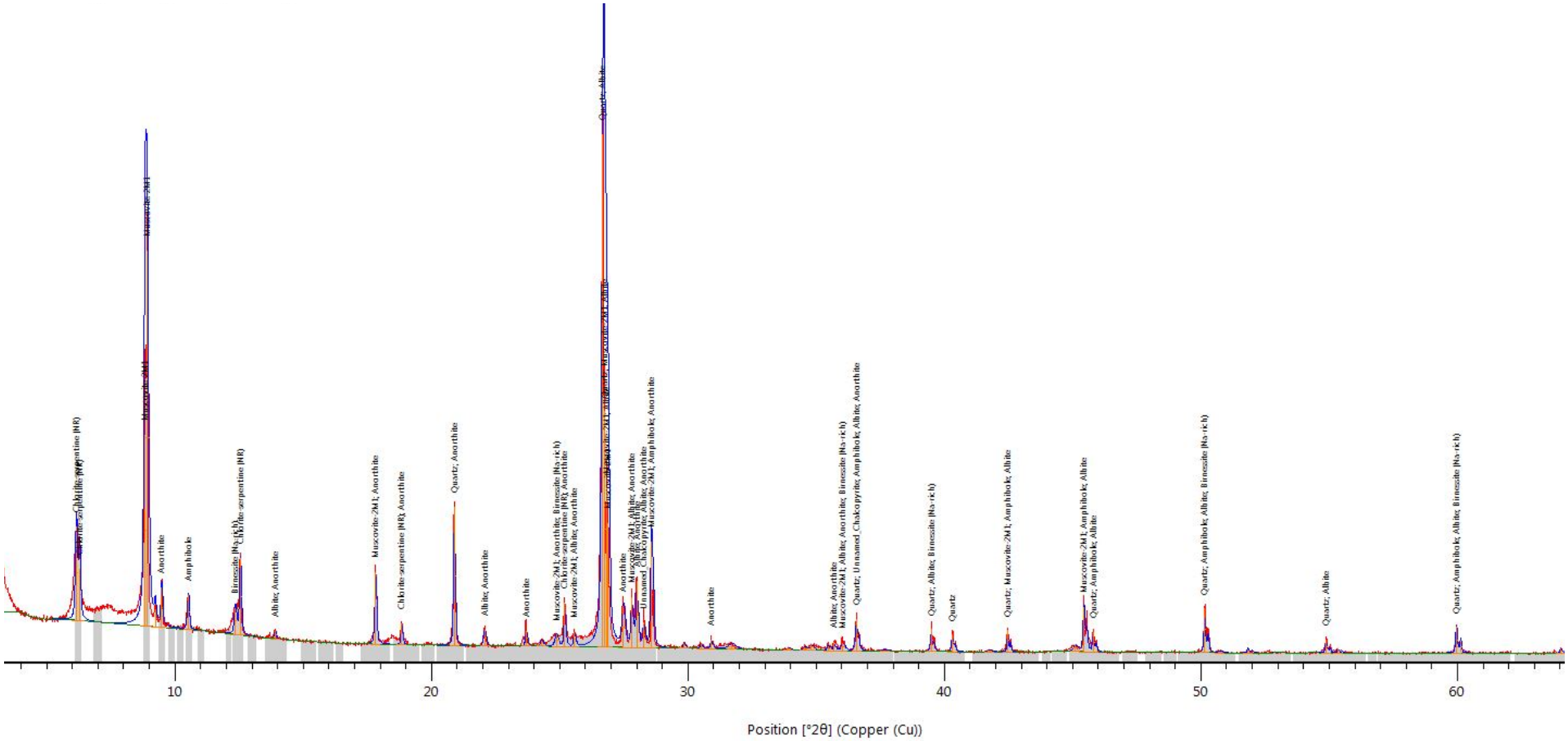

Figure I.3: XRD Spectra Core 1 48-72T

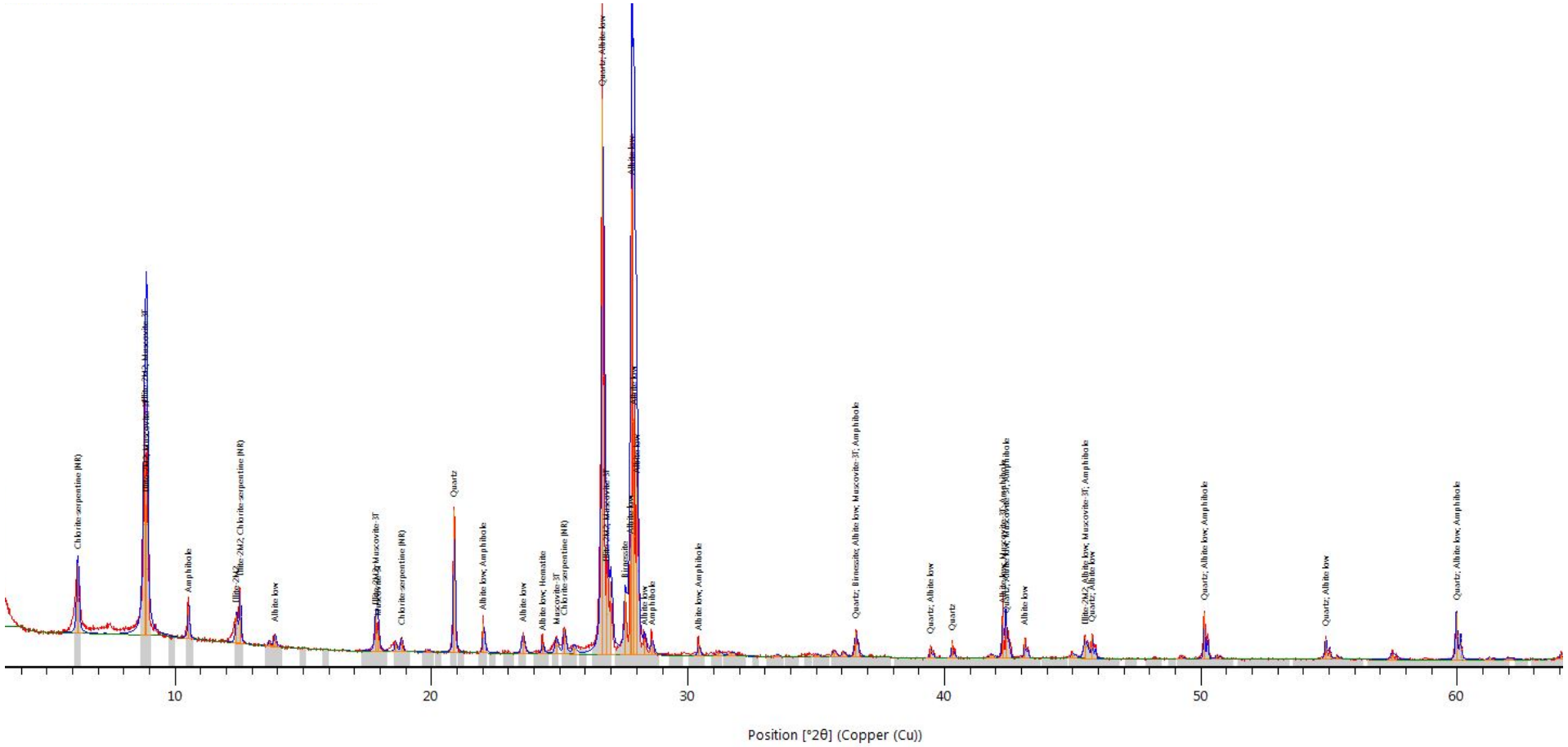

Figure I.4: XRD Spectra Core 1 48-72B

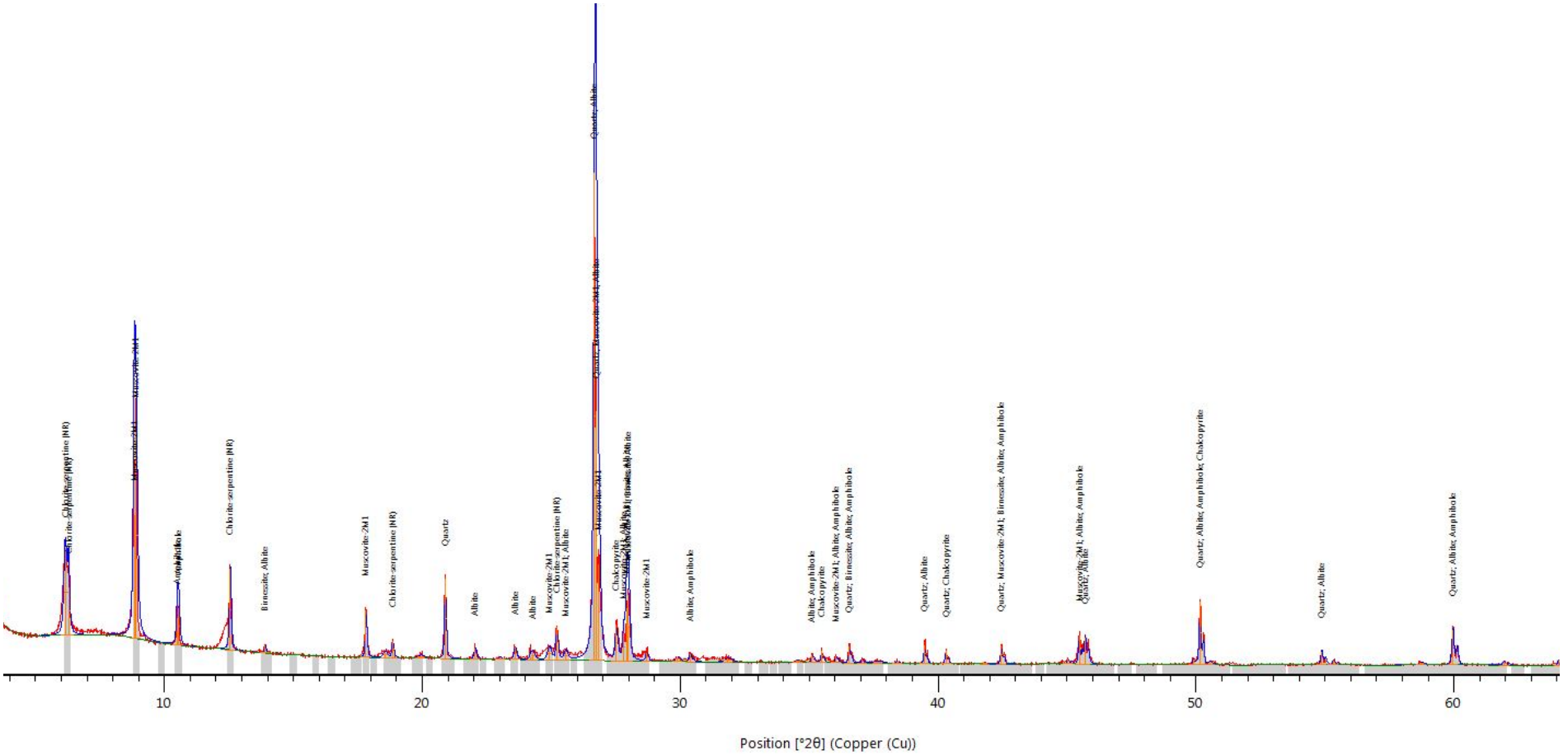

Figure I.5: XRD Spectra Core 1 72-96T

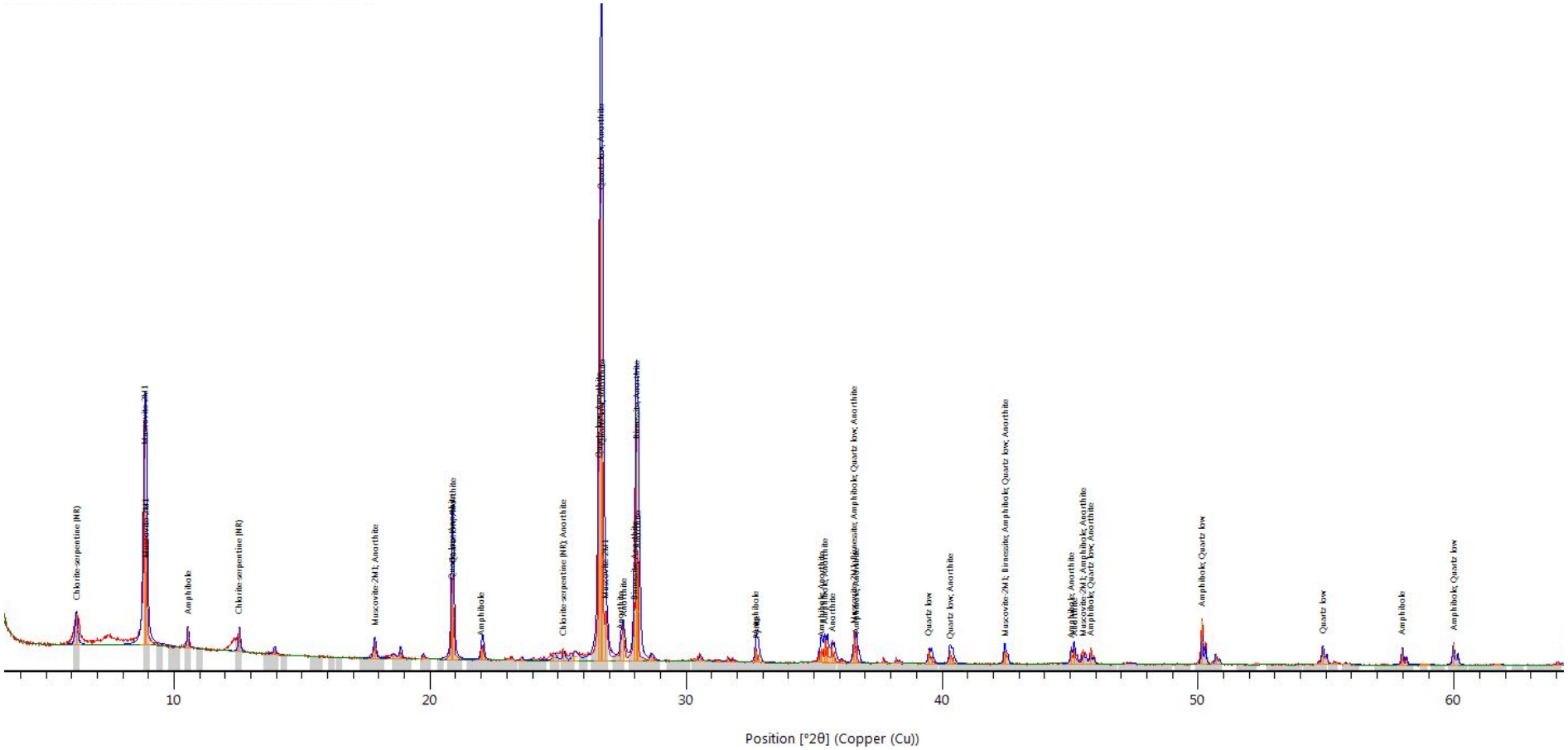

Figure I.6: XRD Spectra Core 1 72-96B

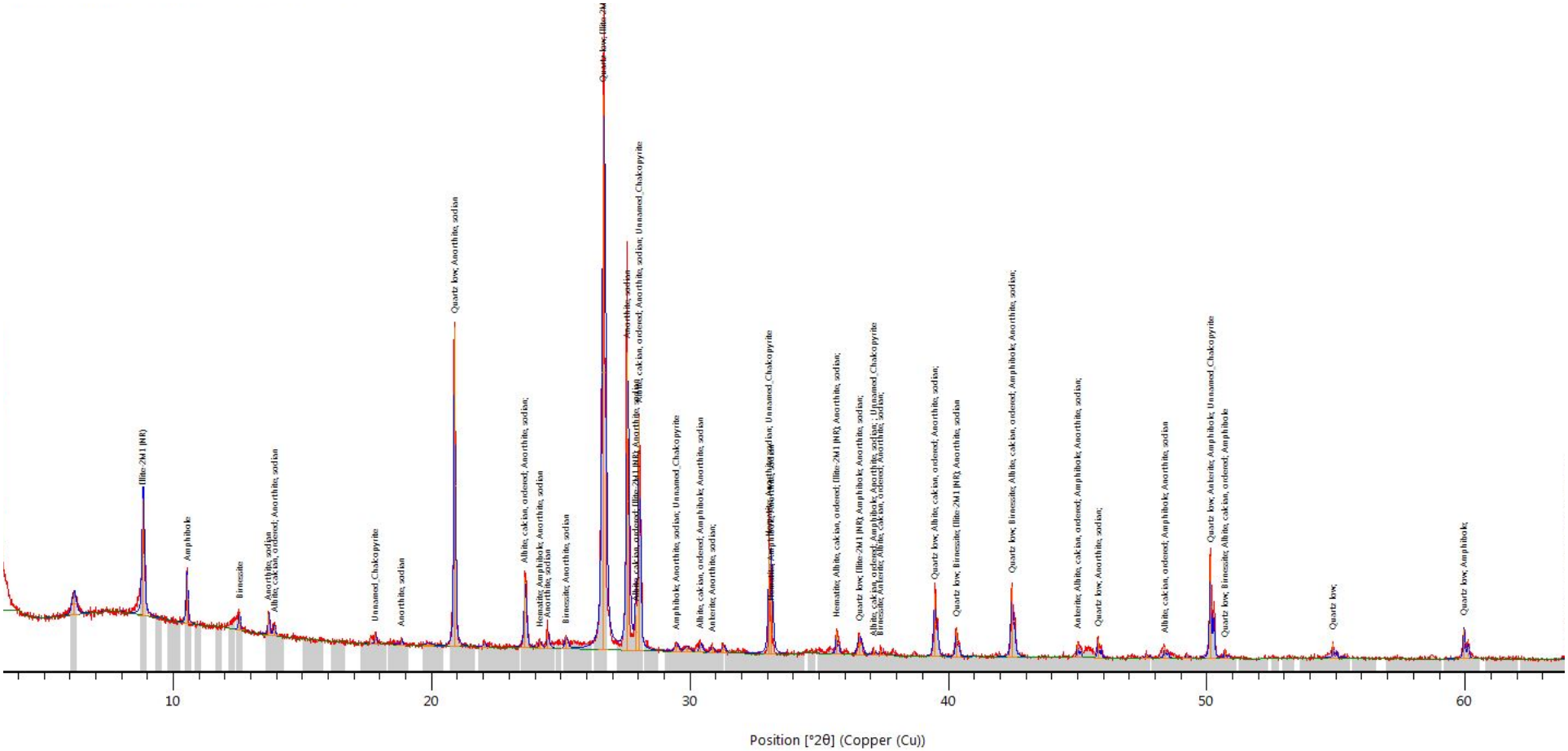

Figure I.7: XRD Spectra Core 1b 0-48T

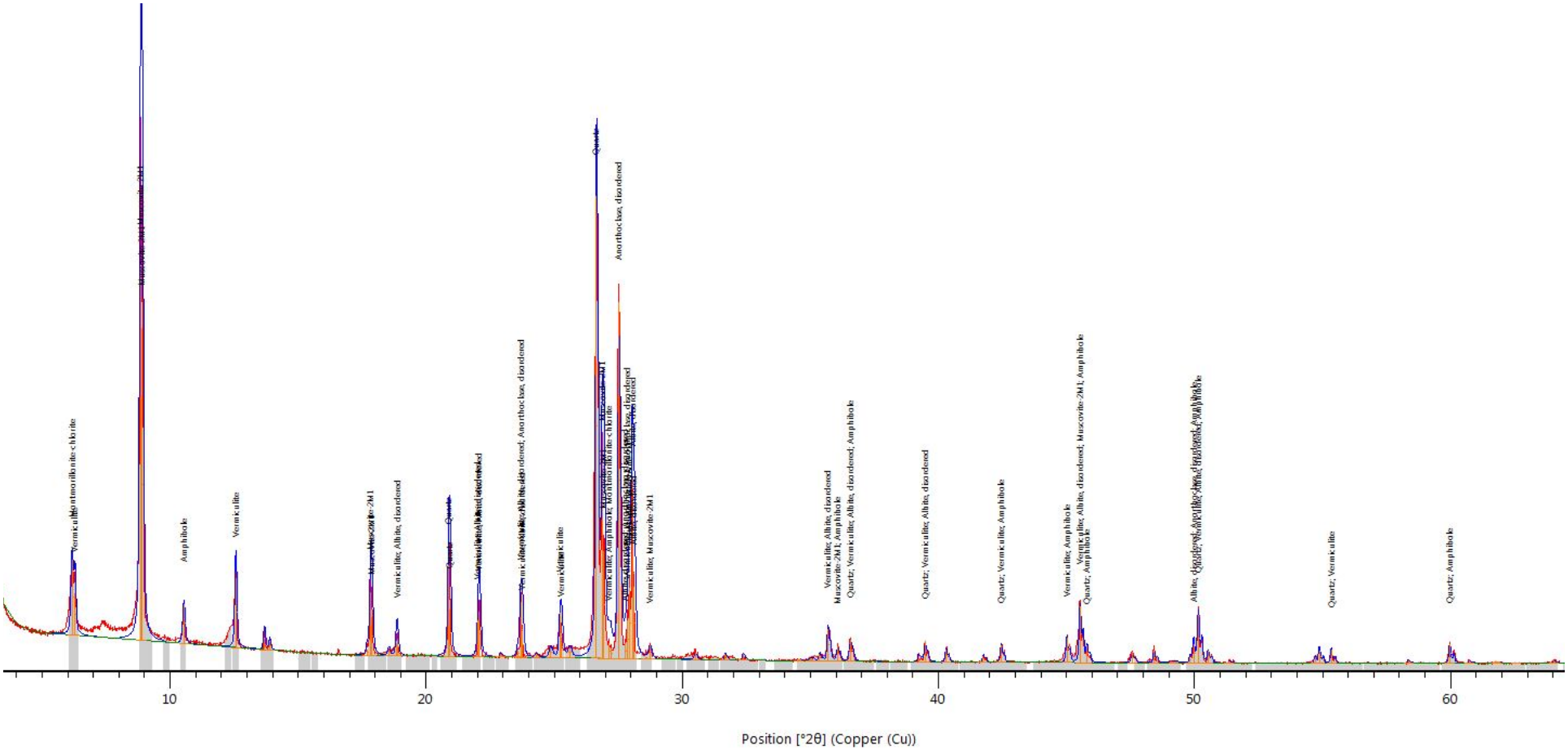

Figure I.8: XRD Spectra Core 1b 0-48B

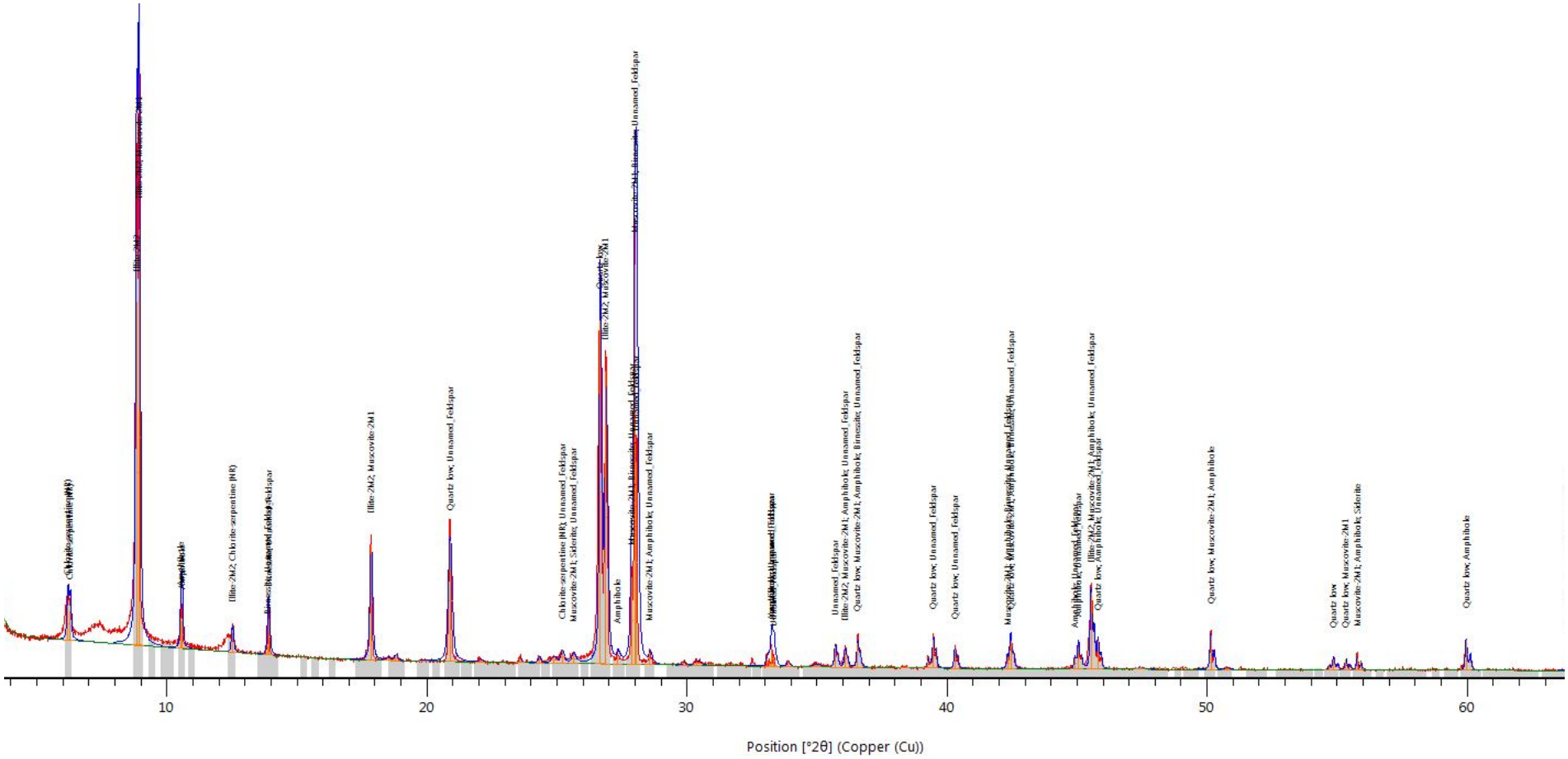

Figure I.9: XRD Spectra Core 2 24-48T

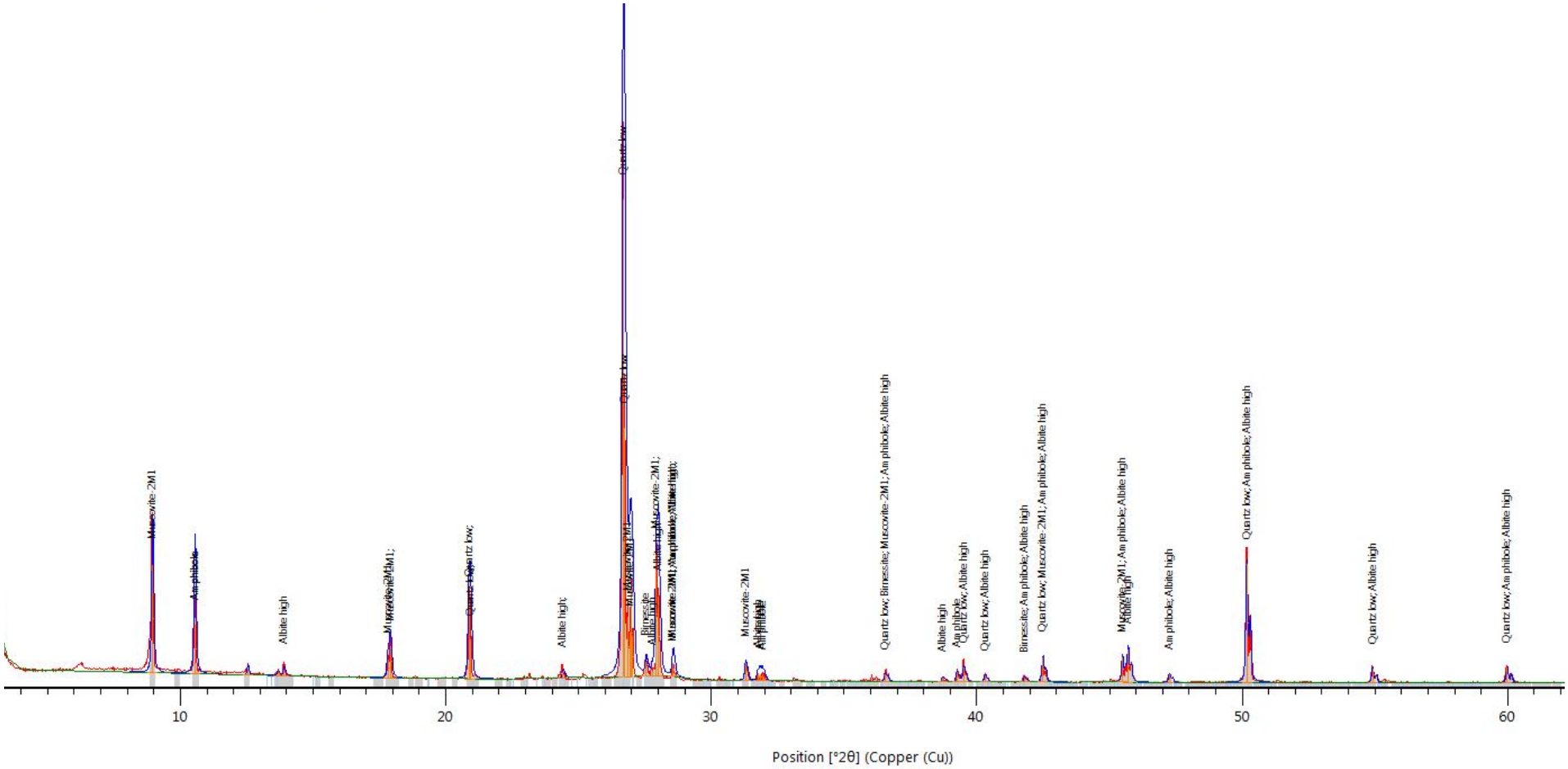

Figure I.10: XRD Spectra Core 2 24-48B

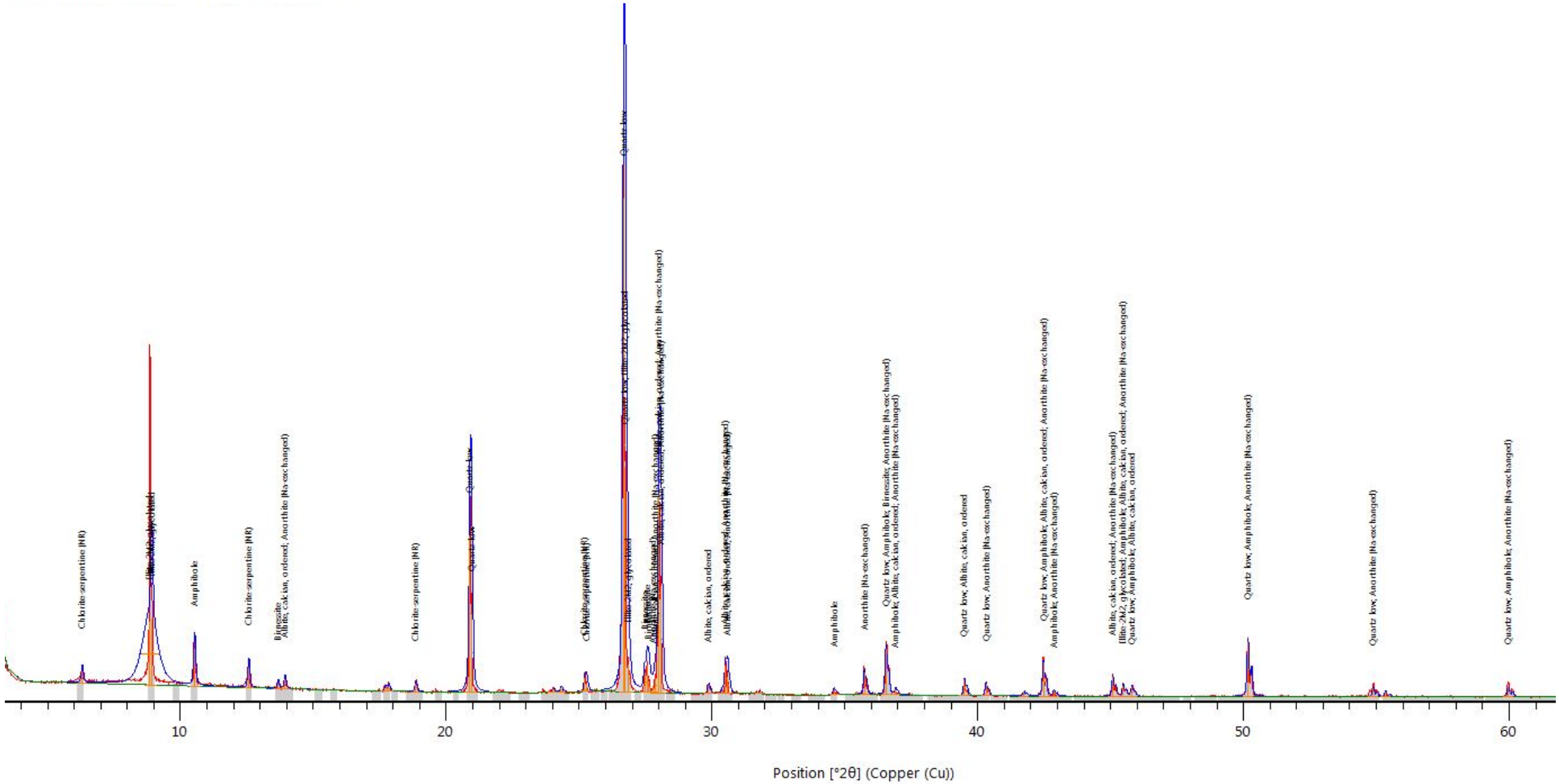

Figure I.1: XRD Spectra Core 3 13-36T

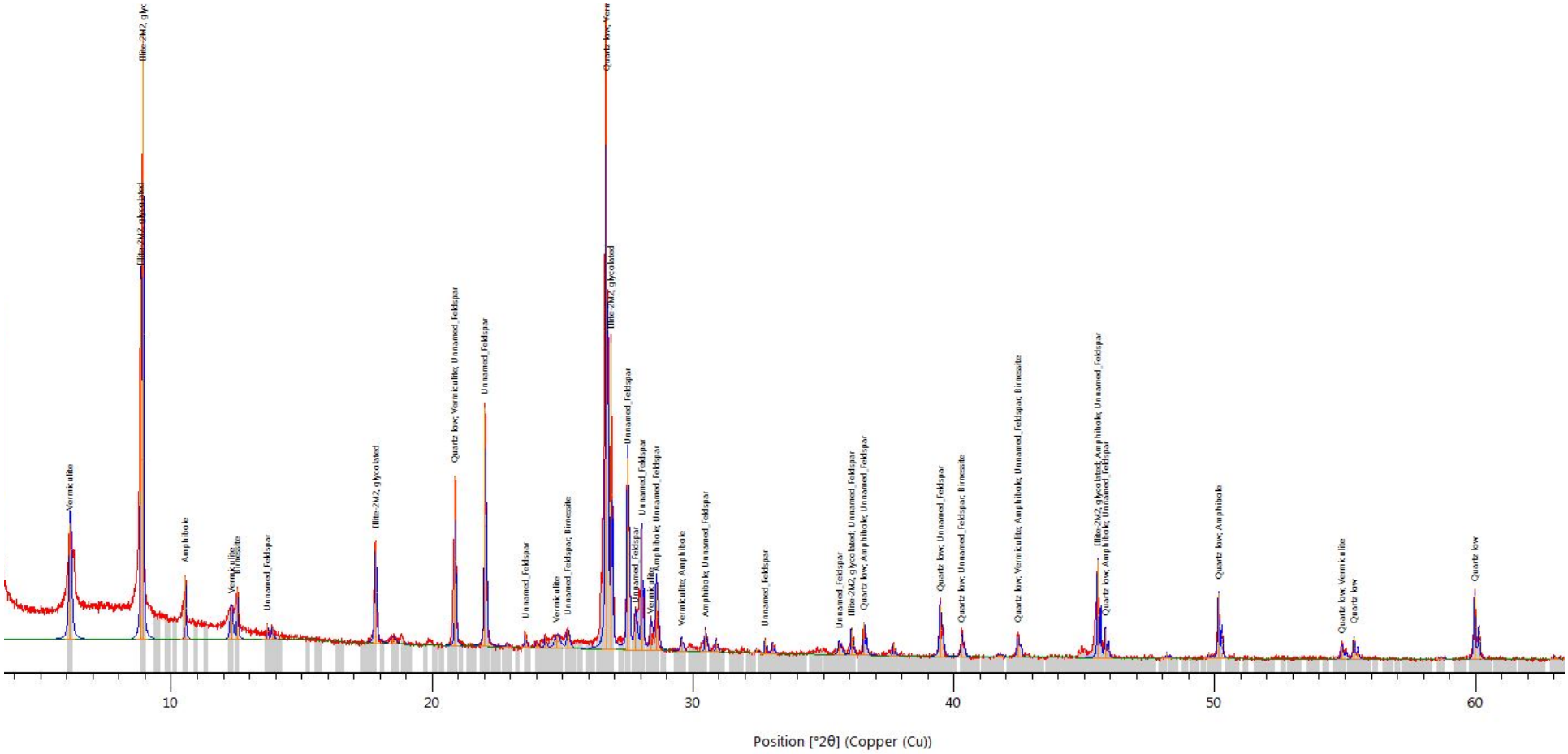

Figure I.12: XRD Spectra Core 3 13-36B

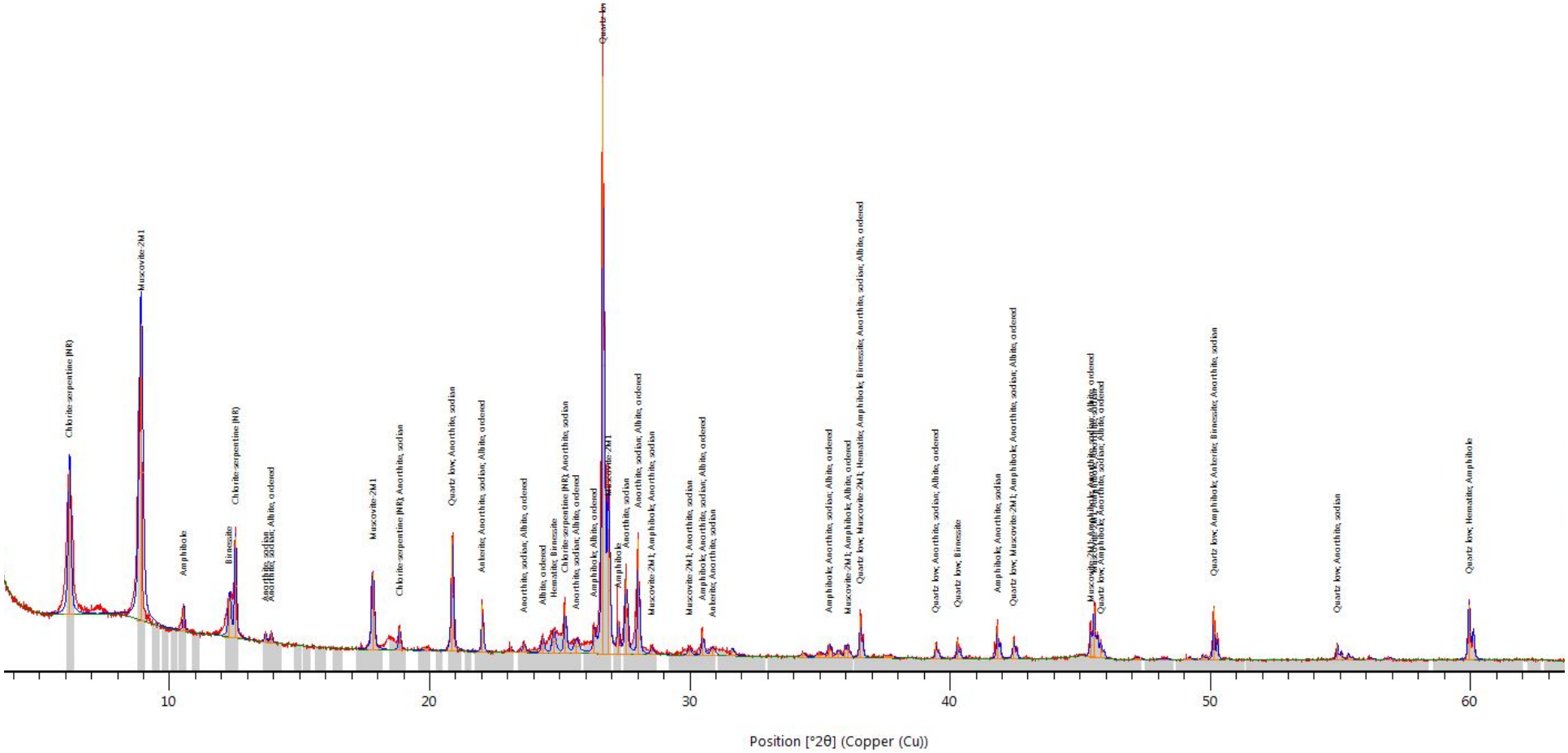

Figure I.13: XRD Spectra Core 3 36-48T

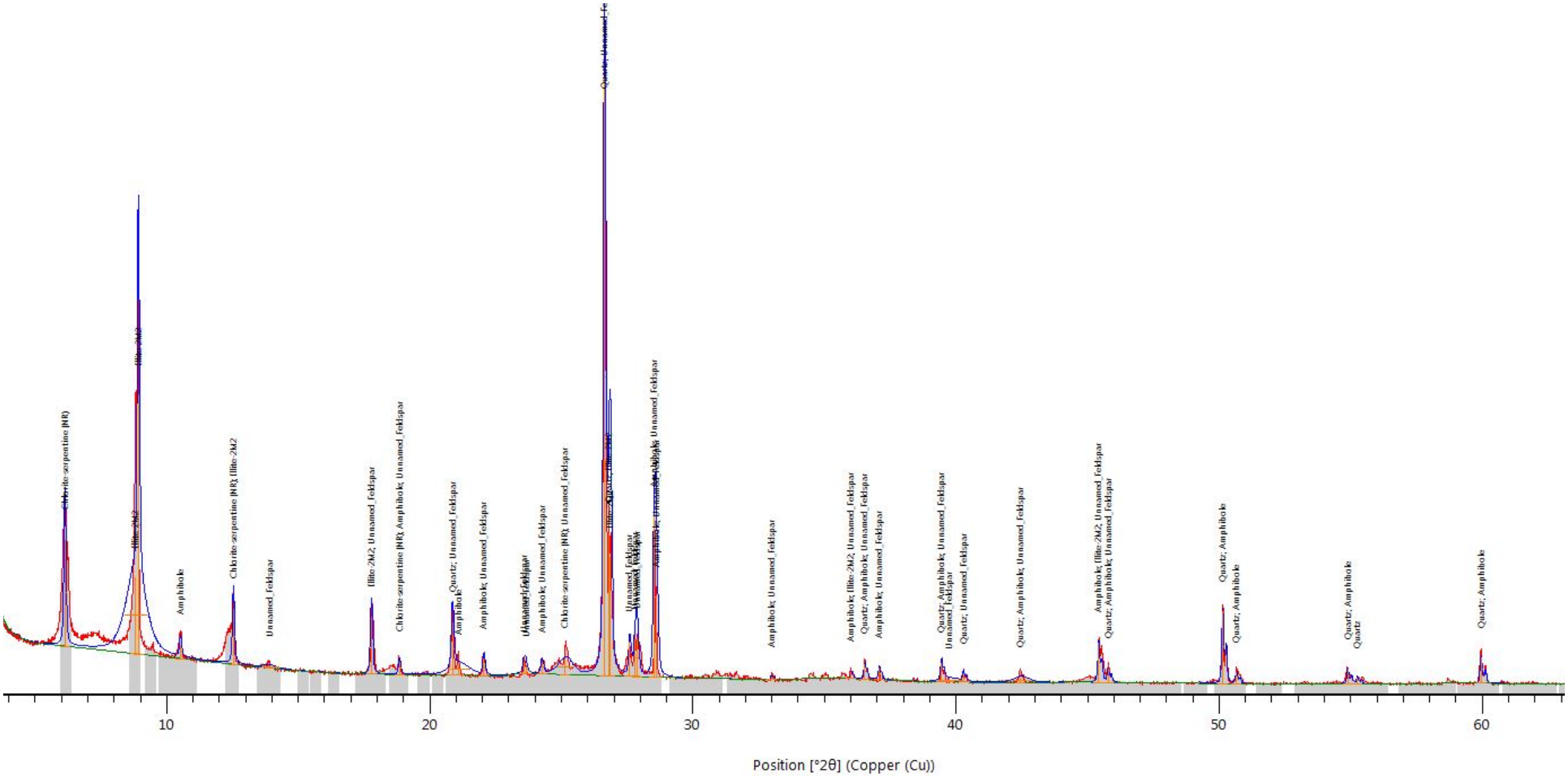

Figure I.14: XRD Spectra Core 3 36-48B

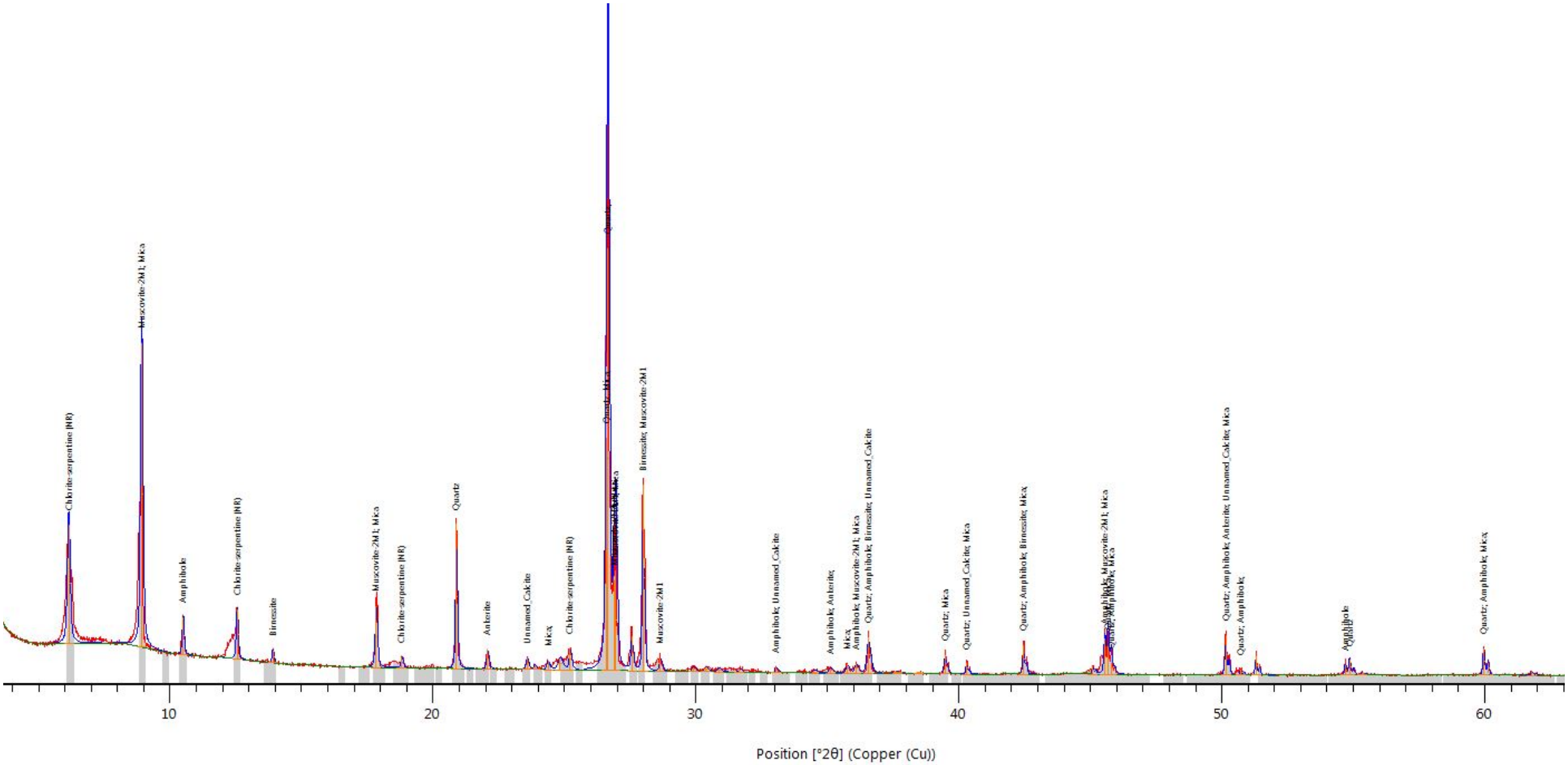

Figure I.15: XRD Spectra Core 4 0-24B

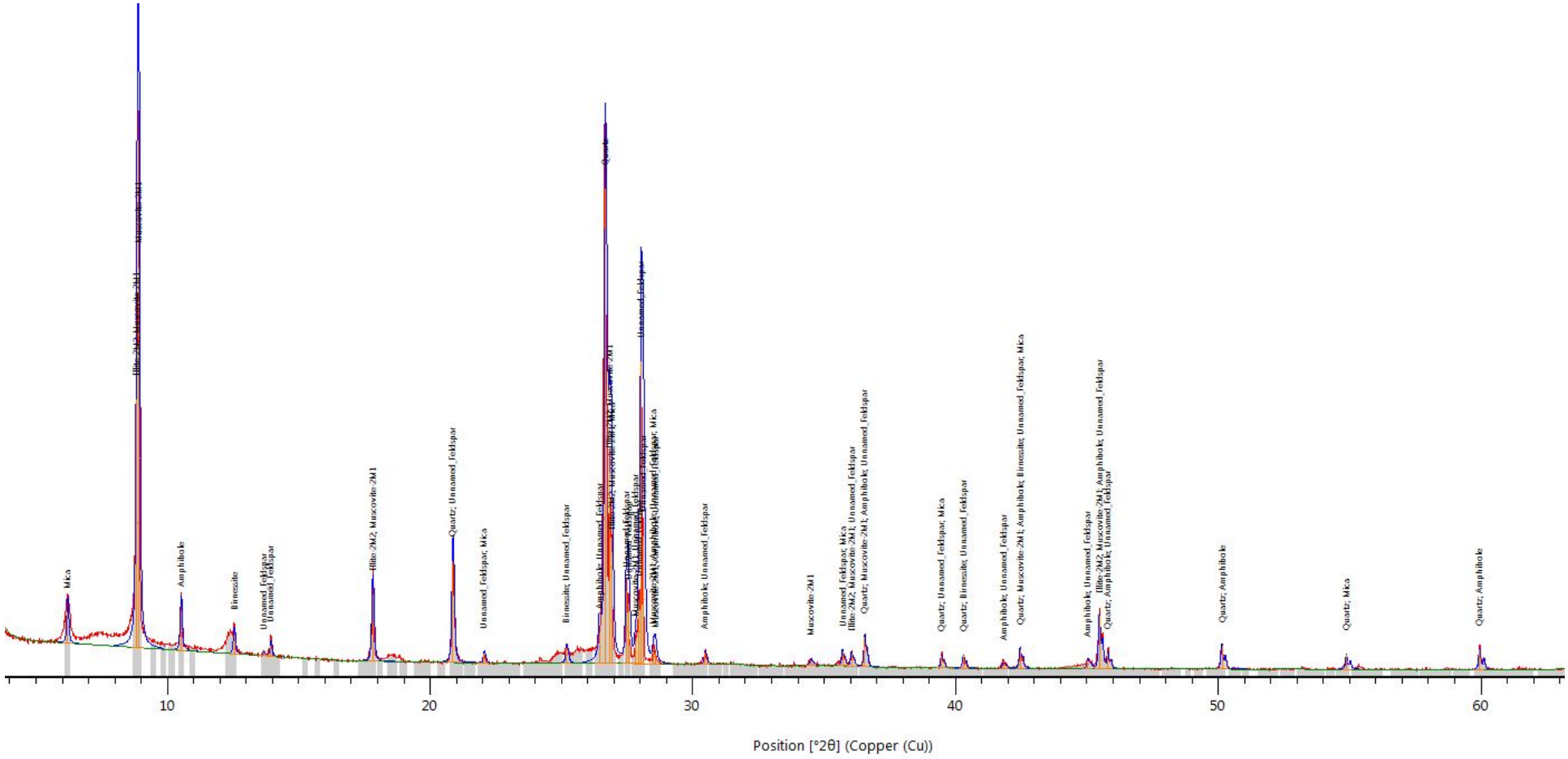

Figure I.16: XRD Spectra Core 4 24-48T

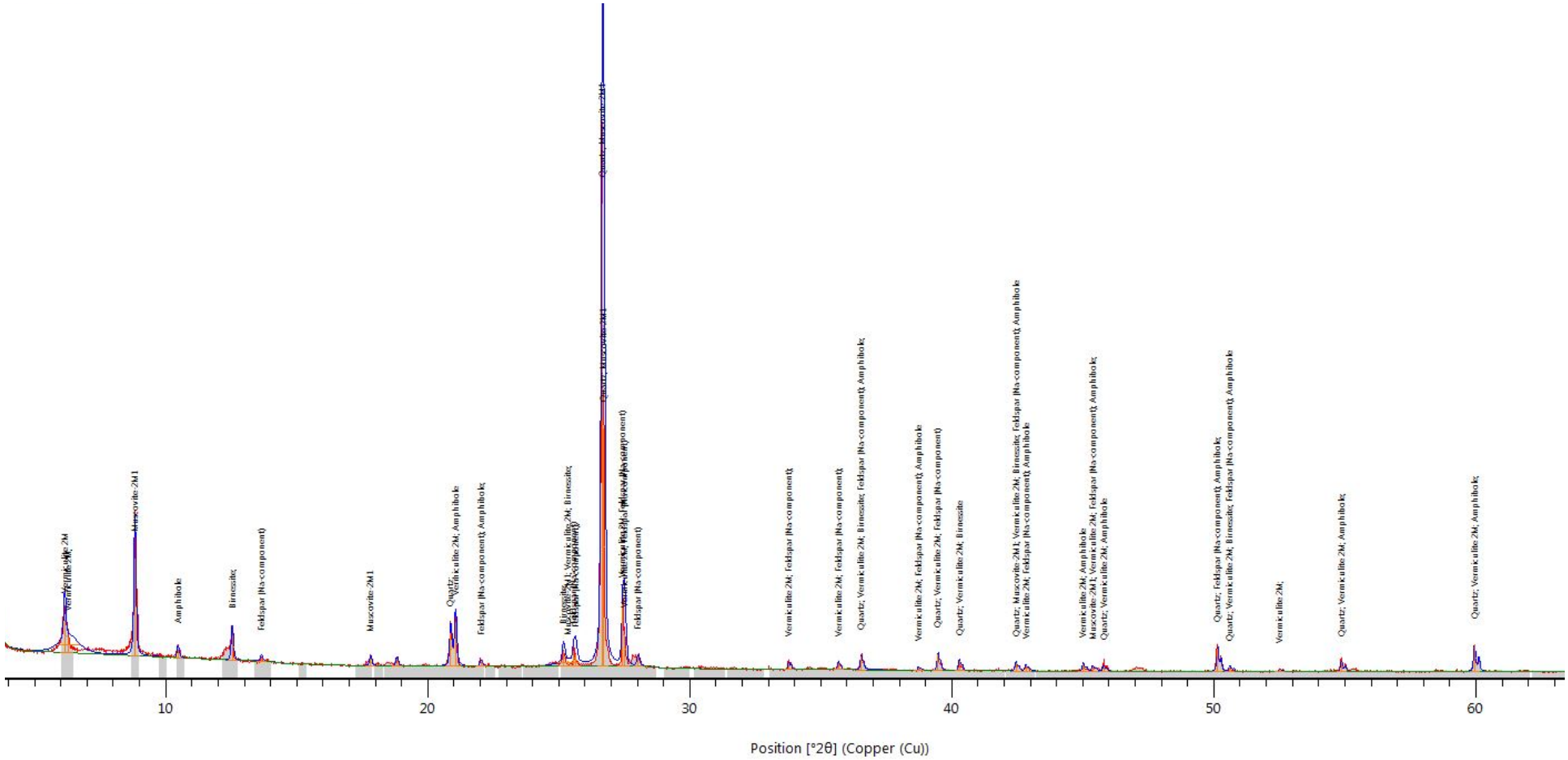

Figure I.17: XRD Spectra Core 5 0-24T

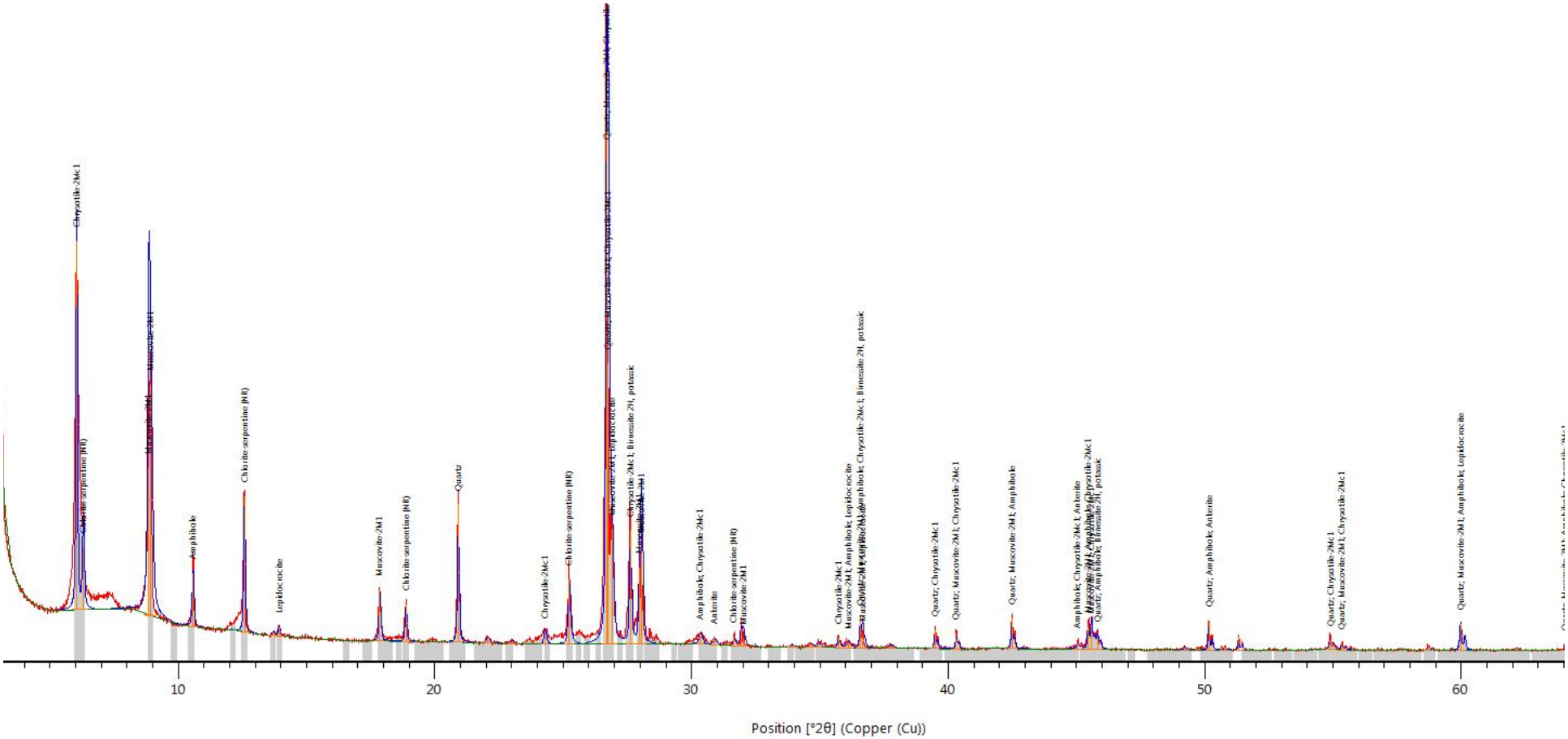

Figure I.18: XRD Spectra Core 5 0-24B

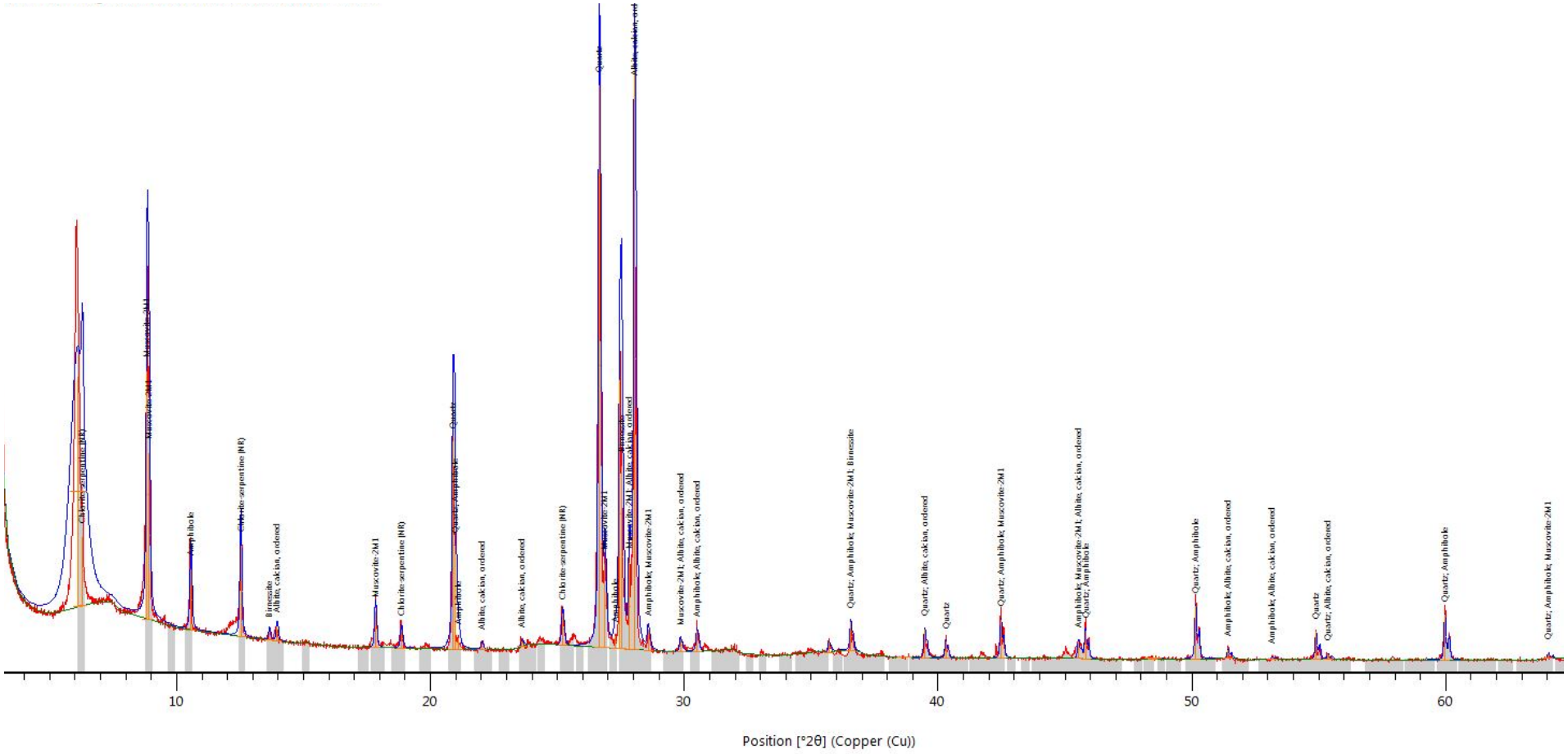

Figure I.19: XRD Spectra Core 5 24-48T

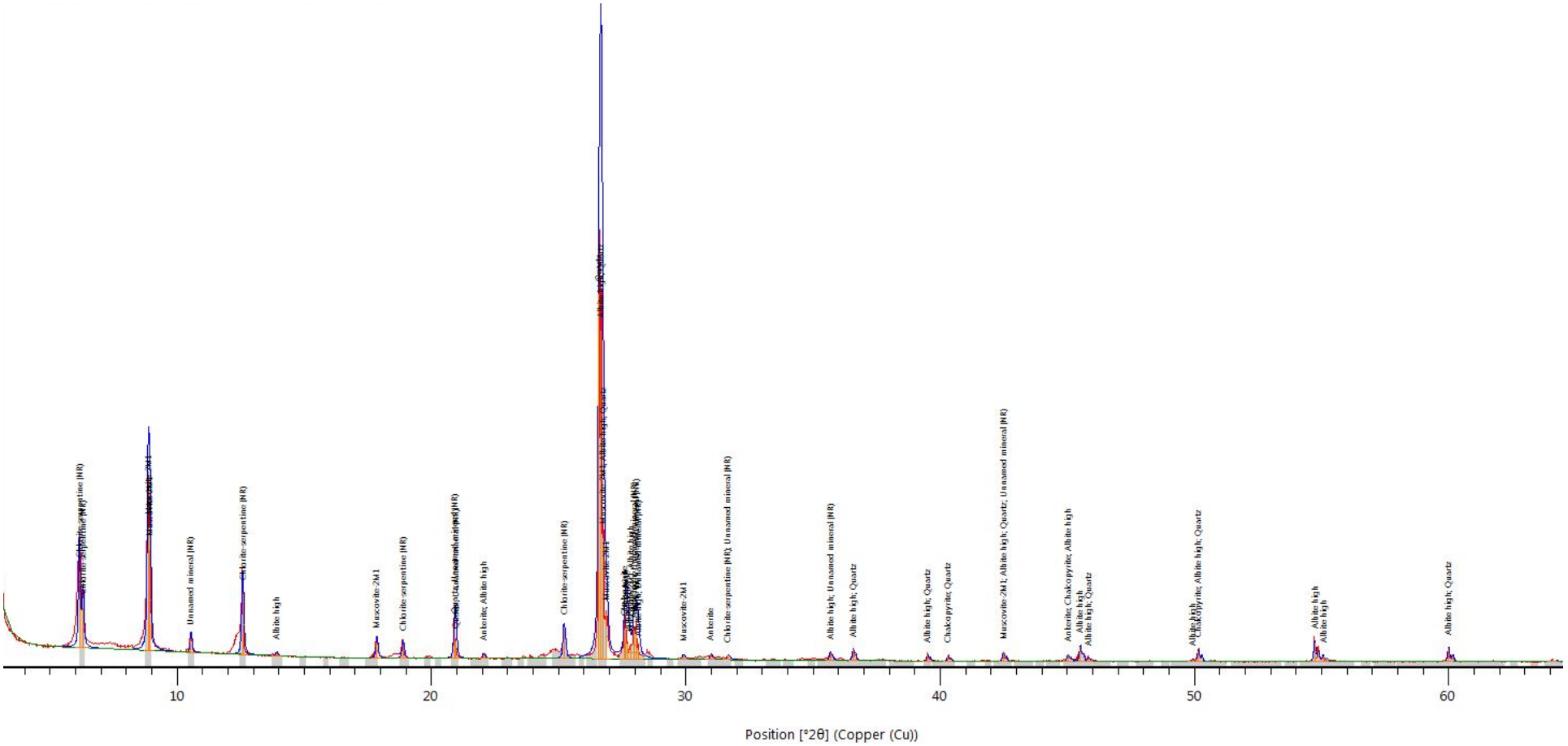

Figure I.20: XRD Spectra Core 5 24-48B

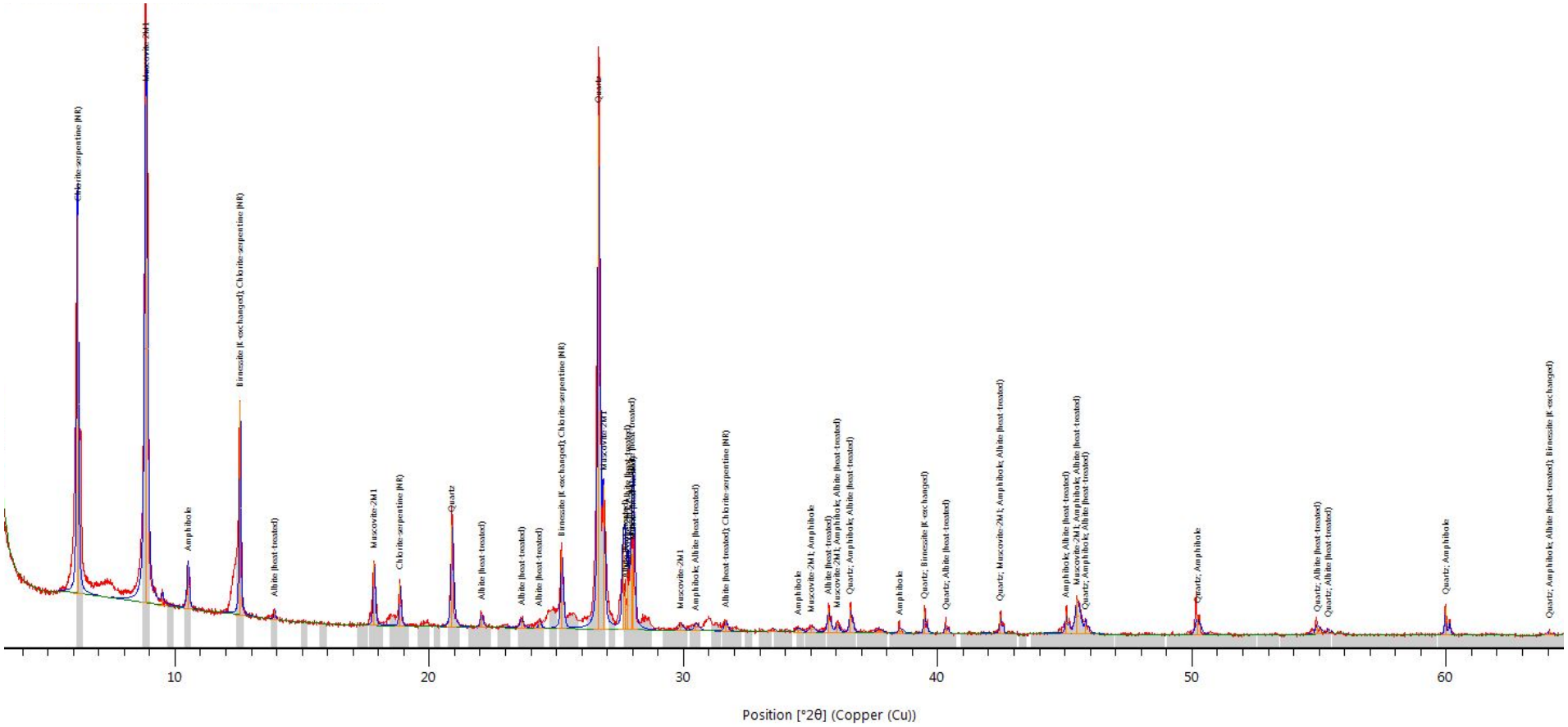

Figure I.21: XRD Spectra Core 5 48-72T

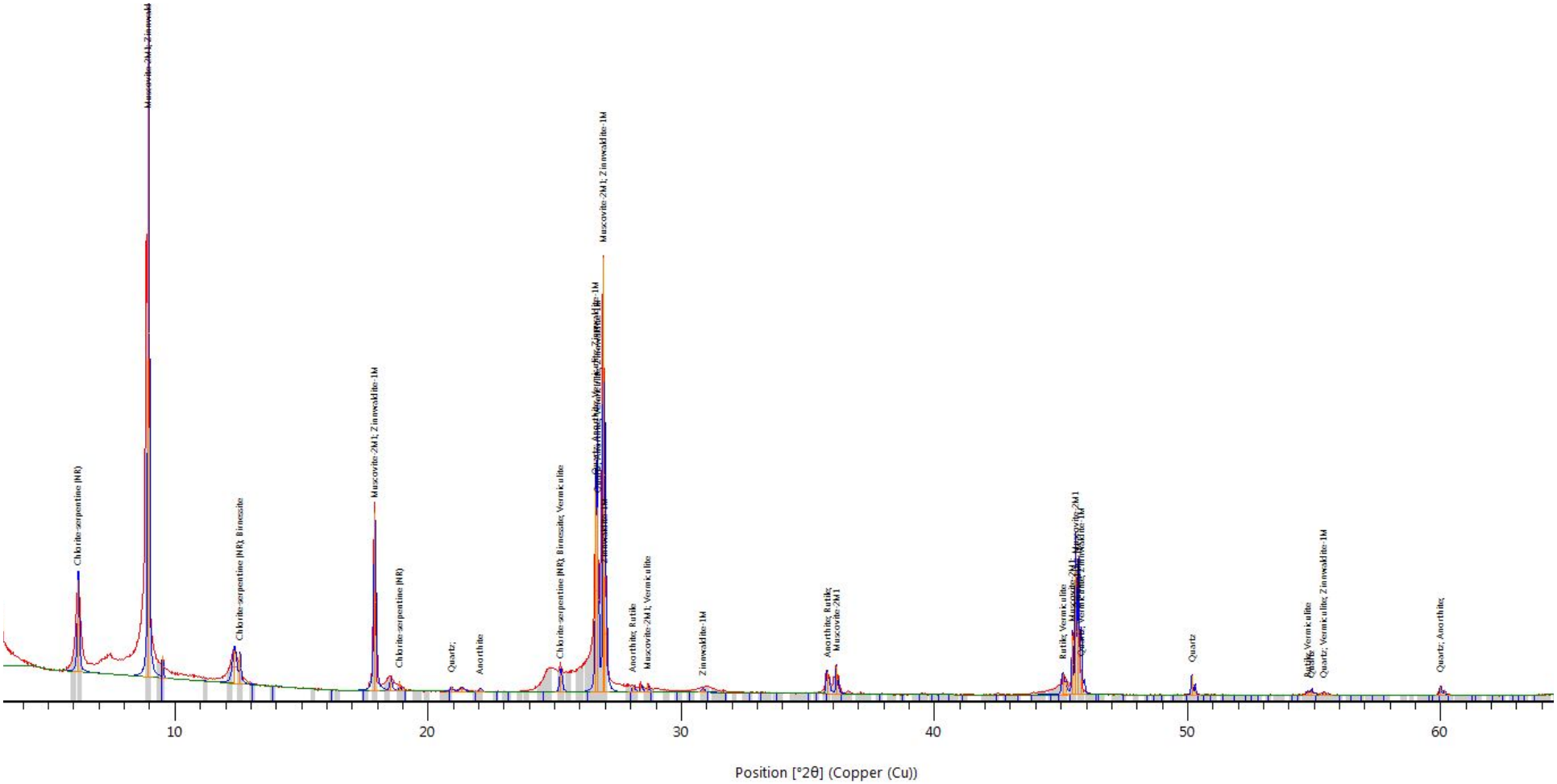

Figure I.22: XRD Spectra Core 5 48-72B

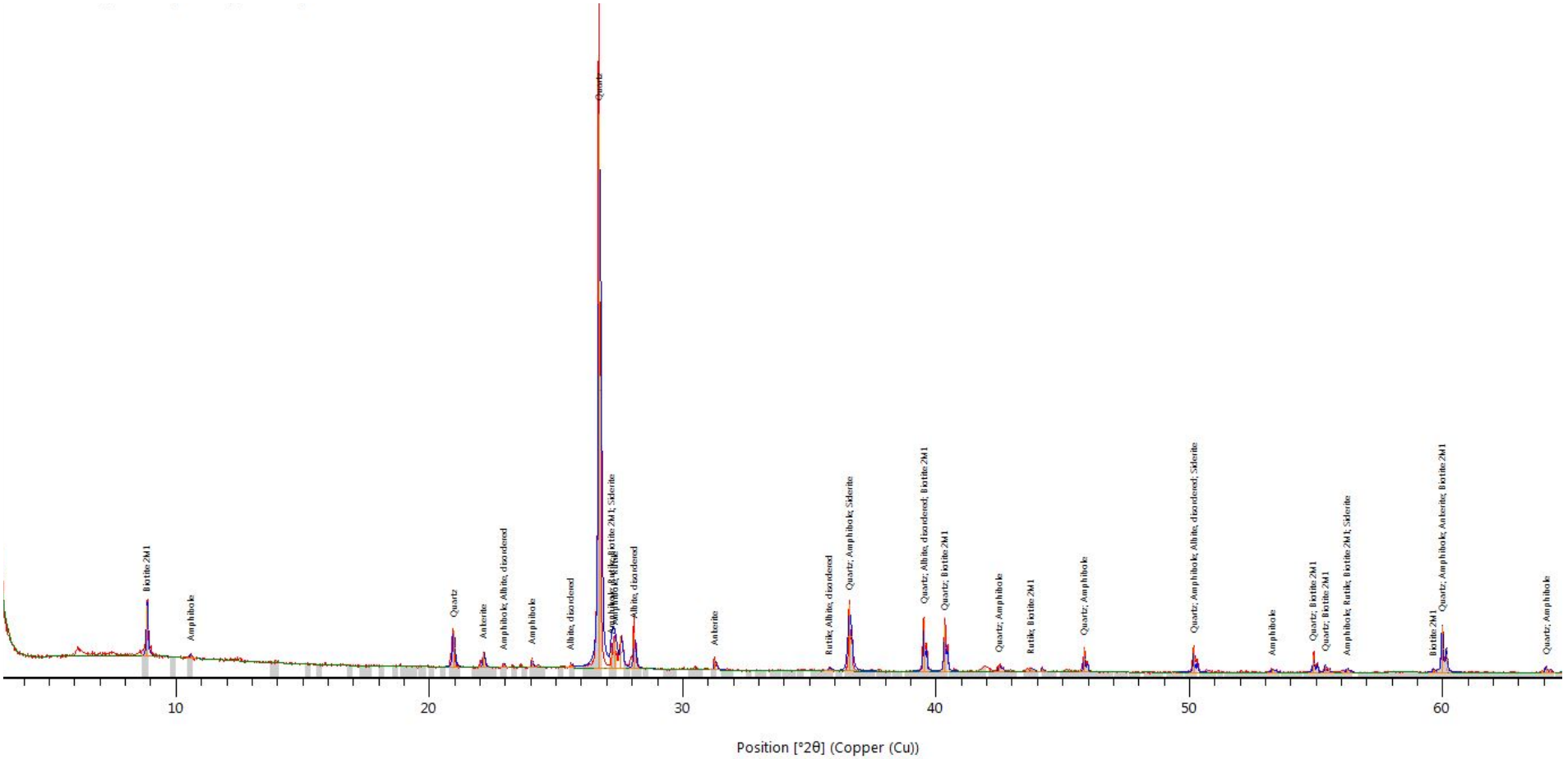

Figure I.23: XRD Spectra Core 6 0-24T

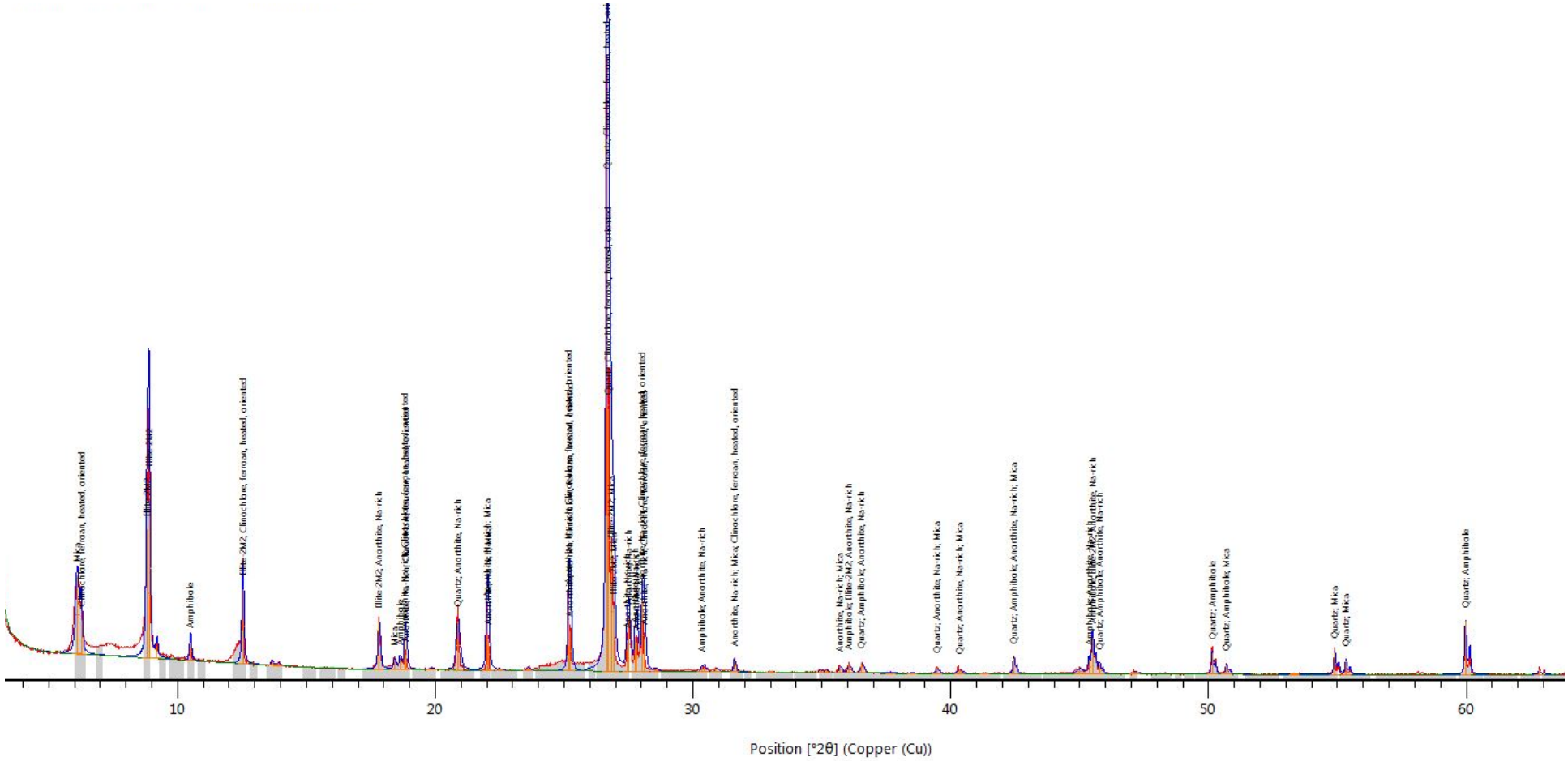

Figure I.24: XRD Spectra Core 6 0-24B

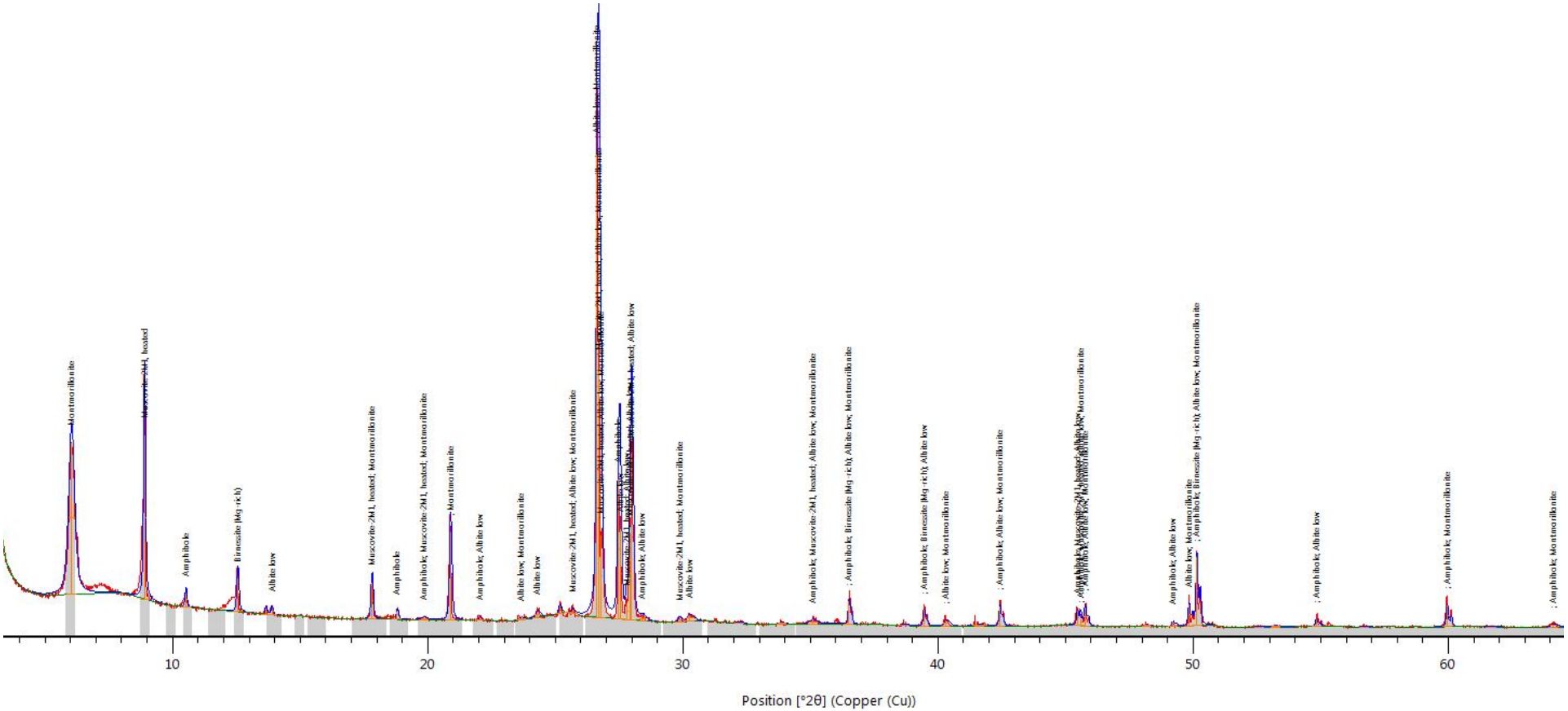

Figure I.25: XRD Spectra Core 6 24-48T

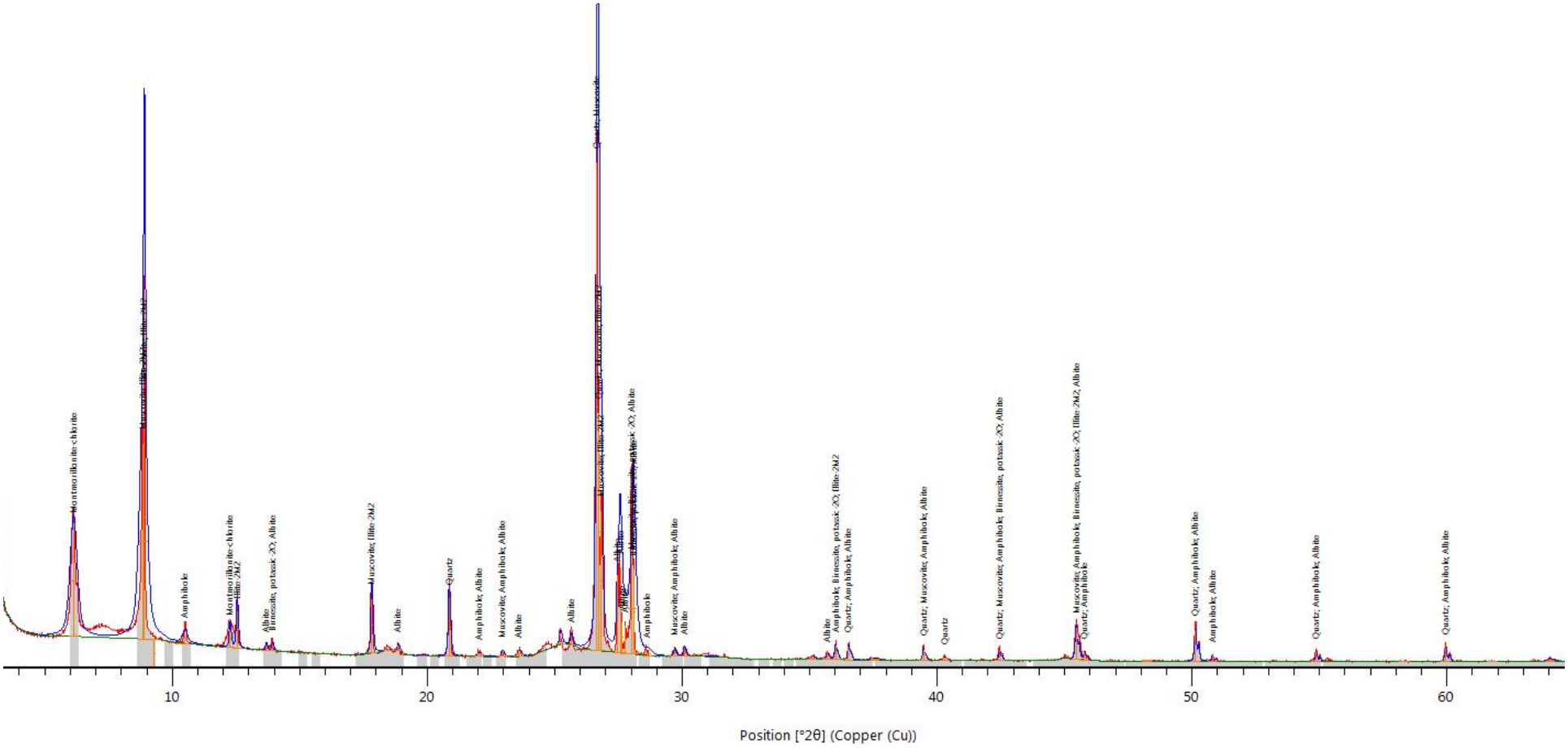

Figure I.26: XRD Spectra Core 6 24-48B

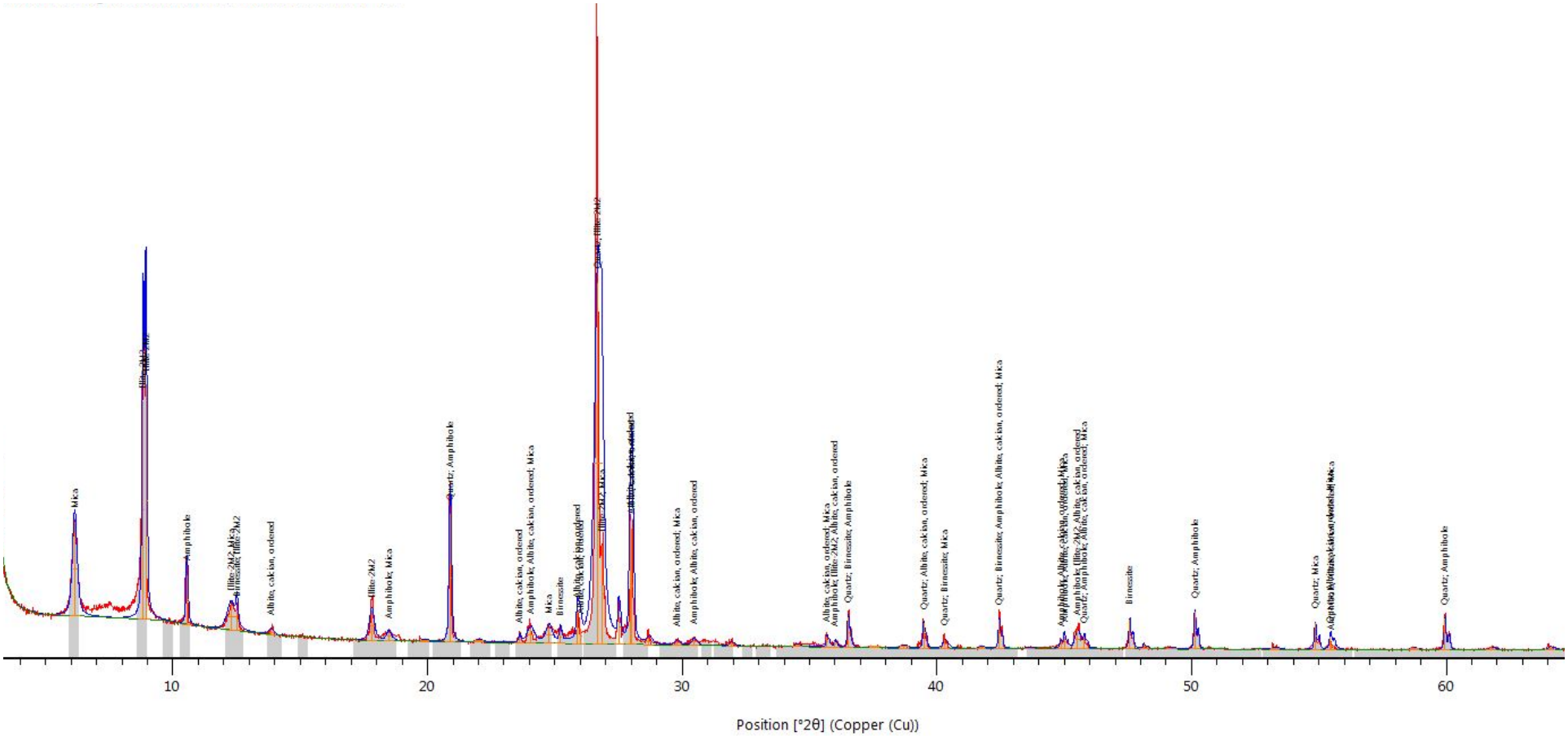

Figure I.27: XRD Spectra Core 7 0-24T

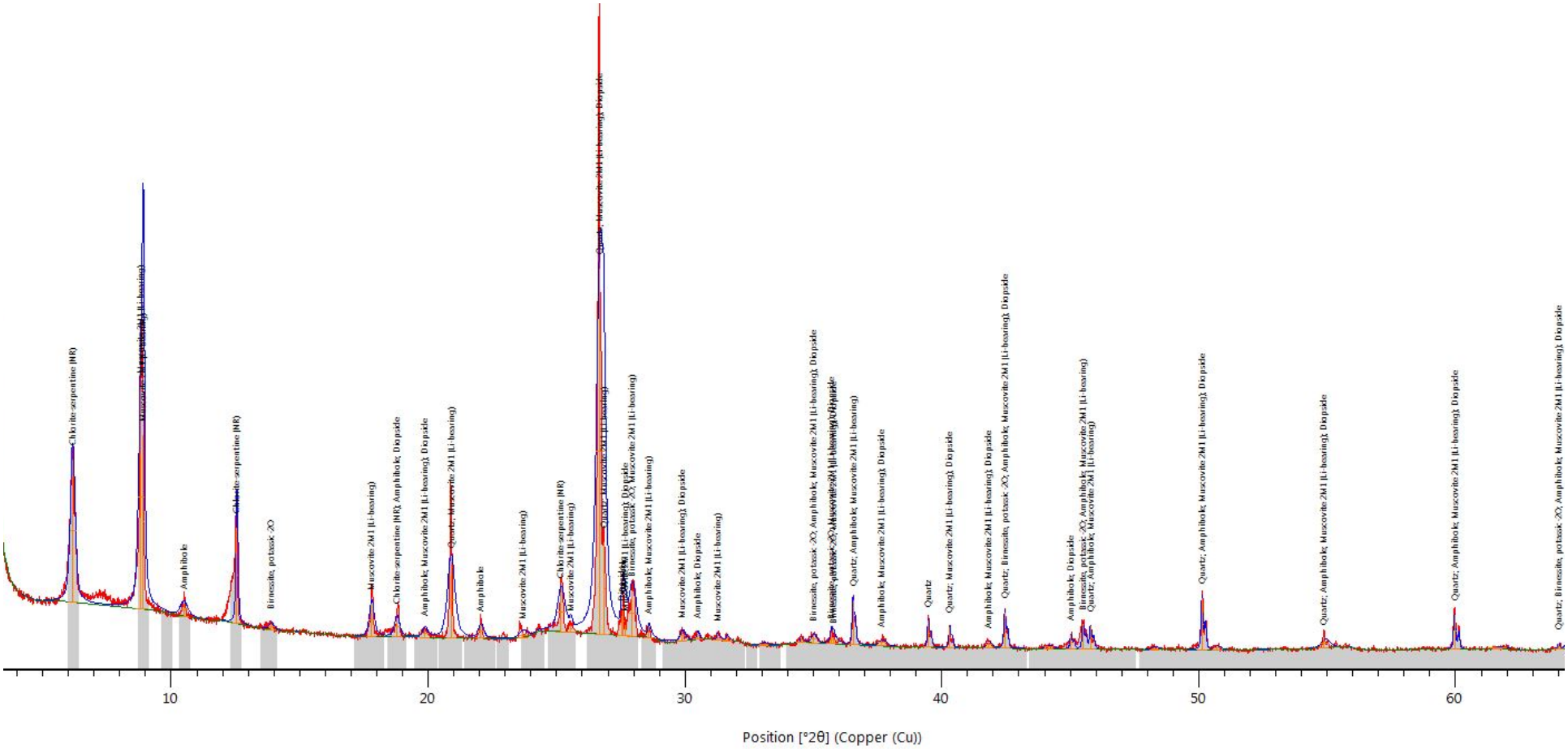

Figure I.28: XRD Spectra Core 7 0-24B

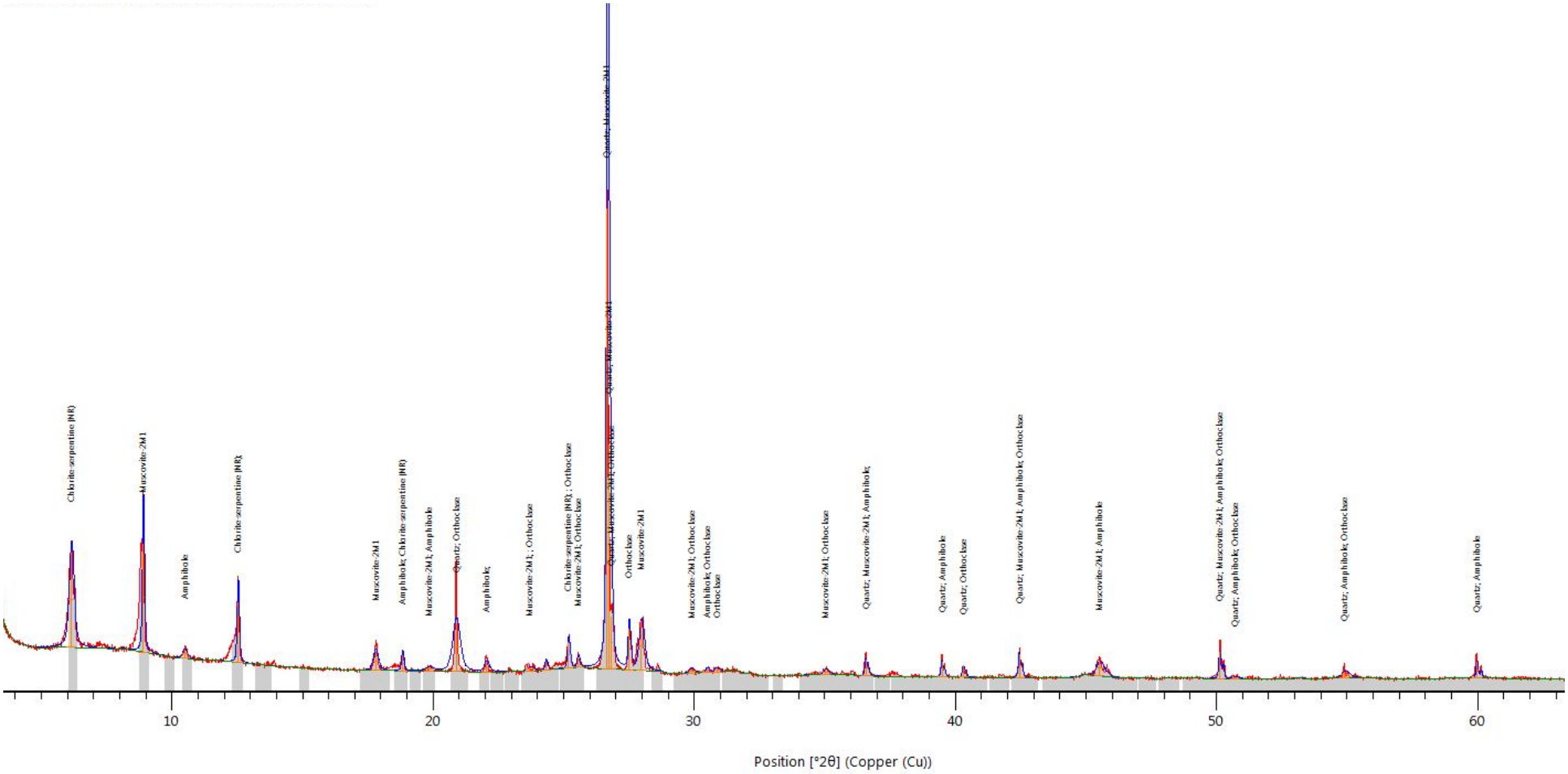

Figure I.29: XRD Spectra Core 7 24-48T

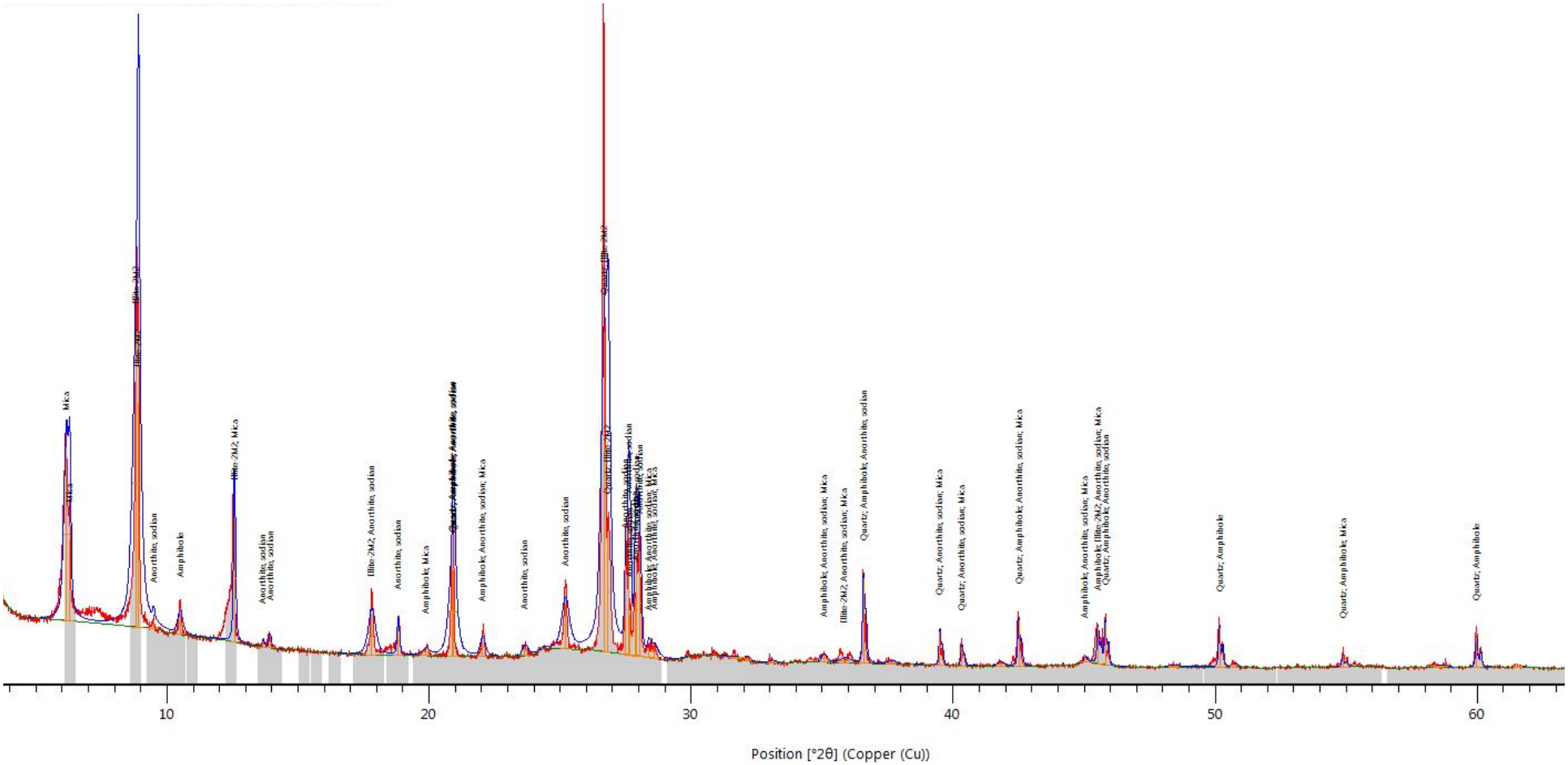

Figure I.30: XRD Spectra Core 7 24-48B

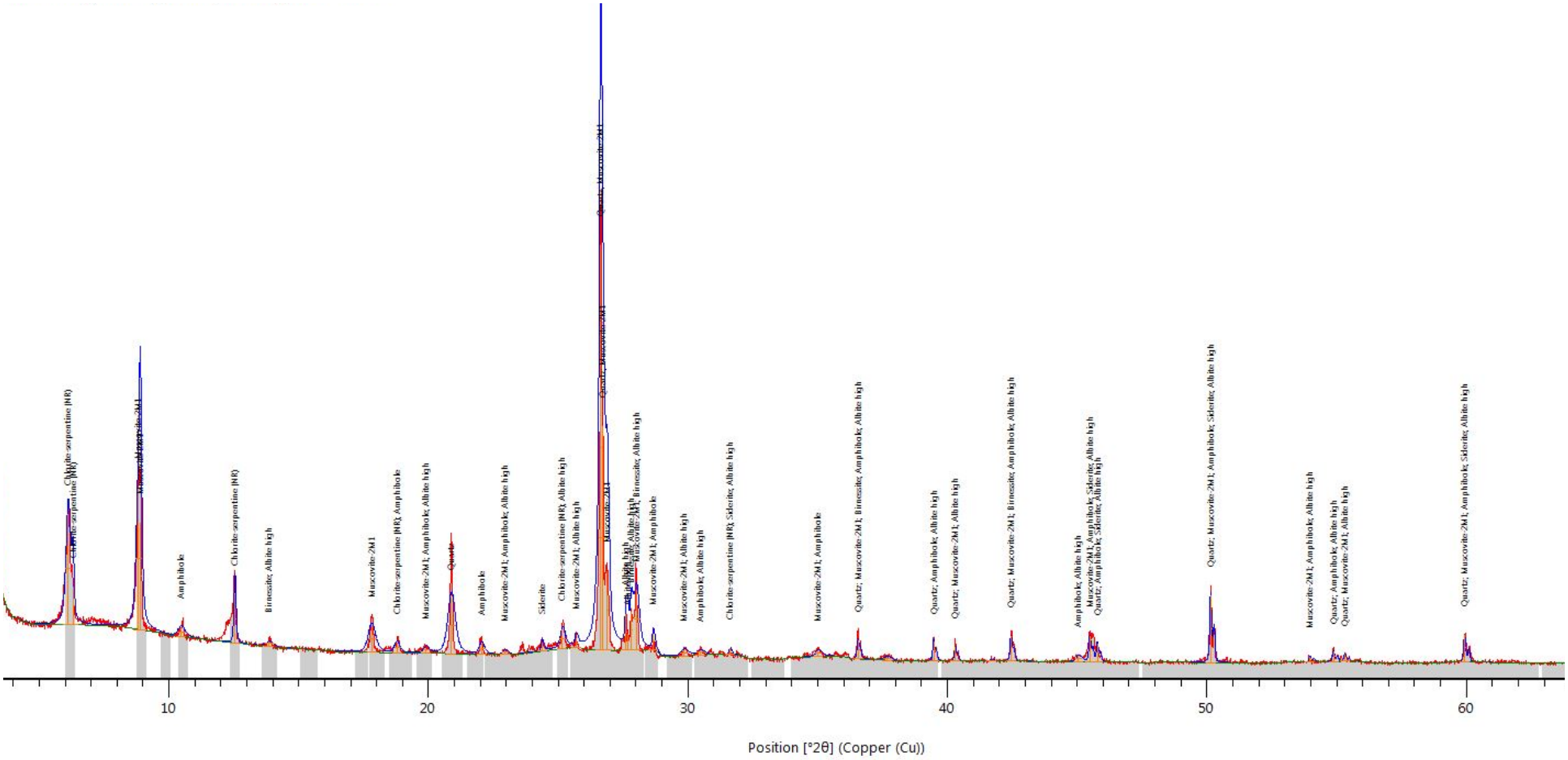

Appendix J - Data for Vertical Profile Figures

Table J.1 X-Ray Fluorescence (XRF) Data used for Sediment Vertical Profiles

			As		distance to		Mn	distance to			Fe	distance to		
Sample Core #	Depth Range (cm)	Depth (cm)	mg/kg	low	high	Stdev.	mg/kg	low	high	Stdev.	mg/kg	low	high	Stdev.
8	0-61 T	0	3.88	3.8	2.33	2.48	456.30	8.80	15.24	9.84	26255.30	731.167	1033.58	773.51
	61-122 T	71	3.11	0	0	0	656.63	25.44	31.68	19.52	34464.26	876.72	463.78	490.66
	122- 173 T	140	4.19	1.22	1.81	1.04	544.14	59.81	27.17	30.50	31884.39	1723.47	1760.09	1647.25
	122- 173 B	183	7.65	0.92	0.810	0.73	757.97	46.05	45.54	42.46	39251.47	5116.38	2880.41	2838.09
	183- 244 T	198	4.80	1.65	1.81	1.29	511.41	39.27	19.46	21.15	32570.45	2805.33	3552.21	2620.26
	183- 244 B	244	5.377	1.82	1.27	1.14	477.51	17.21	30.22	16.05	30679.42	879.41	820.24	588.03
2	0-61 T	0	7.26	2.12	3.66	2.03	688.21	15.61	50.23	25.72	39870.78	374.01	413.29	268.26
	61-122 B	120	2.42	1.78	2.14	1.34	424.81	28.86	32.64	22.99	22356.14	1103.29	840.73	863.54
8b	0-61 T	0	4.31	2.61	1.67	1.66	438.21	11.79	6.91	7.65	25784.40	791.51	1097.60	762.94
	61-122 B	120	3.11	0.82	1.70	0.90	431.96	18.25	25.27	15.340	24993.71	587.19	820.33	490.39
3	0-33 T	0	3.94	1.08	1.16	0.85	498.18	17.78	30.05	18.22	26897.5	654.11	1268.98	838.62
	0-33 B	28	5.05	2.48	3.34	2.05	439.80	20.41	81.12	39.93	23859.99	17686.32	3846.00	8668.25
	33-91 T	40	4.671	1.65	2.41	1.52	647.06	44.47	59.77	43.46	38352.27	2208.39	2399.12	1918.71
	91-122 B	122	4.76	1.74	1.61	1.33	475.16	326.91	102.44	162.41	28443.25	20330.47	4561.56	9965.36
4	0-61 T	0	2.02	1.23	1.96	1.71	467.76	3.58	6.25	5.439	28672.31	256.54	411.24	359.76
	61-122 T	61	5.19	1.38	1.10	1.26	490.66	32.73	19.02	28.47	29068.45	1250.01	704.43	1085.44

			As		distance to		Mn	distance to			Fe	distance to		
Sample Core #	**Depth Range (cm)**	**Depth (cm)**	**mg/kg**	**low**	**high**	**Stdev.**	**mg/kg**	**low**	**high**	**Stdev.**	**mg/kg**	**low**	**high**	**Stdev.**
	61-122 B	122	5.88	1.47	2.19	1.97	416.81	36.96	60.74	34.63	24867.75	2925.97	4339.01	2469.69
6	0-61 T	0	7.00	2.85	2.54	2.46	439.23	37.01	31.52	29.83	26816.18	1388.46	1336.48	1108.65
	61-122 B	122	4.30	2.33	2.63	2.02	408.00	36.84	23.15	20.17	26626.78	1817.88	676.56	933.46
17	0-61 T	0	13.69	3.66	5.97	3.85	934.89	123.82	239.67	180.37	37646.77	8269.63	2809.27	4196.94
	0-61 B	50	9.06	3.26	3.59	2.68	474.32	28.72	83.61	42.23	32984.92	14068.01	3745.29	6927.56
	61-122 T	71	7.04	3.89	3.31	2.61	607.22	30.31	32.83	25.33	44110.49	1757.88	2352.01	1793.82
	61-122 B	112	6.62	1.14	1.05	0.88	565.64	11.06	7.91	7.45	42336.42	642.43	501.76	416.12
	122- 183 T	130	6.21	1.79	2.21	1.34	678.19	121.95	113.38	95.45	57254.03	5336.19	4992.50	4446.93
	122- 183 B	183	4.02	3.26	3.36	2.38	369.06	36.67	43.91	32.74	29820.56	3053.28	4641.83	3686.90
13	0-61 T	0	5.28	1.48	1.54	1.22	652.26	23.65	51.00	25.53	44284.60	520.53	744.25	387.31
	0-61 B	50	6.89	2.41	2.51	2.46	666.96	20.82	20.83	29.45	43641.18	14.33	14.33	20.27
	61-122 T	71	3.91	3.91	2.68	2.70	581.03	48.81	39.64	30.97	39591.69	3133.67	1419.34	1715.20
	61-122 B	122	5.22	2.32	2.73	2.55	684.36	10.70	5.69	9.27	43170.28	582.10	575.22	578.69
14	0-61 T	0	3.94	3.9	2.86	3.14	532.912	28.89	41.67	25.40	36107.94	2219.43	2961.70	1701.28
	0-61 B	50	9.04	1.62	2.45	1.83	560.14	19.98	19.67	13.21	39446.47	2074.67	2291.64	1812.71
	61-122 T	71	6.68	2.23	2.51	1.53	537.78	6.60	10.27	6.40	32683.68	1681.25	1088.46	1165.28
	61-122 B	122	4.05	1.87	1.20	1.09	538.42	53.47	18.52	26.59	32738.25	808.26	277.51	407.36

Table J.2 X-Ray Fluorescence (XRF) Raw Data

Sample ID	Mg	Al	Si	P	S	K	Ca	Ti	V	Cr	Mn	Fe	Co	Ni	Cu	Zn	Ga	As	Rb	Sr	Y	Zr	Nb	Mo	Ba	Pb	Th	U
Core 1																												
RBA-1 T 0-48A	0.00	39833.54	222517.61	223.07	1468.39	15981.64	12920.18	3078.24	70.45	104.69	451.08	27150.85	3.45	15.85	14.02	31.57	6.75	5.47	61.42	91.52	33.85	216.21	14.44	0.00	0.00	8.90	4.74	0.00
RBA-1 T 0-48B	0.00	40585.72	223092.12	224.59	1561.38	16098.88	12915.56	3206.72	89.87	106.16	453.98	27288.89	5.11	32.35	25.55	50.12	11.86	1.75	90.77	151.15	41.11	321.66	12.07	25.58	772.91	10.63	7.20	0.00
RBA-1 T 0-48C	0.00	40263.74	223884.09	220.62	1685.31	14753.57	13149.34	3315.20	55.81	127.91	447.50	25589.03	3.68	31.08	28.23	54.13	10.77	5.63	92.10	148.91	39.63	326.95	11.60	28.77	0.00	10.30	7.25	0.00
RBA-1 T 0-48D	0.00	39976.46	222228.90	166.79	1601.79	14448.16	12920.04	3286.51	41.10	123.86	448.44	25524.14	7.15	25.94	25.52	49.15	10.30	4.25	99.83	153.38	35.31	205.04	10.74	7.44	0.00	9.98	7.60	0.00
RBA-1 T 0-48E	667.26	41578.14	230317.70	356.81	1508.54	13770.13	15070.95	3374.58	69.72	110.76	465.27	25962.61	6.46	23.28	27.08	51.80	11.39	6.22	104.98	163.29	35.12	192.70	11.01	13.90	1363.89	9.87	7.95	0.00
RBA-1 T 0-48F	0.00	40811.68	231217.88	379.29	1498.75	13846.17	15090.87	3367.09	74.94	107.20	471.55	26016.30	0.00	0.00	0.00	0.00	0.00	0.00	0.00	0.00	0.00	0.00	0.00	0.00	0.00	0.00	0.00	0.00
Average (ppm)	111.21	40508.21	225543.05	261.86	1554.03	14816.43	13677.82	3271.39	66.98	113.43	456.30	26255.30	5.17	25.70	24.08	47.36	10.21	4.66	89.82	141.65	37.01	252.51	11.97	15.14	427.36	9.94	6.95	0.00
Standard Dev.	272.41	638.83	4096.27	85.37	80.04	1017.66	1090.52	112.64	16.74	9.94	9.85	773.51	1.64	6.64	5.74	9.02	2.03	1.78	16.90	28.56	3.17	66.09	1.47	12.09	621.37	0.65	1.27	0.00
RBA-1 B 0-48A	489.89	46103.33	212146.58	220.81	1406.01	18267.88	11347.10	3793.97	96.60	100.48	658.46	34697.88																
RBA-1 B 0-48B	408.28	47252.14	213688.11	246.62	1453.41	18350.65	11534.86	3843.65	96.69	99.04	688.31	34206.67																
RBA-1 B 0-48C	791.87	48220.94	207744.34	192.64	1439.62	18414.28	10598.62	3805.80	66.45	101.36	661.32	34928.05																
RBA-1 B 0-48D	977.10	47943.27	207344.66	192.65	1463.64	18501.30	10661.53	3797.74	64.37	100.83	658.77	34725.53																
RBA-1 B 0-48E	742.42	46131.67	214668.79	196.62	1523.06	17317.65	10746.33	3626.57	75.84	103.66	641.74	34639.89																
RBA-1 B 0-48F	326.16	48146.51	211223.87	254.89	1489.19	18151.70	11279.97	4008.74	90.33	107.72	631.18	33587.54																
Average (ppm)	622.62	47299.64	211136.06	217.37	1462.49	18167.24	11028.07	3812.74	81.71	102.18	656.63	34464.26																
Standard Dev.	253.02	977.53	3029.87	28.03	40.44	433.23	405.02	122.20	14.76	3.10	19.51	490.67																
RBA-1 T 48-72A	246.12	49129.12	217776.63	207.21	1470.10	18089.63	11042.68	3388.24	69.90	93.92	552.78	33644.49	11.00	62.06	33.45	73.03	10.80	3.92	119.92	147.26	34.58	184.39	10.97	13.40	250.03	9.85	8.83	0.00
RBA-1 T 48-72B	500.24	49518.21	218717.99	231.06	1477.12	18070.43	11060.68	3482.30	79.26	100.29	556.22	33507.79	6.53	58.31	31.75	66.30	10.93	2.97	110.44	133.51	32.25	176.00	10.71	4.34	174.86	9.19	8.13	0.00
RBA-1 T 48-72C	1629.35	50274.60	222989.49	309.82	1438.37	17806.16	12262.45	4084.70	57.57	104.83	554.90	30257.59	8.09	62.27	31.05	63.62	10.97	3.72	115.55	139.18	33.22	173.73	11.35	4.80	302.47	9.86	8.45	0.00
RBA-1 T 48-72D	181.61	49794.44	222923.11	300.25	1411.89	17788.21	12245.13	3947.72	50.25	102.98	545.33	30160.91	8.66	61.53	31.95	63.27	11.44	6.01	115.50	149.65	33.79	170.86	10.64	3.45	327.88	11.20	8.83	0.00

Sample ID	Mg	Al	Si	P	S	K	Ca	Ti	V	Cr	Mn	Fe	Co	Ni	Cu	Zn	Ga	As	Rb	Sr	Y	Zr	Nb	Mo	Ba	Pb	Th	U
RBA-1T 48-72E	803.44	50230.85	220463.18	259.87	1590.17	18775.13	12007.38	3890.62	79.00	102.74	571.32	32920.53	8.28	54.62	33.90	65.60	13.30	4.70	113.03	144.82	35.92	201.75	11.15	4.53	456.56	11.51	8.49	0.00
RBA-1T 48-72F	326.05	48101.95	219486.72	224.01	1509.69	17148.30	11570.58	3485.40	70.18	103.08	484.34	30815.04	10.20	55.21	34.00	58.16	12.32	3.84	110.79	142.74	35.04	219.39	11.16	8.60	139.08	10.76	8.29	0.00
Average (ppm)	614.47	49508.20	220392.85	255.37	1482.89	17946.31	11698.15	3713.17	67.69	101.31	544.15	31884.39	8.79	59.00	32.68	65.00	11.62	4.19	114.21	142.86	34.13	187.69	11.00	6.52	275.15	10.40	8.50	0.00
Standard Dev.	544.97	813.98	2173.50	42.17	62.36	529.97	559.56	295.06	11.66	3.90	30.51	1647.26	1.60	3.47	1.26	4.86	0.99	1.05	3.56	5.84	1.32	19.12	0.28	3.81	114.58	0.90	0.28	0.00
RBA-1B 48-72A	1691.90	49499.75	192406.89	152.62	1532.34	19994.33	9204.20	4348.22	87.99	83.99	794.73	41629.01	17.25	62.92	46.49	93.41	15.02	6.73	146.66	120.25	33.81	179.89	11.59	0.98	346.78	12.29	11.00	0.00
RBA-1B 48-72B	1287.36	49274.36	191479.41	159.63	1450.22	19958.61	9143.68	4344.41	89.87	86.55	790.87	42131.89	13.69	64.82	45.24	96.07	15.34	8.00	149.99	123.47	33.17	184.22	11.57	6.00	527.40	12.77	11.35	0.00
RBA-1B 48-72C	1248.09	48566.61	201990.62	188.53	1474.60	18828.48	10052.43	4333.03	95.62	88.46	723.89	38946.88	14.18	53.18	38.30	72.78	15.90	7.49	135.27	122.29	34.68	207.72	11.70	3.79	1368.95	12.69	10.29	0.00
RBA-1B 48-72D	1587.72	50137.52	203014.51	244.33	1529.01	19038.39	10173.30	4327.23	88.09	90.42	722.94	39189.74	13.13	60.71	42.47	79.03	15.04	6.90	138.95	128.22	35.52	206.34	11.99	5.84	1077.95	12.41	10.40	0.00
RBA-1B 48-72E	1305.57	49496.91	193967.98	160.32	1523.50	18670.06	9525.53	4031.19	107.74	131.50	803.52	34135.09	14.82	58.44	38.89	82.35	16.41	8.46	136.10	131.67	38.12	197.52	12.14	7.19	942.52	14.15	10.19	0.00
RBA-1B 48-72F	1009.18	47342.23	196478.70	220.03	1468.02	19190.13	10098.58	4020.12	74.30	82.76	711.92	39476.23	12.19	62.19	41.56	88.20	12.68	8.34	134.17	126.39	34.77	196.63	12.06	4.56	637.75	12.30	10.43	0.07
Average (ppm)	1354.97	49052.90	196556.35	187.58	1496.28	19280.00	9699.62	4234.03	90.60	93.94	757.98	39251.47	14.21	60.38	42.16	85.31	15.07	7.65	140.19	125.38	35.01	195.39	11.84	4.73	816.89	12.77	10.61	0.01
Standard Dev.	247.26	978.28	4918.09	37.47	36.06	568.00	467.51	161.62	10.94	18.61	42.47	2838.10	1.74	4.13	3.30	8.89	1.29	0.73	6.58	4.20	1.73	11.34	0.25	2.19	380.95	0.70	0.46	0.03
RBA-1T 72-96A	506.52	43629.52	207213.36	162.09	1358.08	18544.65	10301.68	3727.61	47.06	95.49	524.74	35550.53	5.77	55.59	31.96	62.85	11.70	4.86	118.63	137.22	36.86	244.46	11.27	13.79	582.67	10.68	8.80	0.00
RBA-1T 72-96B	0.00	39921.13	215963.48	221.25	1296.93	16642.61	10953.81	3332.21	62.42	101.57	472.14	29765.12	6.11	55.97	33.50	68.67	12.05	5.25	117.18	136.94	34.48	237.71	11.35	15.33	0.00	11.18	8.95	0.00
RBA-1T 72-96C	0.00	40185.13	206797.70	162.49	1336.96	17067.74	10901.29	3461.32	51.18	91.75	516.45	31018.05	7.81	49.64	32.42	63.93	11.79	6.62	119.73	144.10	33.01	268.81	11.16	20.36	1089.84	11.32	9.21	0.00
RBA-1T 72-96D	0.00	40562.81	205156.20	152.00	1437.41	16746.69	10793.17	3472.10	47.18	92.18	519.63	31178.60	7.69	54.36	31.98	67.09	12.54	3.15	121.01	140.46	33.24	224.99	11.15	15.50	356.89	10.77	9.18	0.00
RBA-1T 72-96E	133.06	44070.93	208618.20	167.87	1401.26	18595.76	10412.70	3724.10	64.12	96.87	530.88	36122.67	3.87	9.92	3.86	23.08	2.36	5.43	58.63	38.26	15.77	96.96	14.85	0.00	0.00	7.61	4.37	0.00
RBA-1T 72-96F	82.38	45178.50	216920.25	192.36	1285.03	18866.37	11082.89	3444.02	89.71	107.19	504.63	31787.74	6.09	51.67	32.35	62.84	13.01	3.50	107.45	149.57	34.35	272.89	11.59	19.87	1002.71	10.89	8.22	0.00

Sample ID	Mg	Al	Si	P	S	K	Ca	Ti	V	Cr	Mn	Fe	Co	Ni	Cu	Zn	Ga	As	Rb	Sr	Y	Zr	Nb	Mo	Ba	Pb	Th	U
Average (ppm)	120.33	42258.00	210111.53	176.34	1352.61	17743.97	10740.92	3526.89	60.28	97.51	511.41	32570.45	6.22	46.19	27.68	58.08	10.57	4.80	107.10	124.43	31.29	224.30	11.89	14.14	505.35	10.41	8.12	0.00
Standard Dev.	197.07	2294.71	5035.28	25.82	59.16	1028.71	313.49	162.02	16.22	5.94	21.16	2620.26	1.45	17.94	11.68	17.31	4.05	1.29	24.24	42.48	7.72	65.03	1.46	7.41	474.93	1.39	1.87	0.00
RBA-1B 72-96A	0.00	44868.02	205072.29	130.01	1351.68	17218.93	9507.22	3124.51	60.09	103.95	460.30	31499.67	8.90	46.05	34.83	65.72	12.81	3.55	115.13	136.77	38.98	361.45	12.43	30.86	0.00	11.54	8.96	0.00
RBA-1B 72-96B	0.00	44691.80	205303.32	156.36	1376.04	17165.24	9537.80	3242.35	72.22	105.28	470.09	31074.25	6.81	47.86	34.81	68.57	12.08	6.65	116.22	132.87	39.49	364.43	12.13	30.09	0.00	11.51	8.99	0.00
RBA-1B 72-96C	404.96	45899.63	212103.25	160.70	1419.82	18193.78	9278.60	3668.68	52.52	82.14	478.04	30678.30	6.36	52.54	35.67	64.95	13.34	5.33	111.75	147.20	33.37	421.12	11.38	46.66	0.00	11.42	8.81	1.80
RBA-1B 72-96D	0.00	45557.84	210984.89	126.96	1390.41	18069.37	9233.27	3677.63	59.77	85.59	472.69	30700.47	5.34	56.54	34.52	67.42	13.00	5.88	115.75	149.11	35.78	418.59	11.33	45.74	709.82	11.64	8.88	0.00
RBA-1B 72-96E	337.52	44261.11	215917.28	289.82	1367.97	16192.56	11343.06	3775.76	49.99	126.26	507.73	30323.87	5.39	50.36	29.50	60.60	12.26	6.21	120.79	143.65	33.90	275.23	10.56	19.20	0.00	11.46	9.20	0.00
RBA-1B 72-96F	0.00	43826.69	214240.60	192.18	1378.55	17581.62	9489.91	3489.92	53.93	103.88	476.19	29800.02	8.43	47.17	34.46	60.68	13.02	4.59	106.69	133.13	39.30	444.89	11.92	42.49	287.58	11.44	8.07	0.00
Average (ppm)	123.75	44850.85	210603.60	176.00	1380.74	17403.58	9731.64	3496.47	58.09	101.19	477.51	30679.43	6.87	50.09	33.97	64.66	12.75	5.37	114.39	140.45	36.80	380.95	11.62	35.84	166.23	11.50	8.82	0.30
Standard Dev.	192.89	777.44	4528.70	60.59	23.04	728.95	799.58	262.09	8.00	15.91	16.06	588.03	1.50	3.94	2.23	3.36	0.49	1.14	4.75	7.15	2.81	61.56	0.67	10.90	290.08	0.08	0.39	0.74
Core 1b																												
RBA-1bT 0-48A	0.00	38030.92	212544.24	164.58	1299.78	14367.17	11654.88	2494.92	99.18	107.42	432.26	24992.89	8.32	35.02	42.57	69.25	10.50	3.03	106.55	147.79	37.91	194.37	11.10	8.61	660.90	9.93	7.84	0.00
RBA-1bT 0-48B	0.00	37583.23	212490.02	160.83	1295.75	14343.43	11647.09	2467.14	92.27	106.38	426.41	25330.85	7.09	30.63	39.76	68.57	10.17	5.02	104.34	149.71	37.76	190.28	10.83	9.41	78.58	9.81	7.82	0.00
RBA-1bT 0-48C	0.00	38868.85	217743.53	131.36	1351.80	15291.23	11300.16	2804.14	73.41	125.79	444.46	25300.59	5.72	33.74	41.23	72.23	10.78	5.99	111.44	155.44	33.71	195.04	10.45	11.46	0.00	11.14	8.61	1.44
RBA-1bT 0-48D	0.00	38522.51	216351.87	131.95	1271.85	15109.37	11247.38	2761.72	66.13	121.17	445.12	25630.95	8.84	36.46	42.43	76.70	10.35	5.74	117.85	155.40	36.14	191.31	10.75	12.48	0.00	10.59	8.75	0.00
RBA-1bT 0-48E	0.00	41104.78	219286.91	194.75	1360.40	16008.11	11512.72	2972.32	91.08	118.40	437.27	26882.01	7.03	35.45	42.58	66.39	10.11	1.69	114.00	149.39	32.14	174.32	9.48	3.47	799.86	9.89	8.48	0.00
RBA-1bT 0-48F	0.00	41144.42	223826.44	212.54	1281.41	15172.71	11683.48	2925.13	122.47	117.08	443.73	26569.16	9.08	37.33	43.77	73.74	12.21	4.41	114.40	139.12	36.78	214.85	11.42	6.30	1220.08	10.25	8.55	0.00
Average (ppm)	0.00	39209.12	217040.50	166.00	1310.16	15048.67	11507.62	2737.56	90.76	116.04	438.21	25784.41	7.68	34.77	42.06	71.15	10.69	4.31	111.43	149.47	35.74	193.36	10.67	8.62	459.90	10.27	8.34	0.24
Standard Dev.	0.00	1546.47	4312.47	32.81	37.06	626.14	191.24	213.22	19.93	7.69	7.65	762.94	1.29	2.37	1.38	3.79	0.79	1.66	5.11	6.01	2.33	12.98	0.67	3.33	510.35	0.51	0.41	0.59
RBA-1bB 0-48A	0.00	42364.52	221287.25	346.19	1096.06	16456.65	13690.34	3400.09	71.06	103.79	413.71	25197.69	3.87	33.65	41.61	70.14	11.20	4.81	91.68	152.02	40.75	374.13	11.50	34.17	0.00	10.33	7.03	0.00
RBA-1bB 0-48B	0.00	42192.61	223896.53	382.05	1174.32	16663.48	13901.32	3465.77	75.35	109.28	421.46	24903.08	4.27	32.78	41.87	66.42	13.11	2.82	92.26	153.89	41.33	379.18	10.95	34.76	0.00	10.22	7.07	0.00
RBA-1bB 0-48C	0.00	42532.80	227737.19	266.18	1225.12	16101.00	13402.94	3283.75	65.80	118.06	438.54	24406.52	7.53	34.75	43.32	69.42	11.43	3.21	97.63	149.76	40.34	395.79	11.88	35.53	903.17	10.66	7.50	0.00

Sample ID	Mg	Al	Si	P	S	K	Ca	Ti	V	Cr	Mn	Fe	Co	Ni	Cu	Zn	Ga	As	Rb	Sr	Y	Zr	Nb	Mo	Ba	Pb	Th	U
RBA-1b B 0-48D	0.00	42724.24	228172.17	252.32	1284.30	16088.11	13392.66	3196.83	64.15	110.79	435.22	24627.05	6.93	32.48	43.21	64.45	14.29	2.28	95.14	146.20	40.14	401.40	11.98	32.15	0.00	10.75	7.45	0.00
RBA-1b B 0-48E	1246.76	45500.09	226677.06	322.55	1316.91	16302.35	14958.11	3665.23	56.22	119.67	457.24	25814.05	6.94	34.89	42.48	65.12	11.55	3.06	96.68	165.26	42.04	383.15	11.72	36.30	463.97	10.10	7.41	0.00
RBA-1b B 0-48F	250.58	43383.00	235635.79	286.97	1220.62	16665.26	13087.17	3557.83	76.87	112.48	425.60	25013.90	6.79	28.10	38.59	62.36	10.43	2.46	95.88	158.09	33.89	283.14	11.54	22.69	106.27	10.08	7.46	0.00
Average (ppm)	249.56	43116.21	227234.33	309.38	1219.55	16379.48	13738.76	3428.25	68.24	112.35	431.96	24993.72	6.05	32.77	41.85	66.32	12.00	3.11	94.88	154.20	39.75	369.46	11.59	32.60	245.57	10.36	7.32	0.00
Standard Dev.	498.70	1238.24	4869.01	49.87	78.74	259.49	659.20	172.96	7.75	5.86	15.34	490.39	1.56	2.49	1.74	2.99	1.42	0.91	2.41	6.72	2.95	43.52	0.37	5.06	368.91	0.29	0.21	0.00
Core 2																												
RBA-2 T 0-24 A	0.00	43804.06	173650.39	87.01	1434.55	16176.52	8224.46	3689.49	72.48	80.25	677.59	39694.27	20.70	63.02	68.46	116.09	17.24	6.23	141.35	102.46	34.74	208.72	12.00	2.35	217.07	13.52	10.75	0.00
RBA-2 T 0-24 B	0.00	43141.91	171161.91	58.37	1440.25	16094.04	8204.55	3774.59	70.11	84.22	692.72	39496.78	21.20	66.31	65.04	113.14	17.59	7.46	147.94	107.49	36.50	207.19	12.91	4.65	0.00	13.49	10.96	0.00
RBA-2 T 0-24 C	0.00	44180.40	175614.04	98.51	1466.20	16320.67	11973.17	3640.56	86.77	83.08	674.53	39936.46	18.75	64.09	60.42	108.78	16.36	6.09	142.90	110.05	38.80	211.73	12.22	8.18	771.96	12.71	10.19	0.00
RBA-2 T 0-24 D	0.00	44427.86	175532.40	131.57	1361.36	16255.57	11966.14	3747.37	85.30	81.16	673.37	39981.06	19.02	61.66	61.87	107.54	16.90	5.14	141.20	100.92	37.40	211.06	12.48	2.30	696.34	12.86	10.25	0.00
RBA-2 T 0-24 E	89.01	48073.01	181781.41	167.19	1526.14	17038.92	8556.91	4010.10	68.02	76.90	738.45	40284.08	20.13	70.29	68.27	121.25	16.78	7.73	143.61	102.83	35.60	233.03	12.95	6.46	1098.85	13.75	10.96	0.00
RBA-2 T 0-24 F	0.00	45933.31	176439.84	87.49	1397.65	16091.67	8018.86	3761.61	58.11	86.73	672.60	39832.07	20.68	70.59	64.41	114.46	16.12	10.93	142.89	105.98	34.85	226.59	12.56	5.16	987.72	14.37	10.84	0.00
Average (ppm)	14.83	44926.76	175696.66	105.02	1437.69	16329.57	9490.68	3770.62	73.46	82.06	688.21	39870.79	20.08	65.99	64.75	113.54	16.83	7.26	143.32	104.95	36.32	216.39	12.52	4.85	628.66	13.45	10.66	0.00
Standard Dev.	36.34	1798.01	3531.61	38.52	56.71	358.95	1928.02	127.66	10.91	3.41	25.72	268.26	0.99	3.77	3.27	5.01	0.54	2.03	2.46	3.48	1.58	10.72	0.38	2.31	433.53	0.61	0.35	0.00
RBA-2 B 24-48A	0.00	29784.59	221175.40	270.82	2047.28	11181.00	13170.62	2548.27	93.01	124.66	405.00	21363.91	7.75	30.83	29.35	51.38	12.34	2.37	76.60	146.57	43.76	406.20	11.87	37.93	44.30	9.79	6.03	0.00
RBA-2 B 24-48B	0.00	29375.85	221297.12	294.03	2052.37	11180.44	13152.68	2632.85	102.09	129.79	395.95	21252.85	6.91	33.66	30.82	51.63	12.37	2.24	79.13	145.52	43.66	412.43	11.72	35.80	0.00	10.28	6.18	0.00
RBA-2 B 24-48C	0.00	28865.59	212050.52	273.10	1695.65	12119.85	13676.41	2907.82	82.32	142.29	427.11	22337.15	5.42	27.74	29.78	54.84	11.61	3.12	80.22	146.22	44.61	408.15	11.91	34.21	0.00	10.12	6.10	0.00
RBA-2 B 24-48D	0.00	28859.98	210207.46	232.98	1671.76	11940.20	13587.81	2856.21	64.64	143.62	420.44	22928.70	4.48	0.00	3.05	10.56	3.22	4.56	29.15	0.00	14.61	169.60	17.27	0.00	0.00	8.98	2.85	0.00
RBA-2 B 24-48E	0.00	28962.45	211998.06	261.60	1413.88	11566.72	13534.61	2796.05	92.04	100.74	442.92	23196.88	4.96	30.95	29.49	52.97	12.71	1.59	85.79	150.70	44.75	398.89	12.38	38.53	914.30	9.52	6.44	0.00
RBA-2 B 24-48F	0.00	30168.88	211863.53	296.16	1435.54	11508.58	13829.87	3061.86	81.41	108.93	457.46	23057.40	5.88	37.33	31.85	53.51	12.41	0.64	77.29	149.76	49.60	441.18	12.63	39.14	503.83	10.04	5.78	0.00
Average (ppm)	0.00	29336.22	214765.35	271.45	1719.42	11582.80	13492.00	2800.51	85.92	125.00	424.81	22356.15	5.90	26.75	25.72	45.81	10.78	2.42	71.36	123.13	40.16	372.74	12.96	30.94	243.74	9.79	5.57	0.00
Standard Dev.	0.00	544.78	5059.17	23.24	281.11	386.07	274.80	186.91	12.92	17.41	22.99	863.55	1.23	13.50	11.15	17.32	3.72	1.34	20.94	60.36	12.71	100.58	2.14	15.27	383.48	0.48	1.35	0.00

Sample ID	Mg	Al	Si	P	S	K	Ca	Ti	V	Cr	Mn	Fe	Co	Ni	Cu	Zn	Ga	As	Rb	Sr	Y	Zr	Nb	Mo	Ba	Pb	Th	U
Core 3																												
RBA-3T 13-36A	327.07	40513.87	221273.19	301.22	1234.12	15248.36	12577.31	4087.96	30.07	126.94	505.49	26675.85	7.19	42.82	47.71	72.07	12.16	2.85	90.41	148.76	44.62	441.75	13.02	41.64	362.53	10.80	7.06	0.00
RBA-3T 13-36B	0.00	40406.27	221351.17	298.07	1200.26	15130.42	12674.95	4032.08	16.24	121.03	504.82	26243.41	9.21	41.29	46.57	70.34	11.98	3.76	92.03	156.85	45.07	436.54	12.70	43.45	167.13	10.62	7.10	0.00
RBA-3T 13-36C	0.00	40414.52	219479.34	310.79	1212.31	14206.16	13395.90	3603.10	37.44	108.55	485.91	26304.52	9.76	45.28	46.98	76.73	14.38	3.14	94.81	143.97	46.66	480.34	12.82	47.29	0.00	11.42	7.55	0.00
RBA-3T 13-36D	0.00	39706.00	219434.90	292.79	1202.48	14323.68	13322.01	3564.66	38.36	104.76	484.25	26270.25	7.15	43.00	44.29	77.19	13.72	5.11	95.32	147.50	45.51	482.06	12.79	47.41	1596.78	11.68	7.60	0.00
RBA-3T 13-36E	340.08	41072.15	224051.29	378.45	1205.90	14309.57	14371.95	3816.25	66.17	112.76	528.23	27724.59	7.85	38.59	43.89	72.78	12.99	4.47	93.65	153.38	39.68	357.58	12.33	30.95	281.78	10.80	7.49	0.00
RBA-3T 13-36F	226.23	40945.51	221476.59	215.40	1381.38	14985.43	13035.34	3510.81	77.89	109.28	480.40	28166.50	6.69	42.12	46.10	70.53	12.60	4.31	91.39	142.34	48.06	496.08	13.15	49.39	195.62	11.17	6.97	0.00
Average (ppm)	148.90	40509.72	221177.75	299.45	1239.41	14700.60	13229.58	3769.14	44.36	113.89	498.18	26897.52	7.97	42.18	45.92	73.27	12.97	3.94	92.94	148.80	44.93	449.06	12.80	43.36	433.97	11.08	7.29	0.00
Standard Dev.	167.80	484.15	1691.61	51.93	70.62	470.18	649.93	248.65	23.15	8.43	18.23	838.63	1.24	2.21	1.52	3.00	0.93	0.85	1.96	5.52	2.86	50.71	0.28	6.71	582.53	0.41	0.28	0.00
RBA-3B 13-36A	0.00	32483.29	211616.67	146.09	1340.96	14500.79	9680.16	2390.71	136.14	118.30	423.92	27430.59	7.33	31.15	27.60	58.60	9.75	4.80	111.03	150.81	30.18	184.03	10.42	5.84	210.07	9.82	8.45	1.11
RBA-3B 13-36B	0.00	33336.99	211114.58	150.44	1335.94	14374.75	9594.83	2403.27	137.39	114.00	425.47	27507.74	8.24	32.45	28.24	58.10	10.21	3.73	115.54	143.63	33.35	185.24	10.30	6.68	0.00	10.47	8.54	0.00
RBA-3B 13-36C	0.00	31383.42	197826.24	94.99	1374.59	14852.04	9177.71	2389.08	86.91	113.19	429.60	27706.00	7.11	33.70	27.70	57.36	11.98	4.51	120.48	160.70	33.04	217.50	10.84	15.40	63.42	10.23	9.24	3.73
RBA-3B 13-36D	0.00	30801.57	195401.15	78.48	1298.34	14581.57	8970.28	2356.50	83.77	109.86	419.51	27410.56	6.70	34.71	30.08	58.35	12.15	2.57	122.12	152.92	33.74	217.51	11.39	11.82	834.93	10.05	9.08	0.00
RBA-3B 13-36E	0.00	30644.65	202732.11	97.52	1313.00	14358.67	9179.46	2305.25	70.91	102.22	419.39	26931.42	11.25	41.66	30.93	63.61	11.45	8.40	122.81	149.33	32.19	222.69	11.20	17.78	165.25	10.66	9.46	0.63
RBA-3B 13-36F	0.00	17221.45	124751.05	0.00	1315.39	8186.49	5529.70	1509.02	185.48	225.28	520.93	6173.67	9.40	41.99	29.62	60.52	11.41	6.31	119.47	140.26	33.38	223.30	11.51	7.12	1159.22	11.03	9.10	0.00
Average (ppm)	0.00	29311.90	190573.63	94.59	1329.70	13475.72	8688.69	2225.64	116.77	130.48	439.80	23859.99	8.34	35.94	29.03	59.42	11.16	5.05	118.58	149.61	32.65	208.38	10.94	10.77	405.48	10.38	8.98	0.91
Standard Dev.	0.00	6012.06	32927.46	54.75	27.01	2597.37	1571.15	352.85	43.83	46.75	39.93	8668.25	1.72	4.71	1.38	2.30	0.97	2.05	4.49	7.19	1.31	18.56	0.51	5.02	475.37	0.44	0.40	1.45
RBA-3T 36-48A	0.00	44383.25	199236.68	150.07	1392.19	18512.77	9432.70	3798.96	103.96	84.26	611.19	37575.94	13.92	55.05	52.70	97.09	14.42	3.89	144.01	120.50	33.62	200.41	10.95	5.93	0.00	11.69	10.78	0.00

Sample ID	Mg	Al	Si	P	S	K	Ca	Ti	V	Cr	Mn	Fe	Co	Ni	Cu	Zn	Ga	As	Rb	Sr	Y	Zr	Nb	Mo	Ba	Pb	Th	U
RBA-3T 36-48B	136.30	43675.95	197984.89	159.42	1419.33	18455.44	9323.82	3674.84	73.70	86.79	602.59	36950.36	14.70	57.84	54.06	95.02	15.19	7.09	142.90	116.26	34.06	196.73	11.03	2.05	601.94	12.43	10.59	0.00
RBA-3T 36-48C	1009.63	47641.53	201294.05	157.54	1462.34	18899.43	9480.84	4019.18	71.90	82.54	694.34	40617.09	16.91	61.10	58.50	100.89	14.00	4.95	148.21	118.99	34.49	205.44	12.25	4.85	0.00	11.87	11.12	0.00
RBA-3T 36-48D	1174.19	46894.65	202202.48	183.24	1431.25	18998.02	9530.59	3979.46	77.59	81.30	706.84	40751.40	19.54	58.83	54.26	98.62	17.39	3.02	145.91	119.39	33.32	205.09	11.77	8.23	473.26	12.24	11.17	0.00
RBA-3T 36-48E	382.78	47306.36	214969.10	244.59	1432.37	18335.18	10517.06	3792.37	79.56	107.49	630.85	36143.88	17.97	55.68	55.09	98.14	17.12	3.47	149.14	122.70	34.35	200.66	11.83	4.09	1307.85	12.37	11.17	0.00
RBA-3T 36-48F	1521.53	48986.03	220551.08	225.31	1501.20	18528.74	10344.85	4069.40	96.33	92.57	636.58	38074.97	15.62	54.71	55.47	95.80	16.10	5.62	145.89	133.84	33.27	192.59	11.12	6.49	79.59	12.43	11.01	0.00
Average (ppm)	704.07	46481.29	206039.71	186.70	1439.78	18621.60	9771.64	3889.04	83.84	89.16	647.07	38352.27	16.44	57.20	55.01	97.59	15.70	4.67	146.01	121.95	33.85	200.15	11.49	5.27	410.44	12.17	10.97	0.00
Standard Dev.	617.08	2036.82	9367.18	39.47	37.66	264.20	518.13	155.55	13.14	9.83	43.47	1918.71	2.11	2.51	1.96	2.11	1.40	1.52	2.38	6.19	0.52	4.93	0.53	2.13	508.40	0.32	0.24	0.00
RBA-3B 36-48A	0.00	37137.44	200769.62	141.62	1420.06	14313.39	9761.29	2951.14	88.14	110.03	502.36	32042.51	13.31	48.88	54.12	90.86	13.26	5.77	130.03	130.73	34.45	214.16	11.29	7.09	0.00	11.38	9.65	0.00
RBA-3B 36-48B	0.00	37525.80	200673.70	133.56	1448.07	14456.25	9896.99	3029.61	80.00	118.48	517.76	32415.30	11.49	48.26	53.75	88.48	13.48	4.30	125.74	137.37	34.72	215.02	11.36	11.96	364.58	11.46	9.51	0.00
RBA-3B 36-48C	0.00	40813.56	209672.67	213.81	1484.78	16329.34	10720.01	3536.31	57.37	99.37	577.61	33004.82	14.01	48.08	53.47	90.53	14.51	3.02	127.41	126.86	34.31	200.19	12.19	4.20	691.25	11.59	9.79	0.00
RBA-3B 36-48D	45.58	41059.72	210543.57	225.50	1447.16	16259.71	10749.63	3484.36	71.17	102.51	553.55	32735.58	14.25	46.74	52.02	91.35	14.10	5.54	128.61	124.76	33.41	202.73	11.75	3.33	973.31	11.58	9.87	0.00
RBA-3B 36-48E	0.00	40091.92	202669.93	172.45	1426.78	15939.27	10584.32	3326.44	80.24	104.02	551.46	32348.51	13.57	54.06	52.22	92.84	13.29	6.37	135.02	133.31	35.73	203.71	11.47	8.70	26.49	11.79	10.09	0.00
RBA-3B 36-48F	5613.04	0.00	20442.71	0.00	832.03	0.00	0.00	0.00	31.39	20.20	148.26	8112.79	13.64	49.31	51.96	89.52	14.22	3.58	133.77	133.98	38.86	202.27	12.63	5.83	1530.30	11.79	9.92	0.00
Average (ppm)	943.10	32771.41	174128.70	147.82	1343.15	12882.99	8618.71	2721.31	68.05	92.44	475.17	28443.25	13.38	49.22	52.92	90.59	13.81	4.76	130.10	131.17	35.25	206.35	11.78	6.85	597.66	11.60	9.80	0.00
Standard Dev.	2287.87	16140.59	75415.89	81.35	251.41	6373.59	4243.62	1353.96	20.80	36.03	162.41	9965.37	0.98	2.53	0.96	1.50	0.53	1.33	3.64	4.71	1.92	6.50	0.53	3.16	592.87	0.17	0.20	0.00
Core 4																												
RBA4 T 0-24A	1270.79	46961.96	221550.81	253.99	1477.89	17376.36	12841.55	3252.78	82.40	105.10	474.03	29083.56	8.57	32.81	6.38	29.15	10.48	1.30	101.25	166.94	37.62	257.49	11.19	24.76	953.09	9.48	7.79	0.00
RBA4 T 0-24B	142.06	47203.14	220081.28	143.92	1498.51	18130.64	11882.97	3315.61	66.91	100.74	464.19	28415.78	5.69	37.36	6.09	35.63	12.85	3.99	116.57	160.85	33.36	239.96	11.52	20.87	1786.61	10.80	9.16	2.46
RBA4 T 0-24C	405.10	46781.26	223046.28	222.80	1495.12	17125.36	12747.51	3381.90	76.92	105.65	465.09	28517.62	7.37	34.93	8.65	30.08	12.50	0.79	93.86	162.40	40.39	363.77	11.90	36.49	822.95	10.00	7.30	0.00
	605.98	46982.12	221559.46	206.90	1490.51	17544.12	12490.68	3316.76	75.41	103.83	467.77	28672.32	7.21	35.04	7.04	31.62	11.95	2.02	103.89	163.39	37.12	287.07	11.54	27.37	1187.55	10.09	8.08	0.00

Sample ID	Mg	Al	Si	P	S	K	Ca	Ti	V	Cr	Mn	Fe	Co	Ni	Cu	Zn	Ga	As	Rb	Sr	Y	Zr	Nb	Mo	Ba	Pb	Th	U
Average (ppm)	605.98	46982.12	221559.46	206.90	1490.51	17544.12	12490.68	3316.76	75.41	103.83	467.77	28672.32	7.21	35.04	7.04	31.62	11.95	2.02	103.89	163.39	37.12	287.07	11.54	27.37	1187.55	10.09	8.08	0.61
Standard Dev.	482.20	172.82	1210.47	46.32	9.03	427.21	431.42	52.72	6.41	2.20	4.44	293.75	1.18	1.86	1.14	2.86	1.05	1.40	9.46	2.58	2.89	54.70	0.29	6.64	426.92	0.54	0.79	1.23
RBA4 T 24-48A	0.00	34954.76	199541.41	118.76	1459.34	13954.20	10038.65	2556.69	74.89	109.91	457.93	27818.45	13.70	49.40	11.66	48.69	13.43	6.30	125.26	127.96	33.80	204.85	11.55	6.67	555.92	11.50	9.50	-4.56
RBA4 T 24-48B	0.00	38429.49	201999.38	111.38	1478.09	14677.23	9907.79	2974.58	92.62	97.92	509.69	29614.02	9.19	42.86	9.95	41.36	14.28	3.81	119.55	135.09	33.78	211.43	11.39	10.12	654.09	11.34	9.34	-1.21
RBA4 T 24-48C	0.00	38017.08	202269.66	128.01	1430.76	14694.67	9913.11	2972.72	91.38	96.03	504.37	29772.89	13.37	47.67	10.08	49.73	13.74	5.48	125.01	140.71	34.42	214.94	10.59	14.77	486.56	10.75	9.39	-2.17
	0.00	37133.77	201270.15	119.38	1456.07	14442.03	9953.18	2834.67	86.30	101.29	490.66	29068.45	12.09	46.64	10.57	46.59	13.82	5.20	123.27	134.59	34.00	210.41	11.18	10.52	565.52	11.20	9.41	0.00
Average (ppm)	0.00	37133.77	201270.15	119.38	1456.07	14442.03	9953.18	2834.67	86.30	101.29	490.66	29068.45	12.09	46.64	10.57	46.59	13.82	5.20	123.27	134.59	34.00	210.41	11.18	10.52	565.52	11.20	9.41	-1.99
Standard Dev.	0.00	1549.97	1227.37	6.80	19.46	345.03	60.48	196.56	8.08	6.15	23.25	886.26	2.05	2.77	0.78	3.72	0.35	1.04	2.64	5.22	0.29	4.18	0.42	3.32	68.73	0.32	0.06	1.93
RBA-4 B 24-48A	0.00	37959.98	213172.51	94.45	1219.53	16858.04	8434.21	2394.63	72.48	101.20	379.86	26689.31	3.77	31.67	27.56	48.91	10.35	7.52	31.70	9.74	5.58	10.52	8.85	0.00	787.46	120.23	160.32	147.55
RBA-4 B 24-48B	0.00	37927.64	222176.25	146.13	1319.51	14724.34	9849.88	2336.89	71.71	139.04	381.62	22981.51	4.70	30.63	28.33	49.07	10.65	8.07	30.77	9.99	5.60	10.99	8.91	0.02	642.76	119.78	158.99	147.17
RBA-4 B 24-48C	0.00	36831.44	223186.39	175.08	1361.23	14847.14	10031.23	2421.30	79.66	139.84	382.69	22886.24	8.48	35.83	29.95	53.25	10.83	4.41	32.40	10.17	3.78	10.82	8.60	0.00	0.00	117.04	145.38	160.31
RBA-4 B 24-48D	265.46	39499.86	223504.81	85.96	1428.81	16616.26	10635.29	2626.30	80.94	121.70	441.96	29206.75	5.09	28.72	25.10	48.42	10.39	3.52	30.75	10.08	0.00	8.84	7.88	0.00	0.00	104.35	151.24	140.53
RBA-4 B 24-48E	0.00	40768.48	218002.04	139.80	1422.43	17136.98	10465.12	2811.74	96.85	105.59	477.56	26426.96	0.00	0.00	0.00	0.00	0.00	0.00	0.00	0.00	0.00	0.00	0.00	0.00	0.00	0.00	0.00	0.00
RBA4 B 24-48F	0.00	45988.51	224343.08	82.41	1553.84	17445.83	9735.96	2671.53	92.58	121.62	423.85	25311.68	0.00	0.00	0.00	0.00	0.00	0.00	0.00	0.00	0.00	0.00	0.00	0.00	73.46	0.00	0.00	0.00
RBA4 B 24-48G	0.00	46381.83	231137.08	152.79	1554.56	18820.42	9719.05	2842.82	61.18	123.38	432.59	23497.70	0.00	0.00	0.00	0.00	0.00	0.00	0.00	0.00	0.00	0.00	0.00	0.00	241.50	0.00	0.00	0.00
RBA4 B 24-48H	0.00	45173.58	232759.62	169.57	1523.42	17991.81	10989.07	2607.01	88.46	118.90	414.38	21941.77	0.00	0.00	0.00	0.00	0.00	0.00	0.00	0.00	0.00	0.00	0.00	0.00	218.52	0.00	0.00	0.00
RBA4 B 24-48I	0.00	45847.97	229413.26	134.92	1543.94	18086.02	10148.03	2707.12	80.74	121.30	423.61	23583.72	7.21	35.04	7.04	31.62	11.95	2.02	37.12	11.54	27.37	10.09	8.08	0.00	1187.55	103.89	163.39	287.07
Average (ppm)	29.50	41819.92	224188.34	131.23	1436.36	16947.43	10000.87	2602.15	80.51	121.40	417.57	24725.07	5.85	32.38	23.59	46.25	10.83	5.11	32.55	10.31	8.46	10.25	8.46	0.00	393.91	113.06	155.87	176.53
Standard Dev.	88.49	3985.64	6267.12	35.27	119.11	1398.68	728.35	181.80	11.14	12.84	32.47	2349.51	1.94	3.00	9.42	8.41	0.65	2.61	2.65	0.71	10.81	0.86	0.46	0.01	433.21	8.25	7.38	62.21
Core 5																												
RBA-5 B 0-24A	841.84	42854.47	200055.72	200.33	1238.38	17410.68	12567.79	3874.07	105.18	93.45	470.38	36730.22	14.28	54.00	43.71	80.99	14.65	12.66	138.85	140.14	34.82	197.12	11.22	5.08	1277.89	14.01	10.64	0.00
RBA-5 B 0-24B	206.65	42043.28	194525.88	172.21	1259.39	17570.67	12381.43	3826.64	101.28	87.53	450.62	35577.86	16.00	53.26	42.58	86.24	13.74	11.32	138.15	130.66	34.96	195.82	11.72	2.41	407.64	13.78	10.45	0.00
RBA-5 B 0-24C	367.58	42970.41	194424.60	182.92	1224.14	17633.79	12508.87	3790.06	92.44	88.91	451.93	35285.88	14.39	55.26	38.30	81.75	15.24	9.84	137.84	144.73	34.58	212.20	10.96	10.35	1379.22	13.67	10.33	0.00

Sample ID	Mg	Al	Si	P	S	K	Ca	Ti	V	Cr	Mn	Fe	Co	Ni	Cu	Zn	Ga	As	Rb	Sr	Y	Zr	Nb	Mo	Ba	Pb	Th	U
RBA-5 B 0-24D	267.01	44695.23	208741.50	216.30	1344.96	17818.95	12422.77	4072.79	102.82	89.02	445.60	34903.69	15.34	57.36	44.80	81.03	14.16	8.15	138.01	153.01	35.77	212.04	10.69	13.52	772.40	13.10	10.36	0.00
RBA-5 B 0-24E	849.87	44306.64	202543.11	215.56	1264.00	17623.10	12572.62	3597.26	84.68	103.26	469.46	36495.00	18.09	57.24	40.70	87.22	14.14	6.61	141.40	137.73	34.69	172.39	11.52	3.45	1177.57	12.77	10.62	0.00
RBA-5 B 0-24F	0.00	34500.49	166787.27	88.06	1109.01	13070.32	8797.11	2825.44	173.21	196.21	557.93	18916.93	16.37	56.27	42.52	81.64	13.88	5.80	136.21	137.98	36.42	193.11	11.94	6.03	1044.77	12.46	10.28	0.00
Average (ppm)	422.16	41895.08	194513.01	179.23	1239.98	16854.58	11875.10	3664.38	109.94	109.73	474.32	32984.93	15.75	55.57	42.10	83.14	14.30	9.07	138.41	140.71	35.20	197.11	11.34	6.81	1009.91	13.30	10.45	0.00
Standard Dev.	349.51	3753.27	14603.96	47.99	76.66	1858.52	1509.86	438.45	31.93	42.76	42.23	6927.57	1.42	1.70	2.31	2.81	0.55	2.69	1.70	7.55	0.73	14.69	0.47	4.28	362.40	0.61	0.15	0.00
RBA-5 B 24-48A	1715.33	47653.11	176240.98	79.15	1605.55	19265.54	10953.78	4224.27	84.52	82.09	554.57	42502.34	25.19	74.91	75.91	118.16	20.71	7.33	161.91	109.38	33.36	198.02	13.58	3.89	229.52	14.86	12.32	0.00
RBA-5 B 24-48B	581.79	46543.16	176652.01	100.94	1615.53	19268.01	10943.69	4193.43	78.17	80.98	561.99	42838.19	25.77	73.50	74.35	122.68	18.56	7.67	167.69	102.54	33.69	202.04	12.59	1.75	0.00	14.05	12.46	0.00
RBA-5 B 24-48C	986.16	48509.19	182314.47	147.60	1575.48	19855.92	11518.59	4431.66	85.27	84.23	573.55	42311.79	25.65	72.71	72.40	122.37	19.97	6.41	159.08	109.25	31.45	202.39	12.69	0.28	1003.84	13.85	12.22	0.00
RBA-5 B 24-48D	1324.78	48272.38	185070.24	127.85	1606.23	20005.70	11898.24	4457.18	75.06	80.53	568.48	41693.99	26.95	71.95	74.69	123.23	18.38	6.22	165.40	108.22	32.39	196.88	12.18	-0.02	2235.15	13.32	12.45	0.00
RBA-5 B 24-48E	1325.10	49946.80	188251.03	151.78	1583.82	20252.23	12066.82	4462.75	90.94	83.31	569.62	42335.82	26.07	73.86	75.49	124.86	17.92	5.48	165.83	110.80	33.38	196.74	13.04	0.69	0.00	13.39	12.52	0.00
RBA-5 B 24-48F	0.00	0.00	0.00	0.00	0.00	0.00	0.00	0.00	0.00	0.00	0.00	0.00	29.97	76.08	77.26	130.61	18.04	7.35	163.12	111.31	34.15	188.40	13.01	1.29	0.00	13.90	12.28	0.00
Average (ppm)	1186.63	48184.93	181705.75	121.47	1597.32	19729.48	11476.22	4353.86	82.79	82.23	565.64	42336.43	26.60	73.84	75.02	123.65	18.93	6.74	163.84	108.58	33.07	197.41	12.85	1.31	578.08	13.89	12.38	0.00
Standard Dev.	425.38	1244.51	5242.49	31.04	16.86	445.46	520.87	133.34	6.26	1.55	7.45	416.12	1.75	1.49	1.64	4.07	1.14	0.84	3.10	3.17	0.98	5.07	0.48	1.42	900.13	0.56	0.12	0.00
RBA-5 B 48-72A	0.00	49371.26	203475.52	91.65	1542.96	21397.30	8845.06	2758.70	90.20	97.88	412.97	34447.09	6.29	28.56	25.47	58.59	12.20	1.91	106.43	168.48	31.41	224.67	10.24	21.65	741.75	9.61	8.23	4.80
RBA-5 B 48-72B	830.56	49262.84	201262.31	75.97	1385.58	21050.23	8718.58	2705.81	103.21	95.99	405.51	34462.40	6.42	25.18	26.23	61.45	9.99	4.45	109.82	152.03	33.12	222.29	10.31	12.71	2037.00	10.06	8.01	0.00
RBA-5 B 48-72C	0.00	47352.10	211583.67	123.15	1159.32	18130.51	10416.82	2589.05	77.20	108.85	346.46	26827.41	5.59	29.62	30.63	63.29	11.28	7.39	105.26	165.32	36.66	285.29	10.69	25.96	0.00	10.87	7.85	0.00
RBA-5 B 48-72D	0.00	48125.25	213085.15	120.19	1245.65	18257.17	10573.37	2662.25	69.79	109.80	362.25	26767.28	6.53	32.16	27.23	62.14	13.05	4.34	103.81	160.36	34.21	281.50	11.25	24.81	350.03	10.44	7.85	0.00
RBA-5 B 48-72E	0.00	47704.27	217241.44	151.79	1230.69	19734.12	10233.64	2513.63	56.61	116.05	354.79	29087.92	5.44	44.56	32.52	75.99	12.13	0.76	135.25	153.21	30.05	181.07	10.06	10.35	240.17	10.27	10.26	3.21
RBA-5 B 48-72F	0.00	44490.77	212579.97	90.59	1272.67	19875.36	8364.12	2393.65	125.28	147.66	332.39	27331.29	6.36	34.58	28.17	63.52	11.23	5.32	112.72	156.78	34.50	198.41	10.71	13.57	1267.53	9.93	8.42	0.00

Sample ID	Mg	Al	Si	P	S	K	Ca	Ti	V	Cr	Mn	Fe	Co	Ni	Cu	Zn	Ga	As	Rb	Sr	Y	Zr	Nb	Mo	Ba	Pb	Th	U
Average (ppm)	138.43	47717.75	209871.35	108.89	1306.14	19740.78	9525.26	2603.85	87.05	112.70	369.06	29820.56	6.10	32.44	28.38	64.16	11.65	4.03	112.22	159.36	33.32	232.21	10.54	18.18	772.75	10.20	8.44	1.33
Standard Dev.	339.08	1779.59	6163.40	27.88	137.42	1361.69	985.58	134.41	24.71	18.74	32.75	3686.90	0.47	6.74	2.71	6.06	1.06	2.38	11.74	6.60	2.35	42.80	0.43	6.77	762.04	0.44	0.92	2.13
RBA-5 T 0-24A	1596.18	43868.07	204550.77	300.52	1292.27	16964.73	11473.53	4038.44	90.40	79.95	815.88	38212.88	13.94	51.51	38.80	79.58	14.40	10.03	122.17	129.59	33.77	215.30	10.83	4.52	845.99	13.53	9.41	0.00
RBA-5 T 0-24B	1281.37	42962.25	203940.81	290.10	1350.60	16920.75	11457.76	4103.58	98.45	75.67	811.08	37806.83	11.89	48.01	40.49	79.00	15.56	10.97	121.87	135.00	34.43	213.31	11.24	7.29	690.84	14.17	9.44	0.00
RBA-5 T 0-24C	2086.49	46592.43	201780.65	295.57	1240.92	18456.47	11608.50	4027.59	93.82	83.09	1174.57	40456.05	15.46	49.23	42.09	77.04	15.32	11.53	131.71	139.92	34.67	223.31	11.21	11.20	404.06	14.30	10.14	0.03
RBA-5 T 0-24D	925.47	45438.74	200121.25	278.15	1151.24	18239.19	11457.69	3984.28	93.34	85.81	1160.22	40360.55	15.52	54.15	41.62	77.53	14.77	12.81	137.97	132.84	35.23	225.33	11.67	11.54	514.23	14.54	10.34	0.00
RBA-5 T 0-24E	2350.96	47615.34	207447.83	285.88	1414.96	18896.83	12273.27	4131.10	115.92	81.17	835.94	39667.21	16.47	55.85	42.18	80.87	15.07	19.67	125.71	153.48	38.24	214.96	11.68	14.97	79.50	16.55	9.88	3.69
RBA-5 T 0-24F	1013.62	42680.32	187638.47	250.49	1203.37	16511.68	10092.38	3407.97	103.93	142.54	811.69	29377.14	12.91	48.86	39.23	77.38	14.13	17.17	127.29	128.75	35.48	232.22	11.02	6.95	750.45	15.24	9.60	0.00
Average (ppm)	1542.35	44859.53	200913.30	283.45	1275.56	17664.94	11393.86	3948.83	99.31	91.37	934.90	37646.78	14.36	51.27	40.74	78.57	14.88	13.70	127.78	136.60	35.30	220.74	11.27	9.41	547.51	14.72	9.80	0.62
Standard Dev.	579.84	2013.18	6967.04	17.90	97.17	984.68	711.03	270.25	9.41	25.29	180.38	4196.94	1.75	3.16	1.47	1.51	0.55	3.85	6.17	9.20	1.56	7.45	0.34	3.82	279.83	1.05	0.38	1.51
RBA-5 T 24-48A	2680.69	59325.42	200244.87	182.47	2177.62	22406.89	11732.53	4659.70	91.65	83.94	576.91	42352.61	21.16	77.66	51.09	104.16	18.26	10.36	155.03	121.40	31.93	186.99	11.85	1.78	273.44	14.62	11.97	0.00
RBA-5 T 24-48B	2976.31	59889.49	200510.91	167.02	2072.83	22279.21	11768.61	4631.65	91.55	83.00	595.54	42856.78	24.85	70.98	52.28	100.83	18.11	9.56	163.40	125.72	33.91	189.90	11.86	1.83	899.29	14.13	12.18	0.00
RBA-5 T 24-48C	4545.84	61039.03	196643.92	192.22	2167.49	23364.44	11270.25	4825.86	111.74	75.53	640.06	45983.46	23.91	75.23	51.90	101.59	18.44	3.15	163.71	112.49	32.57	184.56	12.76	1.10	1195.54	13.39	12.44	0.00
RBA-5 T 24-48D	3978.42	59940.24	194508.37	159.11	2222.08	23104.61	11083.73	4815.24	117.12	72.58	633.64	46462.51	23.68	71.99	53.52	103.94	17.97	7.02	159.09	115.25	32.16	182.75	12.31	0.00	1318.63	13.90	12.08	0.00
RBA-5 T 24-48E	3491.57	60144.09	199600.77	198.85	2102.17	23167.74	11816.96	4796.10	102.19	81.79	609.31	44412.39	20.75	71.34	57.04	98.93	18.40	6.21	157.54	117.39	33.14	210.34	12.45	3.92	935.46	13.58	12.02	0.00
RBA-5 T 24-48F	3090.60	57991.38	198913.19	207.93	2102.15	22483.47	11886.15	4499.03	94.33	83.40	587.90	42595.24	23.98	72.31	56.11	103.31	18.07	6.00	161.38	116.04	30.67	185.88	12.06	0.00	331.40	13.33	12.52	0.00
Average (ppm)	3460.57	59721.61	198403.67	184.60	2140.73	22801.06	11593.04	4704.59	101.43	80.04	607.23	44110.50	23.05	73.25	53.66	102.13	18.21	7.05	160.02	118.05	32.40	190.07	12.22	1.44	825.63	13.82	12.20	0.00
Standard Dev.	696.64	1013.98	2357.68	18.81	57.06	463.15	331.64	130.32	10.93	4.78	25.33	1793.82	1.68	2.63	2.41	2.05	0.19	2.62	3.43	4.76	1.11	10.22	0.36	1.46	435.10	0.50	0.23	0.00
RBA-5 T 48-72A	1035.55	45131.98	176097.16	132.44	1406.61	21207.44	7919.55	4159.65	69.38	67.52	556.25	51917.84	12.41	57.39	50.69	98.45	14.67	4.42	160.63	142.27	29.50	181.07	10.58	8.12	1466.61	12.26	12.29	4.29
RBA-5 T 48-72B	1294.08	45156.83	178381.05	144.37	1371.24	21265.02	8048.74	4173.62	70.19	63.02	579.80	52181.40	15.39	57.93	50.51	92.95	13.82	6.59	163.97	140.37	31.22	179.00	10.24	7.52	301.90	12.07	12.26	0.73

Sample ID	Mg	Al	Si	P	S	K	Ca	Ti	V	Cr	Mn	Fe	Co	Ni	Cu	Zn	Ga	As	Rb	Sr	Y	Zr	Nb	Mo	Ba	Pb	Th	U
RBA-5 T 48-72C	3053.35	49787.38	170449.18	166.50	1462.04	21413.45	7653.10	4986.77	113.44	34.67	767.43	62246.54	11.47	59.11	51.04	97.90	13.80	6.17	152.26	147.68	31.27	147.84	10.51	3.50	739.56	12.24	11.51	3.30
RBA-5 T 48-72D	3711.22	51309.67	172382.55	181.04	1443.06	21490.23	7739.29	5022.71	115.37	37.18	791.58	61627.84	15.33	57.75	50.55	97.75	13.53	6.34	154.22	145.79	31.97	143.63	10.50	5.07	0.00	11.21	11.58	3.47
RBA-5 T 48-72E	3497.23	51229.12	175101.58	247.51	1413.85	23696.36	8026.40	4905.28	111.15	26.87	690.95	57963.46	21.95	63.47	55.03	100.68	14.69	8.43	185.74	138.05	27.38	136.22	9.95	0.00	948.38	12.72	14.01	3.18
RBA-5 T 48-72F	3721.53	51311.49	169694.94	171.82	1568.01	22512.71	8046.74	5231.32	94.07	67.25	683.18	57587.14	19.13	65.05	53.59	103.12	13.46	5.36	174.78	146.80	29.55	139.75	10.17	3.86	1280.50	12.42	13.09	4.40
Average (ppm)	2718.83	48987.75	173684.41	173.95	1444.14	21930.87	7905.64	4746.56	95.60	49.42	678.20	57254.04	15.95	60.12	51.90	98.47	14.00	6.22	165.27	143.49	30.15	154.59	10.32	4.68	789.49	12.15	12.46	3.23
Standard Dev.	1230.56	3033.05	3404.87	40.30	68.27	988.34	171.24	461.92	21.38	18.47	95.46	4446.94	3.99	3.30	1.93	3.40	0.55	1.34	12.84	3.86	1.68	20.10	0.25	2.97	563.63	0.51	0.95	1.33
Core 6																												
RBA-6 B 0-24A	356.76	44133.27	176191.91	256.21	1205.46	16815.35	10501.81	4128.79	63.09	99.35	567.05	41367.95	12.81	55.47	39.36	78.43	14.65	7.41	132.48	128.55	36.95	222.28	11.27	8.42	157.29	12.59	9.89	0.00
RBA-6 B 0-24B	421.71	45069.78	191049.37	244.55	1219.18	16545.87	11495.30	3917.73	73.05	97.54	540.16	37685.69	15.49	50.86	37.83	79.63	15.07	7.64	132.19	135.15	38.42	222.14	11.31	8.58	1170.28	12.10	9.84	0.00
RBA-6 B 0-24AC	153.02	43356.66	176107.71	221.57	1217.29	16675.65	10367.21	4035.14	49.52	98.71	579.81	41738.12	17.86	55.36	45.69	84.43	14.88	11.49	134.04	126.28	35.42	238.21	11.12	9.43	853.10	13.62	10.09	0.00
RBA-6 B 0-24D	548.76	45194.72	192097.87	245.22	1242.45	16689.97	11525.90	3858.08	85.56	95.06	554.12	37371.80	17.24	59.03	41.28	82.81	14.55	11.23	132.50	135.32	35.88	238.62	11.29	9.52	8.35	13.59	9.93	0.00
RBA-6 B 0-24E	41.99	47642.18	196273.79	289.26	1257.31	17928.82	10711.28	3605.71	87.90	103.26	558.86	39328.07	15.06	56.45	38.56	81.79	13.81	8.18	130.59	141.98	34.87	191.95	10.68	8.52	1073.84	12.79	9.83	1.55
RBA-6 B 0-24F	833.79	45784.92	193103.04	347.13	1166.36	16949.33	11622.24	3941.51	86.41	100.45	560.84	39187.23	14.17	48.51	39.14	82.18	13.67	8.29	126.41	130.28	35.97	271.46	12.44	15.59	1012.35	12.65	9.60	0.00
Average (ppm)	392.67	45196.92	187470.62	267.32	1218.01	16934.17	11037.29	3914.49	74.26	99.06	560.14	39446.48	15.44	54.28	40.31	81.54	14.44	9.04	131.37	132.93	36.25	230.78	11.35	10.01	712.54	12.89	9.87	0.26
Standard Dev.	283.37	1473.71	8941.63	44.89	31.53	506.15	571.44	178.74	15.49	2.76	13.21	1812.71	1.88	3.87	2.88	2.18	0.57	1.83	2.67	5.71	1.27	26.18	0.58	2.78	500.78	0.60	0.16	0.63
RBA-6 B 24-48A	965.18	44576.26	206574.83	182.53	1465.58	17199.64	11783.92	3502.43	58.09	97.12	544.77	33015.77	10.86	45.97	35.47	69.59	12.12	4.02	103.52	148.05	37.06	291.11	11.55	21.83	1161.22	10.23	7.93	0.00
RBA-6 B 24-48C	273.75	45146.03	207830.37	223.98	1505.29	17321.14	11840.43	3594.21	50.48	94.67	551.54	32902.66	6.77	28.10	27.29	50.33	9.85	2.18	96.69	160.75	33.65	200.09	10.45	12.54	10.63	9.55	7.47	0.00
RBA-6 B 24-48D	442.19	45512.22	209531.51	213.20	1577.72	17350.65	11984.82	3634.03	56.87	96.49	556.95	32757.78	4.89	28.92	27.38	56.86	9.39	4.59	104.02	149.91	31.04	182.21	10.05	7.45	1009.73	10.44	7.93	0.00
RBA-6 B 24-48E	250.60	45345.09	205467.34	238.05	1527.13	17657.75	12608.89	3667.43	74.36	95.39	545.43	32834.56	5.63	28.41	24.80	55.59	8.43	5.26	112.81	147.62	33.99	184.98	9.85	7.01	871.28	8.82	8.18	0.00
RBA-6 B 24-48F	89.38	43109.61	205200.99	259.12	1394.98	16568.15	12743.07	3651.08	59.36	85.54	484.94	31929.99	4.78	29.97	25.39	53.28	8.45	3.54	110.14	141.54	33.00	179.45	9.87	4.65	0.00	10.22	8.02	0.00

Sample ID	Mg	Al	Si	P	S	K	Ca	Ti	V	Cr	Mn	Fe	Co	Ni	Cu	Zn	Ga	As	Rb	Sr	Y	Zr	Nb	Mo	Ba	Pb	Th	U
RBA-6 B 24-48B	1123.80	45030.40	208874.31	212.11	1522.15	17466.13	11957.26	3599.62	62.39	93.54	546.89	32988.75	5.83	33.42	27.93	50.50	11.12	4.75	105.91	149.50	35.57	214.53	10.65	13.66	362.04	10.38	7.90	0.00
Average (ppm)	524.15	44786.60	207246.56	221.50	1498.81	17260.58	12153.07	3608.13	60.26	93.79	538.42	32738.25	6.46	32.47	28.04	56.02	9.89	4.06	105.52	149.56	34.05	208.73	10.41	11.19	569.15	9.94	7.90	0.00
Standard Dev.	421.27	881.32	1789.56	25.97	62.45	372.81	413.89	59.11	7.95	4.24	26.60	407.37	2.27	6.90	3.84	7.15	1.48	1.10	5.64	6.26	2.08	42.47	0.65	6.25	512.78	0.64	0.24	0.00
RBA-6 T 0-24A	856.58	48355.45	209425.14	245.45	1535.69	19111.66	11071.27	3462.51	87.28	109.79	521.84	35901.55	11.76	44.45	34.30	72.02	12.40	6.45	134.47	148.09	32.90	133.63	10.40	0.00	424.94	11.31	10.01	0.00
RBA-6 T 0-24B	1018.25	48372.66	208756.89	236.47	1557.28	18905.91	11012.04	3388.94	70.62	112.53	528.23	36341.96	12.84	44.21	34.43	73.87	12.12	4.65	134.34	158.71	32.77	135.01	10.44	2.32	567.42	11.10	10.14	2.84
RBA-6 T 0-24C	472.92	47084.54	208782.07	253.18	1508.39	19084.68	11105.03	3455.93	73.79	114.32	518.51	36159.20	10.94	45.92	32.11	71.67	13.34	6.81	137.07	147.65	31.12	148.57	10.12	1.36	0.00	11.63	10.31	0.00
RBA-6 T 0-24D	1359.06	48885.64	202658.22	223.45	1542.80	20101.75	10321.65	3630.66	92.05	85.15	574.59	39069.65	11.68	47.95	34.05	73.37	12.41	5.73	137.97	147.90	32.25	146.96	10.38	2.67	227.08	11.44	10.24	0.00
RBA-6 T 0-24E	798.26	48781.83	208321.79	337.37	1533.15	19148.52	11663.90	4117.40	97.03	90.40	550.31	35286.77	0.00	0.00	0.00	0.00	0.00	0.00	0.00	0.00	0.00	0.00	0.00	0.00	0.00	0.00	0.00	0.00
RBA-6 T 0-24F	1326.65	46687.74	213414.68	263.78	1483.39	18267.08	11163.36	3293.84	76.25	115.55	504.03	33888.51	0.00	0.00	0.00	0.00	0.00	0.00	0.00	0.00	0.00	0.00	0.00	0.00	0.00	0.00	0.00	0.00
Average (ppm)	971.95	48027.98	208559.80	259.95	1526.78	19103.27	11056.21	3558.21	82.84	104.62	532.92	36107.94	11.80	45.63	33.72	72.73	12.57	5.91	135.96	150.59	32.26	141.04	10.34	1.58	304.86	11.37	10.18	0.71
Standard Dev.	337.73	918.28	3443.61	40.37	26.56	589.51	430.09	295.33	10.78	13.30	25.40	1701.29	0.78	1.72	1.09	1.05	0.53	0.95	1.84	5.42	0.81	7.81	0.14	1.19	246.54	0.22	0.13	1.42
RBA-6 T 24-48A	370.00	46069.79	204054.32	166.04	1427.39	17033.48	11894.83	3364.29	61.31	101.71	537.66	31002.43	11.09	64.37	37.11	67.41	11.29	6.32	118.37	129.21	37.48	214.22	11.59	0.10	840.16	11.34	8.73	0.00
RBA-6 T 24-48B	184.48	45739.71	203847.77	208.78	1505.66	17155.02	11989.87	3468.28	79.14	104.38	536.74	31548.16	11.34	61.76	37.07	62.93	12.21	6.64	114.91	135.67	37.46	210.06	11.45	3.28	179.73	11.06	8.73	0.00
RBA-6 T 24-48C	367.10	48397.29	203434.59	205.81	1503.63	17350.89	11860.47	3639.78	77.34	98.21	541.62	33334.01	9.12	61.41	37.42	67.06	13.43	4.44	117.80	150.12	34.63	230.35	11.11	15.05	69.26	11.24	8.97	0.00
RBA-6 T 24-48D	550.80	48425.38	203762.00	235.78	1476.05	17445.12	11852.62	3555.10	72.08	101.10	531.45	33714.93	10.20	62.07	36.34	66.93	12.57	6.33	116.62	151.64	35.38	231.05	11.16	18.49	1276.81	10.67	8.92	0.00
RBA-6 T 24-48E	779.60	48865.78	202489.21	181.78	1489.56	17922.87	12100.41	3567.78	83.86	85.79	531.18	33772.15	7.45	63.22	37.27	68.98	11.79	9.19	113.78	144.45	33.41	217.32	11.01	9.31	92.04	11.55	8.92	0.38
RBA-6 T 24-48F	564.27	48881.31	205621.14	234.77	1532.92	17792.52	12200.99	3811.74	60.91	97.33	548.06	32730.42	13.06	61.94	36.73	71.09	13.56	7.16	118.52	142.21	37.11	209.48	11.89	8.52	897.77	11.64	8.89	0.00
Average (ppm)	469.38	47729.88	203868.17	205.49	1489.20	17449.98	11983.20	3567.83	72.44	98.09	537.78	32683.68	10.38	62.46	36.99	67.40	12.48	6.68	116.67	142.22	35.91	218.75	11.37	9.13	559.30	11.25	8.86	0.06
Standard Dev.	206.58	1432.61	1020.66	27.95	35.73	349.65	142.22	152.43	9.55	6.54	6.40	1165.28	1.94	1.12	0.39	2.70	0.90	1.54	1.95	8.58	1.70	9.69	0.34	6.91	512.02	0.35	0.10	0.15
Core 7																												
RBA-7 T 0-24A	1095.22	49416.38	178829.99	103.88	1377.49	20938.16	10910.44	4670.57	118.95	78.23	631.05	44021.01	28.97	80.15	61.24	110.90	21.23	5.60	171.39	98.92	31.87	206.21	13.19	0.77	0.00	14.21	12.94	0.00

Sample ID	Mg	Al	Si	P	S	K	Ca	Ti	V	Cr	Mn	Fe	Co	Ni	Cu	Zn	Ga	As	Rb	Sr	Y	Zr	Nb	Mo	Ba	Pb	Th	U
RBA-7 T 0-24B	1369.89	52797.17	184870.68	134.38	1481.02	21202.26	11049.76	4713.13	104.95	78.50	639.15	44457.91	25.86	74.48	59.72	109.11	19.76	3.80	166.29	92.80	30.73	202.34	12.81	0.00	1233.26	13.54	12.71	0.00
RBA-7 T 0-24C	1478.80	51544.13	182674.60	130.91	1437.30	21137.92	11264.44	4588.53	91.35	79.92	635.79	43935.53	29.63	73.30	61.28	111.46	20.66	5.69	166.81	109.41	32.44	210.25	13.12	5.64	1344.59	13.38	12.77	0.00
RBA-7 T 0-24D	2024.82	51601.05	183119.17	127.64	1443.49	21260.24	11260.28	4603.21	83.58	76.08	628.61	44034.57	31.97	80.58	61.36	105.47	21.54	3.83	168.57	92.61	32.54	214.34	13.36	0.00	207.31	14.06	12.65	0.00
RBA-7 T 0-24E	2441.72	53822.53	191581.21	161.42	1493.32	22015.23	11291.03	4837.69	118.29	77.59	661.33	44446.88	28.25	75.66	60.67	107.30	20.42	6.82	165.26	105.81	30.64	204.81	12.77	4.46	773.80	14.09	12.75	0.00
RBA-7 T 0-24F	1702.59	51534.54	183939.26	154.36	1486.11	21089.08	11011.61	4675.53	93.47	77.71	645.84	44339.03	27.14	75.38	59.26	106.99	19.32	5.96	171.29	98.46	33.34	199.28	12.69	0.00	1670.75	13.38	12.66	0.00
RBA-7 T 0-24G	3248.82	58318.20	190569.21	162.68	1524.10	22789.66	11094.73	4918.11	113.00	76.59	682.96	44533.60	0.00	0.00	0.00	0.00	0.00	0.00	0.00	0.00	0.00	0.00	0.00	0.00	0.00	0.00	0.00	0.00
RBA-7 T 0-24H	2082.19	54955.27	186693.77	144.96	1518.27	21888.02	11191.94	4748.06	95.02	79.74	642.38	43764.07	0.00	0.00	0.00	0.00	0.00	0.00	0.00	0.00	0.00	0.00	0.00	0.00	0.00	0.00	0.00	0.00
RBA-7 T 0-24I	2648.42	57852.01	193955.60	181.34	1560.47	22782.20	11457.60	4827.44	117.52	72.98	703.27	45028.86	0.00	0.00	0.00	0.00	0.00	0.00	0.00	0.00	0.00	0.00	0.00	0.00	0.00	0.00	0.00	0.00
Average (ppm)	2010.27	53537.92	186248.17	144.62	1480.17	21678.09	11170.20	4731.36	104.01	77.48	652.26	44284.61	28.64	76.59	60.59	108.54	20.49	5.28	168.27	99.67	31.93	206.21	12.99	1.81	871.62	13.78	12.75	0.00
Standard Dev.	685.32	3017.21	4893.04	23.17	54.50	724.54	168.63	111.61	13.51	2.11	25.54	387.31	2.11	3.04	0.90	2.36	0.84	1.22	2.61	6.81	1.07	5.43	0.27	2.55	663.88	0.38	0.11	0.00
RBA-7 B 0-24A	1476.92	50650.44	184110.38	133.46	1431.94	20889.06	10897.85	4453.72	91.05	76.00	687.79	43655.52	31.19	74.39	31.58	90.39	21.18	9.40	170.38	94.96	31.99	185.05	13.11	0.00	561.64	15.06	12.84	0.00
RBA-7 B 0-24B	2071.01	51465.97	189155.68	137.34	1416.78	20570.97	10794.70	4335.93	95.55	80.82	646.13	43626.86	32.10	81.27	32.95	86.97	20.85	6.80	180.03	101.68	31.66	187.77	13.56	0.00	436.57	14.29	13.44	0.00
RBA-7 B 0-24C	0.00	0.00	0.00	0.00	0.00	0.00	0.00	0.00	0.00	0.00	0.00	0.00	32.18	78.06	31.82	89.74	19.59	4.48	177.41	98.76	31.44	185.49	12.98	0.00	1515.80	13.78	13.31	0.00
RBA-7 B 0-24D	0.00	0.00	0.00	0.00	0.00	0.00	0.00	0.00	0.00	0.00	0.00	0.00	31.82	77.91	32.12	89.03	20.54	6.89	175.94	98.47	31.70	186.10	13.22	0.00	1091.07	14.38	13.19	0.00
Average (ppm)	1773.97	51058.20	186633.03	135.40	1424.36	20730.01	10846.27	4394.82	93.30	78.41	666.96	43641.19	31.82	77.91	32.12	89.03	20.54	6.89	175.94	98.47	31.70	186.10	13.22	0.00	901.27	14.38	13.19	0.00
Standard Dev.	420.09	576.66	3567.56	2.75	10.72	224.92	72.93	83.29	3.18	3.41	29.46	20.27	0.45	2.81	0.60	1.48	0.69	2.01	4.07	2.75	0.23	1.19	0.25	0.00	498.32	0.53	0.26	0.00
RBA-7 T 24-48A	0.00	46068.39	185693.04	103.27	1556.95	17801.84	11374.96	4169.88	82.10	86.31	533.77	36816.62	15.59	82.71	51.67	88.25	16.72	5.27	145.34	126.64	36.63	248.12	12.02	13.88	1309.52	12.92	10.92	0.00
RBA-7 T 24-48B	112.26	46856.76	186494.61	120.35	1532.10	17824.83	11410.81	4196.50	79.43	84.35	532.23	36458.02	17.95	79.33	50.61	90.64	18.00	6.54	146.01	129.48	36.45	247.06	12.23	15.02	553.80	13.01	10.95	0.00
RBA-7 T 24-48C	1493.25	52560.40	192392.29	165.68	1575.94	20446.65	11799.12	4446.38	74.75	95.80	595.89	39918.11	16.52	84.93	49.41	93.62	16.76	5.56	143.08	122.54	34.14	245.69	12.31	12.13	0.00	12.50	11.03	0.00
RBA-7 T 24-48D	1541.46	51741.46	192192.07	150.47	1544.43	20252.69	11823.12	4396.08	84.03	94.91	593.40	40214.04	18.58	82.06	53.44	92.60	17.83	4.71	142.36	122.93	36.79	246.16	13.14	9.70	721.37	12.43	10.89	0.00
RBA-7 T 24-48E	1049.14	53114.38	192700.58	189.55	1545.84	20451.77	11495.75	4415.59	78.17	84.34	599.25	41011.04	14.08	65.80	33.51	76.52	12.75	1.30	125.76	96.68	35.52	193.67	12.45	0.00	447.80	10.00	8.78	0.00
RBA-7 T 24-48F	1147.07	51177.54	187204.68	153.98	1545.11	20150.54	11341.63	4360.86	82.96	86.91	581.53	40677.69	19.57	88.51	53.45	93.65	16.91	6.60	152.71	130.12	35.42	256.51	12.76	16.17	661.80	13.14	11.63	0.00

Sample ID	Mg	Al	Si	P	S	K	Ca	Ti	V	Cr	Mn	Fe	Co	Ni	Cu	Zn	Ga	As	Rb	Sr	Y	Zr	Nb	Mo	Ba	Pb	Th	U
RBA-7T 24-48G	971.16	54508.39	192425.37	132.38	1545.39	20362.56	11245.34	4309.89	66.74	82.37	567.21	40072.14	30.06	75.64	29.39	84.87	20.55	5.22	167.77	103.73	30.57	196.74	12.57	0.57	395.47	13.86	12.88	0.00
RBA-7T 24-48H	1786.74	55424.25	194477.40	157.84	1618.90	21468.93	11370.63	4305.17	84.55	86.18	605.37	40307.75	0.00	0.00	0.00	0.00	0.00	0.00	0.00	0.00	0.00	0.00	0.00	0.00	0.00	0.00	0.00	0.00
RBA-7T 24-48I	2470.46	57399.39	196196.81	160.11	1595.53	22398.82	11574.45	4633.97	100.13	81.50	620.67	40849.88	0.00	0.00	0.00	0.00	0.00	0.00	0.00	0.00	0.00	0.00	0.00	0.00	0.00	0.00	0.00	0.00
Average (ppm)	1174.62	52094.55	191086.32	148.18	1562.24	20128.74	11492.87	4359.37	81.43	86.96	581.03	39591.70	18.91	79.85	45.93	88.59	17.07	5.03	146.15	118.87	35.07	233.42	12.50	9.64	584.25	12.55	11.01	0.00
Standard Dev.	779.12	3725.36	3711.17	25.82	28.73	1497.82	202.87	139.33	8.97	5.09	30.98	1715.20	5.26	7.41	10.06	6.20	2.33	1.78	12.59	13.24	2.19	26.37	0.37	6.72	397.36	1.22	1.22	0.00
RBA-7B 24-48A	1931.07	51246.96	182207.15	121.31	1445.82	20806.62	10955.08	4607.81	106.61	74.90	690.06	43745.51	30.49	72.26	28.66	82.67	22.29	2.89	167.74	106.41	30.28	198.15	11.86	0.84	399.55	13.75	12.85	0.00
RBA-7B 24-48B	1427.51	51419.60	186723.05	155.66	1491.36	20940.13	11136.34	4445.07	94.11	79.54	689.37	43177.17	28.55	76.50	29.22	84.17	19.93	7.95	163.73	105.02	28.19	197.71	13.05	0.87	478.43	13.97	13.00	2.03
RBA-7B 24-48C	2188.98	54127.31	194745.23	191.26	1491.60	20720.48	11909.67	4688.39	92.07	87.85	673.66	42588.18	31.14	78.17	30.28	87.77	19.42	4.81	171.83	99.75	33.26	194.37	12.81	0.00	547.82	13.86	12.79	0.00
Average (ppm)	1849.19	52264.62	187891.81	156.07	1476.26	20822.41	11333.70	4580.43	97.60	80.77	684.36	43170.29	30.06	75.64	29.39	84.87	20.55	5.22	167.77	103.73	30.57	196.74	12.57	0.57	475.27	13.86	12.88	0.68
Standard Dev.	387.28	1615.44	6350.23	34.98	26.36	110.67	506.98	123.95	7.87	6.56	9.27	578.70	1.35	3.05	0.83	2.62	1.53	2.55	4.05	3.52	2.55	2.07	0.63	0.49	74.18	0.11	0.11	1.17
Core 8																												
RBA-8B 0-48A	0.00	26868.92	182511.05	0.00	1241.68	12896.41	9906.21	2354.81	96.18	109.69	411.08	26923.36	7.65	42.69	32.02	76.18	12.24	2.28	109.08	147.36	33.92	235.55	11.28	9.48	0.00	10.13	8.43	0.00
RBA-8B 0-48B	0.00	27660.30	182158.66	0.00	1265.63	12828.57	9891.72	2377.13	81.39	105.88	406.30	26493.28	3.75	0.11	4.92	14.81	3.20	6.03	41.87	21.07	11.31	94.35	15.86	0.00	147.32	8.46	3.78	0.00
RBA-8B 0-48C	0.00	29475.90	188872.83	6.16	1203.43	13304.77	9167.49	2613.89	66.79	106.92	419.35	27303.34	4.57	0.63	3.43	15.91	2.32	6.94	44.83	21.57	12.65	94.22	16.20	0.00	0.00	9.08	3.80	0.00
RBA-8B 0-48D	0.00	29472.67	189248.54	0.00	1270.63	13479.75	9205.62	2629.09	69.47	107.53	431.14	27187.08	8.78	42.64	33.21	63.63	10.59	1.97	115.93	147.22	32.49	224.59	10.95	12.55	0.00	10.13	8.91	0.00
RBA-8B 0-48E	0.00	27973.92	185778.86	11.11	1294.24	13173.23	9518.17	2871.20	75.83	99.85	408.99	27044.73	10.72	45.12	32.87	66.63	12.58	3.61	117.28	152.53	33.27	223.44	11.03	12.39	0.00	10.59	8.97	0.00
RBA-8B 0-48F	0.00	25010.95	170049.14	0.00	1214.00	11634.14	8725.77	2352.02	80.51	99.84	371.16	24808.90	8.91	44.18	33.78	62.20	11.82	4.98	113.47	159.34	35.62	248.27	12.11	20.70	1010.07	10.61	8.90	2.71
Average (ppm)	0.00	27743.78	183103.18	2.88	1248.27	12886.15	9402.50	2533.02	78.36	104.95	408.00	26626.78	7.40	29.23	23.37	49.89	8.79	4.30	90.41	108.18	26.54	186.74	12.90	9.19	192.90	9.83	7.13	0.45
Standard Dev.	0.00	1690.15	7069.15	4.73	35.05	660.45	460.09	209.26	10.49	4.15	20.17	933.47	2.71	22.37	14.89	27.19	4.73	2.02	36.57	67.43	11.34	72.17	2.46	8.04	404.64	0.87	2.60	1.11
RBA-8T 0-48A	0.00	34044.50	204400.29	93.27	1218.99	13915.49	9832.02	2722.40	82.35	92.45	470.75	26905.49	8.13	42.85	29.19	58.88	10.57	6.06	119.37	152.40	34.01	222.51	10.49	15.17	1019.35	11.07	8.78	0.00
RBA-8T 0-48B	0.00	34111.24	205088.60	94.26	1254.91	14079.58	9891.95	2741.31	74.07	93.16	461.01	26843.94	8.21	44.87	31.31	55.37	11.95	9.53	114.77	147.99	31.84	219.51	10.44	11.55	757.44	11.27	8.54	0.00
RBA-8T 0-48C	0.00	33102.47	186209.78	49.86	1264.31	14194.99	8952.52	2441.03	74.46	101.71	402.22	25427.72	9.73	43.45	29.73	46.39	12.12	4.41	108.82	159.51	33.62	210.64	10.57	12.57	792.51	10.61	8.15	0.00

Sample ID	Mg	Al	Si	P	S	K	Ca	Ti	V	Cr	Mn	Fe	Co	Ni	Cu	Zn	Ga	As	Rb	Sr	Y	Zr	Nb	Mo	Ba	Pb	Th	U
RBA-8 T 0-48D	0.00	32650.97	185749.07	68.83	1319.28	14125.56	8894.16	2503.66	76.79	98.61	402.73	25683.48	5.84	39.95	29.30	53.54	12.86	4.15	107.52	163.96	32.63	208.74	10.73	14.32	382.41	11.67	8.38	1.55
RBA-8 T 0-48E	0.00	36452.56	198064.84	78.07	1223.39	14663.74	9540.22	2651.51	71.50	156.79	443.08	27883.81	8.84	46.13	28.98	54.35	10.48	8.32	107.48	157.90	32.63	217.13	10.30	11.40	821.45	11.14	8.09	0.00
RBA-8 T 0-48F	0.00	36498.47	206842.85	351.85	1176.26	15352.34	9994.06	2650.46	90.54	111.43	455.59	28152.67	6.42	42.30	30.55	55.16	12.12	9.54	109.18	152.14	31.72	257.55	10.61	19.06	335.72	12.59	8.51	0.18
Average (ppm)	0.00	34476.70	197725.90	122.69	1242.86	14388.62	9517.49	2618.40	78.29	109.03	439.23	26816.18	7.86	43.26	29.84	53.95	11.68	7.00	111.19	155.65	32.74	222.68	10.52	14.01	684.81	11.39	8.41	0.29
Standard Dev.	0.00	1645.22	9571.37	113.48	48.64	534.88	484.67	120.56	7.04	24.39	29.84	1108.66	1.47	2.14	0.91	4.13	0.95	2.46	4.83	5.84	0.92	17.87	0.15	2.89	268.62	0.68	0.26	0.62

Aqua Regia, HCl, and PO_4 Chemical Leaching

Table J.3 Aquaregia Data used for Sediment Vertical Profiles

			As		distance to		Mn	distance to			Fe	distance to		
Sample Core #	Depth Range (cm)	Depth (cm)	mg/kg	low	high	Stdev.	mg/kg	low	high	Stdev.	mg/kg	low	high	Stdev.
8	0-61 T	0	2.64	2.60	4.39	2.68	143.65	2.22	2.22	3.15	15231.78	2069.09	2069.09	2926.13
8	61-122 B	71	59.38	48.47	43.72	39.35	435.44	124.73	176.58	132.17	30683.98	116.21	116.21	164.34
8	122- 183 B	183	4.49	0.46	0.46	0.65	402.68	31.34	31.34	44.32	26442.43	1195.38	1195.38	1690.53
8	183- 244 T	198	32.83	20.62	20.62	29.16	249.89	9.92	9.92	14.04	20682.48	1210.78	1210.78	1712.31
8	183- 244 B	244	3.58	0.35	0.35	0.49	215.88	4.97	4.97	7.03	17637.55	335.72	335.72	474.77
2	0-61 T	0	37.67	31.24	31.24	44.18	133.97	18.58	35.87	31.07	10898.54	260.14	260.14	367.89
2	61-122 T	122	16.36	0.99	0.99	1.412	142.57	5.22	5.22	7.38	13965.44	331.52	331.52	468.84
8b	0-61 B	0	-	-	-	-	222.91	0	0	-	17641.38	0	0	-
8b	61-122 B	122	2.61	0.52	0.52	0.74	302.92	40.15	40.15	56.79	18132.54	248.67	248.67	351.68

Table J.4 HCl Data used for Sediment Vertical Profiles

			As		distance to		Mn	distance to			Fe	distance to		
Sample Core #	**Depth Range (cm)**	**Depth (cm)**	**mg/kg**	**low**	**high**	**Stdev.**	**mg/kg**	**low**	**high**	**Stdev.**	**mg/kg**	**low**	**high**	**Stdev.**
8	0-61 T	0	7.94	6.18	18.17	12.11	58.37	13.14	23.97	20.79	3923.59	1130.48	1795.99	1057.03
	61-122 B	71	10.41	2.20	2.20	3.11	285.37	35.64	36.50	36.08	12465.00	1267.92	826.53	1114.81
	122- 183 T	140	7.75	5.57	9.07	5.47	294.45	0	0	-	13894.40	0	0	-
	122- 183 B	183	39.39	16.09	11.47	14.35	313.55	14.90	18.32	16.87	14908.21	764.68	995.49	902.50
	183- 244 T	198	82.91	48.60	48.60	68.73	84.38	5.90	5.90	8.35	5247.69	1099.65	1135.40	1128.09
	183- 244 B	244	141.61	46.99	46.99	66.46	146.27	2.69	2.69	3.81	7414.06	1464.61	1610.21	1624.66
2	0-61 T	0	660.12	24.86	24.86	24.86	435.86	141.07	141.07	235.28	4746.25	1640.31	4461.15	2976.73
	61-122 B	122	538.15	82.87	97.15	77.80	32.01	1.48	0.85	1.28	2775.21	570.02	554.51	518.12
8b	0-61 T	0	81.51	26.67	29.70	28.31	135.02	23.43	26.65	25.19	7096.50	1988.43	2394.20	1663.19
	61-122 B	122	85.46	16.73	16.734	23.66	56.40	4.64	4.64	6.56	4270.37	1040.19	1088.46	931.31
3	0-33 T	0	61.32	21.57	21.570	30.50	134.09	134.09	0	-	2733.24	2733.24	0	-
	0-33 B	28	35.42	1.75	1.75	2.48	192.43	1.70	1.71	2.41	3905.73	49.68	49.68	70.26
	33-91 T	40	18.40	2.53	2.52	3.57	82.92	1.72	1.73	2.44	2277.57	24.067	24.07	34.03
	33-91 B	91	22.35	7.08	7.08	10.02	170.35	4.91	4.91	6.94	4048.61	27.93	27.93	39.50
	91-122 B	122	18.42	3.76	3.76	5.32	235.72	20.33	20.33	28.75	4612.64	335.79	335.79	474.88
4	0-61 T	0	16.50	5.37	5.37	7.59	327.36	142.88	142.88	202.06	3556.10	1519.99	1519.99	2149.60
	0-61 B	61	19.54	-	-	-	138.69	-	-	-	2009.86	-	-	-
	61-122 B	122	13.84	0.69	0.69	0.97	388.79	10.99	10.99	15.54	3878.41	138.12	138.13	195.34
6	0-61 T	0	16.67	0	0	-	138.79	0	0	-	2664.93	0	0	-
	61-122 B	122	15.911	3.27	3.27	4.62	103.18	4.28	4.28	6.05	2536.96	42.95	42.95	60.75

			As		distance to		Mn	distance to			Fe	distance to		
Sample Core #	**Depth Range (cm)**	**Depth (cm)**	**mg/kg**	**low**	**high**	**Stdev.**	**mg/kg**	**low**	**high**	**Stdev.**	**mg/kg**	**low**	**high**	**Stdev.**
17	0-61 T	0	25.62	9.83	9.83	13.91	557.31	60.47	60.47	85.52	5662.20	140.53	140.53	198.74
	0-61 B	50	775.91	0	0	0	112.07	7.22	7.22	10.21	3591.43	391.21	391.21	553.26
	61-122 T	71	1532.93	119.05	119.05	168.37	229.66	1.81	1.81	2.57	6001.39	51.93	51.93	73.45
	61-122 B	112	17.31	0.07	0.07	0.10	277.52	0.85	0.85	1.21	7054.67	218.17	218.17	308.54
	122- 183 T	130	107.82	0	0	0	190.17	7.66	7.66	10.84	5787.51	255.83	255.83	361.80
	122- 183 B	183	15.047	0	0	-	60.77	0	0	-	2197.06	0	0	-
13	0-61 T	0	692.13	0	0	0	300.83	2.13	2.12	3.01	7192.73	34.25	34.25	48.44
	0-61 B	50	17.86	3.92	3.92	5.54	365.16	4.54	4.54	6.42	7815.59	69.35	69.35	98.08
	61-122 T	71	197.03	0	0	0	290.83	9.40	9.41	13.30	6915.63	211.32	211.32	298.85
	61-122 B	122	17.18	1.99	1.99	2.81	360.89	0.05	0.05	0.08	7583.68	200.98	200.98	284.27
14	0-61 T	0	163.03	0	0	0	158.30	45.51	45.51	64.36	4403.08	175.00	175.00	247.48
	0-61 B	50	578.33	33.44	33.44	47.29	214.24	0.59	0.59	0.84	5615.51	76.83	76.83	108.66
	61-122 T	71	527.44	17.92	17.92	25.35	203.27	3.33	3.33	4.71	3927.91	26.37	26.37	37.29
	61-122 B	122	43.02	22.25	22.25	31.47	82.10	39.96	39.96	56.52	2883.84	124.74	124.74	176.41

Table J.5 PO_4 Data used for Sediment Vertical Profiles

			As		distance to		Mn	distance to			Fe	distance to		
Sample Core #	Depth Range (cm)	Depth (cm)	mg/kg	low	high	Stdev.	mg/kg	low	high	Stdev.	mg/kg	low	high	Stdev.
8	0-61 T	0	2.09	2.00	6.29	3.62	12.42	5.75	3.77	4.01	781.41	120.26	74.88	83.93
	61-122 T	71	0.34	0.347	0.34	0.49	74.05	24.765	24.76	35.02	2452.78	266.43	266.43	376.79
	122- 173 T	140	5.25	3.59	3.59	5.08	161.61	10.57	9.30	9.31	2631.82	784.44	939.39	880.68
	122- 173 B	183	0.95	0.25	0.25	0.35	89.94	15.85	27.71	19.97	2203.54	707.77	851.99	777.13
	183- 244 T	198	4.66	3.01	3.01	4.26	91.55	36.26	33.42	37.41	2092.64	682.18	698.74	744.98
	183- 244 B	244	2.42	2.11	3.74	3.25	50.72	28.69	17.72	17.75	1788.74	490.57	608.92	565.41
2	0-61 T	0	9.49	0.61	0.61	0.86	162.10	41.57	47.55	47.87	2378.01	630.24	1053.34	794.59
	61-122 B	122	6.20	0.90	0.90	1.27	5.49	1.29	1.00	0.95	760.28	88.01	103.08	84.58
8b	0-61 T	0	29.74	29.40	34.40	28.05	38.77	34.76	19.76	18.83	1343.01	205.41	115.96	144.02
	61-122 B	122	39.41	14.156	15.79	12.44	32.71	15.76	19.36	15.31	1111.95	290.62	354.26	322.41
3	0-33 T	0	1.08	0.23	0.23	0.33	97.97	3.03	3.02	4.28	280.57	19.00	19.01	26.87
	0-33 B	28	0.19	0.19	0.19	0.28	54.74	45.78	45.77	64.74	296.70	5.89	5.89	8.34
	33-91 B	91	0.13	0.13	0.13	0.19	35.25	35.25	35.25	49.85	360.18	11.78	11.78	16.67
	91-122 B	122	1.08	0.10	0.10	0.14	112.89	22.01	22.01	31.13	303.06	1.87	1.87	2.64
4	0-61 T	0	0.14	0.14	0.14	0.20	70.36	0.03	0.03	0.04	268.13	2.79	2.79	3.95
	0-61 B	61	0.1	0.00	0.09	0.14	29.54	0.45	0.45	0.64	169.81	2.76	2.76	3.91
	61-122 B	122	0.46	0.07	0.07	0.11	65.69	1.09	1.09	1.54	268.55	2.26	2.26	3.19
6	0-61 T	0	0.22	0.22	0.22	0.31	52.24	0.51	0.51	0.72	237.75	1.79	1.79	2.54
	61-122 B	122	2.76	1.38	1.38	1.96	183.18	84.90	84.90	120.07	292.93	12.56	12.56	17.77
17	0-61 T	0	2.90	1.57	1.57	2.22	216.39	77.91	77.91	110.19	530.88	6.29	6.29	8.90

			As		distance to		Mn	distance to			Fe	distance to		
Sample Core #	**Depth Range (cm)**	**Depth (cm)**	**mg/kg**	**low**	**high**	**Stdev.**	**mg/kg**	**low**	**high**	**Stdev.**	**mg/kg**	**low**	**high**	**Stdev.**
	0-61 B	50	0.83	0.75	0.75	1.17	15.21	15.21	15.20	21.50	398.67	64.79	64.79	91.62
	61-122 T	71	0.75	0.65	0.65	1.06	41.31	41.19	41.19	58.25	296.22	4.54	4.54	6.43
	122- 183 T	130	0.72	0.12	0.12	0.17	37.05	0.04	0.04	0.05	320.46	22.17	22.17	31.35
	122- 183 B	183	0.1	0	0	0	12.08	0.82	0.82	1.16	204.46	6.76	6.76	9.56
13	0-61 T	0	1.06	0.01	0.01	0.01	108.80	0.91	0.91	1.29	361.67	21.66	21.66	30.63
	0-61 B	50	0.1	0	0	0	0.93	0.932	0.93	1.32	571.32	133.31	133.31	188.52
	61-122 T	71	0.1	0	0	0	6.96	6.07	6.07	8.59	337.55	9.91	9.91	14.01
	61-122 B	122	0.55	0.08	0.08	0.12	69.47	3.56	3.56	5.04	315.14	19.89	19.89	28.13
14	0-61 T	0	1.11	0.11	0.11	0.16	123.98	2.00	2.00	2.83	384.22	64.90	64.90	91.78
	0-61 B	50	1.36	0.04	0.04	0.06	153.33	3.55	3.55	5.03	174.58	174.58	174.58	246.90
	61-122 B	122	0.17	0.17	0.17	0.24	74.917	50.17	50.17	70.95	410.49	80.26	80.26	113.51

Table K.1 X-Ray Fluorescence (XRF) Standards

This Study Measured Standards			SARM-41				RTC-W-220 (Woodford Fm.)			
	Wt%	STDEV	Accepted Value	Measured Value	Inter Pellet STDEV	Intra Pellet STDEV	Accepted Value	Measured Value	Inter Pellet STDEV	Intra Pellet STDEV
Fe	2.996595153	0.011591126	2.96	3.2	0.03	0.01	2.39	2.55	0.06	0.02
Ba	0.201390114	0.064178235	0.082	0.0802	0.0214	0.0147	0.209	0.1884	0.0376	0.0083
V	0.094462034	0.000747737	0.0139	0.0167	0.0041	0.0044	0.0928	0.1114	0.0068	0.0066
Cr	0.014937511	0.00066669	0.0123	0.0106	0.0016	0.0009	0.011	0.0098	0.0013	0.0009
Ni	0.014584243	0.00031335	0.0122	0.0079	0.0017	0.0008	0.013	0.0153	0.0026	0.002
Cu	0.018933766	0.000571034	0.0053	0.0065	0.0024	0.0014	0.0083	0.0147	0.002	0.0016
Zn	0.088876788	0.0037892	0.0076	0.0067	0.0007	0.0011	0.0823	0.0844	0.0096	0.003
Th	0.001134741	5.39675E-06	0.0012	0.0007	0.0001	0.0001	0.00084	0.0009	0.0001	0.0002
Rb	0.013807233	0.000273041	0.0059	0.0045	0.0003	0.0003	0.0122	0.0123	0.0012	0.0004
U	0.001373965	0.000550281	0.0002	0.0003	0.0002	0.0003	0.00181	0.0017	0.0006	0.0004
Sr	0.005934777	0.001043929	0.0054	0.0047	0.0002	0.0001	0.00755	0.0087	0.0005	0.0004
Y	0.003255547	2.2356E-05	0.0017	0.0017	0.0001	0.0001	0.00354	0.0034	0.0003	0.0002
Zr	0.011372316	0.000149895	0.0146	0.013	0.0005	0.0004	0.00803	0.0095	0.0007	0.0002
Nb	0.001233761	1.26184E-05	8	5	1	1	9	9	1	1
Mo	0.007165604	0.000455737	5	8	1	1	7	83	4	4

Chemical data for standard material RTC-W-220, pressed powder pellet, Woodford Shale. Accepted values “For RTC-W-220, values for major elements are from lithium borate-fused disk analysis by WD-XRF at SGS; values for trace elements (ppm) from sodium peroxide fusion dissolution and analysis by ICP-MS and ICP-OES. Values for %S determined by LECO combustion/infrared analysis” (Rowe, 2012). Elemental Concentrations Accepted values Rowe et al (2012) measured values, σ Measured values this study: